AWARD NUMBER: W81XWH-17-1-0666

TITLE: Therapeutic Benefit of Hsp90 Inhibition in Pulmonary Fibrosis

PRINCIPAL INVESTIGATOR: Satish K Madala

CONTRACTING ORGANIZATION: Cincinnati, OH

REPORT DATE: JANUARY 2022

TYPE OF REPORT: Final

PREPARED FOR: U.S. Army Medical Research and Materiel Command
Fort Detrick, Maryland 21702-5012

DISTRIBUTION STATEMENT: Approved for Public Release; Distribution Unlimited

The views, opinions and/or findings contained in this report are those of the author(s) and should not be construed as an official Department of the Army position, policy or decision unless so designated by other documentation.

REPORT DOCUMENTATION PAGE

Form Approved
OMB No. 0704-0188

Public reporting burden for this collection of information is estimated to average 1 hour per response, including the time for reviewing instructions, searching existing data sources, gathering and maintaining the data needed, and completing and reviewing this collection of information. Send comments regarding this burden estimate or any other aspect of this collection of information, including suggestions for reducing this burden to Department of Defense, Washington Headquarters Services, Directorate for Information Operations and Reports (0704-0188), 1215 Jefferson Davis Highway, Suite 1204, Arlington, VA 22202-4302. Respondents should be aware that notwithstanding any other provision of law, no person shall be subject to any penalty for failing to comply with a collection of information if it does not display a currently valid OMB control number. **PLEASE DO NOT RETURN YOUR FORM TO THE ABOVE ADDRESS.**

1. REPORT DATE	2. REPORT TYPE	3. DATES COVERED
JANUARY 2022	FINAL	30 Sep 2017 - 29 Sep 2021

4. TITLE AND SUBTITLE

Therapeutic Benefit of Hsp90 Inhibition in Pulmonary Fibrosis

5a. CONTRACT NUMBER

5b. GRANT NUMBER
W81XWH-17-1-0666

5c. PROGRAM ELEMENT NUMBER

6. AUTHOR(S)
Satish K Madala

Email: satish.madala@cchmc.org

5d. PROJECT NUMBER

5e. TASK NUMBER

5f. WORK UNIT NUMBER

7. PERFORMING ORGANIZATION NAME(S) AND ADDRESS(ES)

Children's Hospital Medical Center

Cincinnati, OH 45229

8. PERFORMING ORGANIZATION REPORT NUMBER

9. SPONSORING / MONITORING AGENCY NAME(S) AND ADDRESS(ES)
U.S. Army Medical Research and Materiel Command
Fort Detrick, Maryland 21702-5012

10. SPONSOR/MONITOR'S ACRONYM(S)

11. SPONSOR/MONITOR'S REPORT NUMBER(S)

12. DISTRIBUTION / AVAILABILITY STATEMENT
Approved for Public Release; Distribution Unlimited

13. SUPPLEMENTARY NOTES

14. ABSTRACT: Pulmonary fibrosis is the final common pathway of a number of adult and pediatric diseases that are associated with fibroblast invasion and excessive deposition of the extracellular matrix (ECM) in the lung. In adults, fibrosis occurs in both the idiopathic pneumonias and in the systemic connective-tissue diseases. Idiopathic Pulmonary Fibrosis (IPF) is perhaps the most pernicious and enigmatic form of of lung fibrosis and recent evidence indicates that the prevalence the disease is increasing in the U.S. and around the world. Pirfenidone and nintedanib are two recently FDA-approved therapies that slow the rate of decline in lung function in patients with IPF, but do not halt or reverse fibrosis. Thus, newer therapies that reverse established fibrosis would have significant advantages over these current agents. Rationale: We have made the novel discovery that HSP90 functions as a master regulator of fibroblast activation and excessive deposition of ECM proteins in IPF using bioinformatics, molecular, and biochemical methods. Further, our preliminary data demonstrate that the beneficial effect of 17-AAG is mediated by inhibition of HSP90-dependent degradation of Wilms' Tumor 1 (WT1), a novel fibroblast transcription factor that drives fibroblast activation and ECM production. Inhibition of HSP90 ATPase activity using the pharmacological inhibitor 17-AAG was sufficient to attenuate pulmonary fibrosis both in vitro and in vivo. Hypothesis: We will test the hypothesis that inhibition of HSP90 activity, coupled with anti-fibrotic actions of pirfenidone, will reverse established and progressive pulmonary fibrosis mediated by WT1-driven fibroblast dysfunction. Specific Aims: (1) To determine the role of HSP90 in fibroblast activation in IPF. For this aim, we will determine the role of HSP90AA, HSP90AB and dominant negative HSP90 in IPF fibroblast activation including proliferation, invasiveness, (myo)fibroblast survival and ECM production. Successful completion of this aim will identify HSP90 as a new therapeutic target for pulmonary fibrosis. (2) To define the physiological and functional relevance of HSP90-WT1 interaction in fibroblast activation. For this aim, we will demonstrate functional relevance of HSP90 and WT1 interactions using fibroblast activation assays.

15. SUBJECT TERMS

NONE LISTED

16. SECURITY CLASSIFICATION OF:			17. LIMITATION OF ABSTRACT	18. NUMBER OF PAGES	19a. NAME OF RESPONSIBLE PERSON
a. REPORT	b. ABSTRACT	c. THIS PAGE			USAMRMC
U	U	U	UU	142	19b. TELEPHONE NUMBER *(include area code)*

TABLE OF CONTENTS

	Page
1. Introduction	4
2. Keywords	4
3. Accomplishments	4-17
4. Impact	18-19
5. Changes/Problems	20
6. Products	21-23
7. Participants & Other Collaborating Organizations	24-25
8. Special Reporting Requirements	26
9. Appendices	26

1. **INTRODUCTION:** *Narrative that briefly (one paragraph) describes the subject, purpose and scope of the research.*

IPF is a fatal fibrotic lung disease associated with aberrant activation of fibroblasts and progressive fibrosis. The pirfenidone therapy for IPF has been shown to slow the rate of decline in lung function but do not halt ongoing fibrosis. This application will test whether inhibition of HSP90 activity, coupled with anti-fibrotic therapy of pirfenidone, will attenuate WT1-driven fibroblast activation. The proposed studies will provide robust, highly novel observations to rapidly pursue the *long-term* goal: Translational exploration of the molecular mechanisms by which HSP90 activity positively regulates IPF pathogenesis in order to devise novel preventive and therapeutic strategies for IPF.

2. **KEYWORDS:** *Provide a brief list of keywords (limit to 20 words).*

Idiopathic Pulmonary fibrosis; Fibroblasts; Heat shock protein 90; Wilms' tumor 1; lung; collagens

3. **ACCOMPLISHMENTS:** *The PI is reminded that the recipient organization is required to obtain prior written approval from the awarding agency grants official whenever there are significant changes in the project or its direction.*

What were the major goals of the project?
List the major goals of the project as stated in the approved SOW. If the application listed milestones/target dates for important activities or phases of the project, identify these dates and show actual completion dates or the percentage of completion.

Specific Aim 1: To determine the role of HSP90 in fibroblast activation in IPF
The major task is to determine which HSP90 isoform is involved in fibroblast activation.

Subtask 1: Obtain regulatory approvals: ACURO and HRPO review (Duration: 3-6 months)
Subtask 2: Develop lentiviral plasmids to overexpress HSP90AA or HSP90AB isoforms to assess changes in fibroblasts activation. (Duration: 1-12 months)
Subtask 3: Develop lentiviral plasmids to knockdown HSP90AA or HSP90AB isoforms to assess changes in fibroblast activation (Duration: 7-24 months)
Subtask 4: Develop lentiviral plasmids to overexpress wild type and D88N-HSP90 (a dominant negative mutant of HSP90) to assess changes in fibroblast activation (Duration: 12-24 months)

Specific Aim 2: Define the physiological and functional relevance of HSP90-WT1 interaction in fibroblast activation
The major task is to identify contributions of HSP90 and WT1 on fibroblast activation.

Subtask 1: Knockdown HSP90AB, WT1 or both to assess changes in fibroblast-specific gene networks and function. (Duration: 1-24 months)
Subtask 2: Overexpress HSP90AB, WT1 or both to assess changes in fibroblast-specific gene networks and function (Duration: 12-24 months)
Subtask 3: Overexpress D88N-HSP90 and WT1 alone or together to assess changes in fibroblast-specific gene networks and function (Duration: 12-36 months)

Specific Aim 3: Determine whether combined therapy using pirfenidone and 17-AAG is effective to reverse established and ongoing pulmonary fibrosis

The major task is to determine if combined therapy of 17-AAG and Pirfenidone attenuates fibrosis in vivo.

Subtask 1: Utilize a mouse model of TGFα-induced pulmonary fibrosis to test if combined therapy of 17-AAG and Pirfenidone attenuates fibrosis (Duration: 6-24 months)

Subtask 2: Utilize a mouse model of bleomycin-induced pulmonary fibrosis to test if combined therapy of 17-AAG and Pirfenidone attenuates fibrosis (Duration: 16-36 months)

What was accomplished under these goals?

For this reporting period describe: 1) major activities; 2) specific objectives; 3) significant results or key outcomes, including major findings, developments, or conclusions (both positive and negative); and/or 4) other achievements. Include a discussion of stated goals not met. Description shall include pertinent data and graphs in sufficient detail to explain any significant results achieved. A succinct description of the methodology used shall be provided. As the project progresses to completion, the emphasis in reporting in this section should shift from reporting activities to reporting accomplishments.

Major activities: The first 8-10 months of funding for this project have been focused upon several key start up areas, including i) protocol and manual operation development, ii) obtaining all regulatory approvals including ACURO and HRPO (Completed), iii) developed lentiviral plasmids to overexpress or knockdown WT1, D88N-HSP90, HSP90AA, HSP90AB isoforms and assessed changes in fibroblasts activation and iv) studies using preclinical mouse models to assess therapeutic benefit of 17-AAG, pirfenidone and combination therapy were completed.

Specific objectives: The objectives of this are captured in the specific aims described above but can be succinctly summarized in three aims: Aim 1) To determine the role of HSP90 in fibroblast activation in IPF; Aim 2) Define the physiological and functional relevance of HSP90-WT1 interaction in fibroblast activation, and Aim 3) Determine whether combined therapy using pirfenidone and 17-AAG is effective to reverse established and ongoing pulmonary fibrosis.

Significant results:

Aim 1: To determine the role of HSP90 in fibroblast activation in IPF. We obtained regulatory approvals needed from ACURO and HRPO.

Subaim 1A: To determine which HSP90 isoform involved in fibroblast activation. In this subaim, we will use normal fibroblasts and IPF fibroblasts to assess the effect of HSP90 isoforms and mutant overexpression. We completed cloning and overexpression of dominant negative isoform of HSP90AB (D88N-HSP90) and wildtype HSP90AB **(Figs 1 & 2)**.

Subaim 1B: To determine if the loss of HSP90 attenuates fibroblast activation in IPF (Duration: 7-24 months). In mammalian cells, Hsp90AA and Hsp90AB are the two major isoforms involved in Hsp90-driven functions. We developed the efficient and isoform-specific knockdown method for inhibiting the expression of HSP90AA and HSP90AB isoforms using stealth silencer RNA method (**Fig 3**). Although both isoforms bind similarly to their intracellular co-chaperones and display ATPase activity, in some cases Hsp90AA and Hsp90AB have differential effects on substrate interactions.

To assess the relative contributions of Hsp90 isoforms on fibroblast migration, we measured migration of lung fibroblasts that were treated with siRNA specific to either Hsp90AA or Hsp90AB mRNA, as well as control siRNA. Treatment of fibroblasts with Hsp90AA or Hsp90AB

siRNA specifically knocked down the corresponding isoform expression compared to control siRNA (**Fig 3**). Fibroblast migration was significantly attenuated with the deficiency of either Hsp90AA or Hsp90AB isoform compared to control siRNA treatment (data not shown). Also, we used IPF fibroblasts for HSP90AA or HSP90AB knockdown experiments. IPF fibroblasts were transfected with HSP90AA- and HSP90AB-specific siRNA for 72 hrs. Notably, the genetic knockdown of Hsp90AA was sufficient to attenuate both the proliferation and migration of IPF fibroblasts (**Fig 4**). Further, combined inhibition of both Hsp90AA and HSP90AB had additive effect on proliferation and migration in IPF fibroblasts (**Fig 4**). These findings clearly establish that Hsp90AB and HSP90AA may function as positive regulators of fibroproliferation and migration in IPF. Also, we analyzed HSP90AA or HSP90AB-driven gene transcripts using next generation RNA-seq method. As shown in **Fig 5**, we compared the respective gene expression profiles of HSP90 isoforms to that of IPF and identified multiple transcripts that were either up- or down-regulated in IPF lungs. We performed an enrichment analysis of these negatively correlated gene sets (i.e., genes upregulated in IPF, but downregulated by HSP90AA or HSP90AB knockdown and *vice versa*) using the ToppFun application of the ToppGene Suite. Notably, among the top enriched biological processes were fibroblast motility, proliferation, growth and ECM production (**Fig 6**).

Subaim 1C. To determine if overexpression of a dominant negative mutant of HSP90 attenuates fibroblast activation in IPF. We developed lentiviral plasmids to overexpress wild type and D88N-HSP90 (a dominant negative mutant of HSP90) to assess changes in fibroblast activation. This subaim will determine the effect of wild type and D88N-HSP90 forced expression on activation of IPF fibroblasts, including proliferation, invasion, and apoptosis. Earlier structural studies have demonstrated that Asp93 in HSP90 makes a direct hydrogen bond to the exocyclic N6 group of adenine of bound ATP/ADP nucleotide and site-directed mutagenesis of Asp88 to asparagine (D88N) in HSP90AB resulted in the loss of ATP binding and ATPase activity. We completed the cloning of human-HA-N-Hsp90βDN in pLJMI using standard cloning methods (Addgene Plasmid #22480). Clones were confirmed by DNA sequencing. To determine the effect of D88N-HSP90, we transfected HEK293 cells with control and D88N-HSP90 and measured D88N-HSP90 protein expression and effect on migration of HEK293 cells. In support to our hypothesis, we observed a significant increase in the expression of D88N-HSP90 that resulted in decrease in the migration of HEK293 cells compared to control cells (**Fig 7**). To overexpress D88N-HSP90 using lentivirus, we used pLenti vector (pLJM1-EGFP) to clone HA-N-Hsp90βDN. Agarose gel analysis of pLento-HA-N-Hsp90βDN digestion with restriction enzymes Nhe1 and EcoR1 confirms the generation of lentiviral clone of D88N-HSP90. To assess the effect of Hsp90βDN, we transduced IPF fibrobalsts with either control or Hsp90βDN overexpressing lentiviruses. Overexpression of Hsp90βDN was sufficient to attenuate the expression of Hsp90-driven ECM genes with no effect of endogenous HSP90AA or HSP90AB isoforms (**Fig 8**). However, we observed no significant changes in the proliferation or migration of IPF fibroblasts with the overexpression of Hsp90βDN compared to controls (**Fig 9**).

Aim 2: To define the physiological and functional relevance of HSP90-WT1 interaction in fibroblast activation.

Subaim2A: Knockdown HSP90AB, WT1 or both to assess changes in fibroblast-specific gene networks and function. We obtained regulatory approval for primary cell culture and performed the knockdown HSP90AA and HSP90AB to determine fibroblast specific gene networks (**Fig 5 and 6**).

To determine whether the loss of Hsp90AB, WT1 or both alter ECM production, lung fibroblasts were treated with control, Hsp90AB- , WT1- or both siRNA for 72h. Notably, the loss of Hsp90AB or WT1 was sufficient to attenuate the expression of ECM genes, such as Col1α, and Col3α compared to control siRNA (**Fig 10**). Also, combined inhibition Hsp90AB- and WT1 had no additive effect on the ECM gene expression compared to Hsp90AB- or WT1-specific siRNA treatment. Similarly, we observed no significant changes in the proliferation and invasiveness of IPF fibroblasts treated siRNA for Hsp90AB-, WT1- or both (data not shown).

Subaim 2B: Overexpress HSP90AB, WT1 or both to assess changes in fibroblast-specific gene networks and function. We overexpress WT1 in human fibroblasts using adenovirus and observed a significant increase ECM gene expression (**Fig 11**). Also, we generated HSP90AB lentivirus and validated upregulation of HSP90AB. To determine mechanisms underlying WT1-driven fibroproliferation, we performed the knockdown or overexpression of WT1 in fibrobalsts and assessed changes in the expression of mitotic kinase B (AURKB) involved in fibroproliferation. We performed the knocked down of WT1 using WT1-specific siRNA in fibroblasts isolated from IPF lungs or TGFα mice on Dox for 4 wks. Compared to control siRNA, knockdown of WT1 was sufficient to attenuate the expression of AURKB in lung fibroblasts isolated from both IPF and a mouse model of TGFα-induced pulmonary fibrosis (**Fig 12A & 12B**). We next assessed the effect of adenovirus-mediated overexpression of WT1 on AURKB levels in fibroblasts. Overexpressing WT1 in fibroblasts led to a significant increase in both transcripts and protein of AURKB (**Fig 12C**). Knockdown of WT1 in fibroblasts also abolished the ability of TGFα to increase AURKB expression (Fig 12D). To determine if WT1 is a transcription factor that directly binds to *AURKB*, we performed a computational analysis of the promoter region of human and mouse *AURKB* and found the presence of conserved WT1 binding sites (data not shown). We performed chromatin immunoprecipitation (ChIP) analysis using primary lung-resident fibroblasts isolated from TGFα mice on Dox for 8 wks. ChIP analysis using WT1-specific antibody compared with control isotype antibody revealed that WT1 bound to the *AURKB* gene, suggesting the role of WT1 in AURKB expression (**Fig 12E**). We next overexpressed WT1 in HEK293 cells co-transfected with AURKB-promoter fused with luciferase reporter and observed increased luciferase activity compared to cells transfected with control plasmids (**Fig 12F**). These results support that WT1 functions as a positive regulator of AURKB by directly binding to the AURKB promoter in fibroblasts. The part of these finding is now published in *EMBO molecular medicine* 2020.
Subaim 2C: We overexpressed D88N-HSP90 and WT1 alone or together to assess changes in fibroblast-specific gene networks and function. We completed the overexpression of WT1 in primary fibroblasts and identified WT1-driven gene networks in fibroblasts. We demonstrated the effects of D88N-HSP90 overexpression on fibroblast activation. These new findings are now published in *JCI Insight 2018*.

Aim3: To determine whether combined therapy using pirfenidone and 17-AAG is effective to reverse established and ongoing pulmonary fibrosis. To determine whether combined therapy using pirfenidone and 17-AAG is effective to reverse established and ongoing pulmonary fibrosis. To determine in vivo doses of 17-AAG and pirfenidone, we evaluated the potential benefits of 17-AAG and pirfenidone in pulmonary fibrosis using a mouse model of TGFα-induced pulmonary fibrosis. Our previous studies have demonstrated that conditional overexpression of TGFα induces progressive fibrosis in the adventitia, parenchyma, and subpleural areas of the lung with histologic features and genomic profiles similar to human IPF.

To determine whether in vivo doses of pirfenidone and 17-AAG that influences the progression of established fibrosis, following three wk of Dox treatment when fibrosis is already manifest, TGFα mice were administered 17-AAG or pirfenidone while remaining on Dox for an additional three wk (6 wks total) (**Fig 13A**). The total lung hydroxyproline levels were increased in TGFα mice treated with either vehicle or pirfenidone (**Fig 13B**). However, pirfenidone therapy had no effect on this increase in the lung hydroxyproline levels in TGFα mice treated with pirfenidone compared to vehicle-treated TGFα mice (**Fig 13B**). However, H&E stained lung sections show significant improvement in alveolar size in TGFα mice treated with pirfenidone compared to vehicle-treated TGFα mice (**Fig 13C**). Therefore, we evaluated mean alveolar chord length to determine the potential benefit of pirfenidone therapy on lung alveolar integrity during TGFα-induced pulmonary fibrosis. The mean alveolar chord length was increased in doxycycline induced TGFα mice compared to control mice treated with doxycycline for six weeks (**Fig 13D**). This increase in alveolar chord length was attenuated in TGFα mice treated with pirfenidone when compared to vehicle-treated TGFα mice. Notably, the total lung hydroxyproline levels were decreased in TGFα mice treated with 17-AAG compared to vehicle (**Fig 14A**). However, 17-AAG therapy had no effect on alveolar size or chord length in TGFα mice treated with 17-AAG compared to Vehicle (**Fig 14B**). To determine whether 17-AAG attenuates TGFβ-induced ECM gene expression, human fibroblasts were treated with TGFβ in the presence and absence of 17-AAG and transcripts of ECM genes were quantified by RT-PCR. As predicted, TGFβ induced the expression of COL1α and FN1 (**Fig 15**). Notably, treatment with 17-AAG was sufficient to attenuate TGFβ-driven expression of COL1α and FN1. Together, our in vitro and in vivo results establish that either inhibition of Hsp90 ATPase activity or Hsp90AB expression was sufficient to attenuate myofibroblast transformation and ECM gene expression.

To detremine therapeutic benefit of combined inhibition of 17-AAG and pirfenidone, we treated TGFα mice with the combination of 17-AAG and pirfenidone to test reversal of established and ongoing pulmonary fibrosis. As shown in **Fig 16**, we observed a significant improvement in the lung function of mice treated with 17-AAG, pirfenidone or both compared to vehicle treated mice. However, we observed limited or no additive effect of combination therapy compared to 17-AAG or pirfenidone alone. To assess possible drug-drug interactions, we assessed the levels of 17-AAG and pirfenidone in serum and lungs of TGFα mice treated with vehicle and inhibitors either alone or in combination. We observed combined treatment of 17-AAG and pirfenidone resulted in reduced 17-AAG levels in both serum and lungs of TGFα mice compared to 17-AAG treatment alone (**Fig 17**). To determine whether combined treatment of 17-AAG and pirfenidone can alter fibroblast activation, we treated lung resident fibroblasts isolated from fibrotic lesions of TGFα mice and treated with 17-AAG, pirfenidone or both to assess changes in fibroproliferation, As shown in **Fig 18**, 17-AAG has attenuated fibroproliferation compared to vehicle, pirfenidone or in combination. In support, we observed attenuation of AURKB levels in 17-AAG treated IPF fibroblasts compared to vehicle or pirfenidone treatment. Also, we assessed apoptosis in lung fibroblasts of TGFα mice treated with 17-AAG, pirfenidone or both. As shown in **Fig19**, we observed a significant increase in apoptotic clearance of fibroblast with 17-AAG treatment compared to vehicle or pirfenidone treatment. However, combined treatment of 17-AAG and pirfenidone had limited or no significant change in 17-AAG-induced apoptosis in fibroblasts.

Significant results: As noted above, we have completed the key studies and the major findings are now published in high-impact journal (*JCI insight 2018, 2021 and EMBO Mol Med 2020*). We have completed cloning of D88N-HSP90 and HSP90 isoforms and validated expression using HEK293 cells. Also, we completed the generation of lentiviruses to overexpress human and mouse WT1 (**JCI insight 2018; Figure 3**).

The effects of WT1 overexpression on fibroblast activation are now completed and the findings were published in ***JCI insight 2018*** **(Figures 3-4)**. Also, studies on WT1-induced AURKB expression were published in ***EMBO Mol Med 2020*** **(Figure 12)**. This study also describes the knockdown Hsp90AB isoforms on fibroblast activation. In particular, our knockdown studies have identified effects of WT1 on fibroblast activation. Similarly, we evaluated the specific effects of Hsp90AA or Hsp90AB isoforms on fibroblast activation. In particular, our knockdown studies have identified potential differences between Hsp90AA and Hsp90AB isoforms on fibroblast activation. For Aim3, we completed to set-up breeders to generate wild type and TGFα transgenic mice. Initial studies are completed to evaluate the effects of 17-AAG and pirfenidone in the pathogenesis of TGFα-induced pulmonary fibrosis. In support to our hypothesis, pharmacological inhibition of Hsp90 activity or the genetic loss of WT1 has attenuated fibroblast activation and pulmonary fibrosis. In vivo studies using 17-AAG, pirfenidone or both suggest that combined therapy had limited or no additive effects on TGFα-induced pulmonary fibrosis.

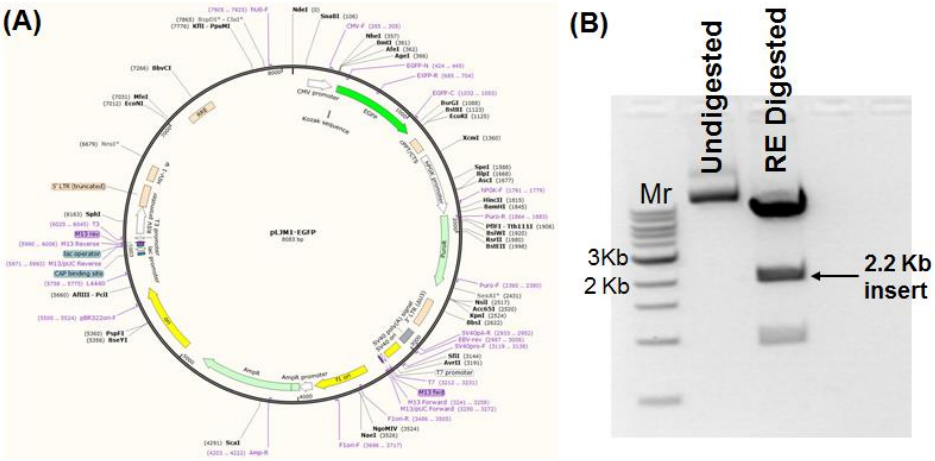


Figure 1. (A) The map of pLJMI-EGFP vector and D88N-HSP90 gene inserted using restriction enzymes, Nhe1 and Age1. (B) Agarose gel showing the right insertion and orientation of D88N-HSP90 in Lenti vector using restriction enzyme digestion (Age1 and EcoR1).

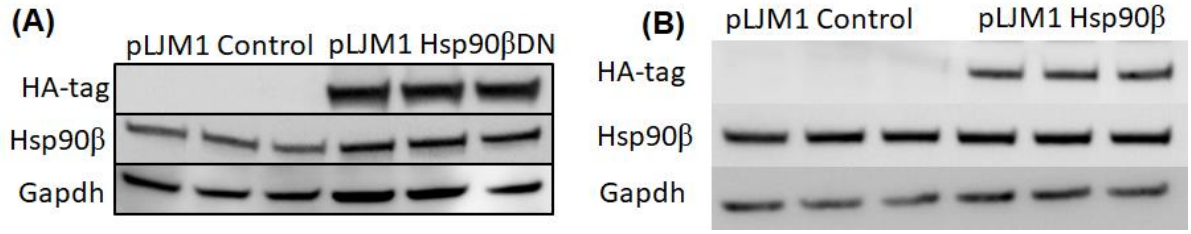


Figure 2. (A) HEK293 cells transfected with control or Hsp90βDN lentivirus for 72hrs and immunoblotted with antibodies against HA-tag, Hsp90β and GAPDH (B) HEK293 cells transfected with control or Hsp90β lentivirus for 72hrs and immunoblotted with antibodies against HA-tag, Hsp90β and GAPDH.

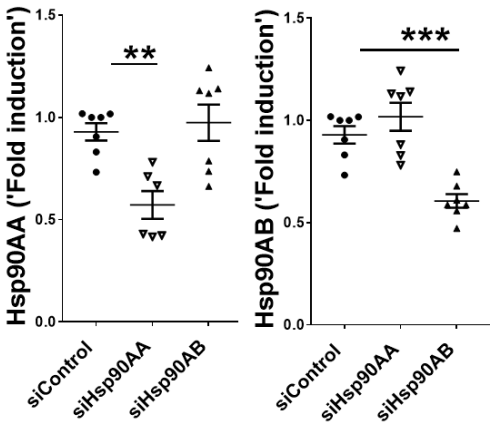


Figure 3: Primary Lung resident fibroblasts ($CD45^{-}Col1^{+}$) were isolated from lung cultures of TGF-α mice which was placed on Dox for 4wk using anti-CD45 magnetic beads and transfected with either control or Hsp90 isoform specific siRNA for 72 hr. The transcripts for Hsp90AA and Hsp90AB isoform are shown as the fold induced by normalizing to hypoxanthine guanine phosphoribosyl transferase (HPRT) control. Data shown are mean + SEM values (n = 7). Statistical significance between groups was measured using an ANOVA. **p<0.005 and ****p<0.00005

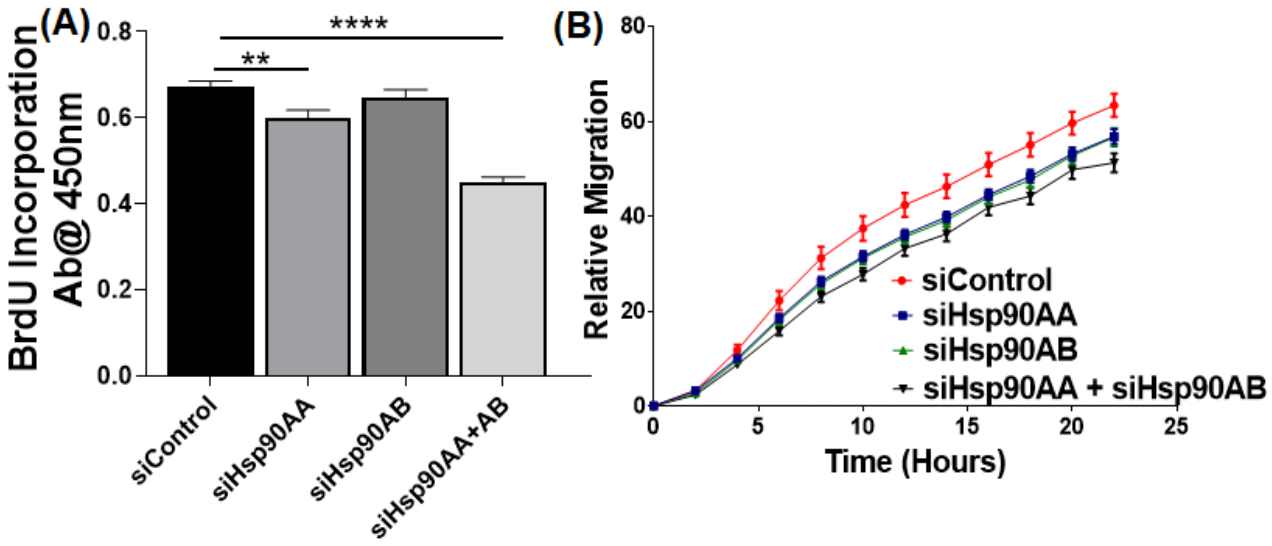


Figure 4. (A) Quantitation of proliferation using the Brdu incorporation assay in lung fibroblasts isolated from IPF lung cultures. Fibroblasts treated with HSP90AA, HSPAB or both for 72hr. ***P*<0.005, *****P*<0.00005. (B) Quantitation of migration in lung fibroblasts isolated from IPF lung cultures. Fibroblasts treated with HSP90AA, HSPAB or both for 72hr.

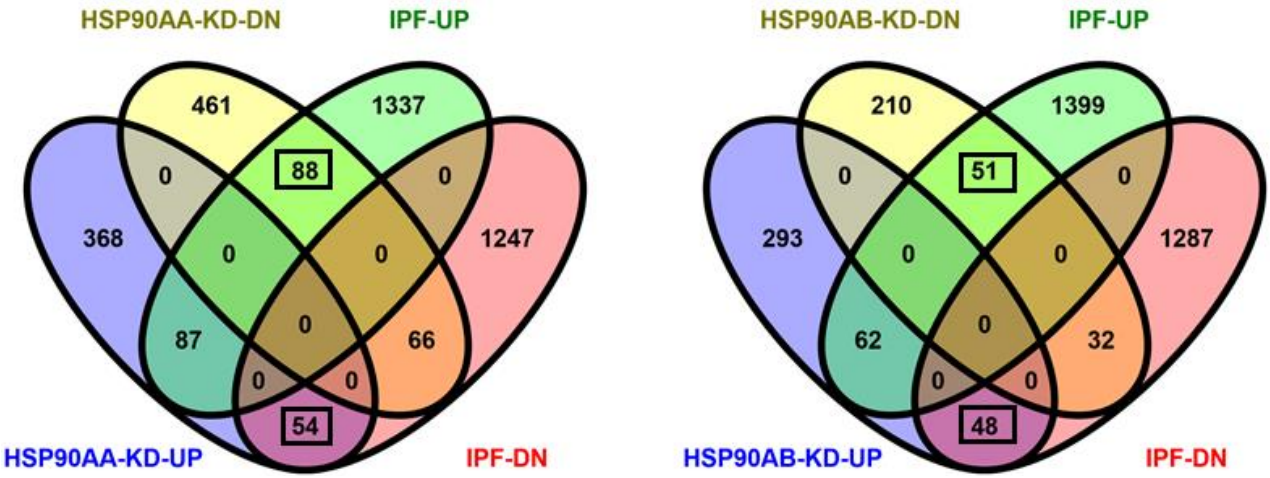


Figure 5: Primary Lung resident fibroblasts ($CD45^{-}Col1^{+}$) were isolated from IPF lung cultures using anti-CD45 magnetic beads and transfected with either control or Hsp90 isoform specific siRNA for 72 hr. Differentially expressed genes in IPF lungs were compared with HSP90AA- and HSP90AB-driven genes in IPF fibroblasts. The overlapping genes that are up or down regulated in IPF or HSP90 isoform deficient fibroblasts are indicated with a box.

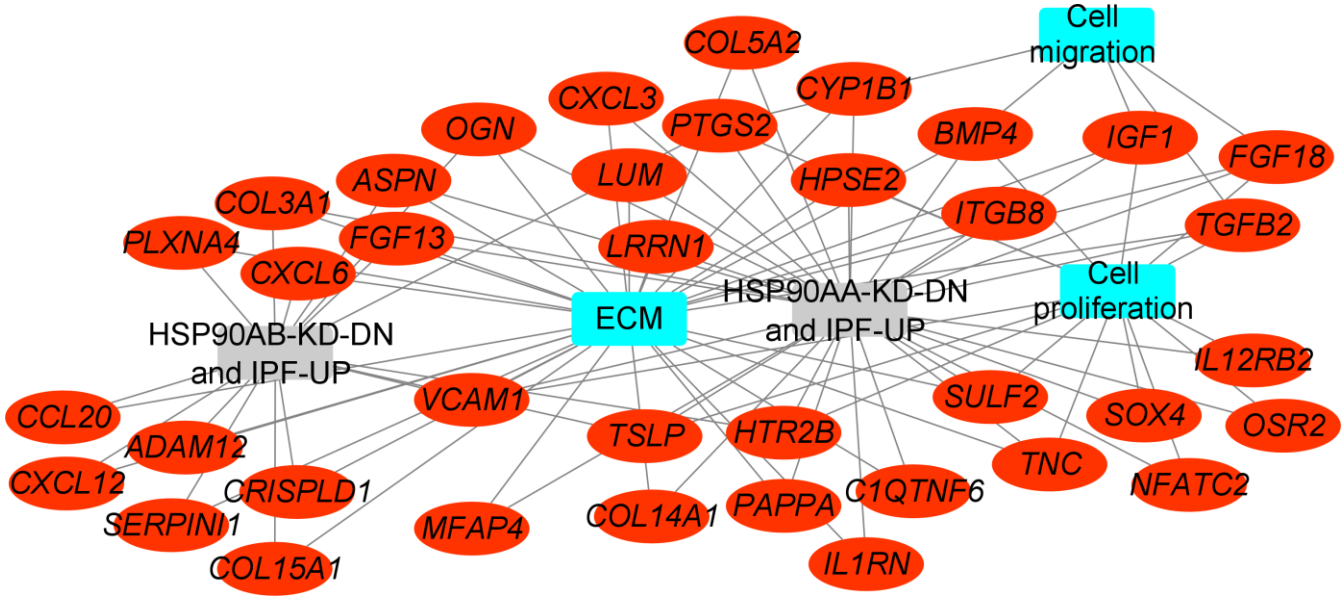


Figure 6: HSP90AA- or HSP90AB-driven genes activated in IPF were analyzed using ToppFun and visualized using Cytoscape. Red-colored circles represent genes that are upregulated in IPF lungs. The turquoise-colored squares represent enriched biological processes for the inversely correlated genes between HSP90AA or HSP90AB siRNA knockdown and IPF.

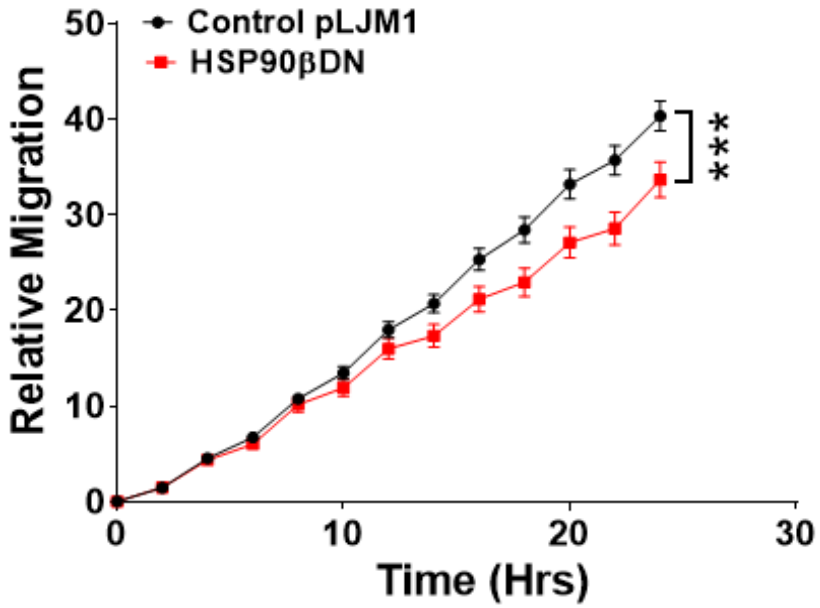


Figure 7. Scratch wound migration assay was performed on HEK293 cells transfected with control or Hsp90βDN overexpressing plasmid for 24hr. Quantitation of migration represented as relative migration over time. Data shown are mean ± SEM values. Statistical significance between groups was measured using ANOVA. ***p<0.0005.

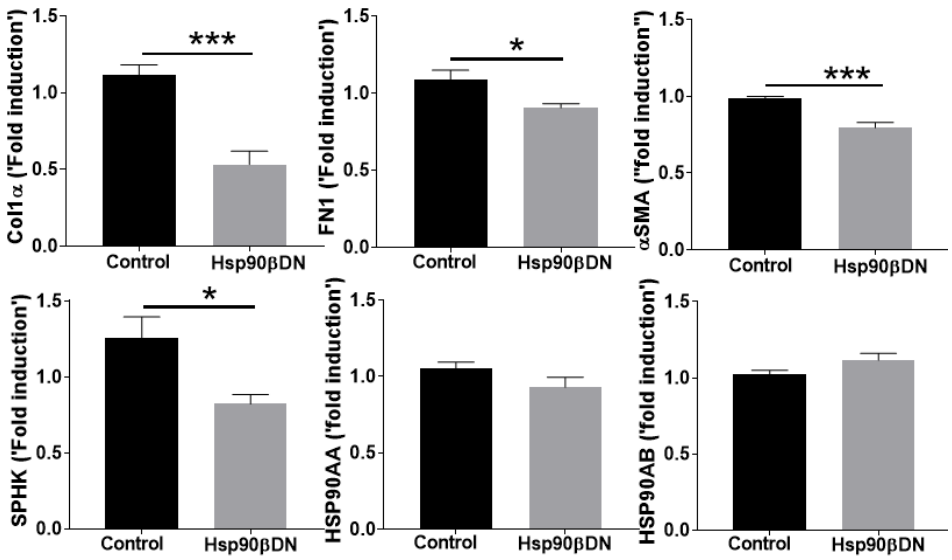


Figure 8. The effect of overexpression of HSP90AB DN on Hsp90-driven ECM gene expression. Primary lung fibroblasts ($CD45^{-}Col1^{+}$) were isolated from IPF lung cultures using anti-CD45 magnetic beads and transduced with either control- or Hsp90AB DN lentivirus for 48 hrs. The levels of Col1a, FN1, αSMA, SPHK, HSP90AA, and HSP90AB gene transcripts relative to HPRT are quantified using qRT-PCR. Data shown are mean ± SEM values (N = 3/group).

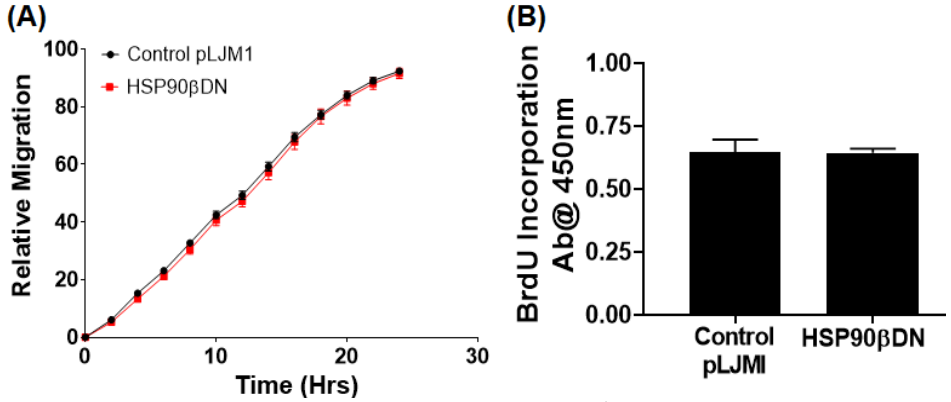


Figure 9. Primary lung fibroblasts ($CD45^{-}Col1^{+}$) were isolated from IPF lung cultures using anti-CD45 magnetic beads and transduced with either control- or Hsp90AB DN lentivirus for 48 hrs. (A) Scratch wound migration assay was performed and quantitation of migration represented as relative migration over time. (B) Quantitation of proliferation using the Brdu incorporation assay.

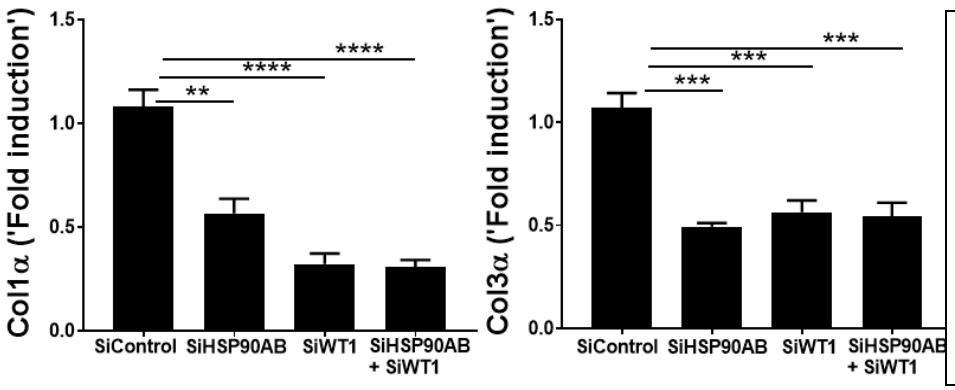


Figure 10. IPF fibroblasts were transfected with either control, Hsp90AB, WT1 or both siRNA for 72 hr. The levels of Col1α and Col3α gene transcripts relative to HPRT are quantified using qRT-PCR.

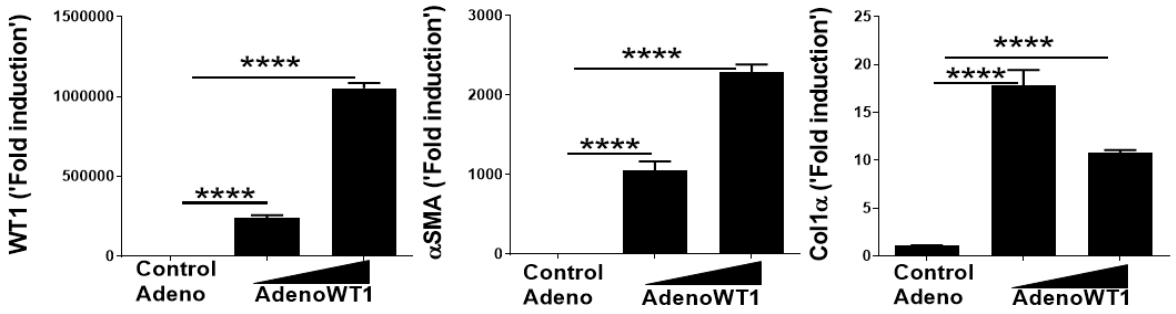


Figure 11. Human lung firboblasts were transduced with either control- or WT1 adenovirus for 72 hrs. The levels of WT1, αSMA, and Colα gene transcripts relative to HPRT are quantified using qRT-PCR.

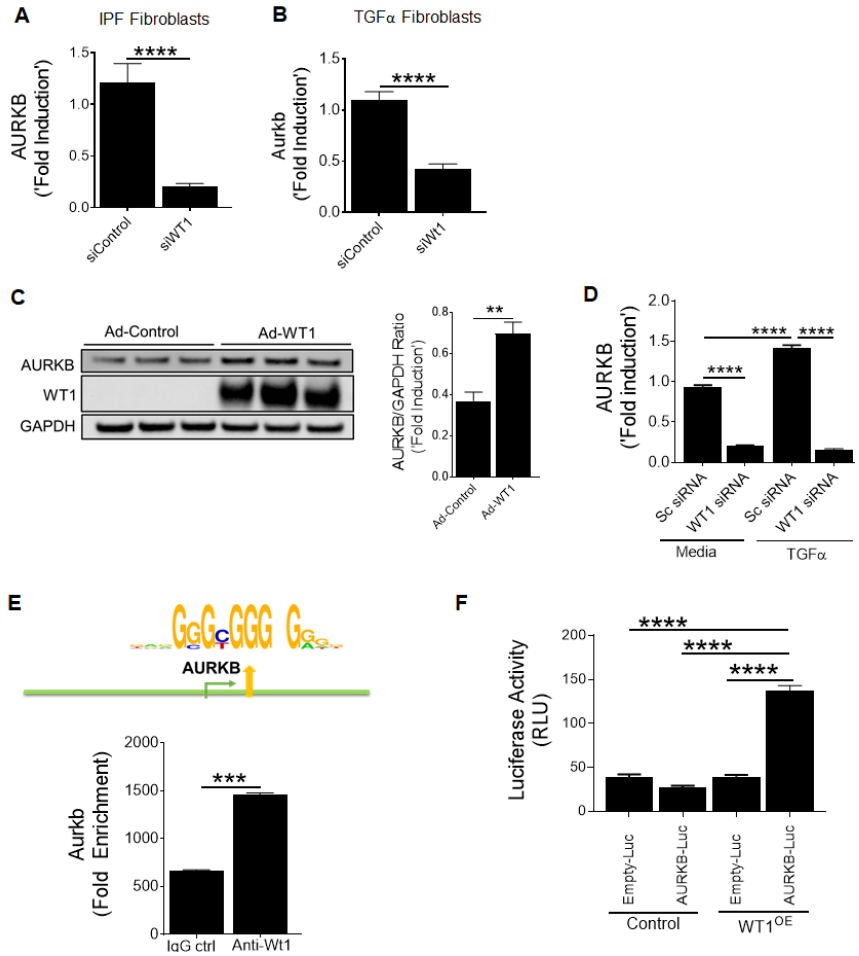


Figure 12. **WT1 induces fibroproliferation by altering AURKB expression. (A)** IPF lung fibroblasts were transiently transfected with control or WT1 siRNA for 72hrs and AURKB transcripts were quantified. **(B)** Lung-resident fibroblasts from TGFα mice on Dox for 4 wks were transiently transfected with control or WT1 siRNA for 72hrs and AURKB transcripts were quantified. **(C)** Immunoblot analysis of AURKB and WT1 in the lysates of non-IPF fibroblasts transduced with control or WT1-adenoviral particles for 72hrs. **(D)** Quantification of AURKB transcripts in primary fibroblasts from IPF lung treated with either control or WT1 siRNA and stimulated with media or TGFα (100ng/mL) for 16hrs. **(E)** The ChIP assay was performed with anti-WT1 antibody or normal rabbit IgG as a negative control. Non-immunoprecipitated DNA is represented as input DNA (product size, 104 bp). **(F)** AURKB-promoter luciferase activity was measured in HEK293 cells transfected with control or WT1 overexpressing (OE) vector.

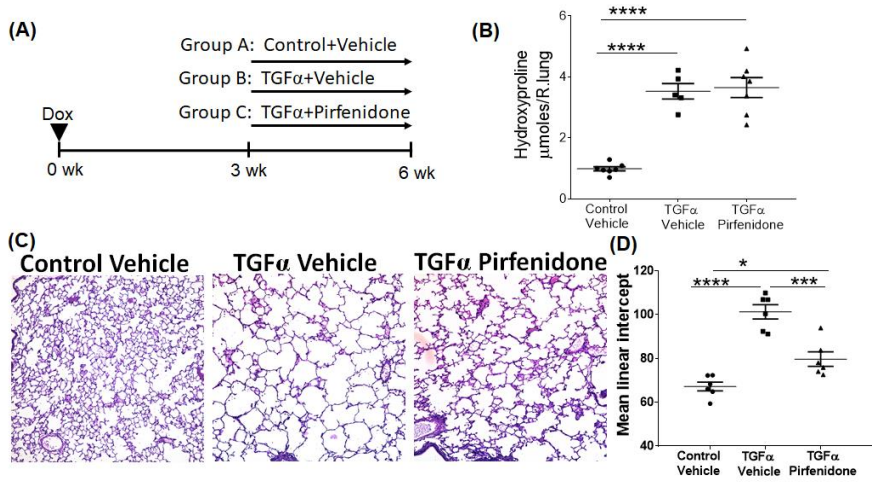


Figure 13. (A) Schematic representation of pirfenidone treatment protocol. Control mice and TGFα mice were placed on Dox for 3 weeks then treated with vehicle or pirfenidone (300 mg/kg; twice a day) for 3 weeks while continued on Dox for a total of 6 weeks. (B) Quantitation of hydroxyproline levels of mice treated with vehicle or pirfenidone. (C) Alveolar regions of H&E stained lung sections from all the groups. Images are representative of each group with N=6-7 per group. (D) Mean linear intercept was quantified in the lung sections of all mice stained with H&E. One-way ANNOVA, *p<0.05, ***p<0.0005 and ****p<0.00005.

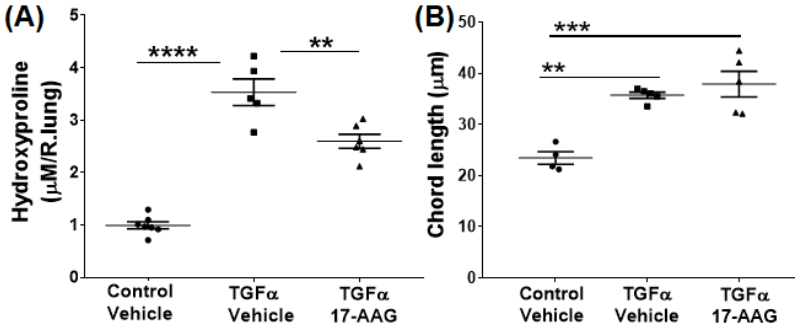


Figure 14. (A) Quantitation of hydroxyproline levels of mice treated with vehicle or 17-AAG. Control mice and TGFα mice were placed on Dox for 3 weeks then treated with vehicle or 17-AAG (15 mg/kg; once a day) for 3 weeks while continued on Dox for a total of 6 weeks. (B) Chord length was quantified in the lung sections of all mice stained with H&E. One-way ANNOVA , **p<0.005, ***p<0.0005 and ****p<0.00005.

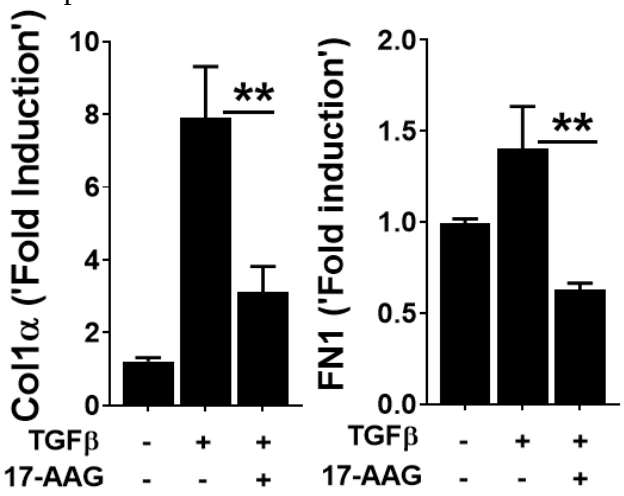


Figure 15. Hsp90 inhibition attenuates TGFβ induced ECM gene expression. Human lung resident fibroblasts ($CD45^{-}Col1^{+}$) were isolated from non-IPF lung fibroblast cultures and treated with TGFβ in the presence and absence of 17-AAG for 24h. Quantified transcripts of ECM genes, COL1α and FN1 using qRT-PCR and shown as the fold induced gene transcripts relative to GAPDH. . $^{**}P < 0.005$, one-way-ANOVA.

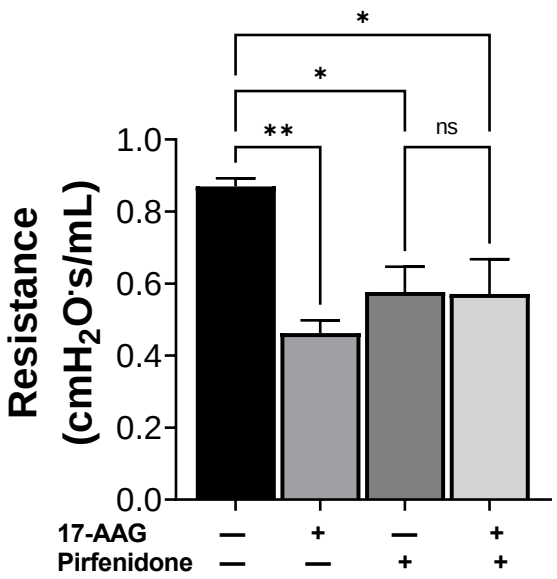


Figure 16. Therapeutic administration of pirfenidone and 17-AAG in combination had limited or no effect on lung function *in vivo.* Improvement in lung resistance was measured using FlexiVent in mice treated with vehicle, 17-AAG (15 mg/kg; once a day), pirfenidone (300 mg/kg; twice a day) or both in combination in vivo. *p<0.05.

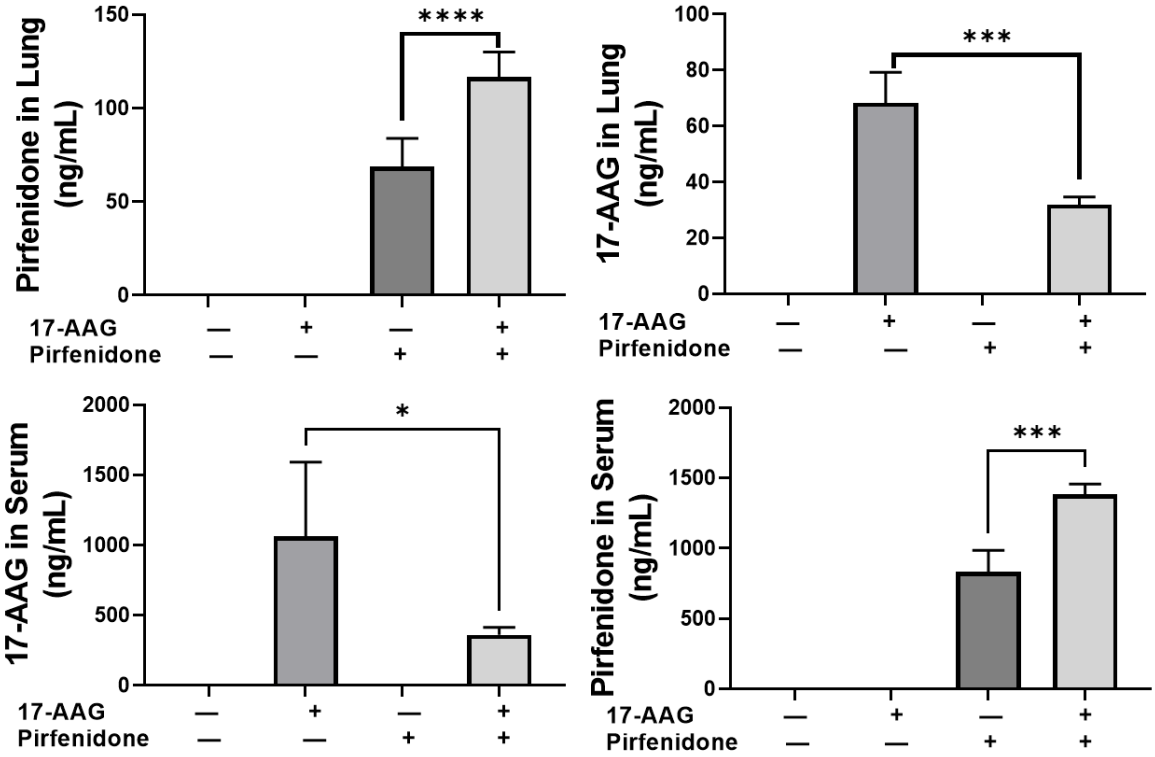


Figure 17. In vivo concentrations of 17-AAG and pirfenidone. Quantitation of pirfenidone and 17-AAG levels in the lungs and serum of mice treated with vehicle, 17-AAG (15 mg/kg; once a day), pirfenidone (300 mg/kg; twice a day) or both in combination in vivo. *p<0.05.

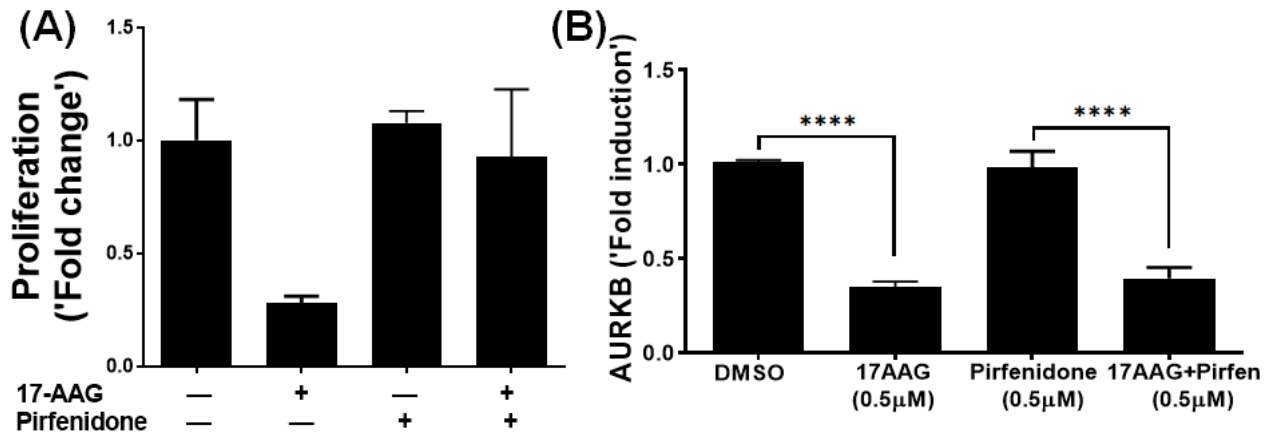


Figure 18. **Hsp90 inhibition attenuates fibroproliferation but limited effect of combined inhibition with pirfenidone.** (A) Quantitation of proliferation using the Brdu incorporation assay in lung fibroblasts isolated from from stromal cultures of TGFα mice placed on Dox for 6 wks and treated with 17-AAG, pirfenidone or both for 72hrs. (B) Human lung resident fibroblasts ($CD45^{-}Col1^{+}$) were isolated from IPF lung fibroblast cultures and treated with 17-AAG, Pirfenidone or both for 24h. Quantified transcripts of AURKB using qRT-PCR and shown as the fold induced gene transcripts relative to GAPDH. . $^{**}P < 0.005$, one-way-ANOVA.

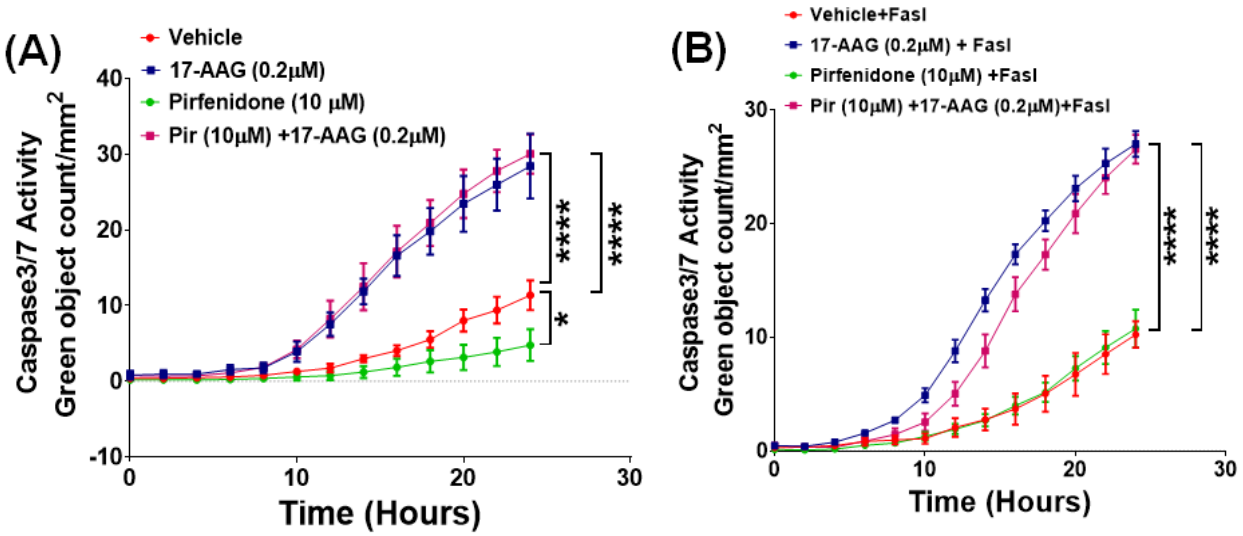


Figure 19. **Hsp90 inhibition attenuates fibroblast survival but limited or no effect of combined inhibition with pirfenidone.** (A) Quantification of apoptosis using Caspase3/7 activity assay in lung fibroblasts isolated from stromal cultures of TGFα mice placed on Dox for 6 wks and treated with 17-AAG, pirfenidone or both for 24hrs in the absence of FasL. (B) Quantification of apoptosis using Caspase3/7 activity assay in lung fibroblasts isolated from stromal cultures of TGFα mice placed on Dox for 6 wks and treated with 17-AAG, pirfenidone or both for 24hrs in the presence of FasL. $^{*}P < 0.005$, one-way-ANOVA.

If the project was not intended to provide training and professional development opportunities or there is nothing significant to report during this reporting period, state "Nothing to Report."

Describe opportunities for training and professional development provided to anyone who worked on the project or anyone who was involved in the activities supported by the project. "Training" activities are those in which individuals with advanced professional skills and experience assist others in attaining greater proficiency. Training activities may include, for example, courses or one-on-one work with a mentor. "Professional development" activities result in increased knowledge or skill in one's area of expertise and may include workshops, conferences, seminars, study groups, and individual study. Include participation in conferences, workshops, and seminars not listed under major activities.

Nothing to report

How were the results disseminated to communities of interest?
If there is nothing significant to report during this reporting period, state "Nothing to Report."

Describe how the results were disseminated to communities of interest. Include any outreach activities that were undertaken to reach members of communities who are not usually aware of these project activities, for the purpose of enhancing public understanding and increasing interest in learning and careers in science, technology, and the humanities.

Nothing to report

What do you plan to do during the next reporting period to accomplish the goals?
If this is the final report, state "Nothing to Report."

Describe briefly what you plan to do during the next reporting period to accomplish the goals and objectives.

Nothing to report

4. **IMPACT:** D*escribe distinctive contributions, major accomplishments, innovations, successes, or any change in practice or behavior that has come about as a result of the project relative to:*

What was the impact on the development of the principal discipline(s) of the project?
If there is nothing significant to report during this reporting period, state "Nothing to Report."

Describe how findings, results, techniques that were developed or extended, or other products from the project made an impact or are likely to make an impact on the base of knowledge, theory, and research in the principal disciplinary field(s) of the project. Summarize using language that an intelligent lay audience can understand (Scientific American style).

IPF is a chronic and ultimately fatal disease in which tissue deep in the lungs becomes increasingly thick and stiff, or scarred, over time, making breathing more and more difficult. With the funding support from the DoD, our team identified that in IPF patients, activity of a particular protein, Hsp90 (Heat shock protein 90), is elevated in fibroblasts. Fibroblasts are cells in connective tissues that produce collagen and other fibers that have not yet progressed to form scar tissue. We also identified Hsp90 inhibitors as a potential effective therapy to stop or possibly even reverse the disease.

What was the impact on other disciplines?
If there is nothing significant to report during this reporting period, state "Nothing to Report."

Describe how the findings, results, or techniques that were developed or improved, or other products from the project made an impact or are likely to make an impact on other disciplines.

Our new findings demonstrate that Hsp90 is a positive regulator of fibroblast activation and ECM production. Increased Hsp90 activity and fibroblast activation has been shown in multiple organs undergoing fibrotic remodeling. Thus, the proposed studies will not only highlight the role of HSP90 activity in initiation and maintenance of pulmonary fibrosis, but also are essential to the development of novel therapeutics for the treatment of fibrosis in the lung and perhaps other organs. Nearly 45% of all deaths in the developed world are attributed to chronic fibroproliferative diseases, emphasizing the potential impact that an anti-fibrotic therapy would provide. Therefore, successful treatment that either reverses fibrosis or prevents disease progression would have an immediate and profound impact on healthcare.

What was the impact on technology transfer?
If there is nothing significant to report during this reporting period, state "Nothing to Report."

Describe ways in which the project made an impact, or is likely to make an impact, on commercial technology or public use, including:

- *transfer of results to entities in government or industry;*
- *instances where the research has led to the initiation of a start-up company; or*
- *adoption of new practices.*

CCHMC has filed a US provisional patent application (D14-0129) on the repurposing of 17AAG for IPF. The Center for Technology Commercialization (CTC) at CCHMC is in the process of initiating discussions with industry partners for joint development of this project based on new findings of this project.

Describe how results from the project made an impact, or are likely to make an impact, beyond the bounds of science, engineering, and the academic world on areas such as:

- *improving public knowledge, attitudes, skills, and abilities;*

- *changing behavior, practices, decision making, policies (including regulatory policies), or social actions; or*
- *improving social, economic, civic, or environmental conditions.*

Nothing to report

5. **CHANGES/PROBLEMS:** *The PD/PI is reminded that the recipient organization is required to obtain prior written approval from the awarding agency grants official whenever there are significant changes in the project or its direction. If not previously reported in writing, provide the following additional information or state, "Nothing to Report," if applicable:*

Nothing to report

Remember that significant changes in objectives and scope require prior approval of the agency.

Actual or anticipated problems or delays and actions or plans to resolve them
Describe problems or delays encountered during the reporting period and actions or plans to resolve them.

Nothing to report

Changes that had a significant impact on expenditures
Describe changes during the reporting period that may have had a significant impact on expenditures, for example, delays in hiring staff or favorable developments that enable meeting objectives at less cost than anticipated.

Nothing to report

Significant changes in use or care of human subjects, vertebrate animals, biohazards, and/or select agents
Describe significant deviations, unexpected outcomes, or changes in approved protocols for the use or care of human subjects, vertebrate animals, biohazards, and/or select agents during the reporting period. If required, were these changes approved by the applicable institution committee (or equivalent) and reported to the agency? Also specify the applicable Institutional Review Board/Institutional Animal Care and Use Committee approval dates.

Significant changes in use or care of human subjects

No changes to report

Significant changes in use or care of vertebrate animals

No changes to report

Significant changes in use of biohazards and/or select agents

No changes to report

6. PRODUCTS: *List any products resulting from the project during the reporting period. If there is nothing to report under a particular item, state "Nothing to Report."*

- **Publications, conference papers, and presentations**

Report only the major publication(s) resulting from the work under this award.

Journal publications. *List peer-reviewed articles or papers appearing in scientific, technical, or professional journals. Identify for each publication: Author(s); title; journal; volume: year; page numbers; status of publication (published; accepted, awaiting publication; submitted, under review; other); acknowledgement of federal support (yes/no).*

Total five manuscripts have been accepted or under consideration for publication.

1. Vadde SR, **Madala SK** and Geereddy BR (2018) Extracellular small heat shock proteins: Exosomal biogenesis and function. ***Cell Stress & Chaperones*** 23(3):441-454. PMID: 29086335
2. Sontake V, Kasam RK, Debora S, Korfhagen TR, Geereddy BR, White ES, Jegga AG and **Madala SK** (2018) Wilms' Tumor 1 Drives Fibroproliferation and Myofibroblast Transformation in Severe Fibrotic Lung Disease. ***JCI insight*** 3(16) PMID: 30135315
3. Sontake V, Gajjala P, Kasam RK, and **Madala SK** (2018) New therapeutics based on emerging concepts in pulmonary fibrosis. ***Expert Opinion On Therapeutic Targets*** 23(1):69-81 PMID: 30468628
4. Kasam RK, Ghandikota S, Soundarajan, D, Reddy GB, Huang SK, Jegga AG, and **Madala SK** (2020) Inhibition of Aurora Kinase B attenuates fibroblast activation and pulmonary fibrosis. ***EMBO Molecular Medicine.*** 12(9):e12131. PMID:32761869
5. Gajjala PR, Kasam RK, Soundararajan D, Debora S, Huang SK, Jegga AG and **Madala SK** (2021) Dysregulated overexpression of Sox9 induces fibroblast activation in pulmonary fibrosis. *JCI Insight* (in press)

dissertation, abstract, or the like published as or in a separate publication, rather than a periodical or series. Include any significant publication in the proceedings of a one-time conference or in the report of a one-time study, commission, or the like. Identify for each one-time publication: author(s); title; editor; title of collection, if applicable; bibliographic information; year; type of publication (e.g., book, thesis or dissertation); status of publication (published; accepted, awaiting publication; submitted, under review; other); acknowledgement of federal support (yes/no).

Nothing to report

Other publications, conference papers and presentations. *Identify any other publications, conference papers and/or presentations not reported above. Specify the status of the publication as noted above. List presentations made during the last year (international, national, local societies, military meetings, etc.). Use an asterisk (*) if presentation produced a manuscript.*

1. Sontake V, Wang Y, Kasam RK, McCormack FK, Debora S, Geereddy BR, Naren AP, White ES, Jegga AG and **Madala SK** (2017) Hsp90 Regulation of Fibroblast Activation in Pulmonary Fibrosis. ***JCI insight*** 2: e91454. PMID: 28239659
2. Kasam RK, Reddy GB, Jegga AG, and **Madala SK** (2019) Dysregulation of mesenchymal cell survival pathways in severe fibrotic lung disease: The effect of nintedanib therapy. ***Front. Pharmacol.*** 10:532 PMID: 31156440
3. Yombo JKD, Mentink-Kane MM, Wilson MS, Wynn TA, and **Madala SK** (2019) Heat Shock Protein 70 is a positive regulator of airway inflammation and goblet cell hyperplasia in a mouse model of allergic airway inflammation. ***Journal of Biological Chemistry*** (In press)
4. Abstract titled "Inhibition of fibroblast activation by integrating multiomics data and preclinical models of severe fibrotic lung disease" presented at 2nd Annual IPF summit, San Francisco, August 20-22, 2018.
5. Kasam RK, Reddy GB, Jegga AG, and **Madala SK** (2019) Dysregulation of mesenchymal cell survival pathways in severe fibrotic lung disease: The effect of nintedanib therapy. ***Front. Pharmacol.*** 10:532 PMID: 31156440
6. Yombo JKD, Mentink-Kane MM, Wilson MS, Wynn TA, and **Madala SK** (2019) Heat Shock Protein 70 is a positive regulator of airway inflammation and goblet cell hyperplasia in a mouse model of allergic airway inflammation. ***Journal of Biological Chemistry*** 294 (41): 15082-94. PMID: 31431507
7. Kasam RK, Gajjala P, Courtney J, Kramer EL, Randell S, Clancy JP, and **Madala SK** (2020) Subacute TGF exposure drives Airway Hyperresponsiveness in CF mice through the PI3K pathway. ***J. Cystic Fibrosis*** 62(5):657-667 PMID: 319322900
8. Yombo JKD, Odayar V, Gupta N, Jegga AG, and **Madala SK** (2021) The protective effects of IL-31RA deficiency during bleomycin-induced pulmonary fibrosis. ***Frontiers Immunology*** 12:645717. PMID: 33815402

- **Website(s) or other Internet site(s)**
List the URL for any Internet site(s) that disseminates the results of the research activities. A short description of each site should be provided. It is not necessary to include the publications already specified above in this section.

News article titled “Computational Analyses Identify New Therapeutic Targets For Idiopathic Pulmonary Fibrosis”
https://www.cincinnatichildrens.org/research/divisions/b/bmi/news/2017/2-27-computational-analyses-identify-new-therapeutic-targets-for-idiopathic-pulmonary-fibrosis

Identify technologies or techniques that resulted from the research activities. Describe the technologies or techniques were shared.

Nothing to report

- **Inventions, patent applications, and/or licenses**
  Identify inventions, patent applications with date, and/or licenses that have resulted from the research. Submission of this information as part of an interim research performance progress report is not a substitute for any other invention reporting required under the terms and conditions of an award.

Methods for Treating Fibrosis.U.S. Patent Pub No.: US201862630866; Role: Principal Investigator

- **Other Products**
  Identify any other reportable outcomes that were developed under this project. Reportable outcomes are defined as a research result that is or relates to a product, scientific advance, or research tool that makes a meaningful contribution toward the understanding, prevention, diagnosis, prognosis, treatment and /or rehabilitation of a disease, injury or condition, or to improve the quality of life. Examples include:
  - *data or databases;*
  - *physical collections;*
  - *audio or video products;*
  - *software;*
  - *models;*
  - *educational aids or curricula;*
  - *instruments or equipment;*
  - *research material (e.g., Germplasm; cell lines, DNA probes, animal models);*
  - *clinical interventions;*
  - *new business creation; and*
  - *other.*

Nothing to report

7. PARTICIPANTS & OTHER COLLABORATING ORGANIZATIONS

What individuals have worked on the project?

Provide the following information for: (1) PDs/PIs; and (2) each person who has worked at least one person month per year on the project during the reporting period, regardless of the source of

Name: *Satish Madala*
Project Role: *PI*
Nearest person month worked during no cost extension: *3.0 calendar months*

Funding Support received during the project:
Name: *Anil Jegga*

Funding Support received during the project:
Name: *Prathibha Gajjala*
Project Role: *Research Fellow*

Funding Support received during the project:
Name: *Rajesh Kasam*
Project Role: *Graduate Assistant*

Funding Support received during the project:
Name: *Divyalakshmi Soundararajan*
Project Role: *Research Assistant*

Funding Support received during the project:
Name: *Sudhir Ghandikota*
Project Role: *Undergraduate Student*

Funding Support received during the project:
Name: *Vishwaraj Sontake*
Project Role: *Graduate Student*

Funding Support received during the project:
Name: *Jaswath Yella*
Project Role: *Undergraduate Student*

Has there been a change in the active other support of the PD/PI(s) or senior/key personnel since the last reporting period?
If there is nothing significant to report during this reporting period, state "Nothing to Report."

If the active support has changed for the PD/PI(s) or senior/key personnel, then describe what the change has been. Changes may occur, for example, if a previously active grant has closed and/or if a previously pending grant is now active. Annotate this information so it is clear what has changed from the previous submission. Submission of other support information is not necessary for pending changes or for changes in the level of effort for active support reported previously. The awarding agency may require prior written approval if a change in active other support significantly impacts the effort on the project that is the subject of the project report.

Nothing to Report

What other organizations were involved as partners?
If there is nothing significant to report during this reporting period, state "Nothing to Report."

Describe partner organizations – academic institutions, other nonprofits, industrial or commercial firms, state or local governments, schools or school systems, or other organizations (foreign or domestic) – that were involved with the project. Partner organizations may have provided financial or in-kind support, supplied facilities or equipment, collaborated in the research, exchanged personnel, or otherwise contributed.

Provide the following information for each partnership:
Organization Name:
Location of Organization: (if foreign location list country)
Partner's contribution to the project (identify one or more)

- *Financial support;*
- *In-kind support (e.g., partner makes software, computers, equipment, etc., available to project staff);*
- *Facilities (e.g., project staff use the partner's facilities for project activities);*
- *Collaboration (e.g., partner's staff work with project staff on the project);*
- *Personnel exchanges (e.g., project staff and/or partner's staff use each other's facilities, work at each other's site); and*

Organization Name: University of Cincinnati
Location of Organization: (if foreign location list country) 51 Goodman Drive, Cincinnati, OH
Contribution to Project: Dr. McCormack has provided human samples and clinical perspective on IPF. The project staff have helped in collection and distribution of clinical samples.

8. SPECIAL REPORTING REQUIREMENTS

COLLABORATIVE AWARDS: *For collaborative awards, independent reports are required from BOTH the Initiating Principal Investigator (PI) and the Collaborating/Partnering PI. A duplicative report is acceptable; however, tasks shall be clearly marked with the responsible PI and research site. A report shall be submitted to* ***https://ers.amedd.army.mil*** *for each unique award.*

QUAD CHARTS: *If applicable, the Quad Chart (available on https://www.usamraa.army.mil) should be updated and submitted with attachments.*

9. APPENDICES:

Attach all appendices that contain information that supplements, clarifies or supports the text. Examples include original copies of journal articles, reprints of manuscripts and abstracts, a curriculum vitae, patent applications, study questionnaires, and surveys, etc.

List of Equipment purchased during Grant:

DSI Buxco – Fine-pointe Whole Body Plethysmography

Qiagen – Tissue Lyser II

List of Residual Inventory of unused supplies exceeding $5,000 in value:

None

Cell Stress and Chaperones (2018) 23:441–454
https://doi.org/10.1007/s12192-017-0856-z

MINI REVIEW

Extracellular small heat shock proteins: exosomal biogenesis and function

V. Sudhakar Reddy[1] · Satish K. Madala[2] · Jamma Trinath[3] · G. Bhanuprakash Reddy[1]

Received: 5 June 2017 / Revised: 17 October 2017 / Accepted: 19 October 2017 / Published online: 30 October 2017
© Cell Stress Society International 2017

Abstract Small heat shock proteins (sHsps) belong to the family of heat shock proteins (Hsps): some are induced in response to multiple stressful events to protect the cells while others are constitutively expressed. Until now, it was believed that Hsps, including sHsps, are present inside the cells and perform intracellular functions. Interestingly, several groups recently reported the extracellular presence of Hsps, and sHsps have also been detected in sera/cerebrospinal fluids in various pathological conditions. Secretion into the extracellular milieu during many pathological conditions suggests additional or novel functions of sHsps in addition to their intracellular properties. Extracellular sHsps are implicated in cell-cell communication, activation of immune cells, and promoting anti-inflammatory and anti-platelet responses. Interestingly, exogenous administration of sHsps showed therapeutic effects in multiple disease models implying that extracellular sHsps are beneficial in pathological conditions. sHsps do not possess signal sequence and, hence, are not exported through the classical Endoplasmic reticulum-Golgi complex (ER-Golgi) secretory pathway. Further, export of sHsps is not inhibited by ER-Golgi secretory pathway inhibitors implying the involvement of a nonclassical secretory pathway in sHsp export. In lieu, lysoendosomal and exosomal pathways have been proposed for the export of sHsps. Heat shock protein 27 (Hsp27), αB-crystallin (αBC), and Hsp20 are shown to be exported by exosomes. Exosomes packaged with sHsps have beneficial effects in in vivo disease models. However, secretion mechanisms and therapeutic use of sHsps have not been elucidated in detail. Therefore, this review aimed at highlighting the current understanding of sHsps (Hsp27, αBC, and Hsp20) in the extracellular medium.

Keywords Small heat shock proteins · Exosomes · Plasma · Export

✉ V. Sudhakar Reddy
sudhakarnin@gmail.com

✉ G. Bhanuprakash Reddy
bhanu@ninindia.org; geereddy@yahoo.com

[1] Biochemistry Division, National Institute of Nutrition, Tarnaka, Jamai-Osmania, Hyderabad 500007, India

[2] Division of Pulmonary Medicine, Cincinnati Children's Hospital Medical Center, Cincinnati, OH, USA

[3] Department of Biological Sciences, BITS-Pilani, 500078, Hyderabad Campus, Hyderabad, Telangana, India

Introduction

Small heat shock proteins (sHsps) constitute a structurally divergent group of heat shock proteins (Hsps) characterized by a conserved sequence of 80–100 amino acid residues termed the α-crystallin domain (Basha et al. 2012; Garrido et al. 2012; Gusev et al. 2002; Sun and MacRae 2005a). The α-crystallin domain is located towards a highly flexible and variable C-terminal extension and is usually preceded by a poorly conserved N-terminal region. The molecular mass of sHsp subunits ranges from 13 to 43 kDa. The sHsps occur as homo- or heteromeric complexes, comprising 2–40 subunits. The subunits assemble into large globular complexes up to 1 mDa and are often polydispersed and dynamic with readily exchangeable subunits. The functional significance of sHsps is attributed to their ability to prevent in vitro aggregation of unfolded proteins through hydrophobic interactions (Horwitz 1992; Horwitz et al. 1998; Reddy et al. 2006). Subsequently, sHsps transfer the bound proteins to ATP-dependent chaperones such as Hsp70. Failure in appropriate protein folding will eventually result in proteasomal degradation of the unfolded

proteins (Haslbeck et al. 2005; Vos et al. 2008). Thus, molecular chaperone function of sHsps may be limited to storing (holding of aggregation-prone proteins as folding-competent intermediates and conferring enhanced stress resistance to cells by preventing aggregation of proteins). There are ten members in the sHsp family: Hsp27/Hsp25 of rodents (HSPB1), MKBP (myotonic dystrophy protein kinase; HSPB2), HSPB3, αA-crystallin (αAC; HSPB4), αB-crystallin (αBC; HSPB5), Hsp20 (HSPB6), cvHsp (HSPB7), Hsp22/H11/H2IG1 (HSPB8), HSPB9, and ODF (sperm outer dense fiber protein; HSPB10). While some sHsps are tissue-specific (MKBP, HSPB3, αAC, cvHsp, HSPB9, and ODF), the rest are ubiquitous (Hsp27, αBC, Hsp20, and Hsp22) (Garrido et al. 2012) Small Hsps can also modulate intracellular redox status suggesting that sHsps are not only involved in the cellular defense mechanisms against protein aggregation but also participate in essential physiological processes including cytoskeletal reorganization and apoptosis. Traditionally, Hsps including sHsps are considered to possess intracellular chaperone activity and confer protection from stress-induced cell death (Arrigo 2005; Sun and MacRae 2005b). However, the emerging evidence envisioned that there is the existence of extracellular Hsps that might contribute toward the alleviation of pathological conditions. Extracellular Hsps are first reported by Tytell et al. (1986) in giant squid axon functioning as a glia-axon transfer protein. Similarly, Hsp70 has been reported to be present in the extracellular milieu independent of ER-Golgi-mediated protein trafficking (Hightower and Guidon 1989). At the molecular level, Hsps lack classical N-terminus signal sequence required for conventional protein secretory pathway (Mambula et al. 2007) similar to that of immune-modulators such as IL-1α, IL-1β, IL-16, and IL-18 (Prudovsky et al. 2003). Extracellular release of Hsps has been reported during necrotic cell death (Basu et al. 2000). However, Hightower and Guidon (1989) noticed that the presence of lysine amino acid analogues/aminoethyl cysteine prevented the release of Hsp70 into extracellular milieu, suggesting that only a structurally intact protein is secreted out from the cells. In support of these results, subsequent studies demonstrated the extracellular presence of large (higher molecular weight) Hsps including Hsp60 and Hsp70 (Luo et al. 2008; Mambula and Calderwood 2006; Merendino et al. 2010; Vega et al. 2008).

Existing literature shed light on the unconventional release of Hsps and their possible extracellular functions in disease conditions including cancer (Calderwood et al. 2007; De Maio 2011; De Maio and Vazquez 2013) (Santos et al. 2017). Adding to this, the presence of sHsps (Hsp27, αBC, and Hsp20) is reported to be present in an extracellular milieu with undefined functions. Intriguingly, these studies also opened up new exploratory research avenues with the possibility of identifying novel functions performed by these secreted sHsps. Therefore, the current review tries to summarize the possible export mechanisms, functions, and therapeutic effects of extracellular sHsps with special emphasis on Hsp27, αBC, and Hsp20, which are known to be well characterized to date.

Hsp27

Hsp27, a member of the sHsp family, responds to stress and acts as a chaperone to facilitate appropriate folding of proteins (Rogalla et al. 1999). Hsp27 acts as an antioxidant and reduces reactive oxygen species (Mehlen et al. 1997) and also protects cells from programmed cell death by interacting with mediators of mitochondria (Havasi et al. 2008). Contrasting observations on the functional role of Hsp27 suggests that Hsp27 can positively and negatively regulate actin polymerization during cellular stress conditions (Benndorf et al. 1994; Huot et al. 1996; Miron et al. 1991).

Extracellular release of Hsp27 from tumor cells with unknown functions has been reported in plasma (4-fold increase) and interstitial fluid (2500-fold increase) in breast cancer patients (Banerjee et al. 2011; Ciocca et al. 1984; Fanelli et al. 1998; Feng et al. 2005; Thuringer et al. 2015). It is reported that secretion of Hsp27 is involved in differentiation of monocytes to macrophages. The secreted protein might be involved in immunological signaling by interacting with plasma membrane proteins thereby promoting tumor growth. Therefore, knock-down or knock-out approach or inhibition of secretion of Hsp27 in tumor cell lines or animal models might be an effective strategy in reducing the tumor growth. The secretion of Hsp27 in the extracellular medium is increased under stressful/pathological insults with different fold changes (Table 1**)**. Elevated levels of Hsp27 are found in the plasma of type 1 diabetic patients in the European population. Interestingly, high levels of Hsp27 are correlated with distal symmetrical polyneuropathy in diabetes and have been reported to be a marker for diabetic neuropathy (Gruden et al. 2008). Further, studies from our laboratory reported altered expression and phosphorylation of intracellular sHsps in target tissues of diabetic rat model (Reddy et al. 2015; Reddy et al. 2014; Reddy et al. 2013; Reddy and Reddy 2015; Reddy and Reddy 2016). In addition, we recently reported elevated levels of Hsp27 in the plasma of nephropathy patients in type 2 diabetes, and its levels were positively correlated with serum creatinine thereby suggesting that Hsp27 might serve as a marker for diabetic nephropathy (Jakhotia et al. 2017). Also, Hsp27 protein and its antibodies are elevated in insulin resistance in glucose-intolerant patients with a history of cardiovascular diseases (Burut et al. 2010). Further, the release of Hsp27 from platelets is accompanied by phosphorylation in type 2 diabetic patients and is correlated with accelerated aggregation of platelets (Tokuda et al. 2015). Taken together, these studies strongly suggest that Hsp27 is released into the serum in diabetes as perhaps a response to stressful events in

Table 1 Secretion of sHsps into the extracellular medium in pathological conditions

sHsp	Pathology	Fold change	Effect	References
Hsp27	Breast cancer	4-fold in serum and 2500-fold increase in tumor interstitial fluid.	Induced differentiation of monocytes to macrophages, anergy in T-cell, and neovascularization	Banerjee et al. (2011)
	Hepatocellular carcinoma (HCC)	Increased levels of Hsp27 found in HCC patients analyzed by 2-DE based serum proteome	Developed as a biomarker for HCC	Feng et al. (2005)
	Colon cancer	4-fold increase (secreted into culture medium from primary tumor derived SW480 cells)	Increased the endothelial gap junction coupling by promoting the phosphorylation of connexin 43	Thuringer et al. (2015)
	Diabetic neuropathy	2-fold increase	Novel biomarker of diabetic neuropathy	Gruden et al. (2008)
	Insulin resistance	Increased antigen and antibodies	Related to glucose intolerance	Burut et al. (2010)
	Chronic obstructive pulmonary disease (COPD)	1.8-fold increase (COPD with severe disease)	Diagnostic marker for immune activation and tissue destruction in COPD	Hacker et al. (2009)
	Multiple sclerosis (MS)	4.8-fold increase in the attack phase	Guiding the accurate detection of an attack in MS	Ce et al. (2011)
	Gastric adenocarcinoma (GA)	1.7-fold increase	Marker for detection of GA	Huang et al. (2010)
	Thymic epithelial tumors (TET)	1.5-fold increase	Can be developed as diagnostic marker for TET	Janik et al. (2016)
	Myasthenia gravis	2.3-fold increase	Can be developed as diagnostic marker for TET	Janik et al. (2016)
	Acute coronary syndromes	2.3-fold increase	Represent the systemic inflammation and oxidative stress	Park et al. (2006)
	Atherosclerosis	20-fold decrease	Could be developed as potential index of atherosclerosis	Martin-Ventura et al. (2004)
	Ovarian cancer (OC)	The secretion of Hsp27 increased after overexpression (2.38-fold) and heat shock	Non-invasive biomarker for OC	Stope et al. (2017)
αBC	Obesity	Increased in Conditioned media of cultured primary human adipocytes derived from obese patients	Could be developed as a novel adipokine	Lehr et al. (2012)
	Renal cell carcinoma (RCC)	Increased	Biomarker of RCC	Holcakova et al. (2008)
	Multiple sclerosis	Increased auto-antibodies	Inflammatory response	Celet et al. (2000); van Noort et al. (2006)
	Multiple sclerosis	5-fold increase	Anti-inflammatory response	Rothbard et al. (2012)
	Experimental auto-immune myelitis	3-fold increase	Anti-inflammatory response	Rothbard et al. (2012)
	Neuro-Behçet's disease	Increased auto-antibodies	Inflammatory response	Celet et al. (2000)
	Guillain–Barré syndrome	Increased auto-antibodies	Inflammatory response	Celet et al. (2000); Hegen et al. (2010)
	Chronic inflammatory demyelinating polyneuropathy			Hegen et al. (2010)
	Brain stroke in mice	2.7-fold at 12 h, 1.7-fold at 2 days, 0.5-fold compared to naïve mice	Anti-inflammatory response	Arac et al. (2011)
	Ischemic brain stroke in humans	1.7-fold at < 4 h, 1.2-fold at 24 h, 1.4 at 48 h in younger patients compared to 0.3-fold in healthy ones	Anti-inflammatory response	Arac et al. (2011)
Hsp20	Cardiomyopathy	126-fold increase	Regulator of platelet function	Kozawa et al. (2002)
	Acute dissecting aneurysm	11-fold increase	Acts as anti-platelet regulator	Niwa et al. (2000)
	Myocardial ischemia/reperfusion (I/R)	3.4-fold increase	Acts as a cardiokine which mediates angiogenesis by directly interacting with VEGFR2	Zhang et al. (2012)

hyperglycemia. Hsp27 and Hsp70 are also elevated in the serum of patients who smoke and have chronic obstructive pulmonary disease (COPD), and these Hsps were found to be diagnostic markers for COPD (Hacker et al. 2009). Extensive tissue damage in COPD patients with chronic disease symptoms correlates with the extracellular release of Hsp27 into circulation (1.8-fold vs healthy). Hsp27 is released not only into plasma but also into cerebrospinal fluid in the central nervous system during ischemia (Hecker and McGarvey 2011). Moreover, elevated serum levels of Hsp27 have been detected in multiple sclerosis (Ce et al. 2011), gastric adenocarcinoma (Huang et al. 2010), pancreatitis (Liao et al. 2009), thymic epithelial tumors, and myasthenia gravis (Janik et al. 2016). Very recently, secretion of Hsp27 into circulation in ovarian cancer (OC) patients has been noticed and considered to be a potential biomarker for prognosis and diagnosis for OC (Stope et al. 2017). The functions of extracellular Hsp27 are unknown, although a few studies have reported that it is involved in signaling by binding to the receptors of immune and endothelial cells (Schmitt et al. 2007; Binder et al. 2004). Additionally, a few studies reported its role in cardiovascular diseases as it was found in the serum of patients with acute coronary syndromes (Park et al. 2006), atherosclerosis (Martin-Ventura et al. 2004), and reperfusion after ischemic clamping during heart bypass surgery (Jin et al. 2014). Additionally, Hsp27 has been shown to be an atheroprotective agent by decreasing the uptake of atherogenic lipids and thereby attenuating inflammation (Rayner et al. 2008). The addition of exogenous Hsp27 to in vitro macrophage culture reduced the acetylated LDL uptake by 41% with a concomitant increase in the expression of anti-inflammatory (IL-10 and GM-CSF) and pro-inflammatory mediators (IL-1β and TNF-α) (Rayner et al. 2008; Salari et al. 2013). Extracellular Hsp27 reduced the LDL uptake by binding to the scavenger receptor-A (SR-A). It reduced the ability of SR-A to engulf acetylated LDL on the surface of macrophages and acquired the foam cell phenotype (Rayner et al. 2008). Hsp27 also activated the NF-kB in mouse coronary endothelial cells by interacting with TLR2 and TLR4 and resulted in upregulation of monocyte chemoattractant protein-1 (MCP-1) and intercellular adhesion molecule-1 (ICAM-1) (Jin et al. 2014). Similarly, Hsp27 engagement on TLR3 was implicated in the activation of NF-κB and secretion of IL-8 and vascular endothelial growth factor (VEGF) in human microvascular endothelial cells (HMECs) (Thuringer et al. 2013). Recombinant Hsp27 rapidly internalized into the endosomal compartment (within 15–30 min) with the pool of TLR3, which is required for NF-κB activation in HMECs. Treatment of bone marrow-derived dendritic cells with recombinant Hsp27 also activated IL-6, TNF-α, IL-1β, IL-12p35, and IL-12p40 by interacting with TLR4 (Yusuf et al. 2009). Estrogen receptor-β is also known to interact with Hsp27 (Al-Madhoun et al. 2007; Miller et al. 2005). In addition to inducing inflammation, extracellular Hsp27 shows chaperone and therapeutic activity in in vitro and experimental disease models. Recombinant Hsp27 inhibited the DTT-induced aggregation of insulin in vitro, indicating that exogenous Hsp27 has effective chaperone activity (Kurnellas et al. 2012). Likewise, intraperitoneal injection of recombinant Hsp27 reduced the paralytic symptoms by modulating inflammatory cytokines IL-2, IL-6, and IFN-λ in the experimental auto-immune encephalomyelitis (EAE) mouse model at the peak of the disease (Kurnellas et al. 2012). However, ceasing of Hsp27 supplementation resulted in complete return of the paralytic symptoms, indicating that Hsp27 acts as a biological inhibitor, and the therapeutic effects seem to depend on consistent circulatory levels of Hsp27, rather than inducing a long-acting immunological state of reduced inflammation or tolerance (Kurnellas et al. 2012). A short sequence of Hsp27 (73 to 92 amino acids; 1 μg/animal) ameliorated the paralytic symptoms in EAE mouse model, suggesting that peptides of Hsp27 also have effective therapeutic activity similar to that of the full-length protein (Kurnellas et al. 2012). In another study, the sequence of 93 to 113 amino acids of Hsp27 (10 μg/ml) protected the HeLa cells from STS- or H_2O_2-induced apoptosis by inhibiting the release of cytochrome c from mitochondria and activating caspase-3 (Nahomi et al. 2015). Intraperitoneal (i.p.) administration of the same peptide (93 to 113 amino acids; 50 μg/animal) for 6 days prevented selenite-induced cataract development in mice by inhibiting the oxidative stress, protein insolubilization, and apoptosis indicating that peptides of Hsp27 are effective in preventing disease phenotype (Nahomi et al. 2015). Detection of injected peptide (i.p.) in the lens confirmed that the peptide is able to traffic through barriers to execute its function. Finally, these observations culminate to suggest that Hsp27 is mainly involved in modulating the inflammatory response by interacting with certain receptors (secretion of cytokines), chaperone activity (prevention or suppression of aggregation of proteins), cell migration (upregulation of MCP-1 and ICAM-1), cell death (preventing apoptosis), and cell proliferation (interacting with ER-β) (Fig. 1).

Export of Hsp27

As discussed earlier, sHsps are not secreted through the classical ER-Golgi secretory pathway. Until now, lysoendosomal or exosomal/extracellular vesicular pathway, direct protein translocation, and release after cell death (necrosis) have been proposed toward the release of Hsps (De Maio 2011; De Maio and Vazquez 2013). Among these, it is unclear whether the release of Hsps after cell death is a valid mechanism for export of Hsps. Some recent studies have provided evidence for the release of sHsps via the lysoendosomal or exosomal pathway (Batulan et al. 2016; Rayner et al. 2009; Sreekumar et al. 2010; Zhang et al. 2012). Rayner et al. (2008) reported that

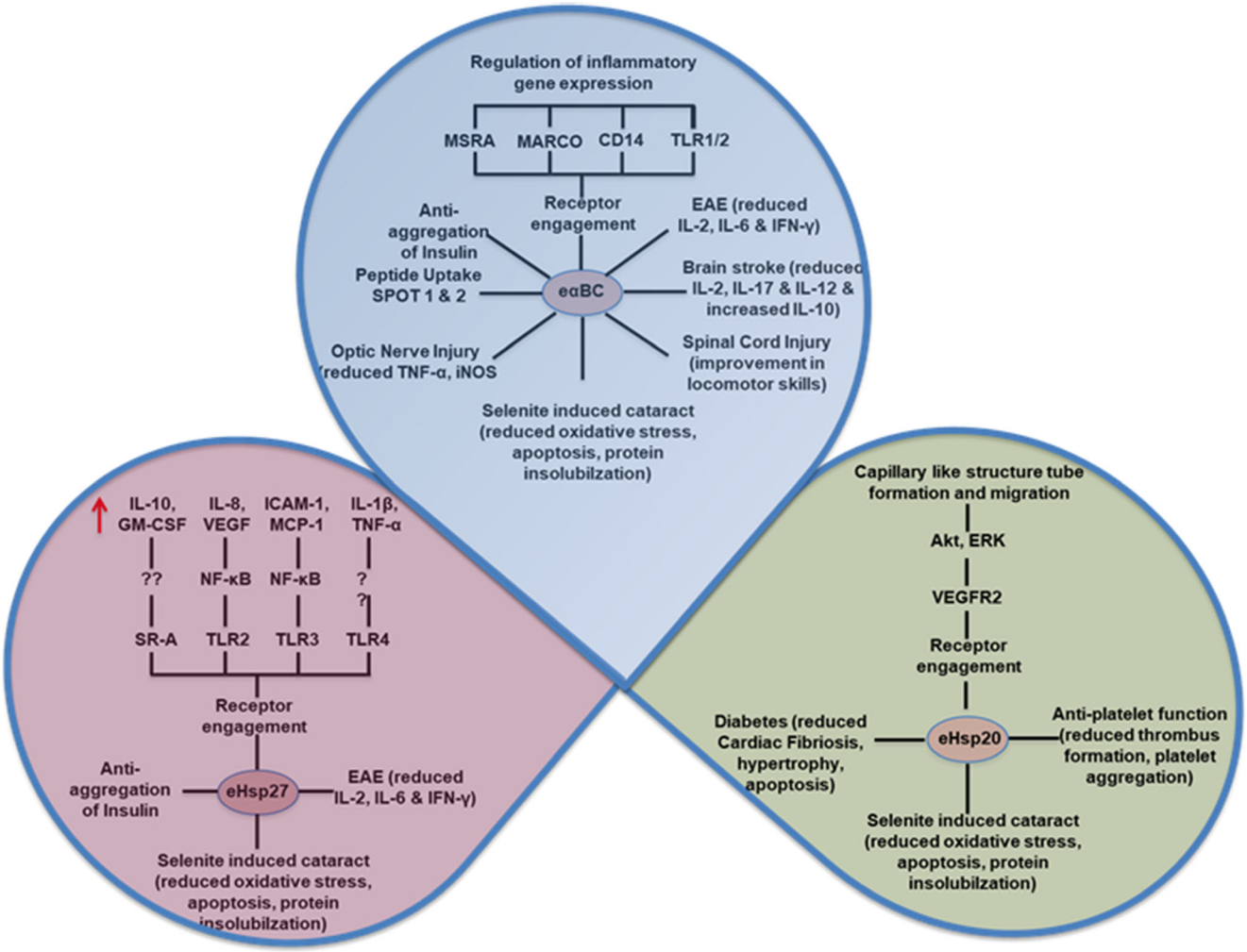


Fig. 1 Functions of extracellular heat shock protein 27 (eHsp27), αB-crystallin (eαBC), and Hsp20 (eHsp20). TLR: toll-like receptor; SR-A: scavenger receptor-A; VEGF: vascular endothelial growth factor; GM-CSF: granulocyte macrophage colony stimulating factor; ICAM-1: intercellular adhesion molecule1; MCP-1: monocyte chemoattractant protein-1; TNF-α: tumor necrosis factor; IL-6: interleukin-6; MSRA: macrophage scavenger receptor A; MARCO: macrophage scavenger receptor with collagenous structure; TNF-α: tumor necrosis factor; IL-2: interleukin-2; SOPT1: sodium oligopeptide transporter 1; VEGFR2: vascular endothelial growth factor receptor 2

treating macrophages with acetylated LDL or estradiol-induced secretion of Hsp27 and co-localization with lysotracker or lysosomal marker LAMP. Another group also reported the co-localization of non-phosphorylatable mutants (S15A/S82A) of Hsp27 fused to GFP with lysosomal marker, LAMP-1, indicating that Hsp27 also exits into the extracellular space through secretory lysosomal-like vesicles (Lee et al., 2012). Utilization of phosphomimetic forms of Hsp27 (S15D/S28D) further confirmed that phosphorylation of Hsp27 at specific serine residues is crucial for its secretion exclusively through the endosomal pathway. Another exit of Hsp27 is through the exosomal pathway, and numerous studies are supporting the release of Hsp27 through the exosomes. Rayner et al. (2009) showed that extracellular levels of Hsp27 are reduced upon treatment of human macrophages with exosomal inhibitor dimethyl amiloride. Nafar et al. (2016) detected Hsp27 in membrane fractions of exosomes originating from rat astrocytes upon treatment with amyloid-β. Under physiological conditions, exosomes are positive for Hsp27, and exposure of lymphoblastoid cells to heat stress (42 °C for 3 h) enhanced the quantity of exosomes with a ratio of 1.2:1 compared to that of exosomes from the control cells. Heat stress not only increased the quantity of exosomes but also selectively enriched Hsp27 along with Hsp70 and Hsp90 (Clayton et al. 2005). Exosomes are small-membrane microvesicles ranging from 4 to 100 nm in diameter and are found in all biological fluids. Lipids (lipid rafts) and proteins are major components of exosome membranes. Exosomes are released into the extracellular space after fusion with the plasma membrane and contain membranous and lumen portions. The inward budding of the plasma membrane forms early endosomes, and the membrane of early endosomes buds inwardly into various late endosomes. Late endosomes contain intraluminal bodies that are also called

multivesicular bodies (MVBs). These MVBs fuse with the plasma membrane to release intraluminal bodies, i.e., exosomes, while the microvesicles, ranging from 100 to 1000 nm directly bud off from the plasma membrane. In the recent past, the exosomes have become crucial in understanding the cell-to-cell communication and as delivery agents of miRNA. Large Hsps including Hsp70 are localized to the membrane (surface) of exosomes (Gastpar et al. 2005) as well as to the luminal compartment (Clayton et al. 2005; Jia et al. 2017). It is also subject to debate whether sHsps are localized in the luminal or membrane portion in exosomes. While the presence of Hsp27 in lumen or membrane of exosomes is still under debate, studies proposed that Hsps are localized in the lumen and as well as on the surface. Localization of Hsps in the lumen but not on the exosome surface suggests that Hsps in exosomes may not interact with target cells through cell surface Hsp receptors. However, the presence of Hsps on the surface can also be accepted, as it is important for secretion of Hsps into circulation and interaction with other cell surface receptors. Furthermore, the presence of sHsps on the cell surface is corroborated by the fact that Hsp27 interacts with cell surface receptors such as SR-A and TLRs (Yusuf et al. 2009). Hsp27 was seen to be released into the extracellular medium through exosomes when OVCAR-3 and SK-OV-3 cells were cultured in vitro (Stope et al. 2017). Blocking of the ER-Golgi pathway with brefeldin-A has not affected the secretion of Hsp27 suggesting secretion of Hsp27 may depend on intracellular levels rather than the phosphorylation status of Hsp27. In support to this, Stope et al. (2017) demonstrated that phosphorylation did not affect the secretion of sHsps. This study further provided significant insights into the understanding of the factors that influence the secretion of Hsp27. Interestingly, heat shock treatment not only increased the expression of intracellular Hsp27 but also enhanced the incorporation of Hsp27 by 10-fold into extracellular exosomes imparting a crucial role of the exosomal pathway in Hsp27 secretion.

αBC

Recently, many studies have demonstrated the extracellular presence and therapeutic functions of exogenous αBC in multiple in vitro cell culture as well as in in vivo disease models. The increased secretion of αBC into the culture medium has been shown during primary human adipocyte culture from obese patients and corroborates with its increased level in plasma and adipose tissue from the patients (Lehr et al. 2012). Therefore, it is concluded that αBC also acts as an adipokine. The secretion of αBC into plasma under several disease conditions with altered fold change is listed in Table 1. One study identified that αBC can act as a biomarker for renal cell carcinoma with its increased levels in serum samples of patients (Holcakova et al. 2008). An increasing number of studies also have been reported that the export of αBC into the extracellular milieu is through the exosomes. Sreekumar et al. (2010) reported the presence of αBC in secreted exosomes when retinal pigment epithelial cells (RPE) were cultured in exosome-free medium (to avoid contamination from endogenous exosomes present in the serum). The presence of αBC in exosomes has been further confirmed by performing immunogold labeling and immunoblotting for CD63, as a marker for exosomes (Sreekumar et al. 2010). Multiple factors including stress stimuli, cell polarity, and inflammation can induce the release of αBC. For example, αBC secreted within exosomes by highly polarized human RPE cells toward the apical photoreceptor facing neural retina confers neuroprotection. Extracellular αBC can also act as an auto-antigen by eliciting auto-antibodies in multiple sclerosis (van Noort et al. 2006). Subsequently, many studies reported the presence of auto-antibodies in CSF and serum of Neuro-Behçet's disease, Guillain–Barré syndrome, and inflammatory neurologic disorders (Celet et al. 2000; Hegen et al. 2010). However, the perception of αBC as an auto-antigen in these disorders is equivocal as recent studies reported that αBC through its chaperone activity can bind immunoglobulin with a high affinity, which contradicts the αBC as an auto-antigen (Rothbard et al. 2011). Of note, αBC promotes anti-inflammatory rather than proinflammatory response. Exogenous administration of 50 μg/100 g of body weight of α-crystallin (combination of αAC and αBC) reduced the expression of cytokines including IL-1α, TNF-α, and NO in the silver nitrate-induced rat inflammation model. Also, α-crystallin treatment in the same experimental model reduced the levels of neurotransmitters including dopamine, 5-hydroxytryptamine, and norepinephrine and increased their metabolites such as 3,4-dihydroxyphenylacetic acid, homovanillic acid, and 5-hydroxyindoleacetic acid in the neocortex and hippocampus regions of the brain (Masilamoni et al. 2005). Additionally, the same group reported alleviation of inflammation-induced expression of NF-κB and GFAP and decreased activation of acetylcholine esterase activity in neurons upon α-crystallin treatment (Masilamoni et al. 2006). However, the mechanism responsible for extracellular αBC in promoting an anti-inflammatory response upon administration remains unclear. The receptors including CD14, TLR1, and TLR2 are a prerequisite for αBC-mediated activation of HEK-293 cells secreting alkaline phosphatase under the control of transfected NF-kB (van Noort et al. 2013). Exogenous αBC activated the cells expressing CD14 and TLR1/2 through initial binding with macrophage scavenger receptor A (MSRA) and macrophage scavenger receptor with collagenous structure (MARCO) (van Noort et al. 2013). Further, it also inhibited the lymphocyte and neutrophil infiltration in the cigarette smoke-induced lung inflammation mouse model (van Noort et al. 2013). It has been observed that there is an increased level of αBC in plasma of individuals with the

disease in advanced stages than that of individuals with later stages of the disease in stroke patients (Arac et al. 2011). Intriguingly, increased levels of αBC have been noticed in patients with stroke at the time of presentation in the hospital (< 4 h from the point of stroke) and subsided within the next 48 h similar to that of mice suffering from a stroke. Supplementation of αBC i.p. to the αBC knock-out mice suffering from brain stroke reduced the lesion size. Administration of αBC 1 h before and 12 h after the onset of stroke in mice did not reduce the lesion size compared to the PBS-treated group. However, administration of αBC 1 h before and 12 and 24 h after followed by daily administration for 7 days after the stroke onset in mice led to a reduction in the lesion size compared to that of PBS-treated group, implicating the neuroprotective function to αBC. Furthermore, systemic augmentation of αBC reduced both the stroke volume and inflammatory cytokines (decreased proinflammatory cytokines and increased anti-inflammatory cytokines) in the stroke-induced mouse model (Arac et al. 2011). Intraperitoneal administration of αBC rapidly and efficiently reduced the paralytic symptoms in EAE mouse model. It is also noted that extracellular αBC does not directly affect T- or B-lymphocyte proliferation; rather, it limits the inflammation induced by TLRs and innate immunity. In support to this, Rothbard et al. (2012) reported that systemic administration of αBC in the EAE (induced by adoptive transfer of myelin-specific Th17 lymphocytes) mice did not ameliorate the clinical symptoms. Another study reported that intravenous administration of human recombinant αBC attenuated the spinal cord injury (SCI) in mice by ameliorating secondary tissue damage, improving locomotor skills, and reducing the recruitment of inflammatory macrophages (Klopstein et al. 2012). The extracellularly administered αBC is able to enter into some of the tissues including the spinal cord. The intravenous administration of αBC is able to enter injured spinal cord when injected into a SCI mouse model and showed 2-fold increase in protein levels at the site of injury 12 h post-injection as compared to a saline-treated group. Altogether, these results indicate that αBC can enter into inflammatory site in neuronal tissues and can show an anti-inflammatory response. However, endogenous αBC protein levels were reduced by 20% in recombinant human αBC-treated SCI mice compared with that of the physiological levels in normal spinal cord (Klopstein et al. 2012). The injected αBC protein has been shown to enter into the white matter at the injured epicenter and into white and gray matter in the adjacent areas (45% taken up by neurons, 38.8% by astrocytes, and 30.7% by oligodendrocytes) and not found in microglial cells, as well as granulocytes. αBC enhanced the survival of retinal ganglion cells, inhibited the retinal microglia cells, and reduced the expression of TNFα and iNOS in the rat model of optic nerve crush (Wu et al. 2014). Wu et al. (2014) administered αBC in a dose-dependent manner (0.05, 0.5, and 5 g/kg of body weight) to optic nerve crush rat model, but 5 g/kg of b.w. showed agitated behavior indicating that higher concentration of αBC is toxic to rats. Therefore, one should be cautious about using higher concentrations of αBC for retinal optic neuropathy, and one has to study the range of concentrations that are deleterious or beneficial to other diseases. However, the mechanism by which extracellular αBC exhibits beneficial functions remains largely unknown. One study revealed that αBC was able to bind to > 70 proteins in plasma of multiple sclerosis, amyloidosis, and rheumatoid arthritis patients, mouse model of EAE, and interestingly, these proteins have been identified to be part of proinflammatory signature including acute phase proteins, members of complement, and coagulation cascade (Rothbard et al. 2012). A study reported that αBC or its peptide blocks the function of platelets by preventing their aggregation in in vitro, ex vivo, and in vivo mouse models induced by thrombin or botrocetin (Kozawa et al. 2001). Inhibition of platelet aggregation is mediated by suppression of Ca^{2+} mobilization and activation of protein kinase C (Kozawa et al. 2001). Furthermore, αBC attenuates the ADP-induced granule secretion via p38 MAPK and p42 MAPK (Enomoto et al. 2009) upon incubation with platelets. Not only full-length αBC but also the intravenous administration of αBC peptides also inhibited thrombus formation in vivo indicating that both extracellular full-length and peptide αBC are important in the regulation of platelet function with an application in anti-platelet therapy (Kanno and Matsuno 2006). αBC is also found to be instrumental in performing extracellular chaperone activity in addition to anti-inflammatory and anti-platelet functions. In support to this, Mannini et al. (2012) showed that extracellular addition of αBC reduced the misfolded oligomer-induced toxicity even at a low level rather than overexpressing in the cytosol implicating the potential role for extracellular αBC to that of cytosolic counterpart. Exogenous recombinant αBC (12.5 μg/ml) protected the human lens' epithelial cells from heat- and oxidative stress-induced cell death indicating that exogenous αBC displays anti-apoptotic activity (Christopher et al. 2014). It is also shown that uptake of αBC is enhanced by fusion with cell penetration peptides (CPP) including TAT protein from human immunodeficiency virus and glycoprotein-C from hepatitis C virus. Cell penetration peptides fused to αBC including TAT-αBC and gC-αBC tagged with fluorophore showed enhanced uptake in HLE-B3 cells within 60 min of exposure to cell. The exogenously added gC-αBC was able to co-localize with endogenous αBC in cytoplasm as revealed by confocal microscopy indicating the efficiency of CPP in increasing the cellular uptake. It is also established that administration of αBC (i.p.) peptides inhibits protein insolubilization, epithelial cell apoptosis, and finally opacification in selenite-induced cataract in mice (Nahomi et al. 2013). This group administered the increasing dose of 2.5, 5, and 10 μg/animal of both αBC peptide and acetyl-αBC

peptide at 6 h prior to selenite injection in rat pups as a single injection separately. For multiple doses, the first dose was given 6 h prior to sodium selenite injection, followed by subsequent injections each day for 4 days. Both the peptides significantly inhibited cataract progression at 10 μg (single dose), as well as multiple doses. Treatment with 5 μg of both peptides also significantly inhibited cataract progression with multiple injections, while acetyl-αBC alone inhibited the cataract with single injection, indicating a dose-dependent therapeutic effect of native as well as modified αBC peptides. This study suggests that peptides of αBC are capable of crossing the blood/aqueous barrier to inhibit the opacification of the lens and shows the efficiency of exogenous αBC peptides in ameliorating the disease phenotype. The above findings suggest that the beneficial effects of exogenous administration of αBC are not only limited to a single disease or mechanism but also to multiple diseases or mechanisms where inflammation, cell death, and protein aggregation are involved in disease initiation or progression. The functions of extracellular αBC were depicted in Fig. 1.

Export of αBC

There is also compelling evidence suggesting the presence of αBC in exosomes. Like Hsp27, αBC secretion occurs independently of the classical secretory pathway wherein inhibiting the classical secretory pathway by using brefeldin and tunicamycin did not alter the secretion of αBC. It has been shown that αBC is secreted from the apical side of polarized human RPE cells (Sreekumar et al. 2010). In exosomes, αBC resides in detergent-resistant membrane microdomains, which are essential sites for exosome biogenesis. Treatment of human RPE cells with β-methyl cyclodextrin (lipid raft and cholesterol depletor) as well as dimethyl amiloride (exosome inhibitor and inhibitor of H^+/Na^+ and Na^+/Ca^{2+} exchanger) significantly inhibited αBC secretion, indicating the need of lipid rafts and exosomes for αBC secretion. Further, the secretory levels of αBC from human RPE cells are only a small fraction to that of the steady-state levels found in mitochondria and cytosolic compartments (Sreekumar et al. 2010). The polarization of cells is also equally important for secretion of αBC, which is further corroborated by the fact that a 5-fold increase in αBC secretion has been found in polarized RPE cells, compared to that of the non-polarized cells. Stress also affects the polarization and secretion of αBC. In support to this, oxidative stress induced by H_2O_2 in RPE cells induced the increased secretion of exosomes on the basolateral side compared to the apical side, and the secretion of αBC is found to be more from the exosomal fraction of the basolateral side when compared to non-stressed cells. Moreover, αBC has been shown to co-localize with tetraspanin CD63 in some of the MVBs/exosomes and perinuclear Golgi in ARPE cells. Interestingly, αBC did not co-localize to some of the CD63 positive exosomes/MVBs in the peripheral regions of the cell (Bhat and Gangulam 2011). Sreekumar et al. (2013) first reported the uptake of the αBC-derived peptide by two novel sodium-dependent oligopeptide transporters SOPT1 and SOPT2 in fetal RPE (fRPE) cells. These transporters are involved in transporting of endogenous and other synthetic opioid peptides and the iron regulatory peptide hormone hepcidin. αBC-derived peptides are transported into fRPE cells by competing with DADLE and deltorphin II that are substrates for SOPT1 and SOPT2. αBC-derived peptides have a high affinity for SOPT1 and SOPT2. On the contrary to Hsp27, exosomal secretion of αBC is influenced by post-translational modification including phosphorylation and O-GlcNAcylation (Kore and Abraham 2016). Phosphorylation and prevention of O-GlcNAcylation deterred the incorporation and exosomal secretion of αBC. αBC plays an crucial role in exosome biogenesis. Using shRNA, inhibition of αBC expression resulted in aggregated staining patterns of CD63 (LAMP3) and inhibited exosome secretion from ARPE19 cells (Gangalum et al. 2016). Further, inhibition of αBC expression increased the number of vacuoles and enlarged (fused) vesicles with increased expression of CD63 (LAMP3) and LAMP1 (a marker of lysosomes) indicating the shift toward the endolysosomal pathway which is further supported by increased levels of Rab7 (a marker for late endosome). This study demonstrates that αBC is crucial in the biogenesis of exosomes and that their secretion and inhibition of αBC cause shift into the endolysosome pathway. Further studies are required to address other mechanistic details of sHsps in the biogenesis of exosomes. It is possible that αBC might be involved in passaging the MVBs to the plasma membrane for the release of exosomes because in the absence of αBC, markers including Rab7 and LAMP1 increased, indicating that MVBs progress toward lysosomes instead of progressing toward the plasma membrane. However, it is also noted that exosome biogenesis normally occurs in many cell types without the involvement of αBC. Therefore, one should address whether αBC acts in a specific manner according to cell type.

Hsp20

Hsp20 is an important member of the sHsp family and is also referred to as HSPB6. It is expressed in multiple tissues with abundant expression in skeletal, cardiac, and smooth muscle cells (Fan et al. 2005; Salinthone et al. 2008). A few studies have reported the secretion of Hsp20 into the extracellular medium in pathological conditions. Whether secretion of Hsp20 in pathological conditions is advantageous or deleterious remains to be elucidated. Kozawa et al. (2002) reported that there is an elevated level of Hsp20 in plasma of cardiomyopathic hamsters. These researchers detected both

dissociated and aggregated forms of Hsp20 with elevated levels of the dissociated form in plasma of cardiomyopathic hamsters. Furthermore, circulating levels of Hsp20 increased 3.4-fold in cardiac-specific Hsp20-overexpressed transgenic mice cardiomyocytes in vitro (Zhang et al. 2012). These researchers also reported the secretion of Hsp20 through exosomes rather than through the classical ER-Golgi secretory pathway. Extracellular Hsp20 promoted the capillary-like structure tube formation and migration in HUVEC cells by interacting with VEGFR2, which is associated with activation of Akt and ERK (Zhang et al. 2012). Hsp20 levels were also elevated up to 11-fold in plasma of acute dissecting aneurysm patients. Extracellular Hsp20 shows anti-platelet activity by inhibiting thrombin-induced platelet aggregation in a dose-dependent manner by inhibiting receptor-mediated calcium influx in vitro and ex vivo (Matsuno et al. 1998; Niwa et al. 2000). Nevertheless, Hsp20 levels were markedly lower in a carotid artery endothelial injury model indicating that Hsp20 is secreted into circulation in response to endothelial injury to act as a regulator of platelets extracellularly (Kozawa et al. 2002). The intravenous administration of Hsp20 into hamsters prevented thrombus formation after endothelial injury, and its peptide also reduced the platelet aggregation implicating the anti-platelet function of exogenous Hsp20 (Kanno and Matsuno 2006). Intraperitoneal administration of recombinant Hsp20 (10 μg/day for 20 days) has shown similar therapeutic activity along with other sHsps by reducing the paralytic symptoms in the EAE mouse model, suggesting that exogenous Hsp20 acts as a therapeutic protein by decreasing the inflammation (Rothbard et al. 2012). In vitro treatment of HeLa cells with Hsp20-peptide (G71HFSVLLDVKHFSPEEIAVK91) caused it to translocate to the nucleus from the cytosol during thermal stress. Hsp20 peptide also prevented apoptosis by blocking the release of cytochrome c from mitochondria and caspase-3 activation in HeLa cells (Nahomi et al. 2015). Intraperitoneal administration of 50 μg of Hsp20 peptide/animal/day for six consecutive days inhibited the protein aggregation and oxidative stress thereby preventing the cataract formation in selenite-treated rats suggesting that exogenous Hsp20 peptide shows therapeutic activity by anti-aggregation and anti-oxidant activities (Nahomi et al. 2015). Previous studies have reported the secretion of Hsp20 through exosomes rather than a classical ER-Golgi secretory pathway. Accumulating evidence suggests that exosomes secreted from cardiomyocytes contain Hsp20 and play crucial role in cardiovascular pathology. Exosomes secreted from diabetic rat cardiomyocytes contain lower levels of Hsp20 compared to that of healthy controls. Exosomes secreted from diabetic cardiomyocytes from cardiac-specific overexpressing-Hsp20 mice (conditional transgenic mice overexpressing Hsp20 in the heart) showed increased levels of Hsp20 compared to those in control rats (Wang et al. 2016). Cardiac-specific overexpression of Hsp20 increased the biogenesis of exosomes upon interaction with tumor susceptibility gene 101 (Tsg101). Tsg101 is the component of Endosomal Sorting Complex Required for Transport-1 (ESCRT-1) which recognizes the ubiquitin tagged proteins and required for the sorting of endocytic ubiquitinated cargos into multivesicular bodies (MVBs). Further, cardiac-specific overexpression of Hsp20 increased the exosomes packed with Hsp20 and protected the cells from hyperglycemia-induced cell death in in vitro and in streptozotocin-induced diabetic mouse model in vivo, altogether suggesting that Hsp20 is instrumental in cardioprotection by increasing the biogenesis of exosomes (Wang et al. 2016). The functions of extracellular Hsp20 are depicted in Fig. 1.

Export of Hsp20

Zhang et al. (2012), for the first time, reported the secretion of Hsp20 from rat cardiomyocytes through exosomes. Hsp20 is released into the extracellular medium in physiological and myocardial infarction conditions, but its secretion is increased in myocardial infarction. It implies that secretion of Hsp20 via exosomes is increased under stress conditions such as ischemia/reperfusion. Interestingly, increased secretion of Hsp20 from cardiomyocytes of cardiac-specific overexpressing Hsp20 mice correlated with increased expression of Rab11a, Rab11b, Rab35, and Tsg101 that are involved in exosome generation/biogenesis. It has also been proven that recombinant Hsp20 is known to interact with Tsg101 but not with Rab11 a/b and Rab35 indicating that Hsp20 increases the generation of exosomes by interacting with Tsg101 (Wang et al. 2016). These studies strongly support that Hsp20 is strongly associated with the biogenesis of exosomes. It is also shown that extracellular Hsp20 promotes angiogenesis by acting as a VEGF-receptor agonist. Furthermore, the same research group has demonstrated that exosomes derived from cardiomyocytes of conditional transgenic-Hsp20 mice are enriched with SOD1, survivin, p-Akt, and Hsp20 and are capable of protecting the mouse cardiac endothelial cells from high glucose-induced stress (Wang et al. 2016). Moreover, exosomes derived from cardiomyocytes of transgenic-Hsp20 mice attenuated the cardiac fibrosis, hypertrophy, and apoptosis when injected into diabetic mice. All these studies indicate that Hsp20 promotes exosome biogenesis and exosomes encased Hsp20 protect the cells from multiple stressful conditions.

Hsp22

Hsp22 is also called as HSPB8 or H11 kinase or E2IG1. Abundant expression of Hsp22 has been noticed in skeletal muscle, heart, retina, brain, and spinal cord. Hsp22 plays an important role in neuronal cell survival by regulating the mitochondrial pathway. However, the extracellular presence

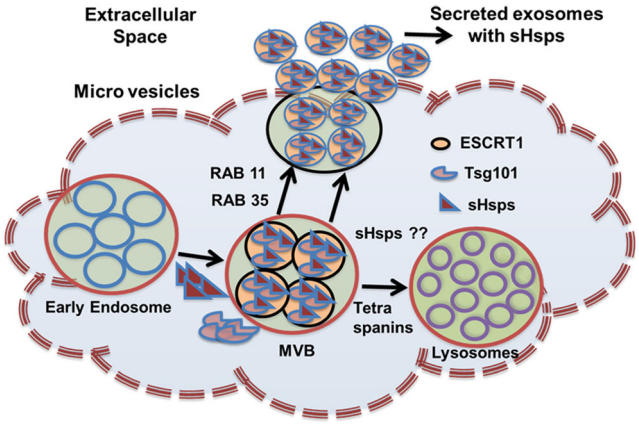


Fig. 2 Hypothetical model for export of small heat shock proteins (sHsps) into the extracellular medium. sHsps may be part of the ESCRT-I complex and involved in the biogenesis of exosomes by directly interacting with Tsg101, an important component of the ESCRT-I machinery, and they might also act as a branch point to decide the fusion of MVBs with plasma membrane or lysosome

of Hsp22 is least studied. Hsp22 is also known to be involved in inflammation of several pathologies. Immunohistochemistry and Western blot analysis in synovial tissues of rheumatoid arthritis patients showed increased expression of Hsp22 (Roelofs et al. 2006). It is also shown that Hsp22 activates dendritic cells upon its engagement with TLR4. Wilhelmus et al. (2009) reported the association of Hsp22 with cerebral amyloid angiopathy, hereditary cerebral hemorrhage, amyloidosis (Dutch type), and senile plaques in Alzheimer's disease. Hsp22 also induced the secretion of IL-6 in human brain pericytes, astrocytes, and microglia. However, the secretory pathway associated with Hsp22 extracellular levels is yet to be elucidated.

Conclusion and future prospects

Heat shock proteins are chaperones that prevent the aggregation of proteins and safeguard the cells from vicious insults. Previous studies reported the intracellular presence of Hsps. However, recently, this perception has changed owing to the extracellular presence of Hsps. Hsp27, αBC, and Hsp20 are secreted into the extracellular medium by a non-classical pathway. Secreted sHsps play an instrumental role in cell-to-cell communication, signaling, immunity, and inflammation. These proteins may act as part of the larger protein complex, for example by interacting with auto-antibodies in plasma or acting by binding to the cell surface receptors on immune/endothelial cells. sHsps also play a pivotal role in the biogenesis of exosomes. These proteins have also been shown to have therapeutic activity when administered extracellularly in in vitro and in vivo disease models. They attenuated the disease phenotype by chaperone, anti-apoptotic, anti-inflammatory, and anti-platelet activities. Many theories have been proposed to explain the secretion of sHsps into the extracellular medium including endolysosomal and exosomal pathways, direct translocation, and release after cell death. Among these, endolysosomal or exosomal pathways are shown to be predominant pathways utilized for the export of sHsps. Hsp27 shown to be secreted via exosomes and endolysosomes while αBC and Hsp20 via exosomes. The crucial role of sHsps in exosome biogenesis/generation should be studied in greater detail as αBC and Hsp20 are involved in exosome biogenesis and their interacting partners like Tsg 101 in the case of Hsp20. The contributory role of all the available sHsps in exosome biogenesis remains to be unanswered till date. Additionally, switching of secretory pathways from exosomes to endolysosomes and vice versa by sHsps and cell type-specific pathways is yet to be elucidated in greater detail. It is also possible that sHsps are involved in exosome biogenesis by participating in the ESCRT machinery in the generation of exosomes. The ESCRT multiprotein complex contains a set of cytosolic proteins that are incorporated into the endosomes by limiting membrane proteins. Proteins recruited to endosomes are usually tagged with ubiquitin on their cytosolic domains. Various types of ESCRT machinery are used in the biogenesis of exosomes including ESCRT-0, -I, -II, and -III. ESCRT-0 is involved in the trafficking of the ubiquitin-tagged proteins to ESCRT-I that are recognized by Tsg-101. It has been established that Hsp20 mediates biogenesis of exosomes by directly interacting with Tsg101. Hsp20 has a high affinity for Tsg101 and less affinity for Rab11 a/b and Rab35 indicating that Hsp20 might be part of the ESCRT-I complex helping Tsg101 to recognize ubiquitin proteins. These studies also support the idea that Hsp20 is localized in the lumen of exosomes as Tsg101 is used as an internal marker of exosomes. Another hypothesis is that, owing to the anti-aggregation effect of sHsps, they might participate in ESCRT complexes to sort out the proteins into vesicles. sHsps might also decide the fate of MVBs in fusion with lysosomes or plasma membrane as suggested in the case of αBC. The role of sHsps in exosome biogenesis was depicted in Fig. 2.

After all these observations, a lot to be resolved regarding the mechanisms by which sHsps find their way to the extracellular milieu with varied functions: in-depth molecular mechanistic details and interactions involved in secretion, role of sHsp auto-antibodies in blood, elucidating the presence of sHsps on the membrane/luminal portion of extracellular vesicles, determining how they bind to cell surface receptors and communicate with distant cells, determining the half-life of extracellular sHsps, and explicating several activities of extracellularly administered sHsp and how they cross the various barriers to exert their effect. Furthermore, studies should be conducted to exploit the benefits of exosomes packed with sHsps in various disease models. The therapeutic effect of exosomes encased with Hsp27, αBC, and Hsp20 should be studied by injecting them in disease models including

neurodegeneration, cancer, diabetes, and ischemia/reperfusion. All these studies are likely to help develop extracellular sHsps as therapeutic molecules and as native proteins/peptides/exosomes encased with sHsps, encapsulation of sHsps with nano- and microparticles or cell penetration peptides.

Acknowledgments This work is supported by the Science and Engineering Research Board-Early Career Research (SERB-ECR) grant (ECR 2017/000277/LS), Government of India to VSR. MSK is supported by a National Institutes of Health grant (NHLBI 1R01 HL134801) and a USA Department of Defense grant (W81XWH-17-1-0666). JT is supported by Research Initiation Grant (BITS/GAU/RIG/2017/77) and OPERA award (FR/SCM/160317/BIO) from BITS-Pilani, Hyderabad Campus, India. GBR is supported by grants from SERB (SB/S0/HS-192/2013), Department of Biotechnology (BT/PR10658/PFN/20/806/201) and Department of Health Research (DHR/HRD/Fellowship/SUG-04/2015-16), Government of India.

References

Al-Madhoun AS, Chen YX, Haidari L, Rayner K, Gerthoffer W, McBride H, O'Brien ER (2007) The interaction and cellular localization of HSP27 and ERbeta are modulated by 17beta-estradiol and HSP27 phosphorylation. Mol Cell Endocrinol 270:33–42

Arac A, Brownell SE, Rothbard JB, Chen C, Ko RM, Pereira MP, Albers GW, Steinman L, Steinberg GK (2011) Systemic augmentation of alphaB-crystallin provides therapeutic benefit twelve hours post-stroke onset via immune modulation. Proc Natl Acad Sci U S A 108:13287–13292

Arrigo AP (2005) Heat shock proteins as molecular chaperones. Med Sci (Paris) 21:619–625

Banerjee S, Lin CF, Skinner KA, Schiffhauer LM, Peacock J, Hicks DG, Redmond EM, Morrow D, Huston A, Shayne M, Langstein HN, Miller-Graziano CL, Strickland J, O'Donoghue L, De AK (2011) Heat shock protein 27 differentiates tolerogenic macrophages that may support human breast cancer progression. Cancer Res 71:318–327

Basha E, O'Neill H, Vierling E (2012) Small heat shock proteins and alpha-crystallins: dynamic proteins with flexible functions. Trends Biochem Sci 37:106–117

Basu S, Binder RJ, Suto R, Anderson KM, Srivastava PK (2000) Necrotic but not apoptotic cell death releases heat shock proteins, which deliver a partial maturation signal to dendritic cells and activate the NF-kappa B pathway. Int Immunol 12:1539–1546

Batulan Z, Pulakazhi Venu VK, Li Y, Koumbadinga G, Alvarez Olmedo DG, Shi C, O'Brien ER (2016) Extracellular release and signaling by heat shock protein 27: role in modifying vascular inflammation. Front Immunol 7:285

Benndorf R, Hayess K, Ryazantsev S, Wieske M, Behlke J, Lutsch G (1994) Phosphorylation and supramolecular organization of murine small heat shock protein HSP25 abolish its actin polymerization-inhibiting activity. J Biol Chem 269:20780–20784

Bhat S, Gangulam RK (2011) Secretion of αB-crystallin via exosomes. New clues to the function of human retinal pigment epithelium. Commun Integr Biol 4:739–741

Binder RJ, Vatner R, Srivastava P (2004) The heat-shock protein receptors: some answers and more questions. Tissue Antigens 64(4):442–451

Burut DF, Borai A, Livingstone C, Ferns G (2010) Serum heat shock protein 27 antigen and antibody levels appear to be related to the macrovascular complications associated with insulin resistance: a pilot study. Cell Stress Chaperones 15:379–386

Calderwood SK, Mambula SS, Gray PJ Jr, Theriault JR (2007) Extracellular heat shock proteins in cell signaling. FEBS Lett 581: 3689–3694

Ce P, Erkizan O, Gedizlioglu M (2011) Elevated HSP27 levels during attacks in patients with multiple sclerosis. Acta Neurol Scand 124: 317–320

Celet B, Akman-Demir G, Serdaroglu P, Yentur SP, Tasci B, van Noort JM, Eraksoy M, Saruhan-Direskeneli G (2000) Anti-alpha B-crystallin immunoreactivity in inflammatory nervous system diseases. J Neurol 247:935–939

Christopher KL, Pedler MG, Shieh B, Ammar DA, Petrash JM, Mueller NH (2014) Alpha-crystallin-mediated protection of lens cells against heat and oxidative stress-induced cell death. Biochim Biophys Acta 1843:309–315

Ciocca DR, Adams DJ, Edwards DP, Bjercke RJ, McGuire WL (1984) Estrogen-induced 24K protein in MCF-7 breast cancer cells is localized in granules. Breast Cancer Res Treat 4:261–268

Clayton A, Turkes A, Navabi H, Mason MD, Tabi Z (2005) Induction of heat shock proteins in B-cell exosomes. J Cell Sci 118:3631–3638

De Maio A (2011) Extracellular heat shock proteins, cellular export vesicles, and the stress observation system: a form of communication during injury, infection, and cell damage. It is never known how far a controversial finding will go! Dedicated to Ferruccio Ritossa. Cell Stress Chaperones 16:235–249

De Maio A, Vazquez D (2013) Extracellular heat shock proteins: a new location, a new function. Shock 40:239–246

Enomoto Y, Adachi S, Matsushima-Nishiwaki R, Niwa M, Tokuda H, Akamatsu S, Doi T, Kato H, Yoshimura S, Ogura S, Iwama T, Kozawa O (2009) alphaB-crystallin extracellularly suppresses ADP-induced granule secretion from human platelets. FEBS Lett 583:2464–2468

Fan GC, Chu G, Kranias EG (2005) Hsp20 and its cardioprotection. Trends in cardiovascular medicine 15:138–141

Fanelli MA, Cuello Carrion FD, Dekker J, Schoemaker J, Ciocca DR (1998) Serological detection of heat shock protein hsp27 in normal and breast cancer patients. Cancer Epidemiol Biomark Prev 7:791–795

Feng JT, Liu YK, Song HY, Dai Z, Qin LX, Almofti MR, Fang CY, Lu HJ, Yang PY, Tang ZY (2005) Heat-shock protein 27: a potential biomarker for hepatocellular carcinoma identified by serum proteome analysis. Proteomics 5:4581–4588

Gangalum RK, Bhat AM, Kohan SA, Bhat SP (2016) Inhibition of the expression of the small heat shock protein alphaB-crystallin inhibits exosome secretion in human retinal pigment epithelial cells in culture. J Biol Chem 291:12930–12942

Garrido C, Paul C, Seigneuric R, Kampinga HH (2012) The small heat shock proteins family: the long forgotten chaperones. Int J Biochem Cell Biol 44:1588–1592

Gastpar R, Gehrmann M, Bausero MA, Asea A, Gross C, Schroeder JA, Multhoff G (2005) Heat shock protein 70 surface-positive tumor exosomes stimulate migratory and cytolytic activity of natural killer cells. Cancer Res 65:5238–5247

Gruden G, Bruno G, Chaturvedi N, Burt D, Schalkwijk C, Pinach S, Stehouwer CD, Witte DR, Fuller JH, Perin PC (2008) Serum heat shock protein 27 and diabetes complications in the EURODIAB prospective complications study: a novel circulating marker for diabetic neuropathy. Diabetes 57:1966–1970

Gusev NB, Bogatcheva NV, Marston SB (2002) Structure and properties of small heat shock proteins (sHsp) and their interaction with cytoskeleton proteins. Biochemistry (Mosc) 67:511–519

Hacker S, Lambers C, Hoetzenecker K, Pollreisz A, Aigner C, Lichtenauer M, Mangold A, Niederpold T, Zimmermann M, Taghavi S, Klepetko W, Ankersmit HJ (2009) Elevated HSP27, HSP70 and HSP90 alpha in chronic obstructive pulmonary disease: markers for immune activation and tissue destruction. Clin Lab 55:31–40

Haslbeck M, Franzmann T, Weinfurtner D, Buchner J (2005) Some like it hot: the structure and function of small heat-shock proteins. Nat Struct Mol Biol 12:842–846

Havasi A, Li Z, Wang Z, Martin JL, Botla V, Ruchalski K, Schwartz JH, Borkan SC (2008) Hsp27 inhibits Bax activation and apoptosis via a phosphatidylinositol 3-kinase-dependent mechanism. J Biol Chem 283:12305–12313

Hecker JG, McGarvey M (2011) Heat shock proteins as biomarkers for the rapid detection of brain and spinal cord ischemia: a review and comparison to other methods of detection in thoracic aneurysm repair. Cell Stress Chaperones 16:119–131

Hegen H, Wanschitz J, Ehling R, Deisenhammer F, Loscher WN, Reindl M, Berger T (2010) Anti-alpha B-crystallin immunoreactivity in Guillain-Barre syndrome and chronic inflammatory demyelinating polyneuropathy. J Peripher Nerv Syst: JPNS 15:150–152

Hightower LE, Guidon PT Jr (1989) Selective release from cultured mammalian cells of heat-shock (stress) proteins that resemble glia-axon transfer proteins. J Cell Physiol 138:257–266

Holcakova J, Hernychova L, Bouchal P, Brozkova K, Zaloudik J, Valik D, Nenutil R, Vojtesek B (2008) Identification of alphaB-crystallin, a biomarker of renal cell carcinoma by SELDI-TOF MS. Int J Biol Markers 23:48–53

Horwitz J (1992) Alpha-crystallin can function as a molecular chaperone. Proc Natl Acad Sci U S A 89:10449–10453

Horwitz J, Huang QL, Ding L, Bova MP (1998) Lens alpha-crystallin: chaperone-like properties. Methods Enzymol 290:365–383

Huang Q, Ye J, Chen W, Wang L, Lin W, Lin J, Lin X (2010) Heat shock protein 27 is over-expressed in tumor tissues and increased in sera of patients with gastric adenocarcinoma. Clin Chem Lab Med 48:263–269

Huot J, Houle F, Spitz DR, Landry J (1996) HSP27 phosphorylation-mediated resistance against actin fragmentation and cell death induced by oxidative stress. Cancer Res 56:273–279

Jakhotia S, Sivaprasad M, Shalini T, Reddy PY, Viswanath K, Jakhotia K, Sahay R, Sahay M, Reddy GB (2017) Circulating levels of Hsp27 in microvascular complications of diabetes: prospects as a biomarker of diabetic nephropathy. J Diabetes Complications. http://dx.doi.org/10.1016/j.jdiacomp.2017.10.004

Janik S, Schiefer AI, Bekos C, Hacker P, Haider T, Moser J, Klepetko W, Mullauer L, Ankersmit HJ, Moser B (2016) HSP27 and 70 expression in thymic epithelial tumors and benign thymic alterations: diagnostic, prognostic and physiologic implications. Sci Rep 6:24267

Jia Y, Chen Y, Wang Q, Jayasinghe U, Luo X, Wei Q, Wang J, Xiong H, Chen C, Xu B, Hu W, Wang L, Zhao W, Zhou J (2017) Exosome: emerging biomarker in breast cancer. Oncotarget 8:41717–41733

Jin C, Cleveland JC, Ao L, Li J, Zeng Q, Fullerton DA, Meng X (2014) Human myocardium releases heat shock protein 27 (HSP27) after global ischemia: the proinflammatory effect of extracellular HSP27 through toll-like receptor (TLR)-2 and TLR4. Mol Med 20:280–289

Kanno Y, Matsuno H (2006) The possibility of novel antiplatelet peptides: the physiological effects of low molecular weight HSPs on platelets. Curr Pharm Des 12:887–892

Klopstein A, Santos-Nogueira E, Francos-Quijorna I, Redensek A, David S, Navarro X, Lopez-Vales R (2012) Beneficial effects of alphaB-crystallin in spinal cord contusion injury. J Neurosci: Off J Soc Neurosci 32:14478–14488

Kore RA, Abraham EC (2016) Phosphorylation negatively regulates exosome mediated secretion of cryAB in glioma cells. Biochim Biophys Acta 1863:368–377

Kozawa O, Matsuno H, Niwa M, Hatakeyama D, Kato K, Uematsu T (2001) AlphaB-crystallin, a low-molecular-weight heat shock protein, acts as a regulator of platelet function. Cell Stress Chaperones 6:21–28

Kozawa O, Matsuno H, Niwa M, Hatakeyama D, Oiso Y, Kato K, Uematsu T (2002) HSP20, low-molecular-weight heat shock-related protein, acts extracellularly as a regulator of platelet functions: a novel defense mechanism. Life Sci 72:113–124

Kurnellas MP, Brownell SE, Su L, Malkovskiy AV, Rajadas J, Dolganov G, Chopra S, Schoolnik GK, Sobel RA, Webster J, Ousman SS, Becker RA, Steinman L, Rothbard JB (2012) Chaperone activity of small heat shock proteins underlies therapeutic efficacy in experimental autoimmune encephalomyelitis. J Biol Chem 287:36423–36434

Lee YJ, Lee HJ, Choi SH, Jin YB, An HJ, Kang JH, Yoon SS, Lee YS (2012) Soluble HSPB1 regulates VEGF-mediated angiogenesis through their direct interaction. Angiogenesis 15:229–242

Lehr S, Hartwig S, Lamers D, Famulla S, Muller S, Hanisch FG, Cuvelier C, Ruige J, Eckardt K, Ouwens DM, Sell H, Eckel J (2012) Identification and validation of novel adipokines released from primary human adipocytes. Mol Cell Proteomics: MCP 11:M111 010504

Liao WC, Wu MS, Wang HP, Tien YW, Lin JT (2009) Serum heat shock protein 27 is increased in chronic pancreatitis and pancreatic carcinoma. Pancreas 38:422–426

Luo X, Zuo X, Zhang B, Song L, Wei X, Zhou Y, Xiao X (2008) Release of heat shock protein 70 and the effects of extracellular heat shock protein 70 on the production of IL-10 in fibroblast-like synoviocytes. Cell Stress Chaperones 13:365–373

Mambula SS, Calderwood SK (2006) Heat shock protein 70 is secreted from tumor cells by a nonclassical pathway involving lysosomal endosomes. J Immunol 177:7849–7857

Mambula SS, Stevenson MA, Ogawa K, Calderwood SK (2007) Mechanisms for Hsp70 secretion: crossing membranes without a leader. Methods 43:168–175

Mannini B, Cascella R, Zampagni M, van Waarde-Verhagen M, Meehan S, Roodveldt C, Campioni S, Boninsegna M, Penco A, Relini A, Kampinga HH, Dobson CM, Wilson MR, Cecchi C, Chiti F (2012) Molecular mechanisms used by chaperones to reduce the toxicity of aberrant protein oligomers. Proc Natl Acad Sci U S A 109:12479–12484

Martin-Ventura JL, Duran MC, Blanco-Colio LM, Meilhac O, Leclercq A, Michel JB, Jensen ON, Hernandez-Merida S, Tunon J, Vivanco F, Egido J (2004) Identification by a differential proteomic approach of heat shock protein 27 as a potential marker of atherosclerosis. Circulation 110:2216–2219

Masilamoni JG, Vignesh S, Kirubagaran R, Jesudason EP, Jayakumar R (2005) The neuroprotective efficacy of alpha-crystallin against acute inflammation in mice. Brain Res Bull 67:235–241

Masilamoni JG, Jesudason EP, Baben B, Jebaraj CE, Dhandayuthapani S, Jayakumar R (2006) Molecular chaperone alpha-crystallin prevents detrimental effects of neuroinflammation. Biochim Biophys Acta 1762:284–293

Matsuno H, Kozawa O, Niwa M, Usui A, Ito H, Uematsu T, Kato K (1998) A heat shock-related protein, p20, plays an inhibitory role in platelet activation. FEBS Lett 429:327–329

Mehlen P, Hickey E, Weber LA, Arrigo AP (1997) Large unphosphorylated aggregates as the active form of hsp27 which controls intracellular reactive oxygen species and glutathione levels and generates a protection against TNFalpha in NIH-3T3-ras cells. Biochem Biophys Res Commun 241:187–192

Merendino AM, Bucchieri F, Campanella C, Marciano V, Ribbene A, David S, Zummo G, Burgio G, Corona DF, Conway de Macario E, Macario AJ, Cappello F (2010) Hsp60 is actively secreted by human tumor cells. PLoS One 5:e9247

Miller H, Poon S, Hibbert B, Rayner K, Chen YX, O'Brien ER (2005) Modulation of estrogen signaling by the novel interaction of heat shock protein 27, a biomarker for atherosclerosis, and estrogen receptor beta: mechanistic insight into the vascular effects of estrogens. Arterioscler Thromb Vasc Biol 25:e10–e14

Miron T, Vancompernolle K, Vandekerckhove J, Wilchek M, Geiger B (1991) A 25-kD inhibitor of actin polymerization is a low molecular mass heat shock protein. J Cell Biol 114:255–261

Nafar F, Williams JB, Mearow KM (2016) Astrocytes release HspB1 in response to amyloid-beta exposure in vitro. J Alzheimer's Dis: JAD 49:251–263

Nahomi RB, Wang B, Raghavan CT, Voss O, Doseff AI, Santhoshkumar P, Nagaraj RH (2013) Chaperone peptides of alpha-crystallin inhibit epithelial cell apoptosis, protein insolubilization, and opacification in experimental cataracts. J Biol Chem 288:13022–13035

Nahomi RB, DiMauro MA, Wang B, Nagaraj RH (2015) Identification of peptides in human Hsp20 and Hsp27 that possess molecular chaperone and anti-apoptotic activities. Biochem J 465:115–125

Niwa M, Kozawa O, Matsuno H, Kato K, Uematsu T (2000) Small molecular weight heat shock-related protein, HSP20, exhibits an anti-platelet activity by inhibiting receptor-mediated calcium influx. Life Sci 66:PL7–P12

van Noort JM, Verbeek R, Meilof JF, Polman CH, Amor S (2006) Autoantibodies against alpha B-crystallin, a candidate autoantigen in multiple sclerosis, are part of a normal human immune repertoire. Mult Scler 12:287–293

van Noort JM, Bsibsi M, Nacken PJ, Gerritsen WH, Amor S, Holtman IR, Boddeke E, van Ark I, Leusink-Muis T, Folkerts G, Hennink WE, Amidi M (2013) Activation of an immune-regulatory macrophage response and inhibition of lung inflammation in a mouse model of COPD using heat-shock protein alpha B-crystallin-loaded PLGA microparticles. Biomaterials 34:831–840

Park HK, Park EC, Bae SW, Park MY, Kim SW, Yoo HS, Tudev M, Ko YH, Choi YH, Kim S, Kim DI, Kim YW, Lee BB, Yoon JB, Park JE (2006) Expression of heat shock protein 27 in human atherosclerotic plaques and increased plasma level of heat shock protein 27 in patients with acute coronary syndrome. Circulation 114:886–893

Prudovsky I, Mandinova A, Soldi R, Bagala C, Graziani I, Landriscina M, Tarantini F, Duarte M, Bellum S, Doherty H, Maciag T (2003) The non-classical export routes: FGF1 and IL-1alpha point the way. J Cell Sci 116:4871–4881

Rayner K, Chen YX, McNulty M, Simard T, Zhao X, Wells DJ, de Belleroche J, O'Brien ER (2008) Extracellular release of the atheroprotective heat shock protein 27 is mediated by estrogen and competitively inhibits acLDL binding to scavenger receptor-A. Circ Res 103:133–141

Rayner K, Sun J, Chen YX, McNulty M, Simard T, Zhao X, Wells DJ, de Belleroche J, O'Brien ER (2009) Heat shock protein 27 protects against atherogenesis via an estrogen-dependent mechanism: role of selective estrogen receptor beta modulation. Arterioscler Thromb Vasc Biol 29:1751–1756

Reddy VS, Reddy GB (2015) Emerging role for alphaB-crystallin as a therapeutic agent: pros and cons. Curr Mol Med 15:47–61

Reddy VS, Reddy GB (2016) Role of crystallins in diabetic complications. Biochim Biophys Acta 1860:269–277

Reddy GB, Kumar PA, Kumar MS (2006) Chaperone-like activity and hydrophobicity of alpha-crystallin. IUBMB Life 58:632–641

Reddy VS, Raghu G, Reddy SS, Pasupulati AK, Suryanarayana P, Reddy GB (2013) Response of small heat shock proteins in diabetic rat retina. Invest Ophthalmol Vis Sci 54:7674–7682

Reddy VS, Kumar CU, Raghu G, Reddy GB (2014) Expression and induction of small heat shock proteins in rat heart under chronic hyperglycemic conditions. Arch Biochem Biophys 558C:1–9

Reddy VS, Jakhotia S, Reddy PY, Reddy GB (2015) Hyperglycemia induced expression, phosphorylation, and translocation of alphaB-crystallin in rat skeletal muscle. IUBMB Life 67:291–299

Roelofs MF, Boelens WC, Joosten LA, Abdollahi-Roodsaz S, Geurts J, Wunderink LU, Schreurs BW, van den Berg WB, Radstake TR (2006) Identification of small heat shock protein B8 (HSP22) as a novel TLR4 ligand and potential involvement in the pathogenesis of rheumatoid arthritis. J Immunol 176:7021–7027

Rogalla T, Ehrnsperger M, Preville X, Kotlyarov A, Lutsch G, Ducasse C, Paul C, Wieske M, Arrigo AP, Buchner J, Gaestel M (1999) Regulation of Hsp27 oligomerization, chaperone function, and protective activity against oxidative stress/tumor necrosis factor alpha by phosphorylation. J Biol Chem 274:18947–18956

Rothbard JB, Zhao X, Sharpe O, Strohman MJ, Kurnellas M, Mellins ED, Robinson WH, Steinman L (2011) Chaperone activity of alpha B-crystallin is responsible for its incorrect assignment as an autoantigen in multiple sclerosis. J Immunol 186: 4263–4268

Rothbard JB, Kurnellas MP, Brownell S, Adams CM, Su L, Axtell RC, Chen R, Fathman CG, Robinson WH, Steinman L (2012) Therapeutic effects of systemic administration of chaperone alphaB-crystallin associated with binding proinflammatory plasma proteins. J Biol Chem 287:9708–9721

Salari S, Seibert T, Chen YX, Hu T, Shi C, Zhao X, Cuerrier CM, Raizman JE, O'Brien ER (2013) Extracellular HSP27 acts as a signaling molecule to activate NF-kappaB in macrophages. Cell Stress Chaperones 18:53–63

Salinthone S, Tyagi M, Gerthoffer WT (2008) Small heat shock proteins in smooth muscle. Pharmacol Ther 119:44–54

Santos TG, Martins VR, Hajj GNM (2017) Unconventional secretion of heat shock proteins in cancer. Int J Mol Sci 18(5):946

Schmitt E, Gehrmann M, Brunet M, Multhoff G, Garrido C (2007) Intracellular and extracellular functions of heat shock proteins: repercussions in cancer therapy. J Leukoc Biol 81(1):15–27

Sreekumar PG, Kannan R, Kitamura M, Spee C, Barron E, Ryan SJ, Hinton DR (2010) AlphaB crystallin is apically secreted within exosomes by polarized human retinal pigment epithelium and provides neuroprotection to adjacent cells. PLoS One 5:e12578

Sreekumar PG, Chothe P, Sharma KK, Baid R, Kompella U, Spee C, Kannan N, Manh C, Ryan SJ, Ganapathy V, Kannan R, Hinton DR (2013) Antiapoptotic properties of alpha-crystallin-derived peptide chaperones and characterization of their uptake transporters in human RPE cells. Invest Ophthalmol Vis Sci 54: 2787–2798

Stope MB, Klinkmann G, Diesing K, Koensgen D, Burchardt M, Mustea A (2017) Heat shock protein HSP27 secretion by ovarian cancer cells is linked to intracellular expression levels, occurs independently of the endoplasmic reticulum pathway and HSP27's phosphorylation status, and is mediated by exosome liberation. Dis Markers 2017:1575374

Sun Y, MacRae TH (2005a) Small heat shock proteins: molecular structure and chaperone function. Cell Mol Life Sci 62:2460–2476

Sun Y, MacRae TH (2005b) The small heat shock proteins and their role in human disease. FEBS J 272:2613–2627

Thuringer D, Jego G, Wettstein G, Terrier O, Cronier L, Yousfi N, Hebrard S, Bouchot A, Hazoume A, Joly AL, Gleave M, Rosa-Calatrava M, Solary E, Garrido C (2013) Extracellular HSP27 mediates angiogenesis through Toll-like receptor 3. FASEB J 27:4169–4183

Thuringer D, Berthenet K, Cronier L, Solary E, Garrido C (2015) Primary tumor- and metastasis-derived colon cancer cells differently modulate connexin expression and function in human capillary endothelial cells. Oncotarget 6:28800–28815

Tokuda H, Kuroyanagi G, Tsujimoto M, Enomoto Y, Matsushima-Nishiwaki R, Onuma T, Kojima A, Doi T, Tanabe K, Akamatsu S, Iida H, Ogura S, Otsuka T, Iwama T, Tanikawa T, Ishikawa K, Kojima K, Kozawa O (2015) Release of phosphorylated HSP27 (HSPB1) from platelets is accompanied with the acceleration of aggregation in diabetic patients. PLoS One 10:e0128977

Tytell M, Greenberg SG, Lasek RJ (1986) Heat shock-like protein is transferred from glia to axon. Brain Res 363:161–164

Vega VL, Rodriguez-Silva M, Frey T, Gehrmann M, Diaz JC, Steinem C, Multhoff G, Arispe N, De Maio A (2008) Hsp70 translocates into the plasma membrane after stress and is released into the extracellular environment in a membrane-associated form that activates macrophages. J Immunol 180:4299–4307

Vos MJ, Hageman J, Carra S, Kampinga HH (2008) Structural and functional diversities between members of the human HSPB, HSPH, HSPA, and DNAJ chaperone families. Biochemistry 47:7001–7011

Wang X, Gu H, Huang W, Peng J, Li Y, Yang L, Qin D, Essandoh K, Wang Y, Peng T, Fan GC (2016) Hsp20-mediated activation of exosome biogenesis in cardiomyocytes improves cardiac function and angiogenesis in diabetic mice. Diabetes 65:3111–3128

Wilhelmus MM, Boelens WC, Kox M, Maat-Schieman ML, Veerhuis R, de Waal RM, Verbeek MM (2009) Small heat shock proteins associated with cerebral amyloid angiopathy of hereditary cerebral hemorrhage with amyloidosis (Dutch type) induce interleukin-6 secretion. Neurobiol Aging 30:229–240

Wu N, Yu J, Chen S, Xu J, Ying X, Ye M, Li Y, Wang Y (2014) Alpha-crystallin protects RGC survival and inhibits microglial activation after optic nerve crush. Life Sci 94:17–23

Yusuf N, Nasti TH, Huang CM, Huber BS, Jaleel T, Lin HY, Xu H, Elmets CA (2009) Heat shock proteins HSP27 and HSP70 are present in the skin and are important mediators of allergic contact hypersensitivity. J Immunol 182:675–683

Zhang X, Wang X, Zhu H, Kranias EG, Tang Y, Peng T, Chang J, Fan GC (2012) Hsp20 functions as a novel cardiokine in promoting angiogenesis via activation of VEGFR2. PLoS One 7:e32765

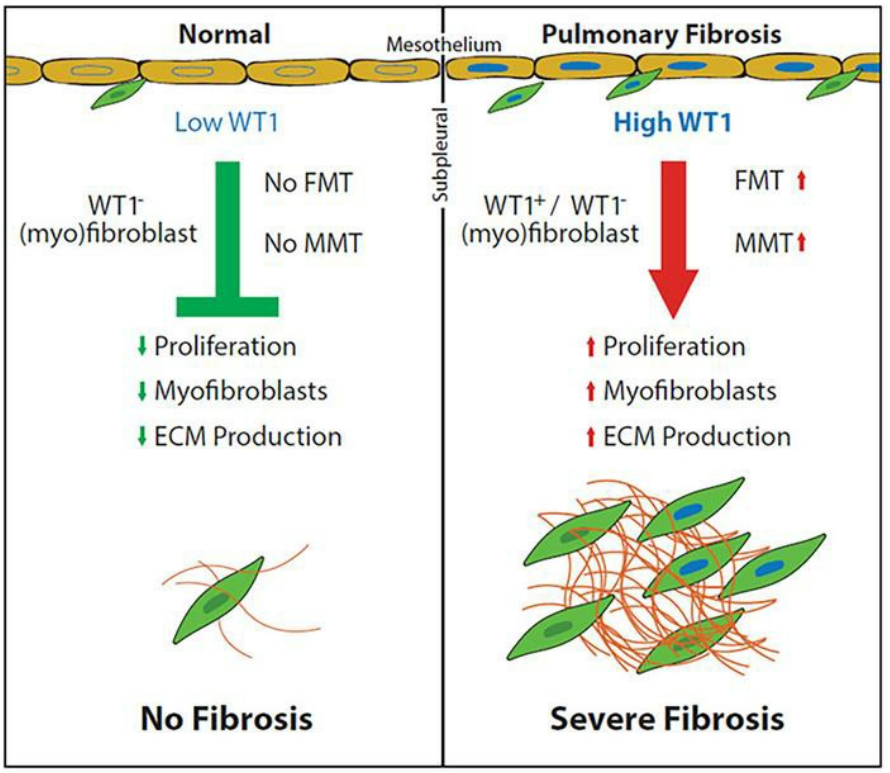
JCI insight

Wilms' tumor 1 drives fibroproliferation and myofibroblast transformation in severe fibrotic lung disease

Vishwaraj Sontake, … , Anil G. Jegga, Satish K. Madala

JCI Insight. 2018;3(16):e121252. https://doi.org/10.1172/jci.insight.121252.

Graphical abstract



Find the latest version:

http://jci.me/121252/pdf

JCI insight

RESEARCH ARTICLE

Wilms' tumor 1 drives fibroproliferation and myofibroblast transformation in severe fibrotic lung disease

Vishwaraj Sontake,[1,6] Rajesh K. Kasam,[1,2,6] Debora Sinner,[3,6] Thomas R. Korfhagen,[3,6] Geereddy B. Reddy,[2] Eric S. White,[4] Anil G. Jegga,[5,6] and Satish K. Madala[1,6]

[1]Division of Pulmonary Medicine, Cincinnati Children's Hospital Medical Center, Cincinnati, Ohio, USA. [2]Department of Biochemistry, National Institute of Nutrition, Hyderabad, Telangana, India. [3]Division of Neonatology and Pulmonary Biology, Cincinnati Children's Hospital Medical Center, Cincinnati, Ohio, USA. [4]Department of Internal Medicine, University of Michigan Health System, Ann Arbor, Michigan, USA. [5]Division of Biomedical Informatics Cincinnati Children's Hospital Medical Center, Cincinnati, Ohio, USA. [6]Department of Pediatrics, College of Medicine, University of Cincinnati, Cincinnati, Ohio, USA.

Wilms' tumor 1 (WT1) is a critical transcriptional regulator of mesothelial cells during lung development but is downregulated in postnatal stages and adult lungs. We recently showed that WT1 is upregulated in both mesothelial cells and mesenchymal cells in the pathogenesis of idiopathic pulmonary fibrosis (IPF), a fatal fibrotic lung disease. Although WT1-positive cell accumulation leading to severe fibrotic lung disease has been studied, the role of WT1 in fibroblast activation and pulmonary fibrosis remains elusive. Here, we show that WT1 functions as a positive regulator of fibroblast activation, including fibroproliferation, myofibroblast transformation, and extracellular matrix (ECM) production. Chromatin immunoprecipitation experiments indicate that WT1 binds directly to the promoter DNA sequence of α-smooth muscle actin (αSMA) to induce myofibroblast transformation. In support, the genetic lineage tracing identifies WT1 as a key driver of mesothelial-to-myofibroblast and fibroblast-to-myofibroblast transformation. Importantly, the partial loss of WT1 was sufficient to attenuate myofibroblast accumulation and pulmonary fibrosis in vivo. Further, our coculture studies show that WT1 upregulation leads to non–cell autonomous effects on neighboring cells. Thus, our data uncovered a pathogenic role of WT1 in IPF by promoting fibroblast activation in the peripheral areas of the lung and as a target for therapeutic intervention.

Introduction

Idiopathic pulmonary fibrosis (IPF) is a severe and chronic fibrotic lung condition that has been shown to associate with aging and is characterized by unrestrained mesenchymal cell activation such as proliferation, migration, differentiation, and extracellular matrix (ECM) deposition (1, 2). The prevalence of IPF is estimated to be between 1.25 and 23.4 cases per 100,000, with IPF incidence at approximately 200,000 in the US alone (3, 4). Histological evaluations of IPF biopsies has revealed the pattern of pulmonary fibrosis that is predominant in subpleural and paraseptal areas with architectural distortion, such as honeycombing, septal thickening, and fibrotic foci in the lung parenchyma (5, 6). Recent pulmonary imaging studies suggest that the early fibrotic lesions are initiated in the subpleural areas of IPF lungs (7, 8). However, cellular and molecular mechanisms of mesenchymal cell activation in the formation of early lesions and progressive expansion in the peripheral areas of IPF lungs remain unknown. In IPF, lung mesenchymal cell genes are transcriptionally dysregulated, leading to uncontrolled profibrotic signaling; this ultimately results in myofibroblast accumulation and ECM deposition, causing impaired lung function. Unfortunately, there are no effective treatments to slow the rate of progression or reverse pathological alterations in IPF. The present study was undertaken with the goal of identifying transcription factors activating profibrotic gene networks in mesenchymal cells in the pathogenesis of IPF. Such transcription factors and gene networks may be targets for modulating the fibrotic processes leading to IPF.

Wilms' tumor 1 (WT1) is a zinc-finger transcription regulator that is shown to play a critical role in Wilms' tumor and hematological malignancies but is not previously known to have a role in the patho-

Conflict of interest: The authors have declared that no conflict of interest exists.

Submitted: March 21, 2018
Accepted: July 11, 2018
Published: August 23, 2018

Reference information:
JCI Insight. 2018;3(16):e121252.
https://doi.org/10.1172/jci.insight.121252.

genesis of pulmonary fibrosis (9–11). Previous studies have demonstrated the ability of WT1 to directly regulate gene expression and RNA metabolism involved in the formation, maintenance, and repair of several vital organs such as lung, heart, and kidney (12–18). WT1 is shown to play an oncogenic role in leukemic blast cells by increasing the proliferation and survival of progenitor cells (9, 11). A considerable body of evidence exists that suggests that WT1 can function as either a positive or negative regulator of proliferation by associating with crucial proteins involved in the checkpoint signaling in multiple cancers (19–21). In embryonic development of the lung, WT1 is selectively expressed by the majority of mesothelial cells lining the lung parenchyma, and its expression is critical for lung development (13). Importantly, the loss of the WT1 gene results in embryonic lethality in mice at E13.5–E14.5 (16). Further, WT1-positive cells of the embryonic lung have been shown to act as progenitors for fibroblasts and smooth muscle cells in perivascular and peribronchial areas of the adult lung (13, 14). After birth, the WT1 expression is downregulated, with limited or no expression in mesothelial cells of the lung. However, our recent study demonstrated that WT1 is upregulated in both mesothelial and mesenchymal cells at the early stages of fibrotic lung disease and remains upregulated in myofibroblasts that accumulate in the subpleural areas of fibrotic lungs (22). Still, the molecular and functional contribution of this potentially novel zinc finger transcription factor in fibroblast activation and the pathogenesis of IPF is unknown. A recent study suggests that WT1 is expressed in mesothelial cells of normal lungs, while it is decreased in IPF lungs (23). The authors that WT1 functions as a negative regulator of mesothelial-to-myofibroblast differentiation in IPF. In contrast, we and others observed limited or no staining for WT1 in normal adult human lungs but elevated staining in lung mesenchymal and mesothelial cells of human IPF (8, 22, 24). Further, our coimmunostaining studies showed that the reactivated WT1 is selectively localized in the nucleus of lung mesenchymal cells positive for either vimentin or α-smooth muscle actin (αSMA) in IPF compared with normal lungs. Therefore, it is essential to understand the mechanisms underpinning the detrimental impact of WT1 upregulation on fibroblast gene expression, which is critical for designing strategies to attenuate IPF and other fibrotic lung diseases.

In the present study, we sought to evaluate the effects of WT1 in fibroproliferation, myofibroblast differentiation, and ECM production in pulmonary fibrosis. We performed pulse-chase studies using lineage-tracing mice for WT1-positive cells to investigate their fate in the pathogenesis of pulmonary fibrosis. Our findings show WT1 is a master regulator of multiple profibrotic processes, including proliferation, myofibroblast transformation, and ECM production. Notably, WT1-positive mesothelial cells lining the lungs transform into myofibroblasts. These data show for the first time to our knowledge that WT1 functions as a positive regulator of fibrosis in peripheral areas of the lung by influencing profibrotic functions of WT1-negative fibroblasts in the pathogenesis of pulmonary fibrosis.

Results

The lineage tracing of postnatal WT1-positive mesothelial cells demonstrates mesothelial-to-myofibroblast transformation in vivo. WT1 is highly expressed in the lung during embryonic stages of lung development but is downregulated later in adult lungs (13). To determine the kinetics of WT1 expression during lung development, we collected lung tissues from E12.5 embryos through 3-week-old adult mice. WT1 was developmentally regulated in murine lungs with higher expression at E12.5 and E13.5, but it was significantly downregulated from E14.5 to postnatal stages, with the maintenance of low expression levels throughout adulthood (Figure 1A). To identify which cell types within embryonic lungs express a WT1 protein, immunostaining was performed on E15.5 lung sections from αSMA reporter mice with antibodies directed against WT1 and calretinin, a mesothelial cell marker. At E15.5, WT1 was selectively expressed by mesothelial cells lining the lung (calretinin-positive) but it was not detected in myofibroblasts (Figure 1B). Indeed, the lung sections show colocalized expression of WT1 and calretinin in mesothelial cells lining the embryonic lungs at E15.5 (Figure 1C). WT1 protein is undetectable in pulmonary epithelial cells or endothelial cells in embryonic or adult lungs (data not shown). In contrast, WT1 was upregulated in mesothelial cells, fibroblasts, and myofibroblasts of subpleural fibrotic lesions in IPF and mouse models of TGFα-induced pulmonary fibrosis (22, 25).

Recent studies from our group and others have shown that $WT1^{CreERT2/-}$ mice can be used to track the genetic lineage of WT1-expressing cells (16, 22). Upon WT1 expression, cells undergo Cre-driven genetic recombination to activate EGFP expression in WT1-expressing cells. The lineage-tracing studies suggest that WT1-positive mesothelial cells of embryonic lungs can give rise to mesenchymal cells that populate in the lung parenchyma. To demonstrate whether postnatal mesothelial cells of the lung transform to

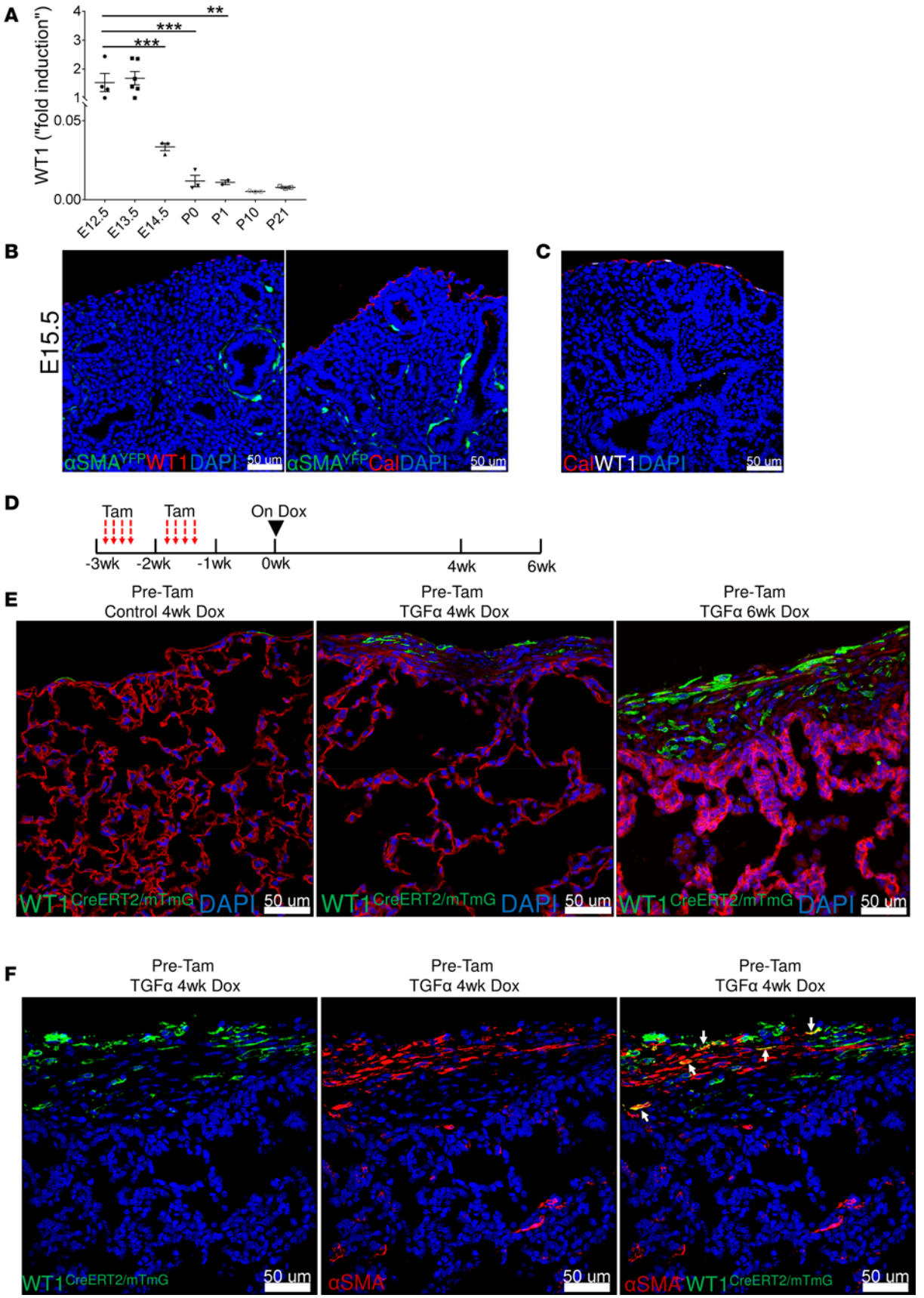


Figure 1. Postnatal WT1-positive mesothelial cell contributions to myofibroblasts in pulmonary fibrosis. (**A**) The dramatic decrease in the expression of WT1 in developing mouse lung at E14.5 and expression levels were normalized to HPRT mRNA (n = 3–5/gestational age). Data are presented as mean ± SEM. Statistical significance was calculated using 1-way ANOVA with Sidak's multiple comparison for multiple comparisons. $^{**}P < 0.005$, $^{***}P < 0.0005$.

(**B**) Immunostaining shows the presence of WT1 protein in mesothelial cells (pleural surface) that coexpress calretinin (red) but not in myofibroblasts (green) of αSMA^{YFP} mice embryos at E15.5. Scale bar: 50 μm. (**C**) WT1 staining (white) is detected in a subset of mesothelial cells positive for calretinin (red) in WT mice embryos at E15.5. Scale bar: 50 μm. (**D**) Schematic diagram of treatments with tamoxifen and Dox. Control or TGFα/WT1$^{CreERT2/mTmG}$ mice were induced with tamoxifen, and 1 week later, pulmonary fibrosis was induced by administering Dox in food for 4 or 6 weeks. (**E**) Immunofluorescence images show progressive accumulation of WT1-derived cells residing in subpleura but not adventitia in TGFα/WT1$^{CreERT2/mTmG}$ mice compared with control WT1$^{CreERT2/mTmG}$ mice on Dox for 4 or 6 weeks. Scale bar: 50 μm. (**F**) Immunostaining shows the presence of αSMA protein in WT1-positive mesothelium-derived mesenchymal cells of TGFα/WT1$^{CreERT2/mTmG}$ mice on Dox for 4 weeks. Note the presence of 2 distinct mesenchymal cells in subpleural fibrotic lesions that are marked by αSMA protein in GFP-positive cells (WT1-positive mesothelial cells) and GFP-negative (WT1-positive mesenchymal cells) cells. Scale bar: 50 μm.

myofibroblasts, we generated WT1 reporter mice (WT1$^{CreERT2/mTmG}$ mice) to trace the fate of WT1-positive mesothelial cells in adult mice during TGFα-induced pulmonary fibrosis. To label WT1-positive mesothelial cells in healthy adult mice, tamoxifen was administered for 4 days per week for a total of 2 weeks, and a week later, mice were kept on doxycycline (Dox) food for 4 or 6 weeks to cause moderate to severe fibrotic lesions by TGFα overexpression in vivo (Figure 1D). Confocal image analysis of the subpleural fibrotic lesions shows a progressive increase in mesenchymal cells that originate from WT1-expressing postnatal mesothelium in subpleural fibrotic lesions (Figure 1E). However, green cells derived from WT1-positive mesothelium were restricted to subpleural fibrotic lesions and did not populate in alveolar and adventitial areas of established fibrotic lesions with 6 weeks on Dox (Supplemental Figure 1, A and B; supplemental material available online with this article; https://doi.org/10.1172/jci.insight.121252DS1). To further establish mesothelium-to-myofibroblast transformation in vivo, the lung sections of WT1$^{CreERT2/-}$ reporter mice on Dox for 6 weeks were immunostained with antibodies against αSMA. We detected several αSMA-positive green cells present in subpleural fibrotic lesions of TGFα/WT1$^{CreERT2/mTmG}$ mice on Dox for 6 weeks, indicating that some myofibroblasts were derived from mesothelial cells (Figure 1F). We observed many αSMA-negative green cells (likely fibroblasts) that may have originated from mesothelial cells. Also, we observed an accumulation of myofibroblasts that derived from WT1-negative mesothelial cells in subpleural fibrotic lesions of TGFα/WT1$^{CreERT2/mTmG}$ mice on Dox for 6 weeks. The above findings suggest accumulation of mesothelial cell– and nonmesothelial cell–derived myofibroblasts in subpleural fibrotic lesions. These data are consistent with our previous data showing that WT1 is reactivated in both mesothelial cells and mesenchymal cells (fibroblast and myofibroblasts) in IPF and mouse models of TGFα-induced pulmonary fibrosis.

WT1 lineage cells are the major source of mesenchymal cells in subpleural fibrotic lesions. To determine whether WT1 lineage cells contribute to the majority of mesenchymal cells, we treated TGFα/WT1$^{CreERT2/mTmG}$ mice or WT1$^{CreERT2/mTmG}$ control mice with tamoxifen for 4 days per week for a total of 2 weeks before Dox food (before tamoxifen; Pre-Tam) or continued with tamoxifen treatments at week 2 and 4 on Dox (Pre-Tam or after tamoxifen [Post-Tam]) (Figure 2A). The lungs were cultured for 7 days and were then analyzed by flow cytometry for GFP-positive fibroblasts (Supplemental Figure 2). In support of our hypothesis, we observed a significant increase in GFP-positive mesenchymal cells in lungs cultured from mice treated with tamoxifen continuously (3.1% ± 0.12%) compared with Pre-Tam–treated TGFα/WT1$^{CreERT2/mTmG}$ (1.75% ± 0.05%) or WT1$^{CreERT2/mTmG}$ control mice (0.3% ± 0.00%) on Dox for 4 weeks (Figure 2, B and C). In addition, confocal imaging of lung sections shows that the majority of mesenchymal cells that accumulate in subpleural fibrotic lesions were derived from WT1-positive postnatal lung cells (Figure 2D). Moreover, we observed a significant increase in WT1-positive cells in reporter mice that were treated with tamoxifen continuously compared with Pre-Tam treated TGFα/WT1$^{CreERT2/mTmG}$ mice or non-TGFα/WT1$^{CreERT2/mTmG}$ mice on Dox for 4 weeks. Taken together, our results demonstrate that most mesenchymal cells within subpleural fibrotic lung lesions originated from WT1-positive mesothelial cells and fibroblasts. Both the above populations were localized in subpleural fibrotic lesions but not in lung parenchyma or adventitia (Supplemental Figure 1B). Together, these findings suggest that myofibroblasts that accumulate in subpleural fibrotic lesions following TGFα overexpression are derived from both mesothelial cells and lung-resident fibroblasts, perhaps through increased induction of WT1 in subpleural fibrotic lesions. These findings further support fibroblast heterogeneity and possible cross-talk between multiple mesenchymal cell types in the pathogenesis of the severe fibrotic disease.

WT1 is a positive regulator of fibroblast-to-myofibroblast transformation. Progressive accumulation of myofibroblasts is an essential determinant of pulmonary fibrosis, as they are responsible for pathological contractures and the excessive ECM deposition in the mature fibrotic lesions of human IPF (26–29). We observed a significant

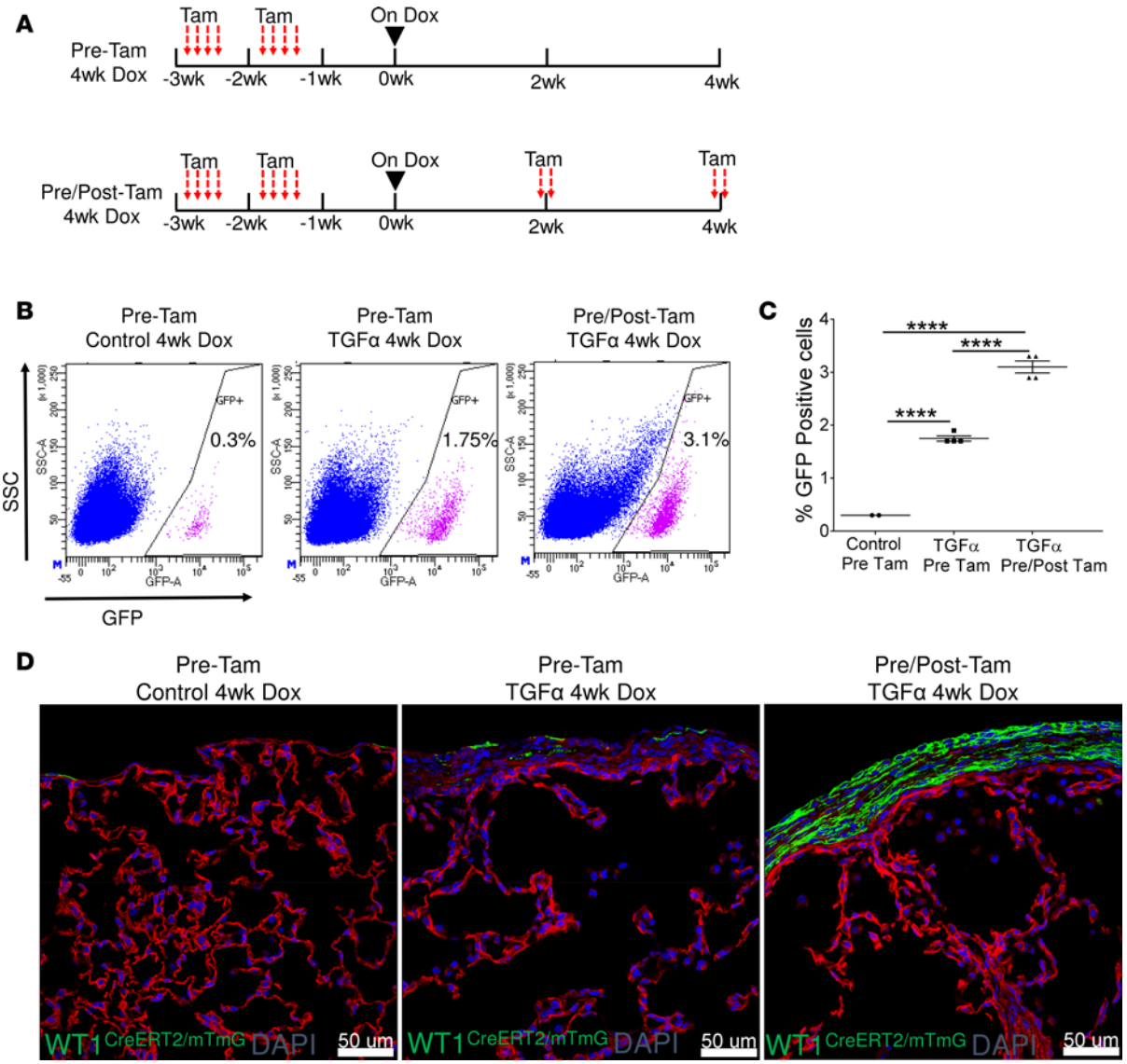


Figure 2. WT1-lineage cells are the major source of mesenchymal cells in subpleural fibrotic lesions in vivo. (**A**) Schematic diagram of treatments with tamoxifen and Dox. For pretamoxifen treatments (Pre-Tam), control, or TGFα/WT1$^{CreERT2/mTmG}$ mice were induced with tamoxifen, and 1 week later, pulmonary fibrosis was induced by administering Dox in food for 4 weeks. For Pre- and posttamoxifen treatments (Pre/Post-Tam), TGFα/WT1$^{CreERT2/mTmG}$ mice were treated with tamoxifen before and after pulmonary fibrosis was induced by Dox in food for 4 weeks. (**B**) Representative FACS plots show increased accumulation of WT1-drived myofibroblasts in Pre-/Post-Tam–treated TGFα/WT1$^{CreERT2/mTmG}$ mice compared with Pre-Tam–treated TGFα/WT1$^{CreERT2/mTmG}$ mice or control mice on Dox for 4 weeks. (**C**) Quantification of GFP-positive myofibroblasts in lung cultures of tamoxifen-treated TGFα/WT1$^{CreERT2/mTmG}$ mice or control mice on Dox for 4 weeks. (**D**) Immunofluorescence images show increased accumulation of WT1-derived mesenchymal cells residing in subpleura but not adventitia in tamoxifen-treated TGFα/WT1$^{CreERT2/mTmG}$ mice compared with control mice on Dox for 4 weeks. Scale bar: 50 μm.

increase in the transcript levels of WT1 and αSMA in primary fibroblasts isolated from fibroblast cultures of non-IPF lungs infected with WT1-overexpressing virus compared with control virus infections (Figure 3A). Also, we detected a significant increase in αSMA protein levels in cells infected with WT1-overexpressing virus compared with control virus infections (Figure 3B). Additionally, lentivirus-mediated (lenti-mediated) overexpression of WT1 was sufficient to increase the αSMA expression in murine lung-resident fibroblasts (Figure 3C).

To evaluate the role of WT1 in fibroblast-to-myofibroblast transformation, we used a cell fate–mapping strategy based on lineage-specific expression of αSMA in lung-resident fibroblasts isolated from αSMA reporter mice (αSMA$^{CreERT2/mTmG}$ mice). In this model, activation of Cre recombinase under control of αSMA promoter removes the STOP cassette between the 2 loxP sites, which irreversibly changes the expression of membrane tomato (mT) to membrane GFP (mG) in αSMA-expressing lung-resident fibroblasts. We isolated the lung-resident fibroblasts from lung cultures of αSMA reporter mice and transduced each with either

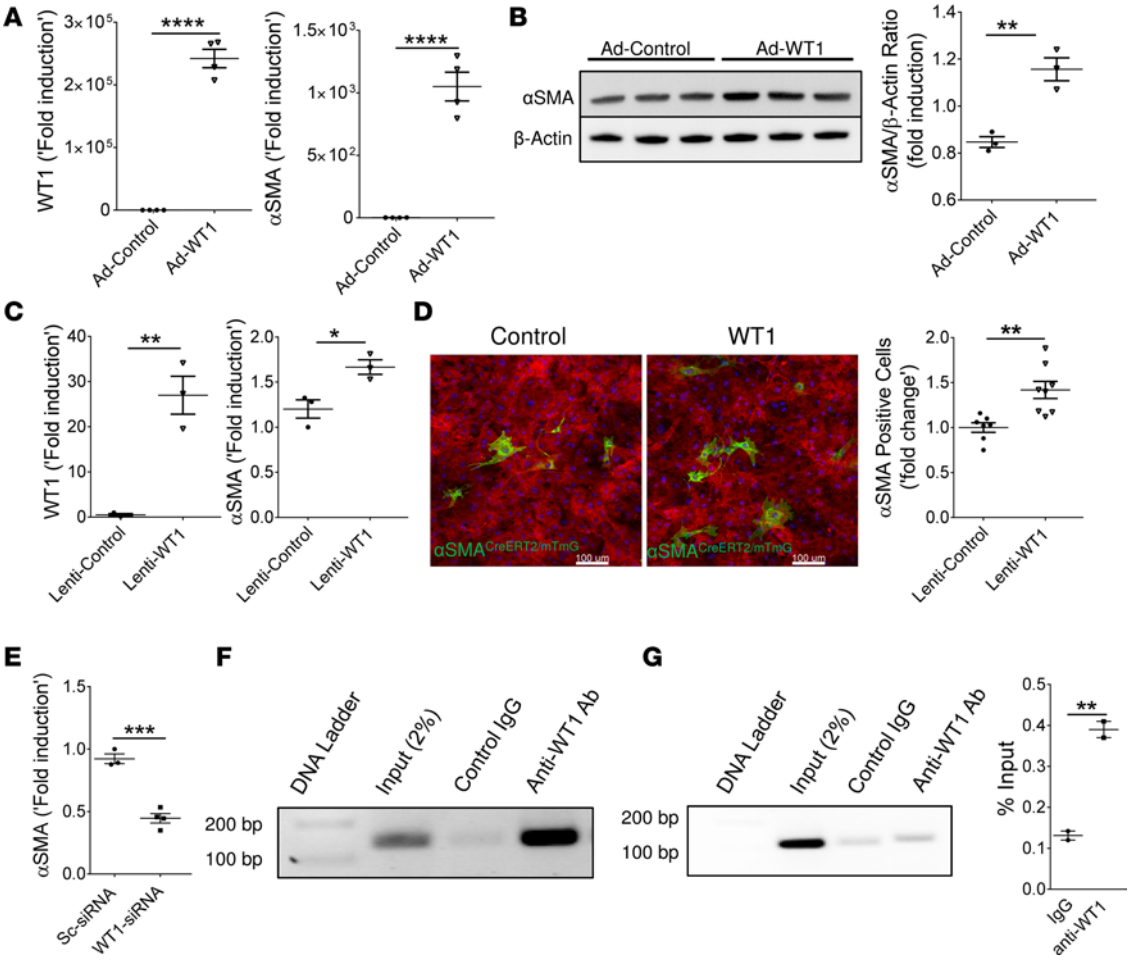


Figure 3. WT1 is a positive regulator of fibroblast-to-myofibroblast transformation. (**A**) Human non-IPF fibroblasts were transduced with either control adenovirusor WT1 adenovirus for 24 hours. Transcripts of WT1 and αSMA were quantified using RT-PCR (n = 6). Results are cumulative, from 2 independent experiments with similar results. (**B**) Human non-IPF fibroblasts were transduced with either control adenovirusor WT1 adenovirus for 72 hours. Protein lysates were immunoblotted for αSMA and β-actin. αSMA quantification was performed by normalizing to the endogenous β-actin control. Results are representative of 2 independent experiments with similar results (n = 3). (**C**) Fibroblasts of nontransgenic mice on Dox for 4 weeks were transduced with either control lentivirus or WT1 lentivirus (10 MOI) for 24 hours. Transcripts of WT1 and αSMA were quantified using RT-PCR (n = 3). Results are representative of 3 independent experiments with similar results. (**D**) Fibroblasts of $\alpha SMA^{CreERT2/mTmG}$ mice were transduced with either control lentivirus or WT1 lentivirus for 72 hours in the presence of 4-hydroxy tamoxifen. Immunofluorescence images were obtained at an original magnification of ×20. Scale bar: 100 μm. The number of αSMA-positive (GFP-positive) myofibroblasts were quantified in images, and the data shown are cumulative of 2 independent experiments with similar results (n = 4). (**E**) Fibroblasts from IPF primary lung cultures were transiently transfected with either control or WT1-specific siRNA for 72 hours, and αSMA gene expression was analyzed by RT-PCR. Results are representative of 2 independent experiments with similar results (n = 4). (**F**) IMR-90 cells were transduced with WT1 adenovirus (100 MOI) for 72 hours. Cell lysates were prepared, and the ChIP assay was performed with anti-WT1 antibody or normal rabbit IgG as a negative control using αSMA gene promoter–specific PCR primers. Nonimmunoprecipitated DNA is represented as input DNA (product size, 140 bp). (**G**) Primary lung-resident fibroblasts were isolated from lung cultures of TGFα mice placed on Dox for 8 weeks. Cell lysates were prepared, and the ChIP assay was performed with anti-WT1 antibody or normal rabbit IgG as a negative control using αSMA gene promoter–specific PCR primers. Nonimmunoprecipitated DNA is represented as input DNA (product size, 104 bp). Data are representative of 2 independent experiments. Data are presented as mean ± SEM. Unpaired Student t test, $^{*}P < 0.05$, $^{**}P < 0.005$, $^{***}P < 0.0005$, $^{****}P < 0.0001$.

control or WT1-overexpressing lentivirus in the presence of hydroxy-tamoxifen. We observed a significant increase in the number of transformed green cells, showing a fibroblast-to-myofibroblast transformation (Figure 3D). Further, the knockdown of WT1 significantly diminished the αSMA gene expression in lung-resident fibroblasts isolated from fibrotic lungs of IPF patients (Figure 3E).

To determine whether the observed increases in αSMA levels and myofibroblast transformation could be due to direct or indirect effects by WT1, we performed a computational analysis of the sequence of human and mouse αSMA promoter regions for possible WT1 binding sites, which revealed the presence of

WT1 binding sites that are highly conserved among mammals, including human and mouse αSMA genes (Supplemental Figure 3). ChIP analysis in WT1-adenoviral–transfected IMR-90 fibroblasts using WT1 specific antibodies revealed that the WT1 bound more efficiently to the αSMA gene (Figure 3F), and no signal was observed with control isotype antibody, suggesting that this site may play an important role in WT1-mediated αSMA expression. Similarly, we performed ChIP analysis of αSMA promoter occupancy by WT1 in primary lung-resident fibroblasts isolated from TGFα mice placed on Dox for 8 weeks. ChIP analysis revealed that WT1 bound more efficiently to the αSMA gene compared with control isotype antibody (Figure 3G). Together, these data confirm that αSMA gene expression during myofibroblast transformation was mediated by binding of the WT1 transcription factor to the αSMA gene promoter. Taken together, our in vitro results establish that WT1 upregulation in lung-resident fibroblasts augments the transformation of fibroblasts to myofibroblasts.

WT1 is a positive regulator of profibrotic gene transcription and fibroproliferation in IPF. The loss of WT1 transcripts has resulted in reduced expression of multiple ECM genes in fibroblasts isolated from IPF lungs or mice with severe fibrotic lung disease (22). To gain insight into the global change in gene transcription due to WT1, we isolated fibroblasts from the lungs of transgenic mice carrying a Dox-regulated transgene leading to TGFα expression in lung epithelium. RNA sequencing (RNA-sequencing; RNA-Seq) showed that the knockdown of WT1 altered the expression of 2,425 genes, half of which were induced (1,193 genes) and half of which were repressed (1,232 genes) by WT1 (Supplemental Figure 4). To identify profibrotic gene transcripts altered by WT1 in IPF, we performed an enrichment analysis of the negatively correlated gene sets between IPF lungs and WT1-specific siRNA-treated lung fibroblasts (30). Gene expression profiles of IPF lungs from a previously published transcriptomic data set (8) (Gene Expression Omnibus [GEO] accession number GSE53845; https://www.ncbi.nlm.nih.gov/geo/query/acc.cgi) were compared with that of WT1 altered genes in fibroblasts, and we identified multiple transcripts that were either upregulated (107 genes) or downregulated (63 genes) by WT1 in IPF (Supplemental Figure 5A, Supplemental Table 1). Using ToppFun application of the ToppGene Suite (31), the top enriched biological processes common to both the IPF and WT1-specific data sets were proliferation, mesenchyme growth, development, and ECM production in IPF (Supplemental Figure 5B). To validate WT1-driven genes in fibroblasts, we performed reverse transcription PCR analysis of several ECM genes. Aside from WT1, we noted a significant reduction in transcripts for *Col14*, *Col15*, *Itg2*, *Itg7*, and *Lum*, suggesting that the maintenance of ECM is WT1 dependent (Supplemental Figure 5C).

Lung-resident fibroblasts have been shown to proliferate and serve as one of the major mesenchymal cell sources in the fibrotic lung lesions of IPF and mouse models of pulmonary fibrosis (32–37). Likewise, we observed higher proliferation capacity of lung-resident fibroblasts isolated from IPF lungs compared with fibroblasts isolated from normal lungs (Supplemental Figure 6). To determine the role of WT1 in fibroproliferation, we overexpressed WT1 in primary lung-resident fibroblasts isolated from normal lungs and quantified changes in proliferation. In order to clarify the status of WT1 in adenovirus-transduced cells, we performed Western blot analysis to demonstrate high amounts of WT1 in WT1–adenovirus-transduced cells compared with empty–adenovirus-transduced cells (Figure 4A). Adeno-mediated overexpression of WT1 caused a significant increase in the amount of proliferative cell nuclear antigen (PCNA) in lung-resident fibroblasts compared with cells infected with empty adenovirus (Figure 4A). Also, the knockdown of WT1 was sufficient to attenuate proliferation of lung-resident fibroblasts isolated from IPF lungs (Figure 4B). Lenti-mediated overexpression of WT1 increased the proliferative capacity of murine lung-resident fibroblasts (Figure 4C). Furthermore, the knockdown of WT1 significantly diminished proliferation of lung-resident fibroblasts isolated from fibrotic lungs of TGFα transgenic mice on Dox for 4 weeks (Figure 4D). Further, we observed a significant decrease in the number of PCNA-positive mouse fibroblasts with knockdown of WT1 using WT1-specific siRNA compared with control siRNA (Supplemental Figure 7). Together, these data demonstrate that the proliferative capacity of lung-resident fibroblasts was largely dependent on WT1 expression and indicates a positive regulation of fibroproliferation by WT1. Levels of WT1-driven proliferative genes in IPF, including *Grem1*, *Runx1*, *Wnt4*, *Stat3*, *Prrx1*, *Igf1*, *Ccnb1*, and *E2f8* were reduced in primary lung-resident fibroblasts of TGFα mice on Dox for 4 weeks treated with WT1 siRNA compared with those treated with control siRNA (Figure 4E). Notably, the genetic knockdown of WT1 was sufficient to attenuate the expression of WT1-driven proliferative genes that are associated with IPF. These findings establish that WT1 functions as a positive regulator of fibroproliferation in IPF.

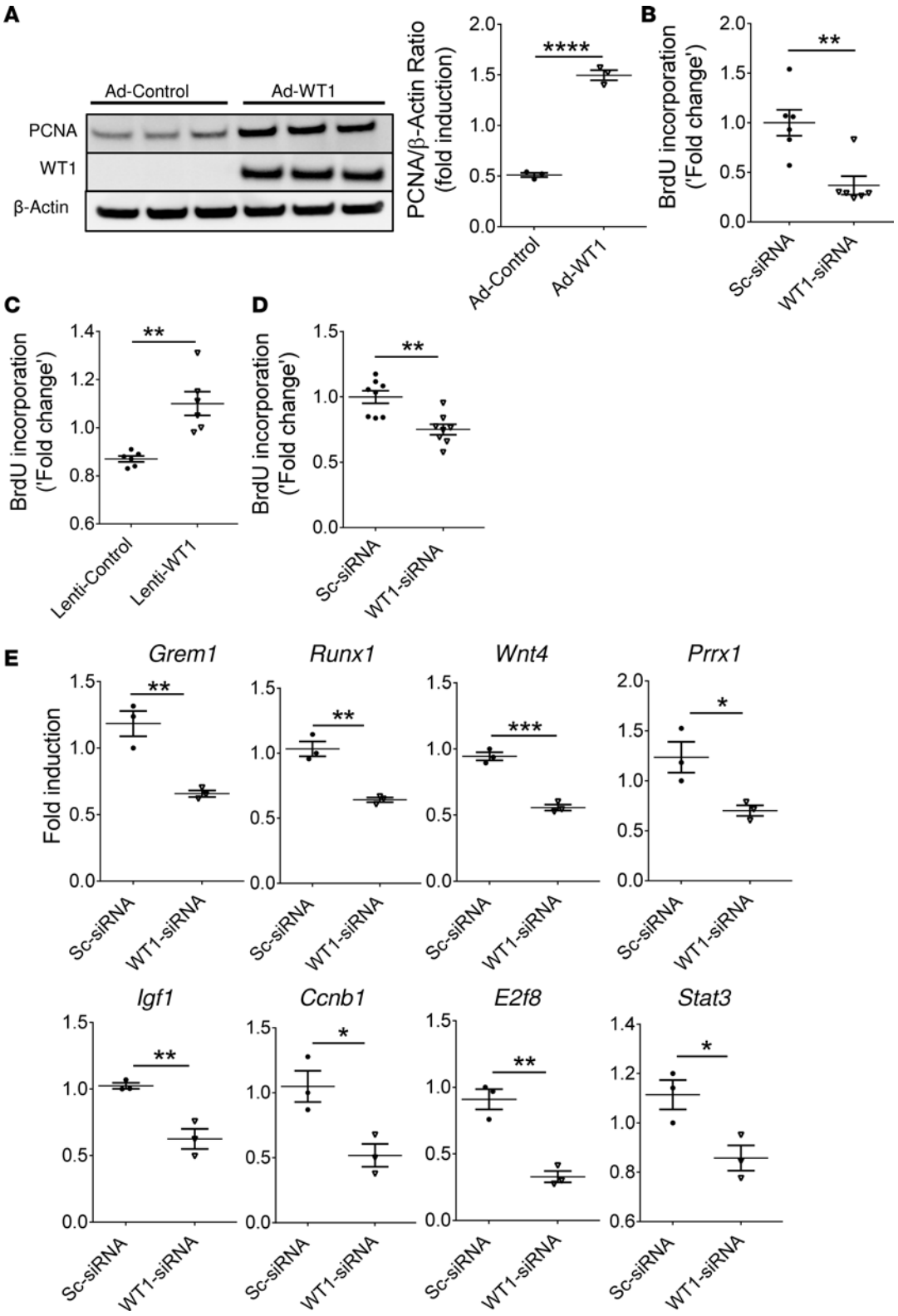


Figure 4. WT1 is a positive regulator of fibroproliferation. Primary lung-resident fibroblasts were isolated from the lung cultures of IPF, non-IPF, WT, or TGFα transgenic mice by negative selection using ant-CD45 magnetic beads. (**A**) Human non-IPF fibroblasts were transduced with either control adeno or WT1 adenovirus for 72 hours. Proliferation was assessed by immunoblotting WT1 and proliferating cell nuclear antigen (PCNA). PCNA quantification was performed by normalizing to the endogenous β-actin control. Results are representative of 2 independent experiments with similar results (n = 3). (**B**) Human IPF fibroblasts were transfected with either control or WT1 siRNA for 72 hours, and proliferation was assessed by BrdU incorporation. Results are cumulative of 2 independent experiments with similar results (n = 4). (**C**) Fibroblasts of nontransgenic mice on Dox for 4 weeks were transduced with either control lenti or WT1 lentivirus for 72 hours. Proliferation was assessed by BrdU incorporation assay. Results are representative of 2 independent

experiments with similar results (n = 6). (**D**) Fibroblasts of TGFα transgenic mice on Dox for 4 weeks were transiently transfected with either control or WT1 siRNA for 72 hours, and proliferation was assessed by BrdU incorporation. Results are cumulative of 2 independent experiments with similar results (n = 4). (**E**) WT1-driven proliferative genes including *Grem1*, *Runx1*, *Wnt4*, *Stat3*, *Prrx1*, *Igf1*, *Ccnb1*, and *E2f8* were quantified in fibroblasts of TGFα transgenic mice on Dox for 4 weeks transfected with either control or WT1 siRNA for 48 hours. Results are representative of 3 independent experiments with similar results (n = 3). Data are presented as mean ± SEM. Unpaired Student t test $^*P < 0.05$, $^{**}P < 0.005$, $^{***}P < 0.0005$, $^{****}P < 0.0001$.

The partial loss of WT1 was sufficient to attenuate pulmonary fibrosis in vivo. Our recent study demonstrated that conditional overexpression of TGFα or bleomycin-induced lung injury caused in WT1 upregulation and severe fibrotic lung disease with histologic features similar to human IPF (22, 38). Heterozygous $WT1^{CreERT2/-}$ mice (knock-in allele) are haploinsufficient for the WT1 allele ($WT1^{+/-}$) but display uninterrupted normal lung development in embryonic and adult stages, with viability similar to WT mice. Loss of a WT1 allele had no effect on lung morphology or collagen deposition (Supplemental Figure 8). We crossed TGFα mice with $WT1^{+/-}$ mice to generate a unique set of double- and triple-transgenic mice carrying mutant WT1 ($WT1^{+/-}$ and TGFα/$WT1^{+/-}$) or WT WT1 ($WT1^{+/+}$ and TGFα/$WT1^{+/+}$). To identify whether WT1 deficiency influences fibrosis susceptibility, mice were placed on Dox for 4 weeks, a time period that leads to significant lung fibrosis upon overexpression of TGFα. The loss of 1 allele of WT1 was sufficient to attenuate subpleural fibrosis in Dox-treated TGFα/$WT1^{+/-}$ mice compared with TGFα/$WT1^{+/+}$ mice (Figure 5A). To determine if WT1 haploinsufficiency affects rtTA-driven TGFα transgene expression, we measured transcripts of TGFα in all 4 groups. As expected, we observed an increase in TGFα transcripts in Dox-treated TGFα/$WT1^{+/+}$ and TGFα/$WT1^{+/-}$ mice, and TGFα transcripts did not differ between mutant and WT WT1 mice (Figure 5B). In support of our hypothesis, WT1 transcripts were attenuated in the lungs of Dox-treated TGFα/$WT1^{+/-}$ mice compared with TGFα/$WT1^{+/+}$ mice (Figure 5C), and reduction of WT1 transcripts was associated with a significant decrease in lung hydroxyproline levels (Figure 5D), as well as improvement in lung compliance (Figure 5E). To further substantiate that WT1 haploinsufficiency contributes to diminished fibrotic responses during bleomycin-induced fibrosis, WT and WT1 haploinsufficient mice were treated by intradermal injections of bleomycin for 5 days a week for a total of 4 weeks (22). Attenuation of Masson's trichrome staining in both subpleural and parenchymal areas of lung sections was detected in $WT1^{+/-}$ mice compared with $WT1^{+/+}$ mice treated with bleomycin (Figure 5F). Also, the transcripts of *Wt1*, *Col1α*, and *Col5α* genes were reduced in bleomycin-treated $WT1^{+/-}$ mice compared with $WT1^{+/+}$ mice (Figure 5, G–I), and lung function was improved in $WT1^{+/-}$ mice compared with $WT1^{+/+}$ mice (Figure 5J). Thus, our findings provide complementary and direct in vivo evidence that WT1 plays a pathogenic role in pulmonary fibrosis.

WT1 augments fibroproliferation and myofibroblast transformation in a non–cell autonomous manner. Using Ki67 as a marker of proliferation, we observed a notable decrease in Ki67-positive cells in both subpleural and adventitial areas in the lungs of TGFα/$WT1^{+/-}$ compared with TGFα/$WT1^{+/+}$ mice on Dox for 4 weeks (Figure 6A). Although WT1-expressing cells were localized to subpleural areas, we observed a significant decrease in the proliferation of parenchymal fibrotic lesions during TGFα- and bleomycin-induced pulmonary fibrosis. To identify myofibroblast accumulation, lung sections were immunostained with antibodies against αSMA. αSMA staining is attenuated in both subpleural and adventitial areas in the lungs of Dox-treated TGFα/$WT1^{+/+}$ mice compared with TGFα/$WT1^{+/-}$ mice (Figure 6B). Consistent with the above findings, we observed attenuation of myofibroblast accumulation in both subpleural and parenchymal areas of the lungs in $WT1^{+/+}$ mice compared with $WT1^{+/-}$ mice treated with bleomycin (Figure 6C). However, our recent studies demonstrated that WT1 expression is limited to subpleural areas of fibrotic lungs during TGFα- and bleomycin-induced pulmonary fibrosis (22).

To investigate possible crosstalk between WT1-positive and WT1-negative fibroblasts, we generated a potentially novel multitransgenic WT1 reporter mice by serial breeding of TGFα transgenic mice with WT1 mutant mice ($WT1^{+/}$) and $ROSA^{mTmG}$ mice. TGFα/$WT1^{CreERT2/mTmG}$ mice were kept on Dox food for 4 weeks, and lung-resident fibroblasts were isolated and treated with either control or WT1-specific siRNA and cultured with tamoxifen to identify the proliferative changes in both WT1-positive and WT1-negative lung-resident fibroblasts (Figure 6D). As expected, we observed a significant decrease in the number of PCNA-positive mouse fibroblasts and a decrease in WT1-expressing cells with the knockdown of WT1 compared with control siRNA (Figure 6, D and E). Notably, the proliferation was reduced in both $WT1^+$/$PCNA^+$ and $WT1^-$/$PCNA^+$ cells (Figure 6, F and G). Further, we performed transwell coculture studies in which WT1-overexpressing lung-resident fibroblasts isolated from TGFα mice on

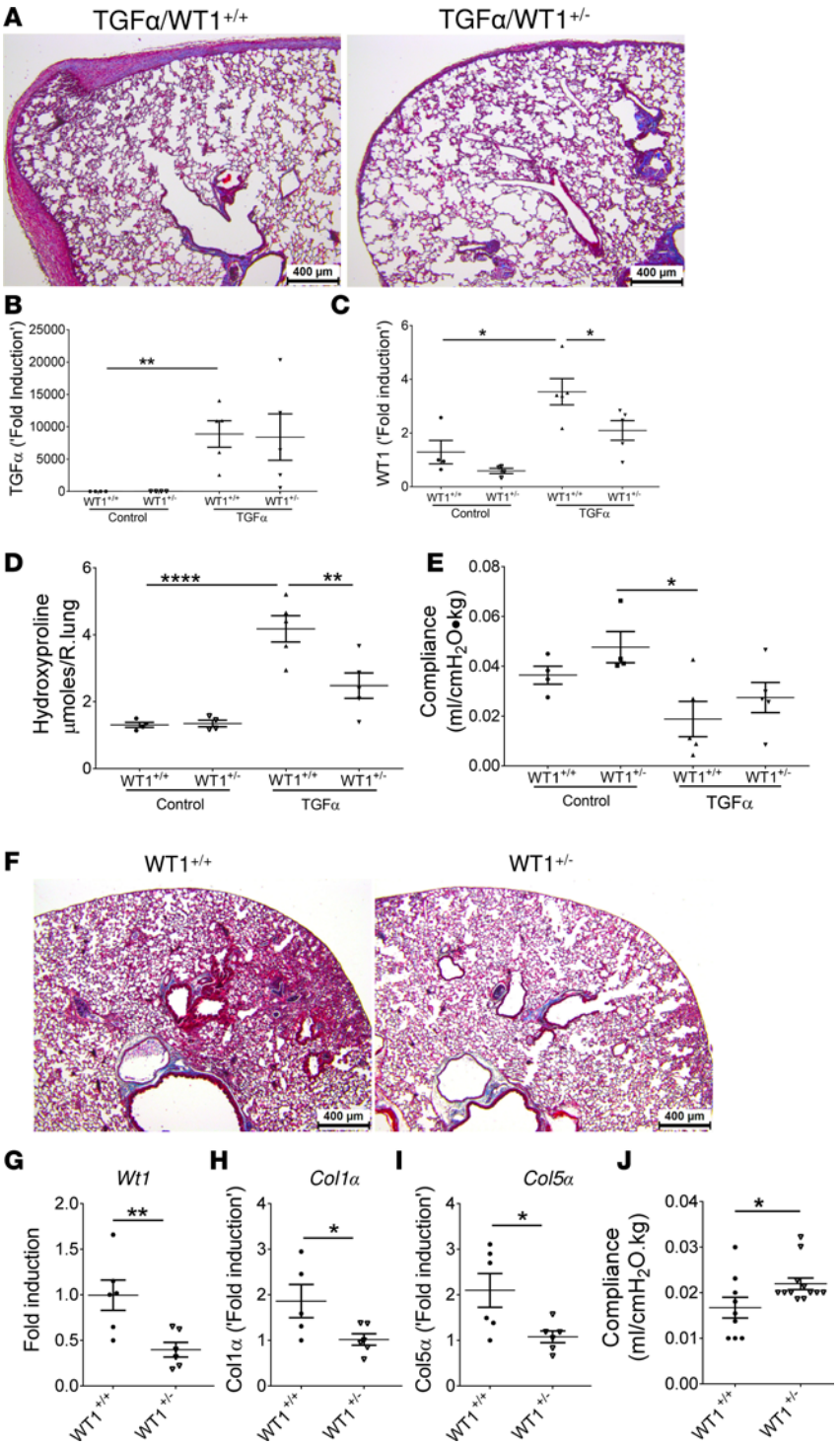


Figure 5. The partial loss of WT1 attenuates pulmonary fibrosis in vivo. CCSP/rtTA and TetO/TGFα transgenes were bred into WT1$^{CreERT2/-}$ knock-in mice (WT1$^{+/-}$) to generate TGFα transgenic mice with WT or mutant WT1 allele, and all groups of mice were administered Dox for 4 weeks. In bleomycin model, WT1$^{+/+}$ and WT1$^{+/-}$ mice were treated with bleomycin (6 units per kg body weight) in 50 μl of saline solution intradermally (i.d.) for 5 days per week for a total of 4 weeks. (**A**) Masson's trichrome–stained lung sections of TGFα/WT1$^{+/+}$ and TGFα/WT1$^{+/-}$ mice on Dox for 4 weeks (n = 4–5/group). Image magnification, ×5. Scale bar: 400 μm. (**B**) TGFα transcripts were measured in WT (WT1$^{+/+}$ and TGFα/WT1$^{+/+}$) and WT1 mutant (WT1$^{+/-}$ and TGFα/WT1$^{+/}$) mice on Dox for 4 weeks (n = 4–5/group). (**C**) WT1 transcripts were measured in WT (WT1$^{+/+}$ and TGFα/WT1$^{+/+}$) and WT1 mutant (WT1$^{+/-}$ and TGFα/WT1$^{+/-}$) mice on Dox for 4 weeks (n = 4–5/group). (**D**) The total lung hydroxyproline levels in WT (WT1$^{+/+}$ and TGFα/WT1$^{+/+}$) and WT1 mutant (WT1$^{+/-}$ and TGFα/WT1$^{+/-}$) mice on Dox for 4 weeks (n = 4–5/group). (**E**) The lung compliance was measured using FlexiVent in WT (WT1$^{+/+}$ and TGFα/WT1$^{+/+}$) and WT1 mutant (WT1$^{+/-}$ and TGFα/WT1$^{+/-}$) mice on Dox for 4 weeks (n = 4–5/group). (**F**) Masson's trichrome–stained lung sections of WT1$^{+/+}$ and WT1$^{+/-}$ mice treated with bleomycin for 4 weeks (n = 6/group). Image magnification, ×5. Scale bar: 400 μm. (**G**) WT1 transcripts were measured in the total RNA isolated from the lungs of WT1$^{+/+}$ and WT1$^{+/-}$ mice treated with bleomycin for 4 weeks (n = 6/group). (**H** and **I**) *Col1α* and *Col5α* transcripts were measured in the total RNA isolated from the lungs of WT1$^{+/+}$ and WT1$^{+/-}$ mice treated with bleomycin for 4 weeks (n = 6/group). (**J**) The lung compliance was measured using FlexiVent in WT1$^{+/+}$ and WT1$^{+/-}$ mice treated with bleomycin for 4 weeks (n = 6/group). Results are representative of 2 independent experiments with similar results. Data are presented as mean ± SEM. Statistical significance was calculated using 1-way ANOVA with Sidak's multiple comparison test or unpaired Student t test for comparison between 2 groups. *P < 0.05, **P < 0.005, ****P < 0.0005.

Dox for 6 weeks were cultured in an upper chamber and control lung-resident fibroblasts were placed in the bottom chamber (Figure 6H). Using immunostaining for PCNA and quantifying the PCNA-positive cells in the bottom chamber, the TGFα fibroblast increased PCNA-positive fibroblasts after 3 days of cocultures (Figure 6H). To demonstrate that the above effect is specific to WT1 upregulation, we prepared conditioned media from primary fibroblasts isolated and treated with either control or WT1-specific siRNA from TGFα mice on Dox for 6 weeks. We observed a significant decrease in the number of PCNA-positive fibroblasts with conditioned medium prepared from the TGFα fibroblasts treated with WT1-specific siRNA compared with control siRNA (Figures 6I). These findings show that WT1 can

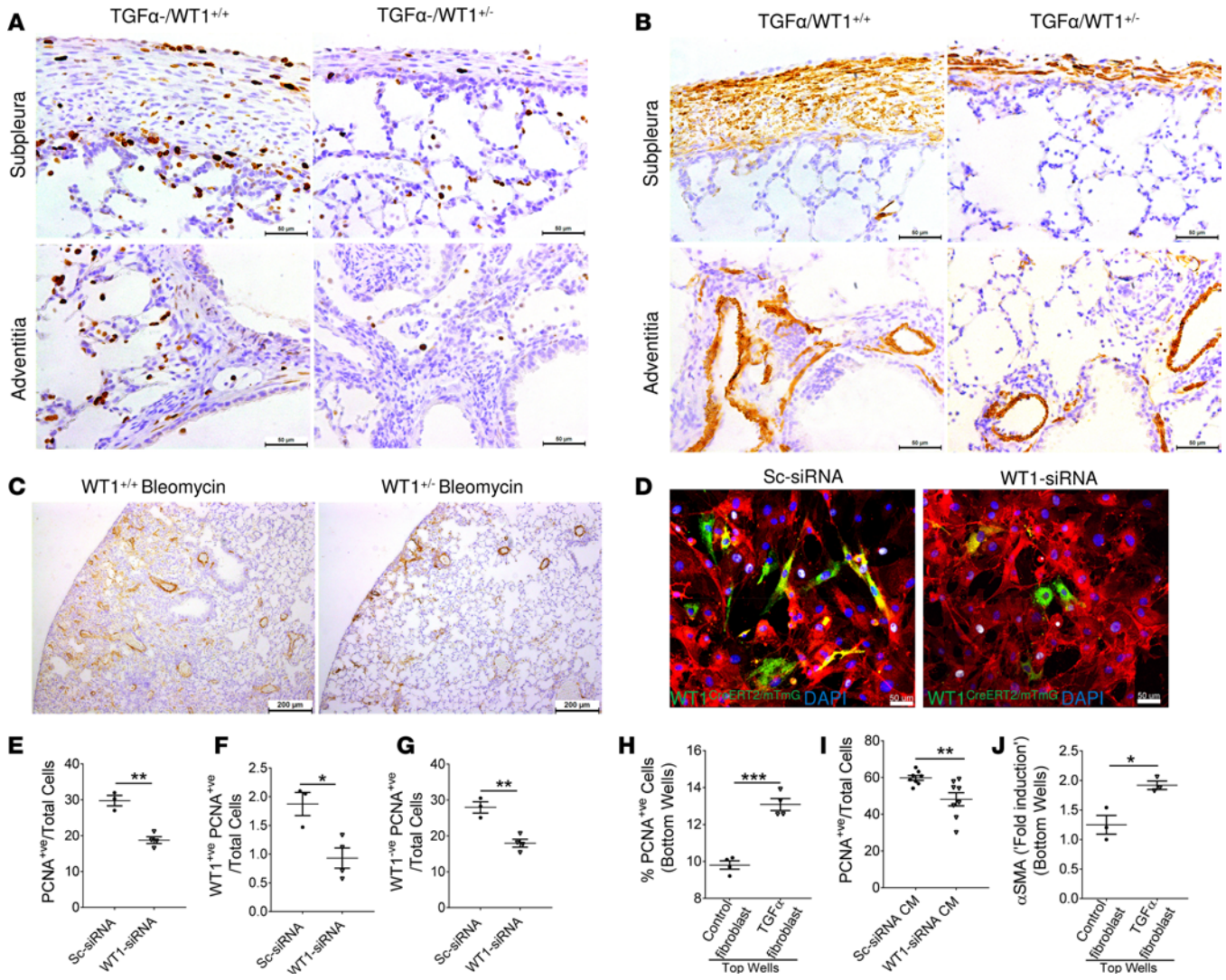


Figure 6. Mechanisms of WT1-driven fibroproliferation and myofibroblast transformation in vivo. (**A**) Immunostainings show Ki67-positive cells residing in subpleura and adventitia were reduced in TGFα/WT1$^{+/-}$ mice compared with TGFα/WT1$^{+/+}$ mice on Dox for 4 weeks. Scale bar: 50 μm. (**B**) Immunostainings show αSMA-positive cells residing in subpleura and adventitia were reduced in TGFα/WT1$^{+/-}$ mice compared with TGFα/WT1$^{+/+}$ mice on Dox for 4 weeks. Scale bar: 50 μm. (**C**) Immunostainings show αSMA-positive cells residing in subpleura and adventitia were reduced in WT1$^{+/-}$ mice compared with WT1$^{+/+}$ mice treated with bleomycin for 4 weeks. Scale bar: 200 μm. (**D**) Primary lung resident fibroblasts were isolated TGFα/WT1$^{CreERT2/mTmG}$ mice on Dox for 4 weeks and treated with either control or WT1 siRNA in presence of 4-hydroxy tamoxifen for 72 hours. Cells were immunostained for PCNA and immunofluorescence images were collected at original magnification ×10 (Scale bar: 50 μm). (**E**-**G**) The number of PCNA-positive cells that coexpresses WT1 (green) in total DAPI-positive cells were quantified using Metamorph image analysis software and were indicated as PCNA$^+$/total cells, WT1$^+$/PCNA$^+$ cells/total cells, or WT1$^-$/PCNA$^+$/total cells. (**H**) Fibroblast cocultures experiments were performed using lung-resident fibroblasts isolated from control mice (bottom chamber) or TGFα transgenic mice on Dox for 6 weeks (top chambers). Cells in the bottom chambers were immunostained for PCNA. Images were collected at original magnification ×10. Total DAPI-positive and PCNA-positive cells were quantified using ND2 analysis software. (**I**) Control mice fibroblasts were cultured for 48 hours in the presence of conditioned media obtained from control or WT1 siRNA transfected fibrotic fibroblasts for 72 hours. After 48 hours, cells were immunostained for PCNA. Images were collected at original magnification ×10. Total DAPI-positive and PCNA-positive cells were quantified using ND2 analysis software. (**J**) Fibroblast cocultures experiments were performed using lung-resident fibroblasts isolated from the lung cultures of control αSMA$^{CreERT2/mTmG}$ mice (bottom chamber) or TGFα transgenic mice on Dox for 6 weeks (top chambers). RNA was isolated from the cell lysates of bottom chamber, and quantification of αSMA gene expression was performed. All data are representative of 2 independent experiments with similar results (n = 3–4/group). All data in the figure are presented as mean ± SEM. Statistical significance was calculated using unpaired 2-tailed Student's t test for comparison between 2 groups. *$P < 0.05$, **$P < 0.005$, ***$P < 0.0005$.

alter the proliferation of WT1-negative fibroblasts in a non–cell autonomous manner through secretion of paracrine factors. Using transwell coculture studies, the effect of the WT1-overexpressing fibroblasts on the myofibroblast transformation was determined by quantifying the transcripts of αSMA gene expression in the bottom chamber after 48 hours of coculture. We observed a significant increase in αSMA gene expression in the bottom chambers of cocultures with WT1-overexpressing fibroblasts compared with cocultures with WT1-negative fibroblasts from normal lungs (Figure 6J). These findings show

that WT-expressing cells can induce fibroblast-to-myofibroblast transformation in a non–cell autonomous manner. Together, our findings suggest that WT1 can augment the proliferation and myofibroblast transformation in a non–cell autonomous manner through secretion of paracrine factors.

Discussion

Our study demonstrates a previously unknown role for WT1 as a positive regulator of pulmonary fibrosis. WT1 was detected in mesothelial and mesenchymal cells, but not epithelial cells, in lungs from patients with IPF. Using in vitro studies with isolated lung fibroblasts from a mouse model of pulmonary fibrosis and in vivo studies of developing pulmonary fibrosis, we demonstrate that WT1 functions to enhance proliferation, myofibroblast transformation, and ECM production. Haploinsufficiency of WT1 reduces fibroblast activation and pulmonary fibrosis in mouse models. WT1 acts by binding the SMA promoter, a marker of myofibroblasts. Using in vivo cell marking in mouse models, we identified WT1 as a key driver of mesothelial-to-myofibroblast and fibroblast-to-myofibroblast transformation. Our study demonstrates the developmental profile of WT1 expression. WT1 is coexpressed with calretinin, indicating expression in mesothelial cells during lung development but no expression in myofibroblasts or other cells in the lung parenchyma at E15.5, during embryonic stages of lung development. This increased WT1 expression in mesothelial cells is significantly downregulated at later prenatal or postnatal stages of lung development in mice. Importantly, our findings demonstrate that a limited number of mesothelial cells express WT1 in adult lungs compared with embryonic stages of lung development (13, 22, 24). These findings are consistent with other published studies on WT1 expression in embryonic and adult lungs (13, 14). In contrast, we observed a robust increase in WT1 staining in both mesenchymal cells and mesothelial cells during TGFα- and bleomycin-induced pulmonary fibrosis in postnatal lungs (20). Localization of WT1 in the mouse models resembles localization of WT1 in subpleural regions of fibrotic lesions in IPF. The cellular localization of WT1 in either mesothelial cells or mesenchymal cells could reflect an early event in fibroblast activation rather than a simple association in the progressive expansion of fibrotic lesions (22, 39). Our findings support a pathogenic role for WT1 in fibroblast activation. Inhibition of WT1 caused a marked reduction in IPF-specific ECM genes such as *Col14*, *Col15*, *Itg2*, *Itg7*, and *Lum* and proliferative genes such as *Grem1*, *Runx1*, *Wnt4*, *Stat3*, *Prrx1*, *Igf1*, *Ccnb1*, and *E2f8*. These findings are consistent with previous studies in fibroblasts isolated from normal and IPF lungs that revealed that activation of Stat3 by IL-6 was mitogenic for IPF fibroblasts due to activation of cyclin D (40–42). Our data show that WT1 affects fibroproliferation in a non–cell autonomous manner, as the loss of WT1 in WT1-positive fibroblasts attenuated the proliferation in both WT1-positive and WT1-negative fibroblasts. In contrast, overexpression of WT1 leads to a marked increase in the proliferation of human and mouse fibroblasts. In vivo, WT1 haploinsufficiency attenuated the proliferation of lung cells in both subpleural and adventitial areas of the lung. Reduced expression of WT1 attenuates the extent of fibrosis by modulating proliferation and ECM production. Taken together, these data highlight the complexity in the WT1 regulation of fibroproliferation and ECM production. Future experiments will need to address how WT1 influences the intracellular signaling and key gene networks in multiple cell types that can affect fibroproliferation and ECM production in the pathogenesis of pulmonary fibrosis.

Our lineage-tracing studies indicate that club-shaped mesothelial cells labeled by WT1 undergo proliferative expansion and differentiate into spindle-shaped myofibroblasts during TGFα-induced pulmonary fibrosis in vivo. It has been reported that, during embryonic lung development, mesenchymal cells develop from pleural mesothelial cells, and recent studies identify a role for mesothelial cells as myofibroblast progenitors in the lung (14, 23, 43), kidney (44–47), and liver (48, 49). However, a recent study by Karki and colleagues suggests that WT1 functions as a negative regulator of mesothelial-to-mesenchymal transition and WT1-derived mesenchymal cells migrate into the parenchyma within 4 hours of TGFβ treatment (23). In contrast, we and others have observed few WT1-positive mesothelial cells on the pleural surfaces of normal adult mice (13, 22, 24), and WT1-positive mesothelial cells of adult mice contribute to myofibroblasts in subpleural fibrotic lesions, albeit in small numbers. A possible explanation for the above differences could be due to intranasal TGFβ causing different signaling or an insufficient dose that does not show WT1 effects compared with intradermal bleomycin- or TGFα-induced pulmonary fibrosis. In support, our published studies have demonstrated that TGFα-induced fibrosis is not altered by blocking αVβ6/TGFβ signaling (50). Findings in human IPF show that WT1 expression occurs in mesothelial cells, fibroblasts, and myofibroblasts of human IPF lungs but has limited or no expression in healthy human lungs (22). Additionally, our cell-tracking studies identified αSMA staining in cells that originate from WT1-positive mesothelial

cells during TGFα- induced pulmonary fibrosis. A recent study by Boren and colleagues showed increases in the pleural mesothelial cells in patients diagnosed with nonspecific pleuritis, as well as mice intrapleurally injected with *S. pneumoniae* to induce pleural injury (51). Nonetheless, we do not know whether early upregulation of WT1 is limited to mesothelial cells alone or both mesothelial cells and mesenchymal cells contributing to myofibroblast transformation that occurs in subpleural fibrotic lesions. Notably, we show that there are more WT1-expressing mesenchymal cells in the subpleural regions of TGFα transgenic mice with continuous tamoxifen treatment compared with mice pretreated with tamoxifen. These observations imply that WT1 upregulation in both mesothelium and mesenchymal cells contribute to subpleural fibrotic lesions in pulmonary fibrosis. With continuous tamoxifen treatment, we found that the majority of mesenchymal cells in subpleura originate from WT1-positive progenitors. Future studies are needed to further delineate mechanisms whereby WT1 leads to differentiation of myofibroblasts in the progressive expansion of subpleural fibrotic lesions. Finally, our results imply that the WT1 upregulation, but not downregulation, is involved in mesothelial-to-myofibroblast transition in the development of pulmonary fibrosis.

Our data show that WT1 functions in a previously unknown manner as a positive regulator of myofibroblast differentiation via 2 potentially novel mechanisms. First, the αSMA gene is the direct target of transcriptional regulation by WT1, and the binding of WT1 induces αSMA transcripts, thus establishing a functional link to myofibroblast accumulation in subpleural areas of IPF lungs. Notably, WT1 binding elements in the αSMA gene are highly conserved among mammals, including mice and humans. Second, WT1-positive cells can induce fibroblast-to-myofibroblast transformation in a non–cell autonomous manner. Data from our coculture studies indicate a significant increase in fibroblast-to-myofibroblast transformation by WT1-overexpressing fibroblasts isolated from TGFα transgenic mice compared with normal fibroblasts that express limited or no WT1. Moreover, the marked upregulation of αSMA transcripts and increased myofibroblast accumulation after WT1 overexpression are consistent with the identification of a significant number of fibroblasts or myofibroblasts that coexpress WT1 in IPF lungs and mouse models of pulmonary fibrosis (22, 24). Furthermore, loss of WT1 attenuated myofibroblast accumulation in both subpleural and adventitial fibrotic lesions in vivo. Considered together, the data indicate that WT1 expression is a critical pathogenic event in myofibroblast transformation and ECM production. In support, we observed a strong correlation between collagen deposition and WT1 levels during TGFα-induced pulmonary fibrosis (22).

Progressive thickening of subpleural and peripheral areas of the lung is a characteristic feature of IPF. Fibrosis in subpleural regions is also a predominant phenotype in other fibrotic lung diseases, including asbestos-related pleural fibrosis, collagen vascular disease resulting in interstitial fibrosis, and drug reactions with pleural involvement (34, 52, 53). A prevailing view has been that lung-resident fibroblasts of subpleural fibrotic lesions invade into lung parenchyma to accumulate in peribronchial fibrotic lesions — a view supported indirectly by the observation that lung-resident fibroblasts are invasive (54–56). Our new findings support a model in which a mesothelial-to-fibroblast transformation is a local event that is confined to the subpleural area of the lung — a view supported by the lack of mesothelium-derived fibroblasts in peribronchial and alveolar areas of lungs of TGFα mice continuously treated with tamoxifen for 4 weeks, while on Dox. However, we find that WT1 expression in subpleural lesions is critical to the development of fibrotic lesions in other areas of the lung, including subpleural, peribronchial, and alveolar regions. By regulating the expression of distinct paracrine factors that may originate in subpleural regions, WT1 can function as a key driver to maintain pulmonary fibrosis in other peripheral areas of the lung. Our coculture studies further imply that no cell-to-cell contact is needed to initiate fibroblast-to-myofibroblast transformation in quiescent fibroblasts by WT1. Our in vivo studies demonstrated that the reduced expression of WT1 in subpleural regions of the lung attenuated both fibroproliferation and myofibroblast accumulation in the parenchymal areas of the lung. While it remains possible that a small amount of WT1 below the threshold of detection is present in lung parenchyma, it is unlikely to account for the large fibrotic phenotypes documented here. However, the identity of fibroblasts in lung parenchyma remains to be determined during TGFα-induced pulmonary fibrosis. More recent findings have suggested that multiple mesenchymal cell lineages exist in distinct anatomical regions of the lung in promoting self-renewal versus a pathological change in injury (35, 38, 56–59). While mesenchymal cells expressing Lgr5 were found mainly in the alveolar area of the lungs, Lgr6-positive mesenchymal cells can be found predominantly in peribronchiolar and adventitial regions of the lung (60). Our findings suggest WT1-expressing mesenchymal cells accumulate in subpleural areas of fibrotic lungs, but none are found in healthy lungs. Thus, within the lung, there appears to be a remarkable heterogeneity in mesenchymal cells and compartmentalization of effector signals that control

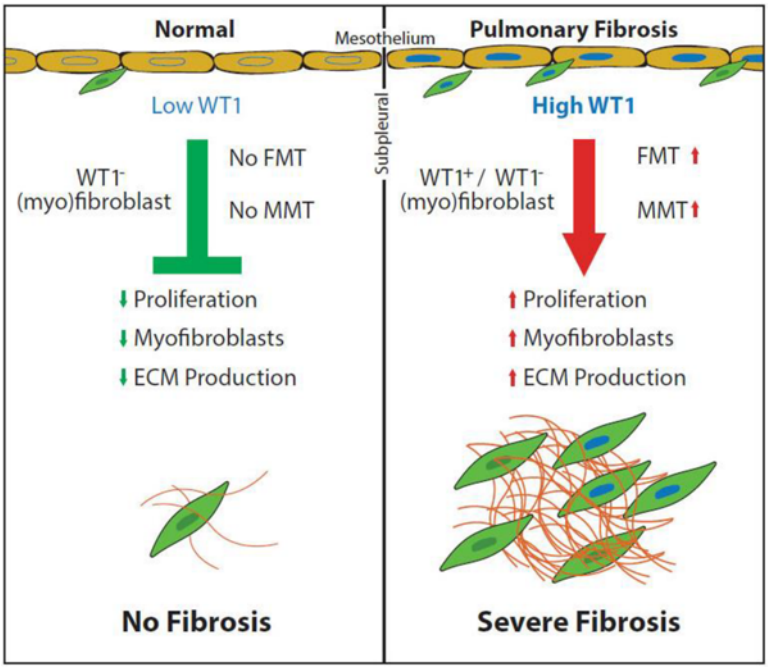


Figure 7. Schematic representation of WT1-driven fibroblast activation in pulmonary fibrosis. In the peripheral areas of the lung, WT1-positive mesothelial cells and mesenchymal cells undergo myofibroblast transformation and activate lung-resident fibroblasts via direct and indirect mechanisms in the pathogenesis of pulmonary fibrosis.

pulmonary fibrosis. Future studies are needed to investigate a possible cross-talk between WT1-positive cells of subpleural regions, with distinct populations documented in multiple areas of the lung. Our data indicate that future pharmacologic interventions targeting WT1-driven events in subpleural fibrotic machinery could target profibrotic processes of the lung in a global and a coordinated fashion.

In summary, our data provides mechanistic insights into the molecular cause of subpleural thickening in IPF by revealing a role of WT1 and targets that are either directly or indirectly involved in fibroblast-specific functions and processes (Figure 7). The largest category of genes altered by WT1 are known to regulate proliferation, growth, differentiation, and ECM production. Concurrently, using 2 different mouse models of pulmonary fibrosis, we have demonstrated that the upregulation of WT1 in subpleural fibrotic lesions causes severe fibrotic lung disease. The findings of this study identify a previously unknown role for WT1 in pathological fibroblast activity in IPF, through acceleration of fibroproliferation and myofibroblast transformation through direct and indirect mechanisms. Overall, our results suggest that WT1 may be a therapeutic target in modulating pulmonary fibrosis.

Methods

Mouse strains. Generation of $WT1^{CreERT2/-}$ transgenic mice has been described previously (16). Heterozygous $WT1^{CreERT2/-}$ knock-in mice are haploinsufficient for the WT1 allele ($WT1^{+/-}$) and display no developmental abnormalities. Clara cell–specific promoter–driven (CCSP-driven) TGFα-overexpression mice were generated as described previously (61). We performed sequential breeding of CCSP/TGFα transgenic mice with $WT1^{CreERT2/-}$ mice to generate control or TGFα transgenic mice with WT ($WT1^{+/+}$ and TGFα/$WT1^{+/+}$) or WT1 mutant allele ($WT1^{+/-}$ and TGFα/$WT1^{+/-}$). The generated $WT1^{CreERT2/mTmG}$ reporter mice were described previously (22). TGFα/$WT1^{CreERT2/mTmG}$ quadruple transgenic mice were generated by crossing the CCSP/TGFα mice with $WT1^{CreERT2/mTmG}$ reporter mice. Ten- to 14-week-old mice were used in all experiments. αSMA^{YFP} reporter mice used in the confocal analysis of WT1 expression in embryonic lung development and transcript analysis were described previously and used to efficiently label embryonic and adult smooth muscle cells (62, 63). The heterozygous $\alpha SMA^{CreERT2/mTmG}$ male transgenic mouse strain was generated as previously described (30). These mice express CreERT2 under the control of the promoter for mouse smooth muscle myosin, heavy polypeptide 11 and have been shown to track the genetic lineage of α-SMA–expressing cells (64).

Mouse models of TGFα- and bleomycin-induced pulmonary fibrosis. TGFα- overexpression was induced by administering food containing Dox (62.5 mg/kg) (catalog D9891, MilliporeSigma) to the CCSP/TGFα transgenic mice. CCSP/- littermate mice fed with Dox-treated food were used as controls (55). For the mouse model of bleomycin-induced pulmonary fibrosis, 10- to 14-week-old mice received bleomycin intradermally (6 U per kg bodyweight/day) suspended in 50 μl saline solution in the center of the shaved back (within a 50-mm radius) for 5 days per week for a total of 4 weeks. At day 28, mice were euthanized and lung samples were collected for further analysis.

Tamoxifen treatments. Tamoxifen (catalog T5648, MilliporeSigma) was dissolved in ethanol and emulsified in sunflower oil (catalog W530285, MilliporeSigma) at 25 mg/ml concentration as described (22), and mice were treated with tamoxifen (i.p. 2.5 mg/day) to induce Cre recombination via i.p. injections.

Histology and IHC. Formalin- or OCT-fixed mouse lung tissue sections were prepared and stained with Masson's trichrome or immunostained with antibodies against α-SMA or Ki67 as described previously (65).

Human and mouse primary lung fibroblast cultures. Human and mouse primary lung fibroblast cell cultures were prepared as previously described (55, 65).

SiRNA transfections. Primary human or mouse fibroblast cells were transfected with stealth siRNA (human WT1 siRNA [catalog HSS111390, Invitrogen], mouse WT1 siRNA [catalog MSS212628, Invitrogen], or stealth negative control siRNA [catalog 12935300, Invitrogen]) using the Lipofectamine 3000 Transfection kit (catalog L3000-015, Invitrogen) as previously described (30). Transfected cells were harvested 72 hours after transfection and used for RNA isolation and whole transcriptome analysis.

Whole-transcriptome shotgun sequencing (RNA-Seq) and bioinformatic analysis. Total RNA was prepared from primary lung fibroblasts isolated from lung cultures of TGFα mice on Dox food for 10 days and transfected with either control or WT1 siRNA as described earlier (22). RNA-Seq was performed using an Illumina HiSeq-1000 Sequencer as described previously (66). Complete RNA-Seq data are available at a gene expression omnibus or GEO database (GEO accession number GSE110177). A previously published transcriptomic data set (GSE53845) derived from analysis of the lung biopsies of 40 IPF patients and 8 healthy controls available in the National Center for Biotechnology Information (NCBI) GEO was used to identify differentially expressed genes (8). Differential analysis for genes was performed using the R package 'limma' or GEO2R (http://www.ncbi.nlm.nih.gov/geo/geo2r/) with *P* value and FDR threshold at 0.05 and fold-change threshold at 1.5. This IPF gene signature was queried against the WT1 siRNA–generated gene expression signature. Functional enrichment analysis of the negatively correlated gene sets between IPF lungs and WT1 siRNA–treated cells were analyzed using the ToppFun application of the ToppGene Suite (31). For network representation of select significantly enriched biological processes and pathways, we used Cytoscape (67).

Viral transductions. Primary lung-resident fibroblasts were isolated from the lung cultures of human or mouse lungs by negative selection for anti-CD45–stained cells using MACS columns (68). Thus, isolated fibroblasts were transduced with control or WT1-overexpressing adenovirus (human WT1) (catalog 000488A, Abm) and lentivirus (mouse WT1) (catalog 41082, Addgene) (69) or Control lentivirus (plasmid lentivirus, catalog 8453, Addgene) (1–10 MOI) for 48–72 hours.

Myofibroblast differentiation. In vitro fibroblast-to-myofibroblast transformation assay was performed using primary lung-resident fibroblasts isolated from the lung cultures of $\alpha SMA^{CreERT2/mTmG}$ mice as previously described (30). Fibroblasts were seeded onto chamber slides and serum starved (0.5% FBS) at 70%–80% confluency overnight and then treated with control or WT1-overexpressing lentivirus in the presence of 2 μM (Z)-4-hydroxytamoxifen (catalog H7904, MilliporeSigma) for 72 hours. For WT1 knockdown studies, isolated lung-resident fibroblasts were transfected with either control or WT1-specific siRNA for 24 hours; after transfection, cells were treated with 2 μM 4-hydroxytamoxifen for an additional 48 hours. After 72 hours, cells were fixed with 4% paraformaldehyde, and the nucleus was stained using ProLong gold DAPI (Thermo Fisher Scientific). Fluorescence images were collected using a Nikon AIR-A1 laser-scanning confocal microscope. Cell quantitation was performed using Metamorph imaging software.

Proliferation assays. Primary lung-resident fibroblast proliferation was examined using BrdU (catalog 6813S, Cell Signaling Technology) incorporation as described previously (30).

Confocal imaging. Mouse lungs were embedded in OCT medium, and sections were prepared as described previously (30). Lungs were immunostained against WT1, calretinin, or αSMA antigens. Appropriate secondary antibodies conjugated with Alexa Fluor 488, Alexa Fluor 594, or Alexa Fluor 647 (Invitrogen), respectively, were used for visualization (antibody details in supplemental Table 4).

For PCNA immunostainings, cells were fixed in ice cold methanol. Nonspecific protein binding was blocked with M.O.M. blocking solution (catalog BMK2202, Vector Laboratories) in PBS, followed by incubation with primary antibodies in M.O.M. diluent solution and subsequent incubation with secondary antibodies. Finally, chamber slides were washed and mounted with ProLong gold DAPI. Confocal images were collected using a Nikon AIR-A1 laser-scanning confocal microscope. Imaris (version 7.2.0; Bitplane) was used for image analysis. For quantitative analysis of PCNA, 5–7 random images were taken for each condition (with the 10× objective). Cell quantitation was performed using Metamorph imaging software.

Chip-Seq PCR assay. ChIP was performed using the ChIP assay kit (catalog 9005, Cell Signaling Technology). Briefly, IMR-90 fibroblasts were treated with WT1-overexpressing adenovirus (10 MOI) for 48 hours. Cells were cross-linked with 1% formaldehyde, and immunoprecipitation was performed with anti-WT1 (catalog 12609-1-AP, Proteintech) or isotype control IgG (catalog 2729, Cell Signaling Technology) at 4°C as described in the manufacturer's protocol. DNA was purified, and PCR was performed in 25 μl of PCR-reaction mix using 1 μl of DNA in a Veriti Thermal Cycler (Applied Biosystems). The primer sequences, annealing temperatures, and PCR product sizes are provided in Supplemental Table 1. The PCR product was electrophoresed through a 2.0% agarose gel with ethidium bromide using 1× TAE buffer (Thermo Fisher Scientific), and resulting fragments were visualized using a UV transilluminator (FotoDyne).

Flow cytometry. The lungs of control or TGFα/WT1$^{CreERT2/-}$/ROSA^{mTmG} mice treated with tamoxifen and Dox were cultured for 7 days, and the total lung fibroblasts were used for flow cytometry analysis. Data were acquired using LSR Fortessa flow cytometer (BD Biosciences). Unstained and single-stained (tdTomato or EGFP) total lung cells were used for compensation and gating. Data were analyzed using FACSDIVA software (BD Biosciences).

RNA preparation and RT-PCR. Total RNA was extracted using the RNAeasy Mini Kit (Qiagen Sciences) as previously described (22). cDNA synthesis was carried out using SuperScript III Reverse Transcriptase (Invitrogen). Quantitative PCR (qPCR) assays were performed with the CFX384 Touch Real-Time PCR Detection system (Bio-Rad). The relative quantities of mRNA for several genes were determined using iTaq universal SYBR green supermix (Bio-Rad). Target-gene transcripts in each sample were normalized to hypoxanthine guanine phosphoribosyl transferase or HPRT or β-actin and expressed as a relative increase or decrease compared with control. All real-time primer sequences used are shown in Supplemental Tables 2 and 3.

Western blot. Purified lung-resident fibroblasts were isolated as described earlier (22) and cultured on 12-well plates to 90% confluence and transduced with control Adenovirus or WT1 adenovirus for 72 hours. Cells were lysed in RIPA lysis buffer, and protein estimation was performed using the BCA method according to manufactures instructions (catalog 23225, Thermo Fisher Scientific). Immunoblotting and quantification were performed using the volume-integration function of Phosphor Imager Software Image Quant 5.2, as previously described (22). Primary antibodies and dilutions used are described in Supplemental Table 5, and the appropriate secondary antibodies conjugated with peroxidase (1:1000) were used for blot development.

Statistics. All data were analyzed using Prism (Version 7; Graph Pad). One-way ANOVA with Sidak's multiple comparison post-test was used to compare different experimental groups. Student's two-tailed *t* test was used to compare between 2 experimental groups. Data were considered statistically significant for P values less than 0.05.

Study approval. All mice were housed under specific pathogen-free conditions, and all animal experimental protocols were approved by the Institutional Animal Care and Use Committee of Cincinnati Children's Hospital Medical Center.

Author contributions

SKM and VS conceived the project, designed experiments, analyzed data, and wrote the manuscript; VS performed most of the experiments. AGJ performed bioinformatic analysis and provided suggestions; RKK performed immunostainings; ESW provided human lung tissues, IPF cells, and RNA; DS provided embryonic mouse lungs and αSMA reporter mice; GBR provided analytical tools and suggestions; and TRK assisted in transgenic mice generation and edited the manuscript.

Acknowledgments

The authors thank the veterinary services, flow cytometry core, and pathology research core at Cincinnati Children's Hospital Medical Center for the help in this study. We thank Frank McCormack and Jeffrey Whitsett for valuable suggestions and Gail Pyne-Geithman for editorial assistance. This research was supported by the NIH grants NHLBI 1R21HL133539 (SKM and AGJ) and 1R01 HL134801 (SKM), the US Department of Defense funds, W81XWH-17-1-0666 (SKM), NHLBI R03HL133420 (DS), and Department of Biotechnology Fellowship, Government of India (RKK).

Address correspondence to: Satish K. Madala, Division of Pulmonary Medicine, Cincinnati Children's Hospital Medical Center, MLC 2021, 3333 Burnet Avenue, Cincinnati, Ohio 45229, USA. Phone: 513.636.9852; Email: satish.madala@cchmc.org.

1. Raghu G, Weycker D, Edelsberg J, Bradford WZ, Oster G. Incidence and prevalence of idiopathic pulmonary fibrosis. *Am J Respir Crit Care Med*. 2006;174(7):810–816.
2. Wynn TA. Cellular and molecular mechanisms of fibrosis. *J Pathol*. 2008;214(2):199–210.
3. Ley B, Collard HR. Epidemiology of idiopathic pulmonary fibrosis. *Clin Epidemiol*. 2013;5:483–492.
4. Nalysnyk L, Cid-Ruzafa J, Rotella P, Esser D. Incidence and prevalence of idiopathic pulmonary fibrosis: review of the literature. *Eur Respir Rev*. 2012;21(126):355–361.
5. Raghu G, et al. An official ATS/ERS/JRS/ALAT statement: idiopathic pulmonary fibrosis: evidence-based guidelines for diagnosis and management. *Am J Respir Crit Care Med*. 2011;183(6):788–824.
6. Smith ML. Update on Pulmonary Fibrosis: Not All Fibrosis Is Created Equally. *Arch Pathol Lab Med*. 2016;140(3):221–229.
7. Cool CD, Groshong SD, Rai PR, Henson PM, Stewart JS, Brown KK. Fibroblast foci are not discrete sites of lung injury or repair: the fibroblast reticulum. *Am J Respir Crit Care Med*. 2006;174(6):654–658.
8. DePianto DJ, et al. Heterogeneous gene expression signatures correspond to distinct lung pathologies and biomarkers of disease severity in idiopathic pulmonary fibrosis. *Thorax*. 2015;70(1):48–56.
9. Chau YY, Hastie ND. The role of Wt1 in regulating mesenchyme in cancer, development, and tissue homeostasis. *Trends Genet*. 2012;28(10):515–524.
10. Bansal H, et al. Heat shock protein 90 regulates the expression of Wilms tumor 1 protein in myeloid leukemias. *Blood*. 2010;116(22):4591–4599.
11. Rampal R, Figueroa ME. Wilms tumor 1 mutations in the pathogenesis of acute myeloid leukemia. *Haematologica*. 2016;101(6):672–679.
12. Duim SN, Goumans MJ, Kruithof BPT. Chapter 13 WT1 in Cardiac Development and Disease. In: van den Heuvel-Eibrink MM ed. *Wilms Tumor*. Brisbane (AU);Codon Publications:2016. https://www.ncbi.nlm.nih.gov/books/NBK373348/doi: 10.15586/codon.wt.2016.ch13. Accessed August 1, 2018.
13. Que J, Wilm B, Hasegawa H, Wang F, Bader D, Hogan BL. Mesothelium contributes to vascular smooth muscle and mesenchyme during lung development. *Proc Natl Acad Sci USA*. 2008;105(43):16626–16630.
14. Moiseenko A, et al. Origin and characterization of alpha smooth muscle actin-positive cells during murine lung development. *Stem Cells*. 2017;35(6):1566–1578.
15. Hohenstein P, Pritchard-Jones K, Charlton J. The yin and yang of kidney development and Wilms' tumors. *Genes Dev*. 2015;29(5):467–482.
16. Zhou B, et al. Epicardial progenitors contribute to the cardiomyocyte lineage in the developing heart. *Nature*. 2008;454(7200):109–113.
17. Gebeshuber CA, et al. Focal segmental glomerulosclerosis is induced by microRNA-193a and its downregulation of WT1. *Nat Med*. 2013;19(4):481–7.
18. Bandiera R, Vidal VP, Motamedi FJ, Clarkson M, Sahut-Barnola I, von Gise A, et al. WT1 maintains adrenal-gonadal primordium identity and marks a population of AGP-like progenitors within the adrenal gland. *Developmental Cell*. 2013;27(1):5–18.
19. Shandilya J, Roberts SG. A role of WT1 in cell division and genomic stability. *Cell Cycle*. 2015;14(9):1358–1364.
20. Shandilya J, Toska E, Richard DJ, Medler KF, Roberts SG. WT1 interacts with MAD2 and regulates mitotic checkpoint function. *Nat Commun*. 2014;5:4903.
21. Vicent S, et al. Wilms tumor 1 (WT1) regulates KRAS-driven oncogenesis and senescence in mouse and human models. *J Clin Invest*. 2010;120(11):3940–3952.
22. Sontake V, et al. Fibrocytes Regulate Wilms Tumor 1-Positive Cell Accumulation in Severe Fibrotic Lung Disease. *J Immunol*. 2015;195(8):3978–3991.
23. Karki S, et al. Wilms' tumor 1 (Wt1) regulates pleural mesothelial cell plasticity and transition into myofibroblasts in idiopathic pulmonary fibrosis. *FASEB J*. 2014;28(3):1122–1131.
24. von Gise A, et al. Contribution of Fetal, but Not Adult, Pulmonary Mesothelium to Mesenchymal Lineages in Lung Homeostasis and Fibrosis. *Am J Respir Cell Mol Biol*. 2016;54(2):222–230.
25. Luzina IG, et al. Transcriptomic evidence of immune activation in macroscopically normal-appearing and scarred lung tissues in idiopathic pulmonary fibrosis. *Cell Immunol*. 2018;325:1–13.
26. Scotton CJ, Chambers RC. Molecular targets in pulmonary fibrosis: the myofibroblast in focus. *Chest*. 2007;132(4):1311–1321.
27. Phan SH. The myofibroblast in pulmonary fibrosis. *Chest*. 2002;122(6 Suppl):286S–289S.
28. Hinz B, Phan SH, Thannickal VJ, Galli A, Bochaton-Piallat ML, Gabbiani G. The myofibroblast: one function, multiple origins. *Am J Pathol*. 2007;170(6):1807–1816.
29. Klingberg F, Hinz B, White ES. The myofibroblast matrix: implications for tissue repair and fibrosis. *J Pathol*. 2013;229(2):298–309.

30. Sontake V, et al. Hsp90 regulation of fibroblast activation in pulmonary fibrosis. *JCI Insight*. 2017;2(4):e91454.
31. Chen J, Bardes EE, Aronow BJ, Jegga AG. ToppGene Suite for gene list enrichment analysis and candidate gene prioritization. *Nucleic Acids Res*. 2009;37(Web Server issue):W305–W311.
32. Hutchison N, Fligny C, Duffield JS. Resident mesenchymal cells and fibrosis. *Biochim Biophys Acta*. 2013;1832(7):962–971.
33. Phan SH. Fibroblast phenotypes in pulmonary fibrosis. *Am J Respir Cell Mol Biol*. 2003;29(3 Suppl):S87–S92.
34. Noble PW, Barkauskas CE, Jiang D. Pulmonary fibrosis: patterns and perpetrators. *J Clin Invest*. 2012;122(8):2756–2762.
35. Xia H, et al. Identification of a cell-of-origin for fibroblasts comprising the fibrotic reticulum in idiopathic pulmonary fibrosis. *Am J Pathol*. 2014;184(5):1369–1383.
36. Moore BB, Kolb M. Fibrocytes and progression of fibrotic lung disease. Ready for showtime? *Am J Respir Crit Care Med*. 2014;190(12):1338–1339.
37. Kleaveland KR, et al. Fibrocytes are not an essential source of type I collagen during lung fibrosis. *J Immunol*. 2014;193(10):5229–5239.
38. Hardie WD, et al. Signaling pathways in the epithelial origins of pulmonary fibrosis. *Cell Cycle*. 2010;9(14):2769–2776.
39. Luzina IG, et al. Transcriptomic evidence of immune activation in macroscopically normal-appearing and scarred lung tissues in idiopathic pulmonary fibrosis. *Cell Immunol*. 2018;325:1–13.
40. Moodley YP, et al. Fibroblasts isolated from normal lungs and those with idiopathic pulmonary fibrosis differ in interleukin-6/gp130-mediated cell signaling and proliferation. *Am J Pathol*. 2003;163(1):345–354.
41. Pechkovsky DV, et al. STAT3-mediated signaling dysregulates lung fibroblast-myofibroblast activation and differentiation in UIP/IPF. *Am J Pathol*. 2012;180(4):1398–1412.
42. Pedroza M, et al. STAT-3 contributes to pulmonary fibrosis through epithelial injury and fibroblast-myofibroblast differentiation. *FASEB J*. 2016;30(1):129–140.
43. Zolak JS, et al. Pleural mesothelial cell differentiation and invasion in fibrogenic lung injury. *Am J Pathol*. 2013;182(4):1239–1247.
44. Kreidberg JA, et al. WT-1 is required for early kidney development. *Cell*. 1993;74(4):679–691.
45. Hartwig S, et al. Genomic characterization of Wilms' tumor suppressor 1 targets in nephron progenitor cells during kidney development. *Development*. 2010;137(7):1189–1203.
46. Kreidberg JA. WT1 and kidney progenitor cells. *Organogenesis*. 2010;6(2):61–70.
47. Motamedi FJ, et al. WT1 controls antagonistic FGF and BMP-pSMAD pathways in early renal progenitors. *Nat Commun*. 2014;5:4444.
48. Asahina K. Hepatic stellate cell progenitor cells. *J Gastroenterol Hepatol*. 2012;27 Suppl 2:80–84.
49. Ijpenberg A, et al. Wt1 and retinoic acid signaling are essential for stellate cell development and liver morphogenesis. *Dev Biol*. 2007;312(1):157–170.
50. Madala SK, et al. Inhibition of the αvβ6 integrin leads to limited alteration of TGF-α-induced pulmonary fibrosis. *Am J Physiol Lung Cell Mol Physiol*. 2014;306(8):L726–L735.
51. Boren J, et al. Inhibition of Glycogen Synthase Kinase 3β Blocks Mesomesenchymal Transition and Attenuates Streptococcus pneumonia-Mediated Pleural Injury in Mice. *Am J Pathol*. 2017;187(11):2461–2472.
52. Schwartz DA, Galvin JR, Yagla SJ, Speakman SB, Merchant JA, Hunninghake GW. Restrictive lung function and asbestos-induced pleural fibrosis. A quantitative approach. *J Clin Invest*. 1993;91(6):2685–2692.
53. Schneider F, Gruden J, Tazelaar HD, Leslie KO. Pleuropulmonary pathology in patients with rheumatic disease. *Arch Pathol Lab Med*. 2012;136(10):1242–1252.
54. Li Y, et al. Severe lung fibrosis requires an invasive fibroblast phenotype regulated by hyaluronan and CD44. *J Exp Med*. 2011;208(7):1459–1471.
55. Madala SK, Edukulla R, Schmidt S, Davidson C, Ikegami M, Hardie WD. Bone marrow-derived stromal cells are invasive and hyperproliferative and alter transforming growth factor-α-induced pulmonary fibrosis. *Am J Respir Cell Mol Biol*. 2014;50(4):777–786.
56. Habiel DM, Hogaboam C. Heterogeneity in fibroblast proliferation and survival in idiopathic pulmonary fibrosis. *Front Pharmacol*. 2014;5:2.
57. Rock JR, et al. Multiple stromal populations contribute to pulmonary fibrosis without evidence for epithelial to mesenchymal transition. *Proc Natl Acad Sci USA*. 2011;108(52):E1475–E1483.
58. O'Dwyer DN, Ashley SL, Moore BB. Influences of innate immunity, autophagy, and fibroblast activation in the pathogenesis of lung fibrosis. *Am J Physiol Lung Cell Mol Physiol*. 2016;311(3):L590–L601.
59. Zepp JA, et al. Distinct Mesenchymal Lineages and Niches Promote Epithelial Self-Renewal and Myofibrogenesis in the Lung. *Cell*. 2017;170(6):1134–1148.e10.
60. Lee JH, et al. Anatomically and Functionally Distinct Lung Mesenchymal Populations Marked by Lgr5 and Lgr6. *Cell*. 2017;170(6):1149–1163.e12.
61. Hardie WD, Le Cras TD, Jiang K, Tichelaar JW, Azhar M, Korfhagen TR. Conditional expression of transforming growth factor-alpha in adult mouse lung causes pulmonary fibrosis. *Am J Physiol Lung Cell Mol Physiol*. 2004;286(4):L741–L749.
62. Li J, Qu X, Bertram JF. Endothelial-myofibroblast transition contributes to the early development of diabetic renal interstitial fibrosis in streptozotocin-induced diabetic mice. *Am J Pathol*. 2009;175(4):1380–1388.
63. Cool J, Carmona FD, Szucsik JC, Capel B. Peritubular myoid cells are not the migrating population required for testis cord formation in the XY gonad. *Sex Dev*. 2008;2(3):128–133.
64. Wirth A, et al. G12-G13-LARG-mediated signaling in vascular smooth muscle is required for salt-induced hypertension. *Nat Med*. 2008;14(1):64–68.
65. Madala SK, Sontake V, Edukulla R, Davidson CR, Schmidt S, Hardie WD. Unique and Redundant Functions of p70 Ribosomal S6 Kinase Isoforms Regulate Mesenchymal Cell Proliferation and Migration in Pulmonary Fibrosis. *Am J Respir Cell Mol Biol*. 2016;55(6):792–803.
66. Madala SK, et al. Dual targeting of MEK and PI3K pathways attenuates established and progressive pulmonary fibrosis. *PLoS ONE*. 2014;9(1):e86536.
67. Shannon P, et al. Cytoscape: a software environment for integrated models of biomolecular interaction networks. *Genome Res*. 2003;13(11):2498–2504.

68. Madala SK, Edukulla R, Schmidt S, Davidson C, Ikegami M, Hardie WD. Bone marrow-derived stromal cells are invasive and hyperproliferative and alter transforming growth factor-alpha-induced pulmonary fibrosis. *Am J Respir Cell Mol Biol*. 2014;50(4):777–86.
69. Buganim Y, et al. Direct reprogramming of fibroblasts into embryonic Sertoli-like cells by defined factors. *Cell Stem Cell*. 2012;11(3):373–386.



Expert Opinion on Therapeutic Targets

ISSN: 1472-8222 (Print) 1744-7631 (Online) Journal homepage: http://www.tandfonline.com/loi/iett20

New therapeutics based on emerging concepts in pulmonary fibrosis

Vishwaraj Sontake, Prathibha R. Gajjala, Rajesh K. Kasam & Satish K. Madala

To cite this article: Vishwaraj Sontake, Prathibha R. Gajjala, Rajesh K. Kasam & Satish K. Madala (2019) New therapeutics based on emerging concepts in pulmonary fibrosis, Expert Opinion on Therapeutic Targets, 23:1, 69-81, DOI: 10.1080/14728222.2019.1552262

To link to this article: https://doi.org/10.1080/14728222.2019.1552262

Accepted author version posted online: 23 Nov 2018.
Published online: 28 Nov 2018.

Submit your article to this journal

Article views: 62

View Crossmark data

Full Terms & Conditions of access and use can be found at
http://www.tandfonline.com/action/journalInformation?journalCode=iett20

EXPERT OPINION ON THERAPEUTIC TARGETS
2019, VOL. 23, NO. 1, 69–81
https://doi.org/10.1080/14728222.2019.1552262

Taylor & Francis
Taylor & Francis Group

REVIEW

Check for updates

New therapeutics based on emerging concepts in pulmonary fibrosis

Vishwaraj Sontake[*a,b], Prathibha R. Gajjala[*a,b], Rajesh K. Kasam[*a,b] and Satish K. Madala[a,b]

[a]Department of Pediatrics, University of Cincinnati, College of Medicine, Cincinnati, OH, USA; [b]Division of Pulmonary Medicine, Cincinnati Children's Hospital Medical Center, Cincinnati, OH, USA

ABSTRACT

Introduction: Fibrosis is an irreversible pathological endpoint in many chronic diseases, including pulmonary fibrosis. Idiopathic pulmonary fibrosis (IPF) is a progressive and often fatal condition characterized by (myo)fibroblast proliferation and transformation in the lung, expansion of the extracellular matrix, and extensive remodeling of the lung parenchyma. Recent evidence indicates that IPF prevalence and mortality rates are growing in the United States and elsewhere. Despite decades of research on the pathogenic mechanisms of pulmonary fibrosis, few therapeutics have succeeded in the clinic, and they have failed to improve IPF patient survival.

Areas covered: Based on a literature search and our own results, we discuss the key cellular and molecular responses that contribute to (myo)fibroblast actions and pulmonary fibrosis pathogenesis; this includes signaling pathways in various cells that aberrantly and persistently activate (myo)fibroblasts in fibrotic lesions and promote scar tissue formation in the lung.

Expert opinion: Lessons learned from recent failures and successes with new therapeutics point toward approaches that can target multiple pro-fibrotic processes in IPF. Advances in preclinical modeling and single-cell genomics will also accelerate novel discoveries for effective treatment of IPF.

ARTICLE HISTORY
Received 28 July 2018
Accepted 21 November 2018

KEYWORDS
Heat shock protein 90; idiopathic pulmonary fibrosis; lung; myofibroblasts; Wilms' tumor1

1. Introduction

Fibrosis is a pathological endpoint in many chronic diseases associated with unresolved inflammation and tissue remodeling. Collagen and other extracellular matrix (ECM) components, such as fibronectin and elastin, are overproduced and accumulate, expanding the inflamed or damaged connective tissue. Fibrosis is a major cause of death through permanent scarring and functional impairment of such vital organs as the heart, intestine, kidney, liver, and lung [1]. Fibrosis has been shown to affect various organ systems in systemic auto-immune diseases, such as scleroderma and systemic lupus erythematosus and also monogenic disease such as cystic fibrosis (Figure 1). It is also a major pathological feature of cancers, regulating the invasion and metastasis of oncogenic cells in tumors. Clearly, developing effective therapeutics against tissue fibrosis is an urgent pursuit in diverse research areas. In the lung, profibrotic responses are essential to maintain the barrier function during injury and establishing immunity against infectious pathogens, such as bacteria and helminths, but repetitive lung injury often, but not always, follows a sequence that results in persistent fibrosis and irreversible fibrotic damage. Fibroblast proliferation and differentiation into ECM-producing myofibroblasts initiate the fibrotic cascade. These mesenchymal cells dictate excessive ECM production and scar tissue formation in the lung. They resist apoptotic clearance to produce excessive ECM in fibrotic lesions. However, the precise molecular events that prompt myofibroblast accumulation in progressive fibrosis as opposed to wound-healing responses are not thoroughly understood. Some clinical evidence in mice and humans suggests that pulmonary fibrosis may resolve in the absence of injury or profibrotic triggers [2]. In genetically susceptible individuals, mutations in telomerase (TERT, TERC, RTEL1), the surfactant proteins (SFTPB, SFTPC), and the MUC5B gene promoter trigger fibroproliferative processes and fibrotic remodeling via mechanisms that remain largely unknown [3].

For decades, fibrosis research has focused on the cellular and molecular triggers of fibroblast proliferation and transformation into ECM-producing myofibroblasts. In this review, we highlight emerging concepts on the cellular and molecular origins of fibrotic lesions in pulmonary fibrosis pathogenesis. In particular, we discuss the mesenchymal cell-specific transcription factors and heat shock proteins involved in myofibroblast activation. We review recent progress in targeting signaling pathway intermediates, which has opened new avenues to inhibiting profibrotic processes while simultaneously attenuating or reversing established, ongoing pulmonary fibrosis.

2. Current evidence

2.1. Emerging cellular targets in pulmonary fibrosis

Myofibroblasts are responsible for ECM deposition in the lung and crucial to scar tissue formation because they produce and secrete excessive amounts of ECM proteins such as collagens, glycoproteins, and proteoglycans. In progressive fibrosis, activation of the contractile protein alpha-smooth muscle actin

CONTACT Satish K. Madala satish.madala@cchmc.org Division of Pulmonary Medicine, Cincinnati Children's Hospital Medical Center, MLC 2021, 3333 Burnet Avenue, Cincinnati OH 45229

*These authors contributed equally to this work

© 2018 Informa UK Limited, trading as Taylor & Francis Group

Article highlights

- Lung resident fibroblasts contribute to the major pool of myofibroblast in fibrotic lung lesions.
- Fibrocytes secrete paracrine factors and induce lung resident fibroblast activation.
- Transcription factors such as FoxF1, FoxM1 and WT1 play an important role in fibroproliferation and myofibroblast transformation.
- Hsp90 is a positive regulator of fibroblast activation and inhibition of Hsp90 ATPase activity attenuates pulmonary fibrosis.
- TGFβ1 is a major fibrogenic factor and improvement in strategies to inhibit TGFβ1-driven signaling may help to combat with fibrosis.
- Infiltration of immune cells and excessive Th2 cytokine production contributes to pulmonary fibrosis.
- Inhibition of multiple signaling pathways that are heightened in IPF lungs such as RhoA, ROCK, MAPK, PI3K, AKT, and mTOR pathways may offer a therapeutic advantage with unclear mechanism of action.
- Elucidating the underlying mechanisms of the ECM clearance and the regenerative capacity in lungs are of interest to improve fibrosis resolution.
- Combinatorial therapeutic strategies are urgently needed that not only delay the progression but also reverse established and ongoing fibrosis in lungs.

This box summarizes key points contained in the article.

(αSMA) transforms fibroblasts into myofibroblasts. However, despite decades of research, the progenitor cells that undergo myofibroblast transformation to cause alveolar destruction in peripheral areas of the lung remain poorly defined [4,5].

This subsection summarizes new findings on the cellular origins of myofibroblasts during lung fibrogenesis. Previous studies have defined five: (i) resident fibroblasts; (ii) hematopoietic fibroblasts, called fibrocytes; (iii) mesothelial cells lining subpleural areas; (iv) pericytes (PCs) that tightly associate with the microvasculature; and (v) epithelial cells.

2.1.1. Resident fibroblasts

These non-hematopoietic cells reside in various parenchymal areas of the lung. They produce matrix proteins and growth factors that provide the structural support essential during lung development and in maintaining mucosal barrier integrity and physiological functions. They are not terminally differentiated and differentiate into myofibroblasts during lung injury and repair [6,7]. Studies from our group and several others emphasize their contribution to αSMA-expressing myofibroblasts that accumulate after fibrotic injury. Using FoxD1-Cre; -TdT-R; Col-GFP^{Tg} mice, Hung et al. showed that, following bleomycin injury, 55 percent of αSMA+ myofibroblasts are derived from collagen-1-(α)1-positive and PDGFRα-expressing resident fibroblasts [8]. A recent study to determine whether lipofibroblasts, a type of resident fibroblast that contains an excess of neutral lipids, can differentiate into αSMA-expressing myofibroblasts, found that they co-expressed αSMA during bleomycin-induced lung injury in Adrp$^{Cre\text{-}ERT2/mT/mG}$ mice. Among lineage-labeled lipofibroblasts, 19 percent became αSMA-positive myofibroblasts during bleomycin-induced fibrosis [9]. Overall, the lung resident fibroblasts represent a heterogeneous population of cells expressing different network of genes that engage in paracrine and autocrine interactions in fibrosing lungs. Thus, therapies that modulate the activation and/or recruitment of resident fibroblasts could emerge as viable treatments for pulmonary fibrosis.

2.1.2. Hematopoietic fibroblasts

Fibrocytes are unique mesenchymal progenitor cells derived from bone marrow that express a variety of cell surface markers related to leukocytes, hematopoietic progenitor cells, and fibroblasts [10,11]. They were originally identified in tissues with active fibrosis and inflammation during

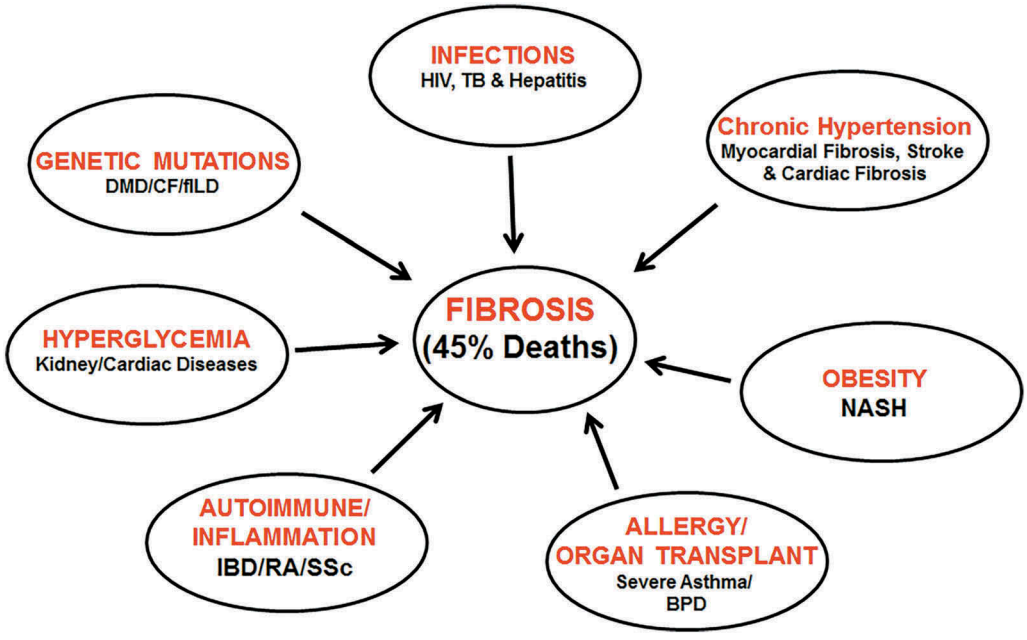


Figure 1. Tissue fibrosis and associated diseases.

Tissue fibrosis is a major cause of death worldwide due to organ failure as several chronic diseases are associated with severe fibrosis leading to organ failure due to impairment in the regulation of inflammation, metabolic pathways and infections. Monogenic mutations could lead to malformed proteins which can manifest into impaired tissue remodeling and fibrosis in chronic diseases such, as Cystic Fibrosis (CF), Duchenne Muscular Dystrophy (DMD), and familial interstitial lung diseases (fILD).

fibroproliferative diseases like idiopathic pulmonary fibrosis (IPF) [12]. The surface markers they express vary with tissue and disease status, but they all express the common leukocyte antigen (CD45) and mesenchymal marker type-I collagen (Figure 2). Their pathogenic role in pulmonary fibrosis is well established in various experimental animal models and clinical samples of IPF [10,13]. Serum amyloid P (SAP), an endogenous blood stream protein inhibits the differentiation of circulating monocytes into pro-fibrotic macrophages (M2) and fibrocytes, which was found to be reduced in IPF patients [14,15]. Recombinant SAP is currently under clinical trials for patients with IPF [16]. However, transformation of fibrocytes into αSMA-positive myofibroblasts is controversial, and recent studies reveal that it is limited. Hashimoto et al. used enhanced green fluorescent protein (EGFP)-chimeric mice and found that most GPF+ cells were negative for αSMA, suggesting that few fibrocytes become myofibroblasts during bleomycin-induced lung injury [17]. Using GFP-chimeric mice, we induced pulmonary fibrosis by overexpressing transforming growth factor alpha (TGFα) in airway club cells. Although fibrocytes accumulated in fibrotic lesions, the majority of them did not become αSMA-expressing myofibroblasts [18]. Note that in the pathogenesis of pulmonary fibrosis, fibrocyte infusion produces severe fibrotic lesions in part due to the paracrine effect on lung-resident (myo)fibroblasts. Fibrocytes infused into wild-type mice challenged with either bleomycin or fluorescein isothiocyanate (FITC) exacerbated pulmonary fibrosis but had no effect on normal mice [19].

These *in vivo* findings suggest that fibrocytes alone cannot induce fibrosis but may play a pathogenic role in ongoing lung injury by secreting paracrine factors that stimulate resident fibroblast proliferation and/or transformation to myofibroblasts [18]. Fibrocytes have been shown to secrete many paracrine factors, including periostin, which is elevated during bleomycin-induced pulmonary fibrosis and IPF [20]. A recent study found that periostin prompts myofibroblast differentiation during bleomycin-induced lung fibrosis [21]. Further studies on the role of fibrocyte-secreted paracrine factors in fibroblast activation could inform new therapeutic strategies.

2.1.3. Mesothelial cells

A single sheet of cuboid pleural mesothelial cells (PMCs) lines the lung. PMCs express both epithelial and mesenchymal cell-specific genes, such as calretinin, cytokeratin, collagen, desmin, and vimentin, but not smooth muscle actin. During embryonic lung development, they become mesenchymal cells in a process called the mesothelial-to-mesenchymal transition (MMT); as a result, mesothelium-derived myofibroblasts populate the perivascular and peribronchial areas of the adult lung [22]. Recent studies using cultured PMCs provide some evidence of MMT in the pathogenesis of pulmonary fibrosis. In particular, the TGFβ1/SMAD3 axis was implicated in MMT and myofibroblast accumulation in the parenchyma of TGFβ1-injured lungs [23]. Although these studies suggest that MMT contributes to pulmonary fibrosis, the lack of robust lineage-tracing models is a significant limitation [24–27].

More recent studies have shown that tamoxifen-dependent Cre recombinases, also known as CreERT2-driven recombination in Wilms tumor ($WT1^{CreERT2}$) mice is more reliable and reproducible than in $WT1^{CreEGFP}$ reporter mice [13,28–30]. Use of $WT1^{CreERT2}$ mice enabled accurate labeling of the WT1-positive mesothelial cells lining embryonic lungs, later shown to engender the mesenchymal cells of the lung parenchyma [28,29]. We demonstrated that WT1 is downregulated in the postnatal stages of lung development but upregulated in mesothelial cells in IPF and a mouse model of severe fibrotic lung disease [13]. Indeed, *in vivo*, postnatal mesothelial lung cells transform into myofibroblasts in TGFα/$WT1^{CreERT2/mTmG}$ reporter mice during TGFα-induced pulmonary fibrosis. They are found in subpleural areas of fibrotic lungs but not in peribronchial or adventitial regions [31] . However, PMCs did not transform into myofibroblasts during single-dose bleomycin-induced injury or adeno TGFβ1-induced pulmonary fibrosis [28], perhaps because TGFβ-driven signaling or other signaling events are less intense. Future studies of myofibroblast formation should be designed to elucidate both up- and downstream WT1 targets and possible cross-talk with the TGFβ/SMAD pathway. Understanding the complex

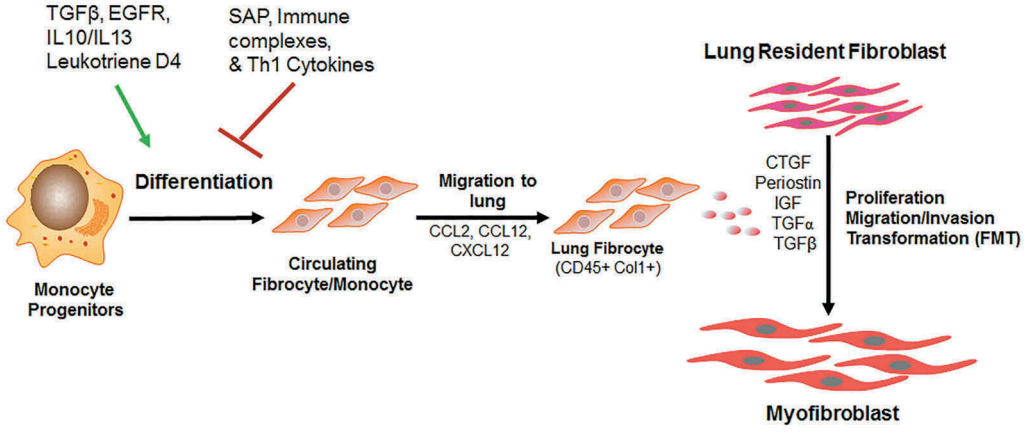


Figure 2. The cellular pathway of fibrocyte-driven (myo)fibrobalst activation in severe fibrotic lung disease.

Fibrocytes originate from monocyte progenitors and migrate to fibrotic lesions of injured lungs to secrete paracrine factors that can cause fibroproliferation and fibroblast-to-myofibroblast (FMT) transformation in the pathogenesis of pulmonary fibrosis.

regulation of myofibroblast formation by TGFβ-dependent and independent pathways in the pathogenesis of pulmonary fibrosis is essential to developing more efficacious therapeutics for IPF.

2.1.4. Pericytes

Pericytes are mural cells that tightly associate with the microvasculature endothelium with the help of multiprotein complexes to strongly support microvascular homeostasis and angiogenesis [32,33]. Pericytes express such markers as neural/glial antigen 2 (NG2), platelet-derived growth factor receptor beta (PDGFR-β), cluster differentiation 90 (CD90), and CD146 [33]. Recent studies using a cell-specific lineage-tracing approach have shown that pericytes become myofibroblasts *in vivo*. Hung et al. used FoxD1-Cre mice to tag pericyte-like cells that co-express NG2. After bleomycin injury, FoxD1-progenitor cells proliferated in fibrosing lungs. These fate-mapped cells have been shown to express αSMA, suggesting a possible pericyte-to-myofibroblast transition, but the myofibroblasts originating from them do not comprise the majority of αSMA-positive cells [8]. In another study, human lung pericytes were grown on decellularized IPF matrix to demonstrate their transformation into myofibroblasts [34]. However, the nonspecific and continuous labeling in FoxD1-reporter mice is a major limitation in assessing the direct conversion of pericytes to myofibroblasts upon injury in adult lungs. The use of inducible Cre to trace the lineage of NG2-positive cells indicates that pericyte-like cells undergo proliferative expansion, but most do not become myofibroblasts during bleomycin-induced injury [35]. Overall, PCs are a potential source of myofibroblasts, but future studies must establish their percent contribution to the pathogenesis of fibrotic lung disease.

2.1.5. Epithelial cells

The epithelial-to-mesenchymal transition (EMT) is a complex molecular process in which a polarized epithelial cell adopts a mesenchymal cell phenotype with enhanced migratory capacity, invasiveness, apoptosis resistance, and production of ECM components, such as collagen and fibronectin. EMT's role in cancer and fibrosis has been described in many organs. Previous studies using patient-derived samples and various *in vivo* models of pulmonary fibrosis demonstrated that EMT is an important cellular phenotypic change that contributes to the mesenchymal cell pool in the pathogenesis of fibrotic lung disease [36–39]. However, a recent lineage-tracing study performed in well-controlled, tamoxifen-inducible Sftpc-CreERT and Scgb1a1-CreERT reporter mice found no EMT during bleomycin-induced pulmonary fibrosis [35]. In the TGFα model, EMT's contribution was determined by generating a quadruple transgenic mouse in which airway epithelial cells were tagged permanently with activation of LacZ reporter gene, and TGFα was overexpressed using doxycycline (dox) to induce severe fibrotic lung disease. Note that the lung epithelial cells showed high LacZ activity and beta-galactosidase (β-gal) staining, but the mesenchymal cells of the fibrotic regions showed no staining, suggesting that airway epithelial cells do not transform to myofibroblasts [40].

Adult lungs are primarily comprised of the epithelial compartment, of which 90 percent consists of morphologically distinct epithelial cell types, including alveolar types I and II. Other studies indicate that activated alveolar epithelial cells produce collagen and secrete other factors in fibrotic lungs, but whether they have capacity to differentiate further into mesenchymal cells or lose their epithelial cell characteristics in the pathogenesis of pulmonary fibrosis remains unknown [41]. During pulmonary fibrosis, epithelial cells not only play a crucial role on their own but also secrete paracrine factors that may activate mesenchymal cells [42]. The EMT is a controversial mechanism that must be further investigated using appropriate epithelial cell reporter models. Understanding epithelial-mesenchymal crosstalk will clarify disease pathogenesis and lead to IPF therapies.

2.2. Emerging molecular targets in pulmonary fibrosis

Mechanistic studies have identified TGFβ as a master regulator of profibrotic processes, including ECM production, inflammation, and myofibroblast formation, particularly the accumulation of these apoptosis-resistant cells in IPF. However, growing *in vitro* and *in vivo* evidence indicates that TGFβ-independent pathways induce myofibroblast transformation and pulmonary fibrosis [43]. This subsection reviews research on emerging molecular targets of (myo)fibroblast activation in pulmonary fibrosis.

2.2.1. Fox proteins

Forkhead box (Fox) proteins are a family of 'winged-helix' DNA-binding domains (DBDs) containing transcription factors that regulate the expression of an array of genes involved in embryonic development and adult tissue homeostasis [44]. Several key subfamilies, such as FoxF1, FoxM1, and FoxO3, are strongly implicated in IPF pathogenesis [45–49]. FoxF1 is critical in regulating the transcription of genes involved in branching morphogenesis during lung development [50,51]. In adult lungs, its expression is observed in bronchiolar smooth muscle cells, connective tissue fibroblasts, endothelial cells, and a subset of alveolar septal cells [51]. Although research has shown that its mRNA and protein levels are downregulated in IPF and a mouse model of bleomycin-induced pulmonary fibrosis, its loss has been associated with increased myofibroblast invasion and collagen production [46].

CDH2 and CDH11 are cadherin family proteins involved in cell-cell adhesion via a calcium-dependent signaling mechanism [52,53]. A molecular switch from CDH2 to CDH11 expression was shown to determine TGFβ fibroblast-to-myofibroblast conversion [52]. Black et al. demonstrated that FoxF1 directly binds to Cdh2 and Cdh11 promoters to activate CDH2 but repress CDH11 expression [46], and the loss of FoxF1 resulted in increased myofibroblast invasion and collagen production during bleomycin-induced pulmonary fibrosis [46]. Moreover, its overexpression was sufficient to attenuate both fibroproliferation and TGFβ1-driven Col1 expression [54]. Selectively deleting it in αSMA-expressing cells was sufficient to exacerbate bleomycin-induced pulmonary fibrosis [46].

FoxM1 and FoxO3a proteins act downstream of the phosphoinositol-3-kinase (PI3K)-AKT signaling cascade [55]. Their axis has been shown to regulate such biological processes as cellular metabolism, proliferation, differentiation, invasion, apoptosis, and DNA-damage response and is thus pivotal in over 20

types of human cancers as well as pulmonary fibrosis [55,56]. FoxM1 regulates proliferation in many types of lung cells by altering expression of the cyclin genes, CCND1 and CCNB1 and serine/threonine-protein kinase (PLK1), involved in the G1/S and G2/M transitions [57] [49]. FoxM1 is elevated in fibroblasts isolated from IPF and the bleomycin model [49]. Several mitogens are implicated in its upregulation via the PI3Kα/PDK1/AKT pathway [49], which a recent study associated with increased fibroproliferation and myofibroblast formation. In contrast, by downregulating FoxM1, FoxO3a has been shown to sensitize IPF fibroblasts to radiation-induced cell death [58]. Mesenchymal cell-specific deletion of the FoxM1 gene or inhibition of FoxM1 using siomycin A was shown to attenuate expression of several profibrotic genes, including αSma, Col1α1, Tgfβ1, and connective tissue growth factor (Ctgf) in the bleomycin model [49]. FoxM1 has been shown to induce expression of the RAD51 and BRCA2 proteins essential for DNA-damage repair after radiation-induced injury [58]. Importantly, FoxM1 levels correlate with IPF fibroblast resistance to the apoptosis after radiation-induced cell death [58]. In this model, FoxM1 was found upregulated in alveolar epithelial cells (AECs) and the conditional deletion of FoxM1 in AECs shown to attenuate radiation-induced pulmonary fibrosis [45]. Therefore, targeting FoxM1 specifically in fibroblasts could be a new therapeutic for the treatment of fibrotic diseases.

2.2.2. WT1

Wilms tumor1 protein is a four zinc finger transcription factor that plays an essential role in the development of such critical organs as lung, heart, and kidney and regulates posttranscriptional modifications and RNA metabolism [59]. Germline mutations or loss of WT1 have been associated with severe developmental defects and embryonic lethality in mice [59,60]. Although expressed at low levels in lung mesothelial cells of adult mice, it can be upregulated in both mesothelial and mesenchymal cells to cause severe fibrosis in the lung [13,31,61]. In gain-of-function studies in primary fibroblasts, we demonstrated that its overexpression alone was sufficient to induce fibroproliferation, myofibroblast formation, and ECM production [31]. Furthermore, its genetic loss markedly reduced expression of ECM genes, such as Col1α and Col5α, and proliferative genes, such as Grem1, Runx1, Wnt4, Igf1, Ccnb1, and E2f8.

Studies using αSMA reporter cells demonstrate that WT1 overexpression is sufficient to induce fibroblast-to-myofibroblast transformation, and chromatin immunoprecipitation experiments indicate that WT1 binds directly to the promoter DNA sequence of αSMA to induce myofibroblasts [31]. WT1 has been shown to maintain the mesenchymal cell phenotype by regulating the genes, such as Snail (Snai1) and E-cadherin (Cdh1), during embryonic stem cell differentiation [62]. Note that haploinsufficiency of WT1 was sufficient to attenuate fibroproliferation, myofibroblast accumulation, and collagen deposition in both TGFα- and bleomycin-induced pulmonary fibrosis *in vivo* [31]. Our new findings suggest that WT1-driven effects on fibroproliferation are non-cell autonomous and may involve paracrine factors secreted by WT1-expressing cells [31]. They highlight the need for more detailed investigation of the molecular mechanisms of WT1-driven fibroblast activation and pulmonary fibrosis and whether crosstalk between WT1 and the TGFβ/SMAD pathway regulates them. By identifying WT1 as a positive regulator of fibroblast activation, they suggest a new target for treating fibrotic lung diseases and possibly regulating fibrosis in other organs.

2.2.3. Heat shock protein 90

The molecular chaperone Hsp90 constitutes 1–2 percent of the total cellular protein pool and plays an essential role in protein folding while stabilizing a variety of client proteins involved in cellular signaling, transcription regulation, and translation [63]. Its molecular functions depend on its ATPase activity and complex formation with other proteins. In mammalian cells, Hsp90α and Hsp90β are the two major isoforms involved in Hsp90-driven functions [64]. They are 86 percent identical, with 93 percent sequence similarity and a characteristic functional MEEVD motif [64]. Both have an N-terminal ATPase catalytic center that binds ATP and assists in chaperoning [64].

Typically, more Hsp90α than Hsp90β is expressed, but in various disease conditions, both may be induced [65,66]. Hsp90β levels are elevated in gastrointestinal stromal tumors, multiple myeloma, breast cancer, and neuroblastomas associated with poor survival [65,67,68]; comparative proteomic analysis shows a significant increase in both Hsp90α and Hsp90β with IPF as compared to healthy lungs [69]. Since many studies confirm the upregulation of Hsp90 expression and its ATPase activity in IPF and mouse models of pulmonary fibrosis [70–74], a recent study proposes a correlation between circulating levels of the Hsp90α isoform and IPF severity [71].

Findings on how Hsp90 regulates signaling pathways to activate fibroblasts have provided new insights into the molecular mechanisms of severe fibrotic lung disease [71–75]. In particular, using tanespimycin (17-AAG) to block Hsp90 ATPase activity hampered the TGFβ1 signaling pathway by inducing proteasomal degradation of TGFβRII, an essential signaling receptor for the TGFβ1 ligand [73]. Similar findings in the tight-skin (Tsk-1) mouse model of dermal fibrosis show that administering alvespimycin (17-DMAG) blocked the TGFβ1 signaling pathway by decreasing SMAD2/3 phosphorylation [75]. Another study showed that Hsp90 forms a complex with TGFβRII to induce fibroblast activation. In human lung fibroblasts treated with exogenous human recombinant Hsp90α, expression of αSMA and other ECM proteins, such as Col1 and fibronectin, increased [72], and a monoclonal anti-Hsp90α antibody (1G6-D7) mitigated these effects by attenuating profibrotic signaling via the kinases ERK, Akt, and P38 [72]. We showed that Hsp90β knockdown in fibroblasts attenuates their proliferation and formation of myofibroblasts, while loss of Hsp90α had a limited or no effect on proliferation and ECM production but attenuated fibroblast migration [74]. Hsp90 inhibition with 17-AAG reduced migratory capacity, proliferation, and ECM production in fibroblasts [74]. New therapeutics inhibiting Hsp90 could target the profibrotic signaling

pathways involved in fibroblast activation and pulmonary fibrosis.

2.3. New advances in inhibiting pulmonary fibrosis signaling pathways

Drugs approved for IPF delay loss of lung function but fail to stabilize or improve IPF patients' lung function or survival. A plethora of mechanisms and pathways are involved in lung fibrosis, including repetitive epithelial cell injury, wound healing, epithelial-mesenchymal crosstalk, and lung fibrotic pathology. To improve clinical outcomes, researchers are pursuing alternative therapeutic approaches to fibrogenesis and its resolution, especially drugs targeting the signaling pathways that maintain the fibrotic networks. Many inhibitors target the downstream signaling molecules involved in fibrogenesis and lesion progression.

2.3.1. TGFβ and integrins

The pathological role of TGFβ as a fibrogenic agent is well documented [76–78]. Of its three forms, TGFβ1 is a potent fibrogenic factor secreted by immune and epithelial cells and fibroblasts. Published studies demonstrate that it promotes fibroblast-to-myofibroblast transformation and collagen deposition both *in vitro* and *in vivo* [79,80]. However, in a phase 1 trial (NCT00125385), an antibody to the TGFβ isoforms (GC1008) showed low efficacy. Targeting TGFβ directly disturbs the other homeostatic effects it regulates in other organs, therefore, more targeted approach toward the molecular mechanisms that activates the latent TGFβ might be advantageous in rescuing from fibrosis. Targeting the integrins or lysophosphatidic acid (LPA) or autotaxins might be a right approach in dealing with fibrosis.

Activation of latent TGFβ is regulated by the integrin αvβ6, expressed more strongly on the epithelial cells of fibrotic than healthy lungs [79,80]. In a TGFα transgenic fibrotic model, genetic deletion of β6 slightly reduced fibrosis, indicating that other signaling mechanisms may act before the αvβ6-TGFβ1 pathway [80] as well as the complexity of fibrotic disease. However, preclinical primate studies with BG00011, a humanized monoclonal antibody against αvβ6 (formerly known as STX-100 and acquired by Biogen), decreased active TGFβ1 signaling in a dose-dependent manner as assessed by pSMAD2 expression in bronchoalveolar lavage fluid (BAL) cells. A phase 2A, randomized, placebo-controlled, dose-escalation study (NCT01371305) on 41 IPF subjects revealed an inverse dose-response relationship with pSMAD2 levels in BAL cells. The data on safety, tolerability, and dose selection led to a phase 2B study [81]. In a phase 1 investigation, another nonpeptidic αvβ6 inhibitor (GSK3008348; GlaxoSmithKline) showed good tolerability in healthy subjects, and its tolerability and safety in IPF patients are currently under investigation (NCT03069989).

2.3.2. T cells, innate lymphoid cells 2 and IL-13

Uncontrolled inflammation and oxidative burst are known to cause progressive lung damage and thickening of peripheral areas of the lung [82]. Histological evaluations of fibrotic lungs revealed infiltration of mononuclear immune cells (T-cells, B-cells and macrophages) into the mature fibrotic lesions in IPF [83]. One of the challenges in studying the role of inflammation in IPF is to identify pathogenic inflammatory cells and their mediators involved in the maintenance of persistent inflammation and progressive fibrosis. Th2-cytokine polarized T cell responses have been shown to mediate tissue damage and fibrosis in IPF [84,85]. In IPF patients, IL-13 levels are elevated and correlate inversely with lung function [86]. Also, IL-4 and IL-13 have been shown to contribute to inflammation and fibrosis in multiple animal models of pulmonary fibrosis including the bleomycin-induced pulmonary fibrosis [87–91]. IL-13 is shown to activate fibroblasts which participate in production and deposition of excess collagen and fibronectin in lung and other organs [92]. Recent studies suggest the innate lymphoid cell 2 (ILC2) are also important source for IL-13 production [93]. Tralokinumab, Lebrikizumab, and SAR156597 were the antibody-mediated targeting either IL-13 alone or IL-4 and IL-13 entered into clinical trials [94–96]. However, anti-IL-13 clinical trials were stopped due to lack of efficacy and could not meet their primary end points. This suggests that targeting the IL-13 alone may not be beneficial to the IPF patients.

2.3.3. Lipids

Apart from proteins, some lipid-mediated signaling pathways are implicated in IPF. LPA levels are high in IPF patients' BAL, acting through receptors LPA_{1-6} [97]. Knockout studies on receptors LPA1 and 2 attenuated lung fibrosis [97,98]. The LPA-LPA1 axis assists in epithelial cell apoptosis after lung injury while opposing apoptosis in fibroblast cells [98]. Xu MY et al. demonstrated that in epithelial cells, the LPA-LPA2 axis activates TGFβ1, mediated by αvβ6, through RhoA-facilitated contraction [99]. However, targeting the enzyme responsible for LPA formation would inhibit the pathogenesis the LPA-LPA1/LPA2 axes mediate.

In this context, Galapagos developed GLPG1690, a selective inhibitor of autotaxin, the phospholipase most responsible for excessive LPA formation in IPF lung tissues [100]. Deleting the autotaxin gene from bronchial epithelial cells and macrophages reduced fibrotic disease [100]. GLPG1690-treated IPF fibroblasts had a marked reduction in fibrotic mediators like CTGF, interleukin-6 (IL-6), and endothelin-1 (ET-1) [101]. Recently, a 12-week, randomized, double-blinded, placebo-controlled phase 2a study (NCT02738801) on 23 IPF patients found GLPG1690 to be well tolerated, and its pharmacokinetic and dynamic profiles were similar to those in healthy subjects as determined by a phase 1 study. LPA concentrations were reduced during the treatment period and reached baseline values without treatment. The mean decline in forced vital capacity (FVC) was consistent with three months of pooled data on the IPF medications nintedanib and pirfenidone [102].

In parallel, Bristol-Myers Squibb developed BMS-986020, a potent antagonist of the LPA1 receptor. Preclinical studies showed antifibrotic effects in, not only the lungs, but liver, kidney, eyes, and skin. It went through phase 1 trials, but although phase 2 (NCT01766817) was completed in 2016, the outcome has not yet been reported.

2.3.4. Cellular senescence and metabolism

IPF is a disease of elderly population and multiple lines of evidence suggest aging-associated factors such as cellular senescence, telomere attrition, and deregulated metabolism role in its pathogenesis [103]. Cellular senescence is well studied in the pathogenesis of IPF. AECs and fibroblasts are crucial cell types that undergo cellular senescence following injury in pulmonary fibrosis. Treatment with senolytic drugs that selectively eliminates senescent cells by inducing apoptosis shown to eliminate pro-fibrotic senescent fibroblasts *in vitro* and alveolar epithelial cells ex vivo [104–106]. In particular, a cocktail of dasatinib and quercetin is shown to improve lung function during bleomycin-induced pulmonary fibrotic mice. However, visible fibrosis was not altered as evidenced by histopathological score [104]. Recent studies suggest that antioxidant and senolytic properties of metformin could be used to dampen bleomycin-induced pulmonary fibrosis [107,108]. However, more work is needed to clarify whether use of senolytic drugs can selectively eliminate pathogenic cell types but not cells required for lung regeneration in fibrosis resolution.

2.3.5. Connective tissue growth factor (CTGF)

In IPF patients, high CTGF expression has been shown to promote ECM deposition, myofibroblast activation, cell adhesion, and invasion, the key processes of tissue remodeling and fibrosis [109,110]. FibroGen identified pamrevlumab (FG-3019) as a candidate monoclonal antibody that efficiently reduces CTGF activity to restore tissue homeostasis. In an irradiated mouse model, FG-3019 treatment eight weeks after lung injury reduced lung density and maintained it for six months. Within two weeks of administration, it also decreased the infiltration of mast cells and macrophages [111]. These promising results led to a phase 1, nonrandomized, open-label, dose-escalation study (NCT00074698) performed on 21 IPF patients, who showed no adverse effects. In the phase 2A, open-label study (NCT01262001) with 89 participants, single doses of either 15mg/kg or 30mg/kg were administered intravenously to two cohorts every three weeks for 45 weeks. FVC declined on average 140 ml, but for 30 percent of patients, FVC increased. Note that this study is the first to show any improvement in pulmonary fibrosis, observing reduced reticular fibrosis and mild adverse effects [112]. Based on these results, a phase 2B, randomized, placebo-controlled study (NCT01890265) was conducted on 103 participants, a subset of whom were treated with FDA-approved drugs. FibroGen announced positive and encouraging results, and combinatorial therapy with either of the FDA-approved drugs was deemed safe. A phase 3 study is planned to evaluate the drug's clinical potential for treating pulmonary fibrosis.

2.3.6. The PI3K/AKT/mTOR pathway

One of the pathways dysregulated in IPF involves phosphoinositide 3-kinase (PI3K), protein kinase B (AKT), and mammalian target of rapamycin (mTOR) [113,114]. It is associated with cell metabolism, growth, proliferation, differentiation, survival, and endoplasmic reticulum-related stress [114,115]. Cell surface receptors, such as tyrosine kinase, activate p110, a catalytic unit of PI3K that converts phosphoinositide bisphosphate (PIP2) to phosphoinositide triphosphate (PIP3) to activate AKT and the pathway. In IPF tissues, expression of phosphatase and tensin homolog (PTEN) and caveolin-1 is suppressed in fibroblasts, and AKT activity is high, leading to fibroproliferation [116,117]. PI3K p110γ expression is also high, and *in vitro* inhibition studies reduced proliferation and α-SMA expression [113].

AKT effector molecules include BCl-2, Fox proteins, and mTOR. They suppress tuberous sclerosis complex (TSC1/2), which indirectly activates mTOR, a kinase that promotes fibroblast proliferation. Of its two complexes, mTORC1 and mTORC2, mTORC1 is sensitive to rapamycin and shows antiproliferative properties. Its phosphorylates, chiefly S6 kinase 1 (S6K1) and 4E-BP1, regulate protein translation. Our studies in TGFα mice showed that LY-2584702, an S6K inhibitor, decreased the subpleural fibrosis TGFα induces [118]. In IPF epithelial cells, phosphorylated S6K (p-S6K) levels are high, and Hippo/YAP signaling active. Expression of the active form of Yes-associated protein (YAP) in human bronchial epithelial cells showed that its stability requires high p-PI3K and p-S6K. Inhibiting p-S6K with temsirolimus blocked YAP entry into the nucleus, thereby suppressing YAP-mediated gene expression of CTGF, AXL, and AJUBA [119]. We propose that in IPF pathogenesis, the interaction of these two signaling pathways prompts cell proliferation and migration and prevents epithelial cell differentiation.

In the bleomycin model, rapid activation of PI3K/AKT and increased protein expression of hypoxia-inducible factor-1alpha (HIF-1α) and VEGF [120] contribute to fibroproliferation and collagen secretion. Studies on treatment with sirolimus, a rapamycin analogue in the bleomycin rat model, reduced IL-13, PDGF-A, and TGFβ1 levels and increased IFN-γ levels in BAL fluid. It also decreased hydroxyproline content [121]. A pilot study (NCT01462006) treated IPF patients with sirolimus and measured circulating fibrocytes since their number is correlated with disease progression. Fibrocytes are recruited into the lung based on CXCL12-CXCR4 chemistry, and mTOR signaling regulates their expression of receptors. Sirolimus significantly reduced the number of circulating fibrocytes, and safety profiles were acceptable [122]. A long-term study in IPF patients is planned.

Omipalisib (GSK2126458) is a highly selective dual inhibitor of PI3K and mTOR. Although originally developed in the oncology setting, it is now tested in IPF patients since the PI3K/mTOR pathway is extremely active in the fibrotic foci of their tissues. Treatment in precision-cut, IPF-tissue BAL cells showed dose-dependent reductions in p-AKT and reduced proliferation of fibroblast cultures [123]. A phase 1B trial (NCT01725139) also showed p-AKT reduction in BAL, and the safety profile in IPF patients was very good [124].

The MAPK (mitogen-activated protein kinase) cascade is another major pathway deregulated in IPF. Our studies in a fibrotic mouse model demonstrate that targeting both the MAPK and PI3K pathways reduced fibrosis and collagen content more efficiently than targeting only one [125]. Thus, targeting several deregulated pathways in IPF may be advantageous.

2.3.7. Lysyl oxidase

Excess deposition of extracellular matrix and tissue stiffening, largely by collagen I, are hallmarks of fibrosis. Two enzymes, transglutaminase 2 (TG2) and lysyl oxidase-like 2 (LOXL2), are primarily responsible for the formation and organization of collagen fibers. They have binding pockets for cytokines and integrins; the latter covalently links collagen and elastin fibers to maintain the mechanical force and modulate tissue stiffness. Serum levels in IPF patients are high and correlate with disease progression and mortality [126]. Immunohistological findings show increased staining for the enzyme in IPF explanted tissue compared to normal lung tissue [127]. Administration of murine monoclonal antibody against LOXL2 (AB0023) in the bleomycin model showed marked reduction in fibrosis, alveolar thickening, TGFβ1 and its signaling, ET-1, CXCL12, and LOXL2. It also reduced the number of fibrocytes in the lungs and the lymphocyte count in BAL as compared to vehicle-treated mice [127]. This study led to the discovery of simtuzumab, a humanized monoclonal antibody to LOXL2. Two phase 2 trials, RAINER (NCT01769196) and ATLAS (NCT01759511), were terminated due to its lack of efficacy. Pharmaxis and Synairgen developed a small-molecule LOXL2 antagonist, PXS-5382A that shown to reduce the fibrotic area as assessed by trichome staining in a murine model. A clinical trial is under way to establish its toxicity.

2.3.8. RhoA/ROCK

Cytoskeletal elements are reorganized during wound healing. One of the major pathways in the context of actin assembly and actomyosin contraction is the rho-associated coiled-coil-forming protein kinase (RhoA/ROCK), which belongs to the serine-threonine kinase family. Its two isoforms, ROCK1 and ROCK2, are activated by rho GTPases residing downstream of many ligand/receptor pairs, such as LPA-LPA1, S1P-S1P1, thrombin-proteinase-activated receptor, and TGFβ-RTK [128,129]. ROCK activity is elevated in the fibrotic lesions of mice and IPF patients and involved in the profibrotic activation of fibroblasts and epithelial and endothelial cells at the injury site [130,131]. ROCK inhibition studies with fasudil reduced the immune cells count in BAL fluid; production of the fibrotic markers TGFβ1, CTGF, α-SMA, plasminogen activator inhibitor-1 (PAI-1), and collagen; and the phosphorylated form of SMAD2/3 in the bleomycin model [132,133]. In ROCK1/2 haploinsufficient studies, Knipe et al. showed that both isoforms afforded comparable protection from bleomycin-induced injury [129]. Together, these preliminary studies show that inhibiting ROCK may benefit IPF patients. Consequently, Kadmon conducted a 24-week, phase 2, open-label trial with KD025, a selective inhibitor of ROCK2 in IPF patients formerly treated with pirfenidone or nintadanib (NCT02688647). The drug was well tolerated and improved lung function as measured by FVC with an absolute median difference of 127ml between the treated and nontreated groups.

3. Conclusion

Therapeutic inhibition of established and ongoing fibrosis remains a major challenge due to an incomplete understanding of cellular and molecular mechanisms that participate in the formation and maintenance of scar tissue. Recent advances have helped to characterize radiological and histological changes from the early to late stages of IPF. Fibrosis has been shown to begin in subpleural areas and progress into the parenchyma of the distal areas. Dysregulated growth-factor signaling in various lung cells (epithelial, mesothelial, endothelial, mesenchymal, macrophage) contributes to IPF. However, the roles of molecular heterogeneity and cell-specific signaling pathways in myofibroblast activation remain unknown. A multipronged approach to disrupt abrupt signaling in various lung cells without interrupting regenerative processes could be a more viable strategy than targeting a single gene or enzyme. In support, the FDA-approved antifibrotic drugs pirfenidone and nintedanib target several pathways and gene networks.

Recent technological advances in identifying molecular signatures at the single-cell level will eventually enable us to map both cellular and molecular differences between IPF and normal lungs. Furthermore, use of systems biology tools will help us to identify an integrated antifibrotic strategy that will simultaneously target relevant pathways and/or gene networks to treat this highly complex and intransigent disease. Future research on the role of cell-specific transcription factors and other druggable targets in pulmonary fibrosis will enable evidence-based combination therapies that can be selected for new clinical trials. We must also learn how to harness the beneficial mechanisms of lung development and inflammation, so damaged lung can be regenerated, the ultimate goal of fibrosis research in all organs.

4. Expert opinion

Over the past two decades, many clinical trials on IPF failed to translate bench findings to the clinic. Despite appropriate study design and well-defined primary endpoints, mortality either increased or showed no change in the treatment arm compared to the placebo group. Studies on warfarin, ambrisentan, bosentan, macitentan, imatinib, corticosteroids, azathioprine, N-acetylcysteine, triple therapy (N-acetylcysteine, prednisolone, azathioprine), SAR156597, lebrikizumab, and carlumab are the best examples [96,134–142]. These disappointments drive clinicians and researchers to improve their definitions of meaningful endpoints and disease parameters.

IPF is an epithelial-fibroblastic disorder, where fibroproliferation and myofibroblast formation and persistence cause excessive ECM deposition [2]. In late 2014, the FDA approved two IPF drugs, nintedanib and pirfenidone, under the brand names Ofev and Esbriet, respectively, which inhibit the key pathways of fibrosis, inflammation, and oxidation. Their exact mechanism of action is unclear, but they prolong IPF patients' survival.

Nintedanib (BIBF 1120) inhibits tyrosine kinases and targets VEGFR, PDGFR, FGFR, and TGFβ-mediated signaling [143]. It also inhibits fibroblast-to-myofibroblast transformation and reduces fibrosis in bleomycin- and silica-induced models [144]. For approval, three randomized, double-blinded, placebo-controlled clinical trials—TOMORROW (NCT00514683), INPULSIS-1 (NCT01335464), and INPULSIS-2 (NCT01335477)—were conducted. Nintedanib's effect on lung function decline was evaluated in 1228 IPF patients at a dosage of 150 mg twice a day for 52 weeks. The outcome was measured as reduction in decline of the lung's forced vital capacity (FVC) over a year as compared to placebo. All the three trails showed significant reduction in FVC decline, but only TOMORROW and INPULSIS-2 showed a significant delay of the first acute IPF exacerbation. Side effects included diarrhoea, nausea, and increases in liver enzymes, bilirubin, and bleeding due to VEGF blockage.

Pirfenidone is a pyridone molecule with as yet unexplained anti-inflammatory, anti-oxidative and antifibrotic properties. Recent studies have shown that it inhibits collagen fibril formation and/or the hedgehog signaling pathway by reducing the glioma-associated oncogene homolog protein (Gli 2) and its target genes [145,146]. Results from a phase 1 trial (NCT02648048) with vismodegib, a molecule that like pirfenidone, inhibits the hedgehog pathway, have not been reported yet. However, in mouse lung fibroblasts, pirfenidone increased the expression of antifibrotic factors, such as nuclear factor-erythroid-related factor 2 (Nrf2), heme oxygenase-1 (Ho-1), and glutathione peroxidase 1 (Gpx1), to reduce oxidative stress [147]. The first trial on pirfenidone, conducted in Japan, established its feasibility for treating advanced pulmonary fibrotic patients, and a later study by Taniguchi et al. showed that it slowed the decline of lung vital capacity and improved patient survival. The results of the CAPACITY 004 and 006 and ASCEND clinical trials paved the way for its approval to treat IPF patients with adverse gastrointestinal events and photosensitivity. The long-term treatment study RECAP proved that the drug does not increase adverse events [148]. A trial of a therapy combining nintetanib with pirfenidone (INJOURNEY) showed acceptable adverse events and tolerability, but reports on lung function have not yet been analyzed [149].

IPF is difficult to treat because of the many distinct immunological and molecular mechanisms that initiate and maintain the progression of fibrotic lung diseases. Dysregulated signaling pathways and (myo)fibroblast activation are major contributors, and inhibiting a single pathway or growth factor in mouse models or human clinical trials has not been effective in attenuating established and ongoing lung fibrosis [1,125,150]. Recent success with nintedanib and pirfenidone, which target the various signaling pathways and cell types in IPF, has changed the landscape. Clinical trials are now dominated by combinatorial designs. Synergistic strategies that more completely arrest or reverse fibrosis are sorely needed and will require a better understanding of the molecular pathways that drive fibroblasts toward dysregulated matrix remodeling. We must also identify patient subtypes based on pathway-specific biomarkers and genetic phenotyping in clinical staging for these new combinatorial trials. Further, we must incorporate our new insights on lung development, regenerative medicine, and the beneficial aspects of inflammation, so we can regrow damaged tissue to duplicate the normal architecture of the lung.

Funding

This paper was not funded. This work was supported by grants from the National Institutes of Health [1R01 HL134801 and 1R21AG059533] and the Department of Defence grant [W81XWH-17-1-0666] for SK Madala and a Cystic Fibrosis Foundation Fellowship for V Sontake

Declaration of interest

The authors have no other relevant affiliations or financial involvement with any organization or entity with a financial interest in or financial conflict with the subject matter or materials discussed in the manuscript. This includes employment, consultancies, honoraria, stock ownership or options, expert testimony, grants or patents received or pending, or royalties.

Reviewer disclosures

Peer reviewers on this manuscript have no relevant financial or other relationships to disclose

References

Papers of special note have been highlighted as either of interest (•) or of considerable interest (••) to readers.

1. Wynn TA, Ramalingam TR. Mechanisms of fibrosis: therapeutic translation for fibrotic disease. Nat Med. 2012;18:1028–1040.
   • **Describes the innate and adaptive immune responses in the pathogenesis of fibrosis in multiple organs.**
2. Glasser SW, Hagood JS, Wong S, et al. Mechanisms of Lung Fibrosis Resolution. Am J Pathol. 2016;186:1066–1077.
   • **Describes the importance fibrosis resolution in pulmonary fibrosis.**
3. Kaur A, Mathai SK, Schwartz DA. Genetics in idiopathic pulmonary fibrosis pathogenesis, prognosis, and treatment. Front Med (Lausanne). 2017;4:154.
   • **Comprehensive review on genome-wide association studies identifying susceptibility loci for IPF.**
4. Zhang HY, Gharaee-Kermani M, Zhang K, et al. Lung fibroblast alpha-smooth muscle actin expression and contractile phenotype in bleomycin-induced pulmonary fibrosis. Am J Pathol. 1996;148:527–537.
5. Sun KH, Chang Y, Reed NI, et al. alpha-Smooth muscle actin is an inconsistent marker of fibroblasts responsible for force-dependent TGFbeta activation or collagen production across multiple models of organ fibrosis. Am J Physiol Lung Cell Mol Physiol. 2016;310:L824–36.
6. Barron L, Gharib SA, Duffield JS. Lung pericytes and resident fibroblasts: busy multitaskers. Am J Pathol. 2016;186:2519–2531.
7. Kendall RT, Feghali-Bostwick CA. Fibroblasts in fibrosis: novel roles and mediators. Front Pharmacol. 2014;5:123.
8. Hung C, Linn G, Chow YH, et al. Role of lung pericytes and resident fibroblasts in the pathogenesis of pulmonary fibrosis. Am J Respir Crit Care Med. 2013;188:820–830.
9. El Agha E, Moiseenko A, Kheirollahi V, et al. Two-way conversion between lipogenic and myogenic fibroblastic phenotypes marks the progression and resolution of lung fibrosis. Cell Stem Cell. 2017;20:261–273 e3.
10. Maharaj S, Shimbori C, Kolb M. Fibrocytes in pulmonary fibrosis: a brief synopsis. Eur Respir Rev. 2013;22:552–557.
    • **Describes the relevance of fibrocytes in pulmonary fibrosis.**

11. Reilkoff RA, Bucala R, Herzog EL. Fibrocytes: emerging effector cells in chronic inflammation. Nat Rev Immunol. 2011;11:427–435.
12. Xu J, Kisseleva T. Bone marrow-derived fibrocytes contribute to liver fibrosis. Exp Biol Med (Maywood). 2015;240:691–700.
13. Sontake V, Shanmukhappa SK, DiPasquale BA, et al. Fibrocytes regulate Wilms tumor 1-positive cell accumulation in severe fibrotic lung disease. J Immunol. 2015;195:3978–3991.
• **Important paper on the cross-talk between fibrocytes and WT1-positive resident fibrobalsts.**
14. Pilling D, Buckley CD, Salmon M, et al. Inhibition of fibrocyte differentiation by serum amyloid P. J Immunol. 2003;171:5537–5546.
15. Murray LA, Chen Q, Kramer MS, et al. TGF-beta driven lung fibrosis is macrophage dependent and blocked by Serum amyloid P. Int J Biochem Cell Biol. 2011;43:154–162.
16. Raghu G, van Den Blink B, Hamblin MJ, et al. Effect of recombinant human pentraxin 2 vs placebo on change in forced vital capacity in patients with idiopathic pulmonary fibrosis: a randomized clinical trial. JAMA. 2018;319:2299–2307.
17. Hashimoto N, Jin H, Liu T, et al. Bone marrow-derived progenitor cells in pulmonary fibrosis. J Clin Invest. 2004;113:243–252.
18. Madala SK, Edukulla R, Schmidt S, et al. Bone marrow-derived stromal cells are invasive and hyperproliferative and alter transforming growth factor-alpha-induced pulmonary fibrosis. Am J Respir Cell Mol Biol. 2014;50:777–786.
19. Moore BB, Murray L, Das A, et al. The role of CCL12 in the recruitment of fibrocytes and lung fibrosis. Am J Respir Cell Mol Biol. 2006;35:175–181.
20. Naik PK, Bozyk PD, Bentley JK, et al. Periostin promotes fibrosis and predicts progression in patients with idiopathic pulmonary fibrosis. Am J Physiol Lung Cell Mol Physiol. 2012;303:L1046–56.
21. Ashley SL, Wilke CA, Kim KK, et al. Periostin regulates fibrocyte function to promote myofibroblast differentiation and lung fibrosis. Mucosal Immunol. 2017;10:341–351.
22. Batra H, Antony VB. The pleural mesothelium in development and disease. Front Physiol. 2014;5:284.
23. Nasreen N, Mohammed KA, Mubarak KK, et al. Pleural mesothelial cell transformation into myofibroblasts and haptotactic migration in response to TGF-beta1 in vitro. Am J Physiol Lung Cell Mol Physiol. 2009;297:L115–24.
24. Chen LJ, Ye H, Zhang Q, et al. Bleomycin induced epithelial-mesenchymal transition (EMT) in pleural mesothelial cells. Toxicol Appl Pharmacol. 2015;283:75–82.
25. Karki S, Surolia R, Hock TD, et al. Wilms' tumor 1 (Wt1) regulates pleural mesothelial cell plasticity and transition into myofibroblasts in idiopathic pulmonary fibrosis. FASEB J. 2014;28:1122–1131.
26. Mubarak KK, Montes-Worboys A, Regev D, et al. Parenchymal trafficking of pleural mesothelial cells in idiopathic pulmonary fibrosis. Eur Respir J. 2012;39:133–140.
27. Zolak JS, Jagirdar R, Surolia R, et al. Pleural mesothelial cell differentiation and invasion in fibrogenic lung injury. Am J Pathol. 2013;182:1239–1247.
28. von Gise A, Stevens SM, Honor LB, et al. Contribution of fetal, but not adult, pulmonary mesothelium to mesenchymal lineages in lung homeostasis and fibrosis. Am J Respir Cell Mol Biol. 2016;54:222–230.
• **Important paper on contribution of mesothelial cells to mesenchymal cells.**
29. Que J, Wilm B, Hasegawa H, et al. Mesothelium contributes to vascular smooth muscle and mesenchyme during lung development. Proc Natl Acad Sci U S A. 2008;105:16626–16630.
•• **Seminal paper defining fetal lung mesothelial cell contribution to smooth muscle cells.**
30. Rudat C, Kispert A. Wt1 and epicardial fate mapping. Circ Res. 2012;111:165–169.
31. Sontake V, Kasam RK, Sinner D, et al. Wilms' tumor 1 drives fibroproliferation and myofibroblast transformation in severe fibrotic lung disease. JCI Insight. 2018;3.e121252
•• **Seminal paper that shows the importance of WT1 in fibroproliferation and myofibroblast transformation in the pathogenesis of pulmonary fibrosis.**
32. Hung CF, Mittelsteadt KL, Brauer R, et al. Lung pericyte-like cells are functional interstitial immune sentinel cells. Am J Physiol Lung Cell Mol Physiol. 2017;312:L556–L567.
33. Maier CL, Shepherd BR, Yi T, et al. Explant outgrowth, propagation and characterization of human pericytes. Microcirculation. 2010;17:367–380.
34. Sava P, Ramanathan A, Dobronyi A, et al. Human pericytes adopt myofibroblast properties in the microenvironment of the IPF lung. JCI Insight. 2017;2.e96352
• **Important paper on contribution of pericytes to mesenchymal cells.**
35. Rock JR, Barkauskas CE, Cronce MJ, et al. Multiple stromal populations contribute to pulmonary fibrosis without evidence for epithelial to mesenchymal transition. Proc Natl Acad Sci U S A. 2011;108:E1475–83.
•• **Seminal paper that desreibes multiple stromal cell contributions and the lack of EMT in pulmonary fibrosis.**
36. Kasai H, Allen JT, Mason RM, et al. TGF-beta1 induces human alveolar epithelial to mesenchymal cell transition (EMT). Respir Res. 2005;6:56.
37. Kim KK, Kugler MC, Wolters PJ, et al. Alveolar epithelial cell mesenchymal transition develops in vivo during pulmonary fibrosis and is regulated by the extracellular matrix. Proc Natl Acad Sci U S A. 2006;103:13180–13185.
38. Tanjore H, Xu XC, Polosukhin VV, et al. Contribution of epithelial-derived fibroblasts to bleomycin-induced lung fibrosis. Am J Respir Crit Care Med. 2009;180:657–665.
39. Willis BC, Liebler JM, Luby-Phelps K, et al. Induction of epithelial-mesenchymal transition in alveolar epithelial cells by transforming growth factor-beta1: potential role in idiopathic pulmonary fibrosis. Am J Pathol. 2005;166:1321–1332.
40. Hardie WD, Hagood JS, Dave V, et al. Signaling pathways in the epithelial origins of pulmonary fibrosis. Cell Cycle. 2010;9:2769–2776.
• **The first report that showed limited or no EMT during TGFα-induced pulmonary fibrosis.**
41. Velikoff MCanalis E, et al. Activated alveolar epithelial cells initiate fibrosis through autocrine and paracrine secretion of connective tissue growth factor. Am J Physiol Lung Cell Mol Physiol. 2014;306:L786-L796.
42. Hewlett JC, Kropski JA, Blackwell TS. Idiopathic pulmonary fibrosis: epithelial-mesenchymal interactions and emerging therapeutic targets. Matrix Biol. 2018;71–72:112–127.
43. Aschner Y, Downey GP. Transforming growth factor-beta: master regulator of the respiratory system in health and disease. Am J Respir Cell Mol Biol. 2016;54:647–655.
44. Lam EW, Brosens JJ, Gomes AR, et al. Forkhead box proteins: tuning forks for transcriptional harmony. Nat Rev Cancer. 2013;13:482–495.
45. Balli D, Ustiyan V, Zhang Y, et al. Foxm1 transcription factor is required for lung fibrosis and epithelial-to-mesenchymal transition. Embo J. 2013;32:231–244.
46. Black M, Milewski D, Le T, et al. FOXF1 inhibits pulmonary fibrosis by preventing CDH2-CDH11 cadherin switch in myofibroblasts. Cell Rep. 2018;23:442–458.
• **Describes the importance FoxF1 in pulmonary fibrosis.**
47. Im J, Hergert P, Nho RS. Reduced FoxO3a expression causes low autophagy in idiopathic pulmonary fibrosis fibroblasts on collagen matrices. Am J Physiol Lung Cell Mol Physiol. 2015;309:L552–61.
48. Nho RS, Peterson M, Hergert P, et al. FoxO3a (Forkhead Box O3a) deficiency protects Idiopathic Pulmonary Fibrosis (IPF) fibroblasts from type I polymerized collagen matrix-induced apoptosis via caveolin-1 (cav-1) and Fas. PLoS One. 2013;8:e61017.
49. Penke LR, Speth JM, Dommeti VL, et al. FOXM1 is a critical driver of lung fibroblast activation and fibrogenesis. J Clin Invest. 2018;128:2389–2405.
• **Describes the importance Foxm1 in pulmonary fibrosis.**

50. Costa RH, Kalinichenko VV, Lim L. Transcription factors in mouse lung development and function. Am J Physiol Lung Cell Mol Physiol. 2001;280:L823–38.
51. Malin D, Kim IM, Boetticher E, et al. Forkhead box F1 is essential for migration of mesenchymal cells and directly induces integrin-beta3 expression. Mol Cell Biol. 2007;27:2486–2498.
52. Chang SK, Noss EH, Chen M, et al. Cadherin-11 regulates fibroblast inflammation. Proc Natl Acad Sci U S A. 2011;108:8402–8407.
53. Agarwal SK, Lee DM, Kiener HP, et al. Coexpression of two mesenchymal cadherins, cadherin 11 and N-cadherin, on murine fibroblast-like synoviocytes. Arthritis Rheum. 2008;58:1044–1054.
54. Melboucy-Belkhir S, Pradere P, Tadbiri S, et al. Forkhead Box F1 represses cell growth and inhibits COL1 and ARPC2 expression in lung fibroblasts in vitro. Am J Physiol Lung Cell Mol Physiol. 2014;307:L838–47.
55. Ho KK, Myatt SS, Lam EW. Many forks in the path: cycling with FoxO. Oncogene. 2008;27:2300–2311.
56. Gomes AR, Zhao F, Lam EW. Role and regulation of the forkhead transcription factors FOXO3a and FOXM1 in carcinogenesis and drug resistance. Chin J Cancer. 2013;32:365–370.
57. Wang IC, Chen YJ, Hughes D, et al. Forkhead box M1 regulates the transcriptional network of genes essential for mitotic progression and genes encoding the SCF (Skp2-Cks1) ubiquitin ligase. Mol Cell Biol. 2005;25:10875–10894.
58. Im J, Lawrence J, Seelig D, et al. FoxM1-dependent RAD51 and BRCA2 signaling protects idiopathic pulmonary fibrosis fibroblasts from radiation-induced cell death. Cell Death Dis. 2018;9:584.
59. Wilm B, Munoz-Chapuli R. The role of WT1 in embryonic development and normal organ homeostasis. Methods Mol Biol. 2016;1467:23–39.
60. Chau YY, Hastie ND. The role of Wt1 in regulating mesenchyme in cancer, development, and tissue homeostasis. Trends Genet. 2012;28:515–524.
61. Luzina IG, Salcedo MV, Rojas-Pena ML, et al. Transcriptomic evidence of immune activation in macroscopically normal-appearing and scarred lung tissues in idiopathic pulmonary fibrosis. Cell Immunol. 2018;325:1–13.
62. Martinez-Estrada OM, Lettice LA, Essafi A, et al. Wt1 is required for cardiovascular progenitor cell formation through transcriptional control of Snail and E-cadherin. Nat Genet. 2010;42:89–93.
63. Csermely P, Schnaider T, Soti C, et al. The 90-kDa molecular chaperone family: structure, function, and clinical applications. A comprehensive review. Pharmacol Ther. 1998;79:129–168.
64. Chen B, Piel WH, Gui L, et al. The HSP90 family of genes in the human genome: insights into their divergence and evolution. Genomics. 2005;86:627–637.
65. Haase M, Fitze G. HSP90AB1: helping the good and the bad. Gene. 2016;575:171–186.
66. Zuehlke AD, Beebe K, Neckers L, et al. Regulation and function of the human HSP90AA1 gene. Gene. 2015;570:8–16.
67. Biaoxue R, Xiling J, Shuanying Y, et al. Upregulation of Hsp90-beta and annexin A1 correlates with poor survival and lymphatic metastasis in lung cancer patients. J Exp Clin Cancer Res. 2012;31:70.
68. Rong B, Zhao C, Liu H, et al. Identification and verification of Hsp90-beta as a potential serum biomarker for lung cancer. Am J Cancer Res. 2014;4:874–885.
69. Korfei M, Schmitt S, Ruppert C, et al. Comparative proteomic analysis of lung tissue from patients with idiopathic pulmonary fibrosis (IPF) and lung transplant donor lungs. J Proteome Res. 2011;10:2185–2205.
70. Bellaye PS, Burgy O, Causse S, et al. Heat shock proteins in fibrosis and wound healing: good or evil? Pharmacol Ther. 2014;143:119–132.
71. Bellaye PS, Shimbori C, Yanagihara T, et al. Synergistic role of HSP90alpha and HSP90beta to promote myofibroblast persistence in lung fibrosis. Eur Respir J. 2018;51:1700386.
• **Describes the importance of HSP90 in pulmonary fibrosis.**
72. Dong H, Luo L, Zou M, et al. Blockade of extracellular heat shock protein 90alpha by 1G6-D7 attenuates pulmonary fibrosis through inhibiting ERK signaling. Am J Physiol Lung Cell Mol Physiol. 2017;313:L1006–L1015.
73. Sibinska Z, Tian X, Korfei M, et al. Amplified canonical transforming growth factor-beta signalling via heat shock protein 90 in pulmonary fibrosis. Eur Respir J. 2017;49:1501941.
74. Sontake V, Wang Y, Kasam RK, et al. Hsp90 regulation of fibroblast activation in pulmonary fibrosis. JCI Insight. 2017;2:e91454.
•• **Seminal paper that used pharmacogenomic screening and identified HSP90 inhibitors as a novel therapeutic targets in IPF.**
75. Tomcik M, Zerr P, Pitkowski J, et al. Heat shock protein 90 (Hsp90) inhibition targets canonical TGF-beta signalling to prevent fibrosis. Ann Rheum Dis. 2014;73:1215–1222.
76. Biernacka A, Dobaczewski M, Frangogiannis NG. TGF-beta signaling in fibrosis. Growth Factors. 2011;29:196–202.
77. Pohlers D, Brenmoehl J, Loffler I, et al. TGF-beta and fibrosis in different organs - molecular pathway imprints. Biochim Biophys Acta. 2009;1792:746–756.
78. Meng XM, Nikolic-Paterson DJ, Lan HY. TGF-beta: the master regulator of fibrosis. Nat Rev Nephrol. 2016;12:325–338.
79. Munger JS, Huang X, Kawakatsu H, et al. The integrin alpha v beta 6 binds and activates latent TGF beta 1: a mechanism for regulating pulmonary inflammation and fibrosis. Cell. 1999;96:319–328.
80. Madala SK, Korfhagen TR, Schmidt S, et al. Inhibition of the alphav-beta6 integrin leads to limited alteration of TGF-alpha-induced pulmonary fibrosis. Am J Physiol Lung Cell Mol Physiol. 2014;306:L726–35.
81. Raghu G, Mouded DA, Culver MJ, et al. Randomized, double-blind, placebo-controlled, multiple dose, dose-escalation study of BG00011 (Formerly STX-100) in patients with idiopathic pulmonary fibrosis (IPF). Am J Respir Crit Care Med. 2018;197:A7785.
82. Gieseck RL 3rd, Wilson MS, Wynn TA. Type 2 immunity in tissue repair and fibrosis. Nat Rev Immunol. 2018;18:62–76.
• **Comprehensive review that discussed type 2 immunity role in tissue repair and injury**
83. Heaney LG, Djukanovic R, Woodcock A, et al. Research in progress: medical research council United Kingdom Refractory Asthma Stratification Programme (RASP-UK). Thorax. 2016;71:187–189.
84. Wilson MS, Madala SK, Ramalingam TR, et al. Bleomycin and IL-1beta-mediated pulmonary fibrosis is IL-17A dependent. J Exp Med. 2010;207:535–552.
•• **Seminal paper that described IL-17A role during inflammation-induced fibrosis**
85. Wynn TA. Type 2 cytokines: mechanisms and therapeutic strategies. Nat Rev Immunol. 2015;15:271–282.
86. Park SW, Ahn MH, Jang HK, et al. Interleukin-13 and its receptors in idiopathic interstitial pneumonia: clinical implications for lung function. J Korean Med Sci. 2009;24:614–620.
87. Murray LA, Zhang H, Oak SR, et al. Targeting interleukin-13 with tralokinumab attenuates lung fibrosis and epithelial damage in a humanized SCID idiopathic pulmonary fibrosis model. Am J Respir Cell Mol Biol. 2014;50:985–994.
88. Ramalingam TR, Pesce JT, Sheikh F, et al. Unique functions of the type II interleukin 4 receptor identified in mice lacking the interleukin 13 receptor alpha1 chain. Nat Immunol. 2008;9:25–33.
89. Kolodsick JE, Toews GB, Jakubzick C, et al. Protection from fluorescein isothiocyanate-induced fibrosis in IL-13-deficient, but not IL-4-deficient, mice results from impaired collagen synthesis by fibroblasts. J Immunol. 2004;172:4068–4076.
90. Fichtner-Feigl S, Strober W, Kawakami K, et al. IL-13 signaling through the IL-13alpha2 receptor is involved in induction of TGF-beta1 production and fibrosis. Nat Med. 2006;12:99–106.
91. Singh B, Kasam RK, Sontake V, et al. Repetitive intradermal bleomycin injections evoke T-helper cell 2 cytokine-driven pulmonary fibrosis. Am J Physiol Lung Cell Mol Physiol. 2017;313:L796–L806.
• **Investigated Th2-cytokine signaling role in severe fibrotic lung disease using novel intradermal bleomycin mouse model**
92. Gause WC, Wynn TA, Allen JE. Type 2 immunity and wound healing: evolutionary refinement of adaptive immunity by helminths. Nat Rev Immunol. 2013;13:607–614.

93. Hams E, Armstrong ME, Barlow JL, et al. IL-25 and type 2 innate lymphoid cells induce pulmonary fibrosis. Proc Natl Acad Sci U S A. 2014;111:367–372.
94. Parker JM, Glaspole IN, Lancaster LH, et al. A phase 2 randomized controlled study of tralokinumab in subjects with idiopathic pulmonary fibrosis. Am J Respir Crit Care Med. 2018;197:94–103.
95. Swigris JJ, Ogura T, Scholand M, et al. The RIFF study (Cohort A): a phase II, randomized, double-blind, placebo-controlled trial of lebrikizumab as monotherapy in patients with idiopathic pulmonary fibrosis. Am J Respir Crit Care Med. 2018;197:A6167.
96. Raghu G, Richeldi L, Crestani B, et al. Safety and efficacy of SAR156597 in Idiopathic Pulmonary Fibrosis (IPF): a phase 2, randomized, double-blind, placebo-controlled study. Am J Respir Crit Care Med. 2018;197:A2441.
97. Tager AM, LaCamera P, Shea BS, et al. The lysophosphatidic acid receptor LPA1 links pulmonary fibrosis to lung injury by mediating fibroblast recruitment and vascular leak. Nat Med. 2008;14:45–54.
98. Funke M, Zhao Z, Xu Y, et al. The lysophosphatidic acid receptor LPA1 promotes epithelial cell apoptosis after lung injury. Am J Respir Cell Mol Biol. 2012;46:355–364.
99. Xu MY, Porte J, Knox AJ, et al. Lysophosphatidic acid induces alphavbeta6 integrin-mediated TGF-beta activation via the LPA2 receptor and the small G protein G alpha(q). Am J Pathol. 2009;174:1264–1279.
100. Oikonomou N, Mouratis MA, Tzouvelekis A, et al. Pulmonary autotaxin expression contributes to the pathogenesis of pulmonary fibrosis. Am J Respir Cell Mol Biol. 2012;47:566–574.
101. Coornaert B, Duys I, Van Der Schueren J, et al. Autotaxin inhibitor GLPG1690 affects TGFβ-induced production of the pro-fibrotic mediators CTGF, IL-6 and ET-1 in fibroblasts. Am J Respir Crit Care Med. 2017;195:A2404.
102. Maher TM, van der Aar EM, Van de Steen O, et al. Safety, tolerability, pharmacokinetics, and pharmacodynamics of GLPG1690, a novel autotaxin inhibitor, to treat idiopathic pulmonary fibrosis (FLORA): a phase 2a randomised placebo-controlled trial. Lancet Respir Med. 2018;6:627-635.
103. Zank DC, Bueno M, Mora AL, et al. Idiopathic pulmonary fibrosis: aging, mitochondrial dysfunction, and cellular bioenergetics. Front Med (Lausanne). 2018;5:10.
104. Schafer MJ, White TA, Iijima K, et al. Cellular senescence mediates fibrotic pulmonary disease. Nat Commun. 2017;8:14532.
•• **This article demonstrated importance of senolytic drug usage in pulmonary fibrosis**
105. Lehmann M, Korfei M, Mutze K, et al. Senolytic drugs target alveolar epithelial cell function and attenuate experimental lung fibrosis ex vivo. Eur Respir J. 2017;50:1602367.
106. Zhu Y, Tchkonia T, Pirtskhalava T, et al. The Achilles' heel of senescent cells: from transcriptome to senolytic drugs. Aging Cell. 2015;14:644–658.
107. Sato N, Takasaka N, Yoshida M, et al. Metformin attenuates lung fibrosis development via NOX4 suppression. Respir Res. 2016;17:107.
• **This article demonstrated therapeutic advantage of metformin during pulmonary fibrosis.**
108. Rangarajan S, Bone NB, Zmijewska AA, et al. Metformin reverses established lung fibrosis in a bleomycin model. Nat Med. 2018;24:1121–1127.
• **This study demonstrated AMPK dependent theraputic effects of metformin in bleomycin-induced fibrotic model.**
109. Wang Q, Usinger W, Nichols B, et al. Cooperative interaction of CTGF and TGF-beta in animal models of fibrotic disease. Fibrogenesis Tissue Repair. 2011;4:4.
110. Lipson KE, Wong C, Teng Y, et al. CTGF is a central mediator of tissue remodeling and fibrosis and its inhibition can reverse the process of fibrosis. Fibrogenesis Tissue Repair. 2012;5:S24.
111. Huber PE, Sebastian B, Peschke P, et al. Reversal of established fibrosis by treatment with the Anti-CTGF monoclonal antibody FG-3019 in a murine model of radiation-induced pulmonary fibrosis. Am J Respir Crit Care Med. 2010;181:A1054.
112. Raghu G, Scholand MB, de Andrade J, et al. FG-3019 anti-connective tissue growth factor monoclonal antibody: results of an open-label clinical trial in idiopathic pulmonary fibrosis. Eur Respir J. 2016;47:1481–1491.
113. Conte E, Gili E, Fruciano M, et al. PI3K p110gamma overexpression in idiopathic pulmonary fibrosis lung tissue and fibroblast cells: in vitro effects of its inhibition. Lab Invest. 2013;93:566–576.
114. Lawrence J, Nho R. The Role of the Mammalian Target of Rapamycin (mTOR) in pulmonary fibrosis. Int J Mol Sci. 2018;19:778.
• **Describes the importance of mTOR pathway in pulmonary fibrosis.**
115. Hsu HS, Liu CC, Lin JH, et al. Involvement of ER stress, PI3K/AKT activation, and lung fibroblast proliferation in bleomycin-induced pulmonary fibrosis. Sci Rep. 2017;7:14272.
116. White ES, Atrasz RG, Hu B, et al. Negative regulation of myofibroblast differentiation by PTEN (Phosphatase and Tensin Homolog Deleted on chromosome 10). Am J Respir Crit Care Med. 2006;173:112–121.
117. Xia H, Khalil W, Kahm J, et al. Pathologic caveolin-1 regulation of PTEN in idiopathic pulmonary fibrosis. Am J Pathol. 2010;176:2626–2637.
118. Madala SK, Thomas G, Edukulla R, et al. p70 ribosomal S6 kinase regulates subpleural fibrosis following transforming growth factor-alpha expression in the lung. Am J Physiol Lung Cell Mol Physiol. 2016;310:L175–86.
119. Gokey JJ, Sridharan A, Xu Y, et al. Active epithelial Hippo signaling in idiopathic pulmonary fibrosis. JCI Insight. 2018;3:e98738.
120. Lu Y, Azad N, Wang L, et al. Phosphatidylinositol-3-kinase/akt regulates bleomycin-induced fibroblast proliferation and collagen production. Am J Respir Cell Mol Biol. 2010;42:432–441.
121. Tulek B, Kiyan E, Toy H, et al. Anti-inflammatory and anti-fibrotic effects of sirolimus on bleomycin-induced pulmonary fibrosis in rats. Clin Invest Med. 2011;34:E341.
122. Axell-House DB, Yu V, Zhang Z, et al. Fibrocytes in pulmonary fibrosis: double-blind placebo-controlled crossover pilot study of sirolimus in idiopathic pulmonary fibrosis. Am J Respir Crit Care Med. 2018;197:A4353.
123. Mercer PF, Woodcock HV, Eley JD, et al. Exploration of a potent PI3 kinase/mTOR inhibitor as a novel anti-fibrotic agent in IPF. Thorax. 2016;71:701–711.
124. Maher TM, Bareille P, Costa MJ, et al. Marshall a randomised, placebo-controlled, double-blind, repeat dose escalation study with Omipalisib (gsk2126458) in patients with Idiopathic Pulmonary Fibrosis (ipf). Am J Respir Crit Care Med. 2017;195:A7010.
125. Madala SK, Edukulla R, Phatak M, et al. Dual targeting of MEK and PI3K pathways attenuates established and progressive pulmonary fibrosis. PloS one. 2014;9:e86536.
• **Important paper on combinatorial therapies in pulmonary fibrosis.**
126. Chien JW, Richards TJ, Gibson KF, et al. Serum lysyl oxidase-like 2 levels and idiopathic pulmonary fibrosis disease progression. Eur Respir J. 2014;43:1430–1438.
127. Barry-Hamilton V, Spangler R, Marshall D, et al. Allosteric inhibition of lysyl oxidase-like-2 impedes the development of a pathologic microenvironment. Nat Med. 2010;16:1009–1017.
128. Knipe RS, Tager AM, Liao JK. The Rho kinases: critical mediators of multiple profibrotic processes and rational targets for new therapies for pulmonary fibrosis. Pharmacol Rev. 2015;67:103–117.
129. Knipe RS, Probst CK, Lagares D, et al. The Rho Kinase Isoforms ROCK1 and ROCK2 each contribute to the development of experimental pulmonary fibrosis. Am J Respir Cell Mol Biol. 2018;58:471–481.
130. Shimizu Y, Dobashi K, Sano T, et al. ROCK activation in lung of idiopathic pulmonary fibrosis with oxidative stress. Int J Immunopathol Pharmacol. 2014;27:37–44.
131. Zhou Y, Huang X, Hecker L, et al. Inhibition of mechanosensitive signaling in myofibroblasts ameliorates experimental pulmonary fibrosis. J Clin Invest. 2013;123:1096–1108.

132. Jiang C, Huang H, Liu J, et al. Fasudil, a Rho-kinase inhibitor, attenuates bleomycin-induced pulmonary fibrosis in mice. Int J Mol Sci. 2012;13:8293–8307.
133. Bei Y, Hua-Huy T, Duong-Quy S, et al. Long-term treatment with fasudil improves bleomycin-induced pulmonary fibrosis and pulmonary hypertension via inhibition of Smad2/3 phosphorylation. Pulm Pharmacol Ther. 2013;26:635–643.
134. Alagha K, Secq V, Pahus L, et al. We should prohibit warfarin in idiopathic pulmonary fibrosis. Am J Respir Crit Care Med. 2015;191:958–960.
135. Noth I, Anstrom KJ, Calvert SB, et al. A placebo-controlled randomized trial of warfarin in idiopathic pulmonary fibrosis. Am J Respir Crit Care Med. 2012;186:88–95.
136. Raghu G, Behr J, Brown KK, et al. Treatment of idiopathic pulmonary fibrosis with ambrisentan: a parallel, randomized trial. Ann Intern Med. 2013;158:641–649.
137. King TE Jr, Behr J, Brown KK, et al. BUILD-1: a randomized placebo-controlled trial of bosentan in idiopathic pulmonary fibrosis. Am J Respir Crit Care Med. 2008;177:75–81.
138. Raghu G, Million-Rousseau R, Morganti A, et al. Macitentan for the treatment of idiopathic pulmonary fibrosis: the randomised controlled MUSIC trial. Eur Respir J. 2013;42:1622–1632.
139. Daniels CE, Lasky JA, Limper AH, et al. Imatinib treatment for idiopathic pulmonary fibrosis: randomized placebo-controlled trial results. Am J Respir Crit Care Med. 2010;181:604–610.
140. Martinez FJ, de Andrade JA, Anstrom KJ et al. Randomized trial of acetylcysteine in idiopathic pulmonary fibrosis. N Engl J Med. 2014;370:2093–2101.
• **Important clinical paper on anti-inflammatory and anti-oxidant therapy in IPF.**
141. Raghu G, Anstrom KJ, King TE Jr, et al.; Idiopathic Pulmonary Fibrosis Clinical Research N. Prednisone, azathioprine, and N-acetylcysteine for pulmonary fibrosis. N Engl J Med. 2012;366:1968–1977.
142. Raghu G, Martinez FJ, Brown KK, et al. CC-chemokine ligand 2 inhibition in idiopathic pulmonary fibrosis: a phase 2 trial of carlumab. Eur Respir J. 2015;46:1740–1750.
143. Hilberg F, Roth GJ, Krssak M, et al. BIBF 1120: triple angiokinase inhibitor with sustained receptor blockade and good antitumor efficacy. Cancer Res. 2008;68:4774–4782.
144. Wollin L, Maillet I, Quesniaux V, et al. Antifibrotic and anti-inflammatory activity of the tyrosine kinase inhibitor nintedanib in experimental models of lung fibrosis. J Pharmacol Exp Ther. 2014;349:209–220.
145. Bahudhanapati H, Kass DJ. Unwinding the Collagen Fibrils: elucidating the mechanism of pirfenidone and nintedanib in pulmonary fibrosis. Am J Respir Cell Mol Biol. 2017;57:10–11.
•• **Mode of action of the FDA approved drugs on collagen structure.**
146. Didiasova M, Singh R, Wilhelm J, et al. Pirfenidone exerts antifibrotic effects through inhibition of GLI transcription factors. FASEB J. 2017;31:1916–1928.
147. Liu Y, Lu F, Kang L, et al. Pirfenidone attenuates bleomycin-induced pulmonary fibrosis in mice by regulating Nrf2/Bach1 equilibrium. BMC Pulm Med. 2017;17:63.
148. Costabel U, Albera C, Lancaster LH, et al. An open-label study of the long-term safety of pirfenidone in patients with idiopathic pulmonary fibrosis (RECAP). Respiration. 2017;94:408–415.
• **Evaluation of Pirfenidone safety for a longer duration.**
149. Vancheri C, Kreuter M, Richeldi L, et al. Nintedanib with add-on pirfenidone in idiopathic pulmonary fibrosis. Results of the INJOURNEY trial. Am J Respir Crit Care Med. 2018;197:356–363.
• **Effect of combination therapy of pirfenidone and nintedanib in IPF patients.**
150. Noble PW, Barkauskas CE, Jiang D. Pulmonary fibrosis: patterns and perpetrators. J Clin Invest. 2012;122:2756–2762.

Article

SOURCE DATA | TRANSPARENT PROCESS | OPEN ACCESS

EMBO Molecular Medicine

Inhibition of Aurora Kinase B attenuates fibroblast activation and pulmonary fibrosis

Rajesh K Kasam[1,2], Sudhir Ghandikota[3,4], Divyalakshmi Soundararajan[1], Geereddy B Reddy[2], Steven K Huang[5], Anil G Jegga[3,4,6,*] & Satish K Madala[1,6,**]

Abstract

Fibroblast activation including proliferation, survival, and ECM production is central to initiation and maintenance of fibrotic lesions in idiopathic pulmonary fibrosis (IPF). However, druggable molecules that target fibroblast activation remain limited. In this study, we show that multiple pro-fibrotic growth factors, including TGFα, CTGF, and IGF1, increase aurora kinase B (AURKB) expression and activity in fibroblasts. Mechanistically, we demonstrate that Wilms tumor 1 (WT1) is a key transcription factor that mediates TGFα-driven AURKB upregulation in fibroblasts. Importantly, we found that inhibition of AURKB expression or activity is sufficient to attenuate fibroblast activation. We show that fibrosis induced by TGFα is highly dependent on AURKB expression and treating TGFα mice with barasertib, an AURKB inhibitor, reverses fibroblast activation, and pulmonary fibrosis. Barasertib similarly attenuated fibrosis in the bleomycin model of pulmonary fibrosis. Together, our preclinical studies provide important proof-of-concept that demonstrate barasertib as a possible intervention therapy for IPF.

Keywords Aurora Kinase B; Barasertib; fibroproliferation; pulmonary fibrosis; Wilms' tumor 1

Subject Categories Pharmacology & Drug Discovery; Respiratory System

DOI 10.15252/emmm.202012131 | Received 5 February 2020 | Revised 8 July 2020 | Accepted 13 July 2020

EMBO Mol Med (2020) e12131

Introduction

Idiopathic pulmonary fibrosis (IPF) is a chronic and progressive fibrotic lung disease characterized by increased proliferation and survival of mesenchymal cells that are involved in excessive production and deposition of extracellular matrix (ECM) proteins in the distal areas of the lung (Wynn & Ramalingam, 2012; Barratt *et al*, 2018). The median survival rate of IPF patients is 3–5 years from diagnosis, and IPF claims more lives annually than many types of cancer (Gribbin *et al*, 2006; Ley *et al*, 2011). The increasing burden of IPF is not simply reflective of an aging population, as age-adjusted mortality for IPF is increasing as well (Pardo & Selman, 2016). Currently, two FDA-approved drugs, Ofev (nintedanib) and Esbriet (pirfenidone), are available for the treatment of patients with IPF. However, neither of these drugs provide a cure, and both of them are associated with several serious drug-related side effects (King *et al*, 2014; Richeldi *et al*, 2014; Hughes *et al*, 2016). Pirfenidone and nintedanib both cause gastrointestinal events, while pirfenidone also causes skin disorders including rash and photosensitivity (Costabel *et al*, 2014; Wollin *et al*, 2015; Lancaster *et al*, 2017; Kasam *et al*, 2019). Intolerance to these medicines and their variable efficacy justify the need to identify other therapeutic alternatives.

In the pathogenesis of IPF, lung-resident fibroblasts have been shown to proliferate and differentiate into contractile mesenchymal cells, called myofibroblasts, which participate in continuous ECM production, secretion, and deposition in distal areas of the lung (Phan, 2008; Sontake *et al*, 2017). Multiple cytokines and growth factors released by immune cells, fibrocytes, and the lung epithelium are known to enhance the fibrogenic activity of lung-resident fibroblasts (Baughman *et al*, 1999; Allen & Spiteri, 2002). Published reports indicate that pathological processes in IPF are often stimulated by 1) receptor tyrosine kinases activated by ligands of the epidermal growth factor receptor (EGFR), as well as platelet-derived growth factor (PDGF), connective tissue growth factor (CTGF), insulin-like growth factor 1 (IGF1), basic fibroblast growth factor (FGF), and vascular endothelial growth factor (VEGF) receptors; 2) SMAD and non-SMAD (PI3K and MAPK) signaling pathways activated by TGFβ and PDGF receptors; and 3) STAT3 and STAT6 signaling pathways activated by IL-6 cytokines (IL-6 and IL-10) and Th2 cytokines (IL-4 and IL-13), respectively (Wilson & Wynn, 2009; Wynn, 2011; Madala *et al*, 2012; Prele *et al*, 2012; Grimminger *et al*, 2015; Walton *et al*, 2017). These data illustrate several unanswered

1 Division of Pulmonary Medicine, Cincinnati Children's Hospital Medical Center, Cincinnati, OH, USA
2 Department of Biochemistry, National Institute of Nutrition, Hyderabad, India
3 Division of Biomedical Informatics, Cincinnati Children's Hospital Medical Center, Cincinnati, OH, USA
4 Department of Computer Science, University of Cincinnati College of Engineering, Cincinnati, OH, USA
5 Division of Pulmonary and Critical Care Medicine, Department of Internal Medicine, University of Michigan Medical School, Ann Arbor, MI, USA
6 Department of Pediatrics, College of Medicine, University of Cincinnati, Cincinnati, OH, USA
*Corresponding author. Tel: +1 513 636 0261; E-mail: anil.jegga@cchmc.org
**Corresponding author. Tel: +1 513 636 9852; E-mail: satish.madala@cchmc.org

© 2020 The Authors. Published under the terms of the CC BY 4.0 license

questions, but also suggest a possible redundant function and synergism between multiple cytokines and fibrogenic pathways. In support of this, inhibition of a single pathway or growth factor in mouse models or human clinical trials has not been effective in reversing established and ongoing fibrosis in the lung (Chaudhary *et al*, 2007; Vallath *et al*, 2014; Raghu, 2017). As fibrosis is likely heterogeneous in etiology and molecular pathophysiology, attempts to block or counteract single upstream or downstream pathways may not be sufficient to inhibit cellular processes associated with ongoing fibrosis. Therefore, identification of converging or overlapping pathways downstream of growth factors involved in fibroblast activation could result in more effective therapies. In a recent study, we used an unbiased chemical genomics approach to identify drug targets that regulate multiple pro-fibrotic processes including fibroproliferation, migration, invasiveness, and ECM production (Sontake *et al*, 2017). This novel *in silico* screening platform has identified several small molecule inhibitors including inhibitors of Hsp90, tyrosine kinases, and mitotic kinases, whose gene expression profiles were inversely correlated with differentially expressed gene networks in IPF lungs.

Aurora kinase B (AURKB) is a ubiquitously expressed mitotic kinase that belongs to the family of serine/threonine kinase (STKs) (Nigg, 2001; Fu *et al*, 2007). AURKB regulates multiple key events during cell division, which includes, but is not limited to chromatin condensation, chromosome bi-orientation, and cytokinesis (Kollareddy *et al*, 2008; Lampson & Cheeseman, 2011). Moreover, recent studies have identified interphase functions of AURKB during various pathophysiological settings (Wu *et al*, 2011; Gully *et al*, 2012; Frangini *et al*, 2013). It is well-documented that overexpression of AURKB in numerous cancer types causes uncontrollable tumor cell proliferation and helps in evading apoptotic death (Sorrentino *et al*, 2005; Jha *et al*, 2013; Tang *et al*, 2017). The role of AURKB in fibroblast activation in the pathogenesis of IPF has remained unexplored. We had previously shown that WT1 is a critical transcription factor that promotes fibrogenesis (Sontake *et al*, 2015, 2018). We recently performed RNA-seq in fibroblasts for which WT1 was knockdown, and AURKB was identified as a major target of WT1 (Sontake *et al*, 2018). Here, we show for the first time that AURKB is upregulated in fibroblasts of IPF and a mouse models of pulmonary fibrosis. Multiple growth factors such as TGFα, CTGF, and IGF1 upregulate AURKB in lung fibroblasts. WT1 acts as a key transcription factor involved in TGFα-induced AURKB expression in fibroblasts. In support of its pro-fibrotic functions, we found that inhibition of AURKB expression or activity attenuated proliferation, survival, and ECM production in lung fibroblasts. *In vivo* studies using the TGFα- and bleomycin-induced mouse models of pulmonary fibrosis demonstrate that barasertib, a known AURKB inhibitor, attenuates fibroproliferation, myofibroblast survival, and ECM deposition in established and ongoing pulmonary fibrosis.

Results

AURKB is upregulated in IPF fibroblasts

To determine the fibroproliferative effects of multiple pro-fibrotic growth factors on AURKB expression, we treated primary fibroblasts isolated from human lungs with multiple growth factors including TGFα, TGFβ, CTGF, and IGF1. We found a significant increase in the expression of AURKB in fibroblasts treated with TGFα, CTGF, and IGF1 but none with TGFβ (Fig 1A). To determine whether AURKB is overexpressed in IPF fibroblasts, we isolated fibroblasts from the lungs of patients with IPF and non-fibrotic controls and measured the amount of AURKB transcripts. We observed a significant increase in AURKB transcripts in fibroblasts of IPF compared to non-IPF controls (Fig 1B). To determine the expression of AURKB in the lungs of IPF, we immunostained lung sections with antibody against AURKB and observed a marked increase in AURKB staining in spindle-shaped fibroblasts located in subpleural regions and fibrotic foci of IPF lung tissue compared to normal lungs (Fig 1C).

AURKB is upregulated during TGFα- and bleomycin-induced pulmonary fibrosis

To determine whether AURKB is upregulated during TGFα-induced pulmonary fibrosis, Western blot analysis was performed on total lung lysates from control (CCSP/-) and TGFα (CCSP/TGFα) mice on Dox for 6 weeks using antibodies against AURKA and AURKB. We observed a significant increase in the protein levels of AURKB but not AURKA in TGFα mice compared to controls (Fig 1D). In support, we observed increased staining for AURKB in the nucleus of spindle-shaped cells localized in the subpleural fibrotic lesions of TGFα mice on Dox for 6 weeks, but limited or no staining in the lungs of control mice (Fig 1E). Further, we found that the majority of AURKB is localized in the nucleus of vimentin-positive fibroblasts (Fig EV1). Similarly, we observed a significant increase in AURKB protein levels in the lungs of bleomycin-treated mice compared to saline-treated control mice (Fig 1F).

Wilm's tumor 1 regulates the AURKB expression

Recent studies from our laboratory have shown that WT1 is upregulated in mesenchymal cells of subpleural fibrotic lung lesions and that it contributes to pulmonary fibrosis pathogenesis (Sontake *et al*, 2015). To test whether WT1 affects AURKB expression, we knocked down WT1 expression using WT1-specific siRNA in fibroblasts isolated from IPF lungs or TGFα mice on Dox for 4 weeks. Compared to control siRNA, knockdown of WT1 was sufficient to attenuate the expression of AURKB in lung fibroblasts isolated from both IPF and a mouse model of TGFα-induced pulmonary fibrosis (Fig 2A and B). We next assessed the effect of adenovirus-mediated overexpression of WT1 on AURKB levels in fibroblasts. Overexpressing WT1 in fibroblasts led to a significant increase in both transcripts and protein of AURKB (Figs EV2A and 2C). Knockdown of WT1 in fibroblasts also abolished the ability of TGFα to increase AURKB expression (Fig 2D). To determine whether WT1 is a transcription factor that directly binds to *AURKB*, we performed a computational analysis of the promoter region of human and mouse *AURKB* and found the presence of conserved WT1 binding sites (Fig EV2B). We performed chromatin immunoprecipitation (ChIP) analysis using primary lung-resident fibroblasts isolated from TGFα mice on Dox for 8 weeks. ChIP analysis using WT1-specific antibody compared with control isotype antibody revealed that WT1 bound to the *AURKB* gene, suggesting the role of WT1 in AURKB

 © 2020 The Authors

expression (Fig 2E). We next overexpressed WT1 in HEK293 cells co-transfected with AURKB promoter fused with luciferase reporter and observed increased luciferase activity compared to cells transfected with control plasmids (Fig 2F). These results support that WT1 functions as a positive regulator of AURKB by directly binding to the AURKB promoter in fibroblasts.

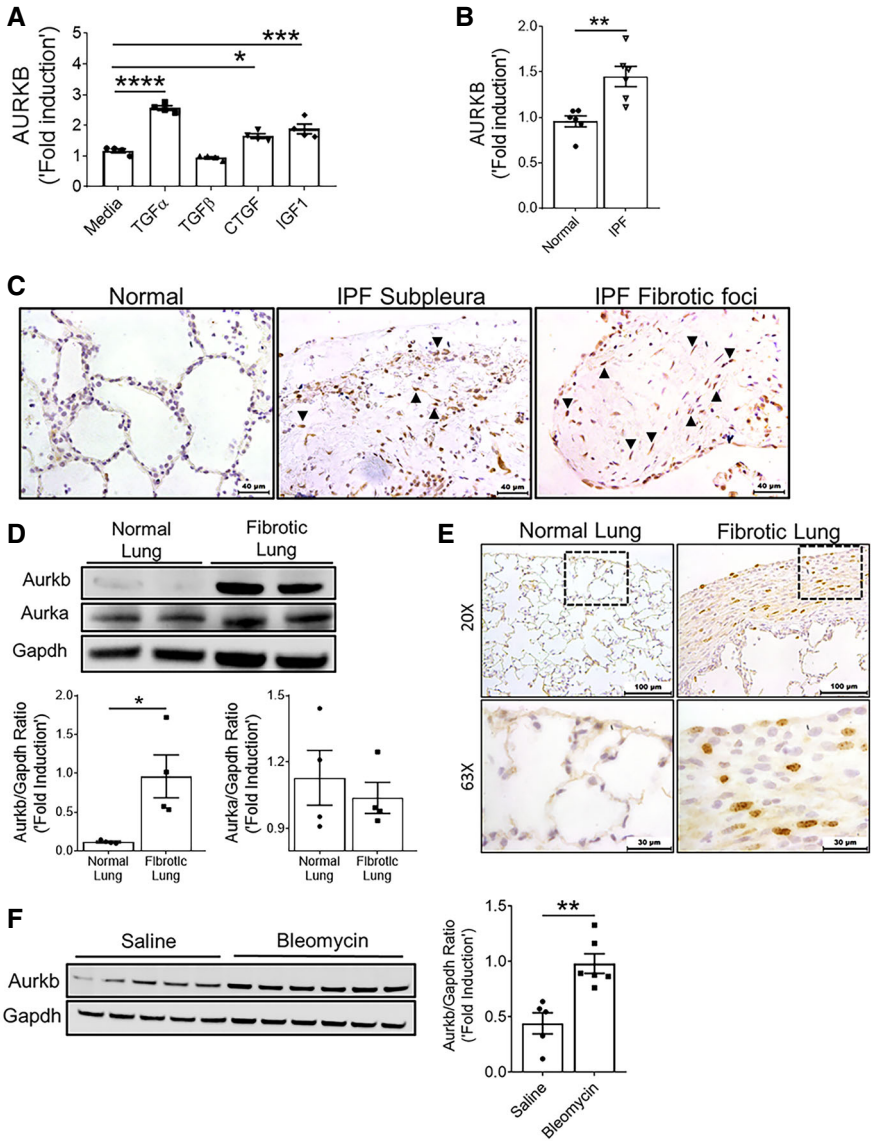


Figure 1. Multiple growth factors upregulate AURKB in severe fibrotic lung disease.

A Quantification of AURKB transcripts in non-IPF lung-derived resident fibroblasts treated with indicated mitogens for 16 h. *$P < 0.05$, ***$P < 0.0005$, and ****$P < 0.00005$, 1-way ANOVA ($n = 4$).

B Quantification of AURKB gene transcripts in isolated fibroblasts from non-IPF and IPF lung stromal cell cultures. **$P < 0.005$, unpaired t-test ($n = 6$).

C IPF and non-IPF lung sections were immunostained using AURKB antibody ($n = 4$). Representative images were obtained at 40× magnification. Scale bar: 40 μm. Dotted area: black; myofibroblastic core, blue; active fibrotic front. Arrows indicate AURKB positive cells.

D Immunoblots of Aurkb and Aurka in total lung lysates of normal (CCSP/—) and fibrotic (CCSP/TGFα) mice fed with Dox for 6 weeks. Quantification was performed using phosphor imager software and normalization was done using loading control Gapdh. *$P < 0.05$, unpaired t-test ($n = 4$).

E Immunostaining was performed using AURKB antibody in lung sections of control (CCSP/—) and TGFα (CCSP/TGFα) mice on Dox for 6 weeks ($n = 6$). Representative images were obtained at 20× (low; Scale bar: 100 μm) and 63× (high; Scale bar: 30 μm) magnification. Dashed box indicates area of the section showing in high magnification.

F Western blot analysis of Aurkb in total lung lysates from saline and bleomycin-treated mice. Quantification was performed using phosphor imager software, and normalization was done using loading control Gapdh. **$P < 0.005$, unpaired t-test ($n = 4$–5).

Data information: All data were presented as mean ± SEM. Exact P values are shown in Appendix Table S6.
Source data are available online for this figure.

© 2020 The Authors

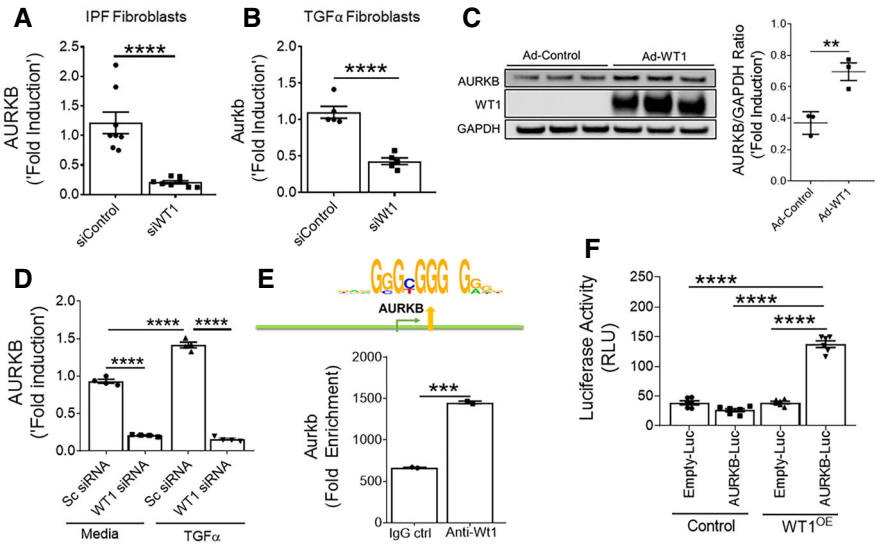


Figure 2. WT1 regulates AURKB expression.

A Human IPF lung fibroblasts were transiently transfected with control or WT1 siRNA for 72 h and AURKB transcripts were quantified. ****$P < 0.00005$, unpaired t-test ($n = 4$).

B Lung-resident fibroblasts from TGFα mice on Dox for 4 weeks were transiently transfected with control or WT1 siRNA for 72 h, and AURKB transcripts were quantified. ****$P < 0.00005$, unpaired t-test ($n = 4$).

C Immunoblot analysis of AURKB and WT1 in the lysates of non-IPF fibroblasts transduced with control or WT1-adenoviral particles for 72 h. **$P < 0.005$, unpaired t-test ($n = 3$).

D Quantification of AURKB transcripts in primary fibroblasts from IPF lung treated with either control or WT1 siRNA and stimulated with media or TGFα (100 ng/ml) for 16 h. ****$P < 0.00005$, unpaired t-test ($n = 4$).

E Primary lung-resident fibroblasts were isolated from stromal cultures of TGFα mice placed on Dox for 8 weeks. Cell lysates were prepared, and the ChIP assay was performed with anti-WT1 antibody or normal rabbit IgG as a negative control using AURKB gene promoter-specific PCR primers. Non-immunoprecipitated DNA is represented as input DNA (product size, 104 bp). ***$P < 0.0005$, unpaired t-test ($n = 2$).

F AURKB promoter luciferase activity was measured in HEK293 cells transfected with control or WT1 overexpressing (OE) vector. ****$P < 0.00005$, one-way-ANOVA ($n = 6$).

Data information: All data were presented as mean ± SEM. The above data were a representative of two independent experiments with similar results. P values were shown in Appendix Table S6.
Source data are available online for this figure.

AURKB functions as a positive regulator for fibroblast proliferation and survival

To gain insight into the role of AURKB in fibroblast activation, we assessed gene expression changes using next-generation sequencing in fibroblasts isolated from the lungs of TGFα mice on Dox for 10 days treated with either control- or AURKB-specific siRNA for 72 h. Knockdown of AURKB resulted in significant loss of its transcripts in resident fibroblasts (Fig EV3A). As shown in the heat map, the knockdown of AURKB has resulted in 800 upregulated and 1248 downregulated genes (≥ 1.5-fold change; P value FDR ≤ 0.05) (Fig EV3B). To identify potential AURKB-driven pro-fibrotic gene transcripts in IPF, we next compared differentially expressed genes in IPF lungs (GSE53845) (DePianto *et al*, 2015) and AURKB-specific siRNA-treated lung fibroblasts. We identified multiple transcripts that were either upregulated (141 genes) or downregulated (50 genes) by AURKB in IPF (Fig 3A and Appendix Table S1). Functional enrichment analysis of these negatively correlated gene sets (i.e., genes upregulated in IPF lungs but downregulated in AURKB-specific siRNA-treated lung fibroblasts and vice versa) using the ToppFun application of the ToppGene Suite (Chen *et al*, 2009) identified several major fibroblast-specific biological processes. These include cell proliferation, apoptosis, and ECM production (Fig 3B). Co-immunofluorescence staining was performed with anti-AURKB and anti-Ki-67 antibodies on lung sections from normal and TGFα mice on Dox for 4 weeks. We observed a notable increase in the number of AURKB and Ki-67-positive cells in the fibrotic lesions of TGFα mice on Dox for 4 weeks compared to control mice (Fig 3C). Both AURKB and Ki-67 co-localized to the same cells by immunofluorescence staining, and the number of dual positive cells for both AURKB and Ki-67 was significantly greater in the lungs of TGFα mice compared to normal mice (Fig 3D).

To test whether AURKB induces fibroproliferation, we assessed the impact of AURKB knockdown on BrdU incorporation in fibroblasts isolated from the lungs of IPF or TGFα mice on Dox for 2 weeks. We observed a significant decrease in BrdU incorporation in fibroblasts treated with AURKB-specific siRNA compared to control siRNA (Fig 3E). With the loss of AURKB in fibroblasts, we observed a significant decrease in TGFα-induced fibroproliferation (Fig 3F). To establish the mechanisms in AURKB-driven fibroproliferation, we assessed changes in AURKB-driven IPF network genes predicted to regulate fibroproliferation, such as PLK1 and CCNA2, in fibroblasts treated with AURKB-specific siRNA compared with control siRNA. Notably, the genetic knockdown of AURKB was

 © 2020 The Authors

sufficient to attenuate the expression of AURKB-dependent genes involved in fibroproliferation (Fig 3G). These findings establish that AURKB functions as a positive regulator of fibroproliferation in IPF.

In progressive fibrosis, fibroblasts transform to myofibroblasts and develop resistance to apoptosis, thereby promoting excessive ECM deposition and the expansion of fibrotic lung lesions (Thannickal & Horowitz, 2006; Kasam *et al*, 2019). To test whether myofibroblasts express AURKB, we performed co-immunofluorescence staining of AURKB and αSMA in lung sections from control and TGFα mice at 6 weeks on Dox, when fibrosis is well established. Our co-immunostaining show that AURKB localized in the nucleus and αSMA being in cytoplasm of myofibroblasts in the subpleural fibrotic lesions of TGFα mice on Dox for 6 weeks (Fig 3H). To test whether AURKB induces fibroblast survival, the mature fibrotic lesions of IPF or TGFα mice on Dox for 6 weeks were cultured to isolate fibroblasts and apoptosis was quantified in fibroblasts treated with either control or AURKB-specific siRNA. Notably, the loss of AURKB transcripts was sufficient to induce apoptosis in fibroblasts from IPF or TGFα mice (Fig 3I). To understand the mechanisms in AURKB-driven fibroblast survival, we quantified the expression of genes involved in apoptosis by RT–PCR. The genetic loss of AURKB was sufficient to induce the expression of pro-apoptotic gene transcripts such as Bak, Bax, and Fas in fibroblasts isolated from the lungs of IPF or TGFα mice on Dox for 6 weeks (Fig 3J and K). Together, the above findings establish that increased AURKB expression contributes to apoptosis resistance in mesenchymal cells.

Barasertib attenuates fibroblast activation

To test whether the inhibition of AURKB activity alters fibroblasts activation, we assessed the proliferation of fibroblasts isolated from the lungs of IPF or TGFα mice on Dox for 4 weeks. Upon treatment with barasertib, a known AURKB inhibitor, we observed a

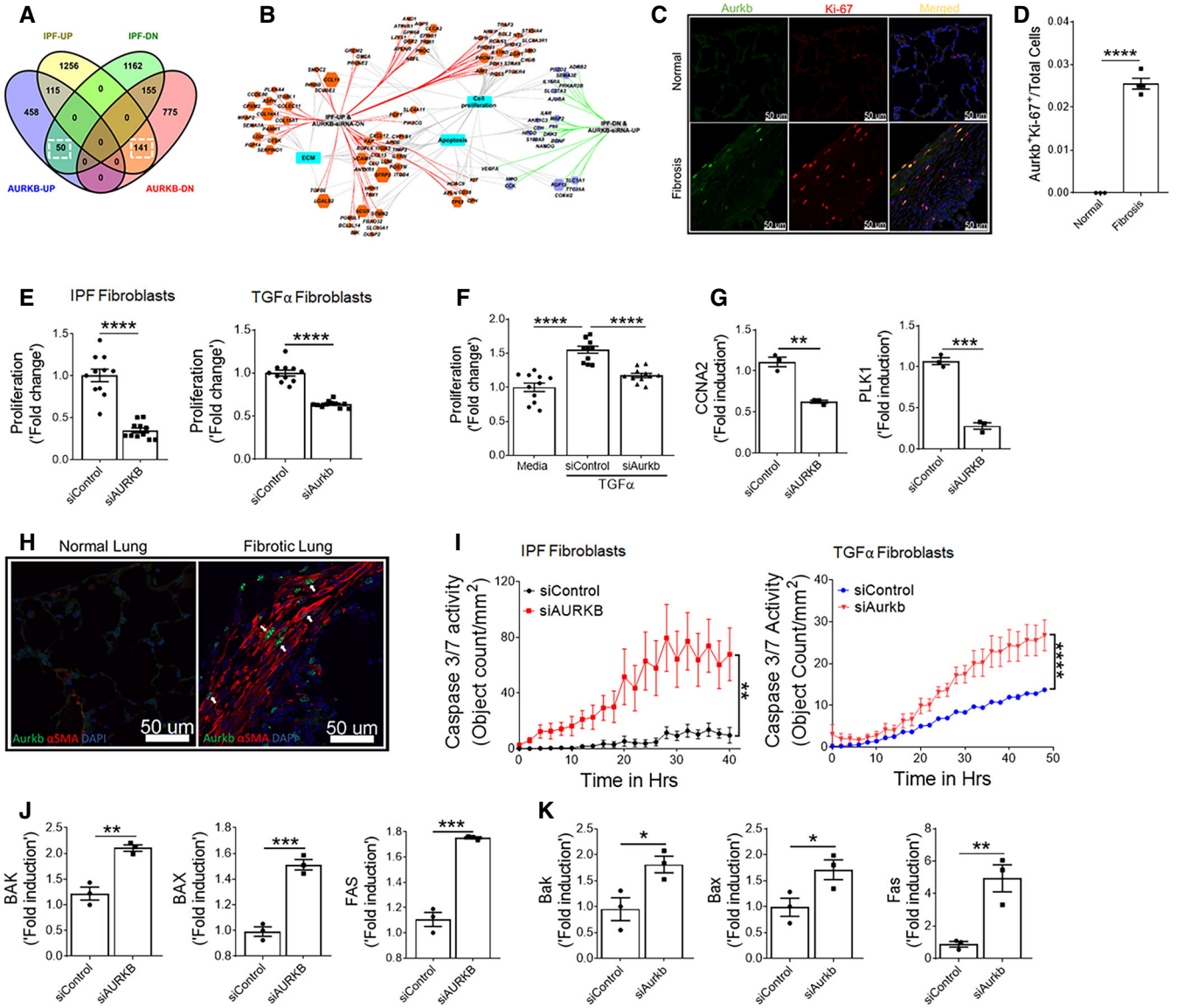


Figure 3.

Figure 3. AURKB functions as a positive regulator of fibroproliferation and survival.

A Venn diagram depicting the comparison and overlap of differentially expressed genes in IPF lungs and AURKB siRNA-treated fibrotic fibroblasts. The dashed box indicates genes that were up- (141 genes) or downregulated (DN, 50 genes) in IPF lungs compared with AURKB siRNA knockdown gene expression signatures.

B AURKB-driven genes activated in IPF were analyzed using ToppFun and visualized using Cytoscape. Red- and blue-colored circles represent genes that are up or downregulated, respectively, in IPF lungs. The turquoise-colored circle represents enriched biological processes for the inversely correlated genes between AURKB siRNA knockdown and IPF.

C Lung sections from control and TGFα mice fed with Dox food for 4 weeks were stained for AURKB (green) and Ki-67(red). Merged image shows cells that co-express AURKB and Ki-67 (yellow).

D Quantification of Ki-67$^+$ and AURKB$^+$ double-positive cells was performed using five confocal images per mice in control and TGFα mice. Images were obtained at 40× magnification. Scale bar: 50 μm. ****$P < 0.00005$, unpaired t-test ($n = 4$).

E Proliferation was measured in primary lung-resident fibroblast isolated from either IPF lung or TGFα mice and treated with either control or AURKB siRNA. ****$P < 0.00005$, unpaired t-test ($n = 9$–11).

F Proliferation was measured in primary lung-resident fibroblasts isolated from stromal cultures of TGFα mice on Dox for 2 weeks and transiently transfected with control or AURKB siRNA and stimulated with TGFα (20 ng/ml) for 24 h. ****$P < 0.00005$, 1-way ANOVA ($n = 9$–11).

G Quantification of CCNA2 and PLK1 transcripts in human IPF fibroblasts transiently transfected with control or AURKB siRNA for 72 h. **$P < 0.005$, ***$P < 0.0005$, unpaired t-test ($n = 3$).

H Lung sections from control and TGFα mice fed with Dox food for 6 weeks were stained for AURKB (green) and αSMA (red). Images were obtained at 40× magnification. Scale bar: 50 μm. ($n = 4$).

I Quantification of apoptotic cells using Incucyte ZOOM (caspase 3/7-positive cells) in lung-resident fibroblasts isolated from IPF and TGFα mice on Dox for 6 weeks and treated with control or AURKB siRNA for 72 h. **$P < 0.005$, ****$P < 0.00005$, 2-way ANOVA ($n = 4$).

J Quantification of Bak, Bax, and Fas gene transcripts in human IPF lung-resident fibroblasts treated with either control or AURKB siRNA for 72 h. **$P < 0.005$, ***$P < 0.0005$, unpaired t-test ($n = 3$).

K Quantification of Bak, Bax, and Fas gene transcripts in lung-resident fibroblasts isolated from TGFα mice and treated with either control or AURKB siRNA for 72 h. *$P < 0.005$, **$P < 0.005$, unpaired t-test ($n = 3$).

Data information: All data were presented as mean ± SEM. The above data were a representative of two independent experiments with similar results. Exact P values are shown in Appendix Table S6.

significant reduction in BrdU incorporation in fibroblasts isolated from IPF and TGFα model (Fig 4A and B). In support, the percent of PCNA-positive cells was significantly reduced in barasertib-treated IPF fibroblasts compared with vehicle (Fig 4C). Consistent with the loss of AURKB in fibroblasts, we observed a dose-dependent attenuation of TGFα-induced fibroblast proliferation when treated with barasertib compared to vehicle (Fig 4D). Similar to the loss of AURKB expression, inhibition with barasertib reduced the expression of AURKB-driven genes involved in fibroproliferation such as CCNA2 and PLK1 (Fig EV4). Previous studies from our group, and others, have demonstrated a pathogenic role for enhanced survival of multiple mesenchymal cells in the development and maintenance of pulmonary fibrosis (Kasam *et al*, 2019). To evaluate the effect of AURKB inhibition on apoptotic clearance of fibroblasts, we isolated fibroblasts from IPF lungs and assessed the impact of barasertib treatment on cleaved caspase 3 activity. Treatment with barasertib resulted in a significant increase in caspase 3/7 activity compared to vehicle (Fig 4E). Thus, either the loss of expression or activity of AURKB is sufficient to mitigate fibroblast activation, including fibroproliferation and survival in IPF fibroblasts and in lung fibroblasts from the TGFα mouse model.

Barasertib attenuates TGFα-induced pulmonary fibrosis *in vivo*

To test whether treatment with barasertib prevents the development of lung fibrosis, TGFα mice were concomitantly treated with Dox to induce TGFα expression and either barasertib (40 mg/kg body weight) or vehicle twice per day for 4 weeks (Fig 5A). Induction of TGFα caused extensive subpleural, perivascular, and peribronchial fibrosis (Fig 5B). TGFα-activated mice that were concomitantly given barasertib showed reduced collagen staining with infrequent scattered small fibrotic areas. Further, we observed a significant decrease in the lung weights and hydroxyproline levels in TGFα mice treated with barasertib compared to vehicle-treated mice (Fig 5C and D). In agreement with the transcriptional changes, we observed a significant decrease in lung collagen levels in TGFα mice treated with barasertib compared to vehicle-treated TGFα mice on Dox for 4 weeks (Fig 5C). Further, gene expression analysis by RT–PCR demonstrated a reduction in the expression of ECM genes such as Col1α, Col5α, and Fn1 in barasertib-treated TGFα mice compared to vehicle-treated TGFα mice (Fig 5E). Together, these findings suggest that inhibition of AURKB activity by barasertib attenuates progressive fibrotic changes in TGFα mice.

To determine whether the anti-fibrotic effects of barasertib *in vivo* are due to decreased proliferation in fibrotic lung lesions, we next immunostained the lung sections with Ki-67 and found a significant increase in immunoreactivity for Ki-67 in the subpleural and adventitial fibrotic lesions of TGFα mice treated with vehicle compared to non-fibrosis control mice (Fig 6A). Notably, TGFα mice treated with barasertib displayed a significant reduction in Ki-67 staining in both subpleural and adventitial fibrotic lesions. Additionally, immunoblot analysis in lung lysates demonstrated decreased PCNA levels in the barasertib-treated TGFα mice compared to vehicle-treated TGFα mice (Fig 6B). The transcript levels for genes implicated in cell proliferation, including Aurkb, were significantly reduced in barasertib-treated TGFα mice lungs compared to vehicle-treated mice (Fig 6C). Also, we observed a significant reduction in the expression of Wt1 in the lungs of TGFα mice treated with barasertib compared to vehicle-treated TGFα mice (Fig EV5).

To determine whether AURKB inhibition influences the progression of established and ongoing pulmonary fibrosis following 3 weeks of Dox treatment when fibrosis is already manifest, TGFα mice were administered barasertib while remaining on Dox for an additional 3 weeks (Fig 7A). The right lung weights were increased in TGFα mice compared to control mice on Dox for 6 weeks. This increase in lung weights was attenuated in TGFα mice treated with

 © 2020 The Authors

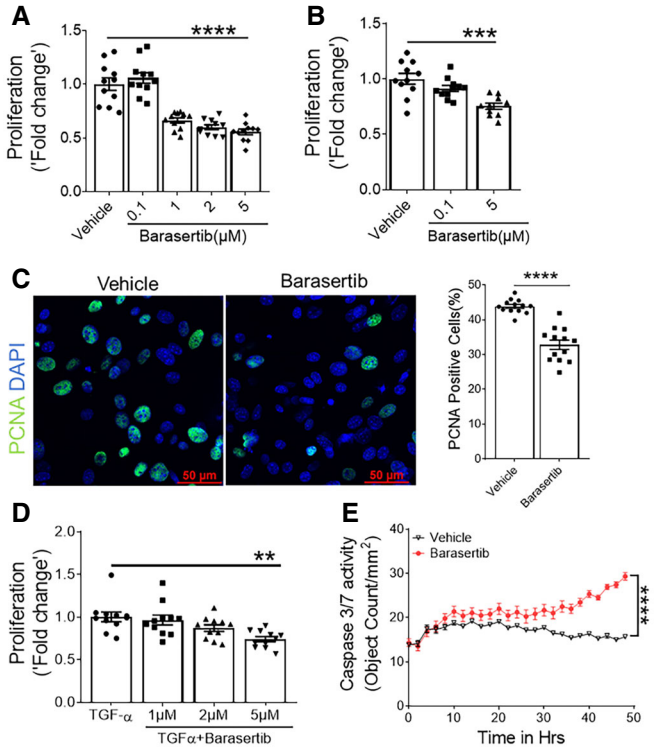


Figure 4. Blockade of AURKB activity impacts fibroblast proliferation and survival.

A Proliferation was assessed using BrdU incorporation assay in human IPF fibroblasts treated with indicated doses of barasertib for total of 48 h. ****$P < 0.00005$, 1-way ANOVA (n = 9–11).

B Proliferation was assessed using BrdU incorporation assay in fibroblasts isolated from TGFα mice lung and treated with indicated doses of barasertib for total of 48 h. ***$P < 0.0005$, 1-way ANOVA (n = 9–11).

C Primary lung-resident fibroblasts isolated from TGFα mice on Dox for 4 weeks were treated with vehicle or 5 μM barasertib for 48 h and immunostained using PCNA antibody. Images were obtained at 40× magnification. Scale bar: 50 μm. The number of PCNA-positive cells and total DAPI-positive cells was quantified using MetaMorph image analysis software. Proliferation is indicated as the percentage of proliferating cells in total DAPI-positive cells. ****$P < 0.00005$, unpaired t-test (n = 3–4).

D Proliferation was measured in primary fibroblasts treated with TGFα (20 ng/ml) and indicated doses of barasertib for 48 h. **$P < 0.005$, 1-way ANOVA (n = 9–11).

E Quantification of apoptotic cells using Incucyte ZOOM (caspase 3/7-positive cells) in resident fibroblasts isolated from IPF lung stromal cultures and treated with vehicle or 5 μM Barasertib. ****$P < 0.00005$, 2-way ANOVA (n = 4).

Data information: All data were presented as mean ± SEM. The above data were a representative of two independent experiments with similar results. P values were shown in Appendix Table S6.
Source data are available online for this figure.

barasertib when compared to vehicle-treated TGFα mice (Fig 7B). Western blot analysis revealed a significant decrease in Col1α and Fn1 protein levels in barasertib-treated TGFα mice lungs compared to vehicle-treated (Fig 7C). TGFα mice on Dox for 6 weeks develop severe fibrotic lung disease including subpleural and adventitial thickening and the loss of lung function. Intervention therapy with barasertib resulted in a marked reduction in subpleural and adventitial fibrosis as evidenced by masons trichrome staining (Fig 7D). Notably, barasertib treatment resulted in improvements in resistance and elastance and prevented a decrease in lung compliance during TGFα-induced pulmonary fibrosis (Fig 7E). To assess possible effects of doxycycline and DMSO treatments individually on inflammation and fibrosis, CCSP-rtTA and TetO-TGFα mice were treated with Dox-containing food for 6 weeks or vehicle containing 5% DMSO for 3 weeks. We observed no significant effect of doxycycline or DMSO treatments on inflammation, lung collagen deposition, and lung function compared to untreated littermate control mice (Appendix Fig S1).

Barasertib attenuates bleomycin-induced pulmonary fibrosis *in vivo*

To substantiate our hypothesis that AURKB inhibition with barasertib attenuates pulmonary fibrosis, we used an alternative mouse model of bleomycin-induced pulmonary fibrosis (Singh *et al*, 2017; Sontake *et al*, 2018). Pulmonary fibrosis was induced in wild-type mice by treating with bleomycin intradermally 5 days per week for 4 weeks, while the last 2 weeks they received either vehicle or barasertib (Fig 8A). Lung sections stained with Masson's trichrome demonstrated significant increase in collagen staining in the lung parenchyma of bleomycin-treated mice compared with vehicle-treated control mice. This increase in Masson's trichrome staining was attenuated with barasertib treatment compared to vehicle-treated mice during bleomycin-induced pulmonary fibrosis (Fig 8B). Similarly, barasertib treatment resulted in a significant decrease in the lung hydroxyproline levels compared to vehicle-treated fibrotic mice (Fig 8C). To determine whether barasertib treatment has any negative effect on AURKB-regulated gene network, we analyzed total lung transcripts using RT–PCR. In particular, transcripts of Col1α, Col3α, Col5α, Col14α, Col15α, Ccna2, Ccnb1, and Fas were significantly decreased in barasertib-treated mice compared to vehicle-treated fibrotic mice (Fig 8D). Barasertib treatment also caused a significant decrease in the αSMA protein levels in the lung lysates of barasertib-treated mice compared to vehicle-treated fibrotic mice (Fig 8E). Taken together, our findings provide complementary *in vivo* evidence that barasertib treatment attenuates collagen deposition and plays a protective role in pulmonary fibrosis.

Discussion

We report a mitotic kinase called aurora kinase B that links fibroblast activation with fibrotic lung remodeling in IPF. AURKB is a member of the aurora kinases family and a mitotic kinase that plays a critical role in multiple steps of the cell cycle, including cytokinesis (Willems *et al*, 2018). AURKB is overexpressed in a wide range of tumor types and has been considered a marker of prognosis (Portella *et al*, 2011; Tang *et al*, 2017; Chieffi, 2018). Our results demonstrate that AURKB is upregulated in fibroblasts isolated from fibrotic lung lesions of IPF and a mouse model of TGFα-induced pulmonary fibrosis. Our immunostainings suggest upregulation of AURKB in a subset of mesenchymal cells in subpleural fibrotic lesions and fibrotic foci of IPF lungs. Co-immunostainings with Ki67 and αSMA show that AURKB is upregulated in both proliferating fibroblasts and myofibroblasts that populate the fibrotic lung lesions.

© 2020 The Authors

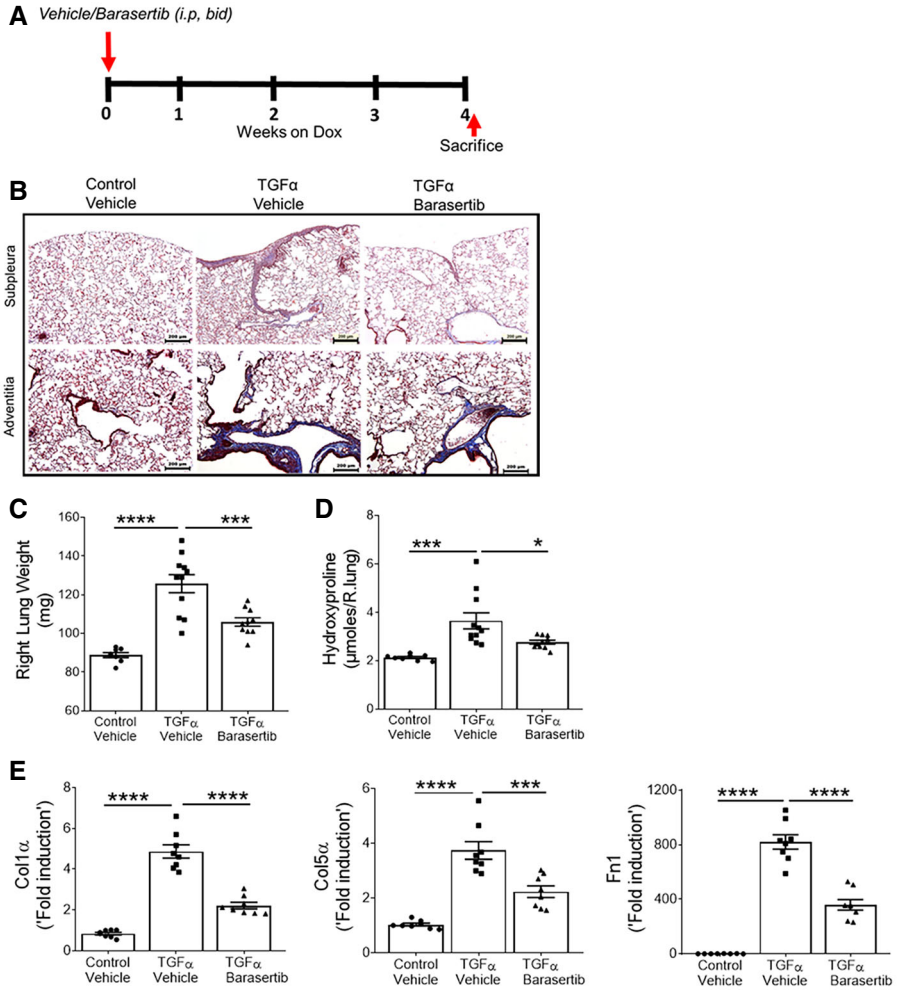


Figure 5. ***In vivo*** **Barasertib treatment prevents from TGFα induced lung fibrosis.**

A Schematic illustration of barasertib preventive treatment protocol. Control and TGFα mice were treated with either vehicle or barasertib (40 mg/kg; twice a day) for 4 weeks, while they were fed with Dox-containing food.

B Representative images of Masson's trichrome-stained lung sections from the vehicle- and barasertib-treated mice. Images were obtained at 10× magnification. Scale bar: 200 μm.

C Quantification of right lung weight of mice treated with vehicle or barasertib. ***$P < 0.0005$, ****$P < 0.00005$, 1-way ANOVA (n = 8–10 mice/group).

D Quantification of total lung hydroxyproline levels in mice treated with vehicle or barasertib. *$P < 0.05$, ***$P < 0.0005$, 1-way ANOVA (n = 8–10 mice/group).

E Quantification of Col1α, Col5α, and Fn1 gene transcripts in total lung of mice treated with vehicle or barasertib. ***$P < 0.0005$, ****$P < 0.00005$, 1-way ANOVA (n = 8 mice/group).

Data information: All data were presented as mean ± SEM. P values were shown in Appendix Table S6.

Using knockdown studies, we identified AURKB-driven gene networks that were fibroblast-specific and dysregulated in IPF, such as genes involved fibroproliferation, survival, and ECM production. In support of its pro-fibrotic actions, loss of AURKB resulted in attenuation of fibroproliferation and increased apoptotic clearance of fibroblasts, suggesting that AURKB is a positive regulator of fibroblast activation. Furthermore, AURKB is known to induce proliferation and survival in cancer cells during tumor development. Elevated expression of AURKB in thyroid anaplastic carcinoma cells can induce higher growth rate, and inhibition of AURKB expression by RNA interference has resulted in reduced proliferation of these cells (Sorrentino *et al*, 2005). Similarly, the knockdown of Epstein–Barr nuclear antigen 3C (EBNA3C)-induced AURKB expression resulted in increased activity of caspases 3 and 9 along with poly (ADP-ribose) polymerase 1 (PARP1) cleavage (Jha *et al*, 2013). Inhibition of AURKB activity by barasertib attenuated fibroproliferation and induces the apoptotic clearance in fibroblasts of IPF and TGFα mice. We confirmed that pharmacological inhibition of AURKB activity or siRNA-mediated inhibition of AURKB expression is sufficient to inhibit the expression of genes such as Plk1 and CcnA2 implicated in fibroblast proliferation. With AURKB inhibition, we observed a significant increase in the expression of pro-apoptotic genes such as Bak, Bax, and Fas, which are downstream effectors in caspase-mediated apoptotic clearance. This agrees with our recent report that apoptosis-resistant fibroblasts isolated from fibrotic lung express low levels of pro-apoptotic genes such as Bak and Bax

 © 2020 The Authors

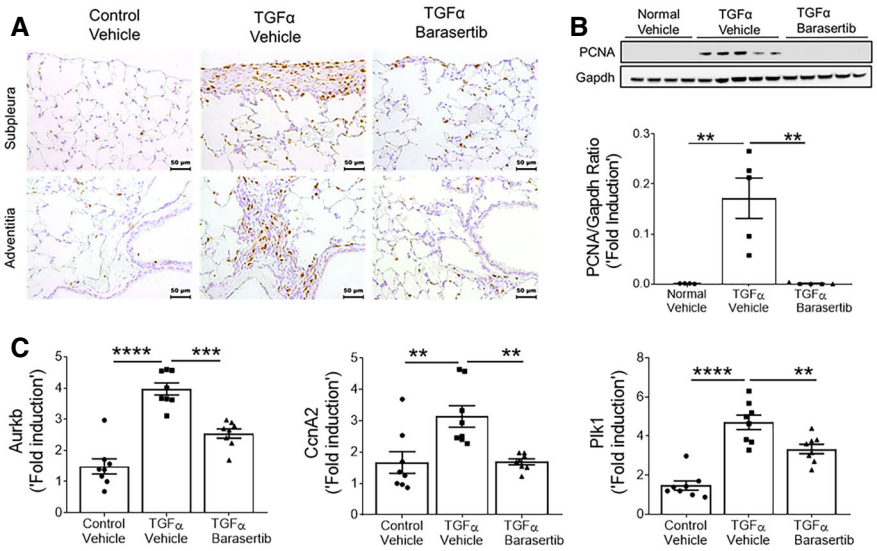


Figure 6. ***In vivo*** **barasertib treatment attenuates mesenchymal proliferation.**

A Lung sections from vehicle- and barasertib-treated mice were immunostained using Ki-67 antibody. Representative images were obtained at 20× magnification. Scale bar: 50 μm.

B Immunoblot analysis in lung lysates from vehicle- and barasertib-treated mice using PCNA antibody. Gapdh is used as loading control. $^{**}P < 0.005$, 1-way ANOVA (n = 4–5 mice/group).

C Quantification of Aurkb, Plk1, and CcnA2 gene transcripts in total lungs of mice treated with vehicle or barasertib. $^{**}P < 0.005$, $^{***}P < 0.0005$, $^{****}P < 0.00005$, 1-way ANOVA (n = 8 mice/group).

Data information: All data were presented as mean ± SEM. P values were shown in Appendix Table S6.
Source data are available online for this figure.

compared to normal fibroblasts (Kasam *et al*, 2019). Similarly, a recent publication from Bogen *et al* showed that barasertib induces apoptosis in multiple types of MYCN-amplified neuroblastoma cell lines (Bogen *et al*, 2015). This phenomenon was also documented in multiple cancer types, including breast cancer, colorectal cancer, melanoma, and leukemia (Gully *et al*, 2010; Alferez *et al*, 2012; Yamauchi *et al*, 2013; Porcelli *et al*, 2015).

Our previous work demonstrates a role for WT1 in fibroblast activation, including fibroproliferation, myofibroblast transformation, and ECM gene expression in the pathogenesis of IPF (Sontake *et al*, 2015, 2018). This work expands upon these findings, demonstrating that WT1 upregulates AURKB expression in fibroblasts. The fibroproliferative changes detected in TGFα mice may be the result of WT1-driven AURKB expression. ChIP analysis and the use of an AURKB promoter-driven luciferase assay revealed that WT1 directly interacts with the promoter elements of AURKB to drive its expression in fibroblasts. Our previous study demonstrates that WT1 regulates the myofibroblast transformation by interacting with αSMA promoter region and promoting its expression (Sontake *et al*, 2018). Hence, we speculate that WT1 promotes the fibroblasts activation at least in part by regulating the expression of AURKB. These findings posit a new role for WT1-AURKB axis in fibroproliferation. However, future studies are needed to evaluate possible binding partners and other molecular regulators downstream of WT1 and AURKB in fibroblast activation and pulmonary fibrosis.

These findings have therapeutic implications as they suggest targeting AURKB activity inhibits fibroblast activation, particularly when multiple pro-fibrotic growth factors promoting alternative fibroproliferative pathways are present. We evaluated the *in vivo* effects of AURKB inhibition by barasertib using mouse models of TGFα- and bleomycin-induced pulmonary fibrosis. Published studies have shown elevated levels of TGFα in the lung lavage fluid and fibrotic lung lesions of IPF patients compared to healthy controls (Madtes *et al*, 1988; Baughman *et al*, 1999). In support, overexpression of TGFα in mice has resulted in the development of pathologic fibrotic lesions similar to those found in IPF, including fibroproliferation, resistance to apoptosis, and subpleural fibrosis migrating into the interstitium, myofibroblast transformation, and a progressive decline in lung function (Hardie *et al*, 2004, 2010; Sontake *et al*, 2018; Kasam *et al*, 2019). Moreover, gene expression profiles after expression of TGFα were more similar to IPF samples compared to bleomycin model (Hardie *et al*, 2007; Kasam *et al*, 2019). In a recent study, we demonstrated that the FDA-approved anti-fibrotic agent nintedanib inhibited TGFα-induced pulmonary fibrosis by limiting both fibroproliferation and myofibroblast survival (Kasam *et al*, 2019). Similarly, in the TGFα model used in the current study, *in vivo* treatment with barasertib either as a preventive or as a therapeutic strategy led to decreased fibroproliferation and myofibroblast accumulation in the pathogenesis of pulmonary fibrosis. Our lung physiology measurements using FlexiVent have demonstrated that treatment of mice with barasertib improved lung function during TGFα-induced pulmonary fibrosis. These physiological changes are in agreement with observed changes in the expression of genes associated with proliferation, apoptosis, and ECM. Furthermore, we demonstrated anti-fibrotic effects of barasertib using a chronic mouse model of bleomycin-induced pulmonary fibrosis (Madala

© 2020 The Authors

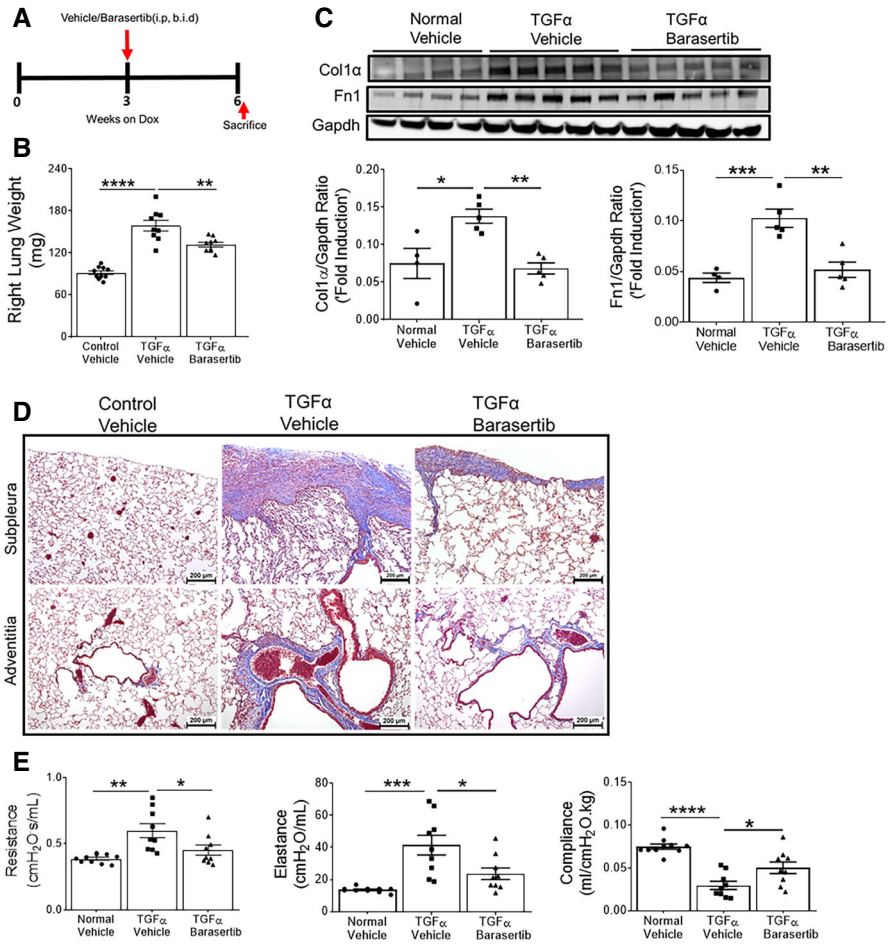


Figure 7. Therapeutic barasertib treatment reduces established and ongoing lung fibrosis.

A Schematic illustration of barasertib treatment protocol. Control and TGFα mice were treated with either vehicle or barasertib (40 mg/kg; twice a day) for last 3 weeks, while they were fed with Dox-containing food for total of 6 weeks.

B Quantification of right lung weight of mice treated with vehicle and barasertib. $^{**}P < 0.005$, $^{****}P < 0.00005$, 1-way ANOVA (n = 9–10 mice/group).

C Western blot analysis in lung lysates from vehicle- and barasertib-treated mice using Col1α and Fn1 antibodies. Gapdh is used as loading control. $^{*}P < 0.05$, $^{**}P < 0.005$, $^{***}P < 0.0005$, 1-way ANOVA (n = 4–5 mice/group).

D Representative images of Masson's trichrome-stained lung section from mice treated with vehicle and barasertib. Images were obtained at 10× magnification. Scale bar: 200 μm.

E Quantification of lung mechanics in mice treated with vehicle and barasertib. $^{*}P < 0.05$, $^{**}P < 0.005$, $^{***}P < 0.0005$, $^{****}P < 0.00005$, 1-way ANOVA (n = 9–10 mice/group).

Data information: All data were presented as mean ± SEM. P values were shown in Appendix Table S6.

et al, 2016a; Singh *et al*, 2017; Sontake *et al*, 2018). A large body of evidence supports the concept that macrophages, fibrocytes, and other immune cells secrete paracrine factors to cause excessive fibroproliferation (Madala *et al*, 2014; Desai *et al*, 2018). Importantly, the frequency of proliferating fibroblasts was elevated in the expanding areas of fibrotic foci and infusion of these proliferating mesenchymal progenitors resulted in the progressive fibrosis in mice (Xia *et al*, 2017). However, the expansion of fibrotic lesions is also attributed to the resistance to programmed cell death in myofibroblasts that accumulate in the mature fibrotic lesions (Horowitz & Thannickal, 2019; Hinz & Lagares, 2020). In support, myofibroblasts isolated from IPF lungs displayed abnormalities in apoptotic pathways, senescence, and defective autophagy (Patel *et al*, 2012; Alvarez *et al*, 2017; Kasam *et al*, 2019). Also, it is now increasingly recognized that the pathogenesis of IPF is complex likely in part due to the molecular and functional heterogeneity of fibroblasts and other lung cells (Rock *et al*, 2011; Reyfman *et al*, 2018; Tsukui *et al*, 2020). Therefore, use of inhibitors that block both proliferation and myofibroblast survival could be more beneficial to attenuate established and ongoing pulmonary fibrosis. Barasertib is currently in clinical studies, and it has been evaluated in patients with solid malignant tumors and myeloid leukemia (Lowenberg *et al*, 2011). Moreover, barasertib treatment in murine xenograft model has potentiated the anti-proliferative properties of vincristine and daunorubicin (Yang *et al*, 2007). In human xenograft models, administration of barasertib was effective against various

 © 2020 The Authors

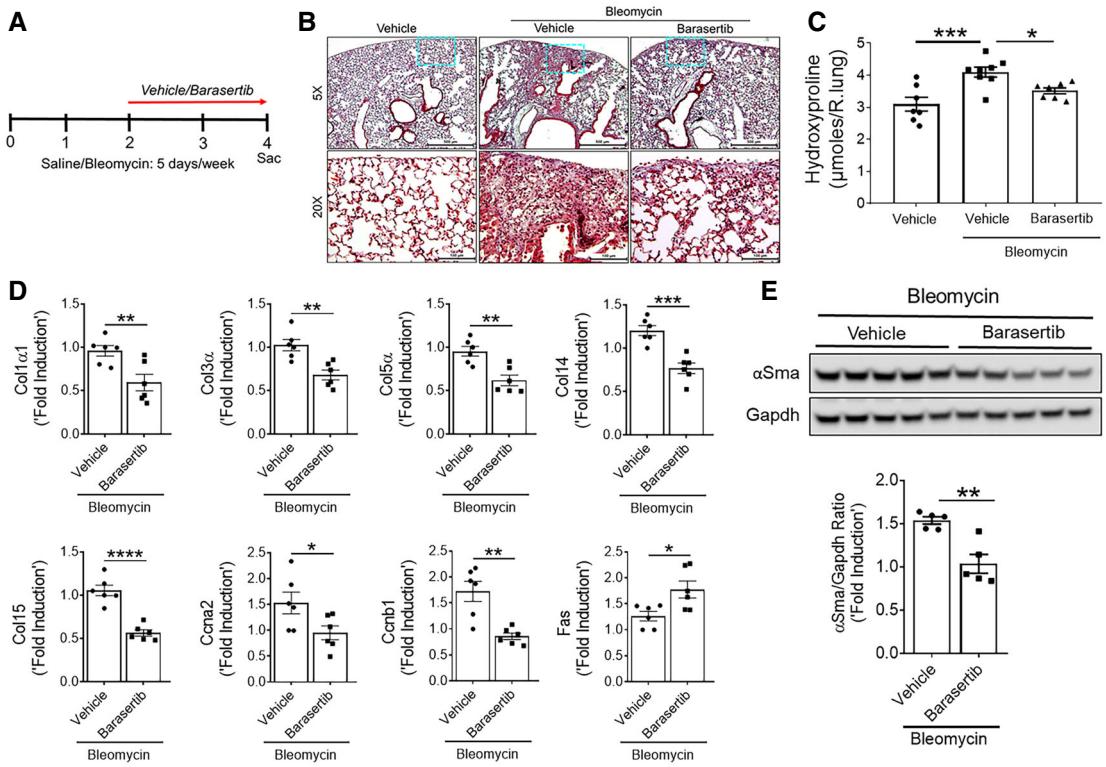


Figure 8. Therapeutic barasertib treatment attenuates bleomycin-induced lung fibrosis.

A Schematic illustration of barasertib treatment protocol. Mice were treated with either vehicle or barasertib (40 mg/kg; twice a day) for last 2 weeks, while they were injected intradermally with either saline or bleomycin 5 days per week for total of 4 weeks.

B Representative images of Masson's trichrome-stained lung section from mice treated with vehicle and barasertib. Images were obtained at 10× magnification. Scale bar: 200 μm.

C Quantification of total lung hydroxyproline in mice treated with vehicle and barasertib. *$P < 0.05$, ***$P < 0.0005$, 1-way ANOVA (n = 7–8 mice/group).

D Quantification of Col1α1, Col3α, Col5α, Col14, Col15, αSma, Ccna2, and Fas gene transcripts in total lungs of mice treated with vehicle or barasertib. *$P < 0.05$, **$P < 0.005$ ***$P < 0.0005$, ****$P < 0.00005$, 1-way ANOVA (n = 6 mice/group).

E Quantification of αSma protein levels in lung lysates from vehicle- and barasertib-treated mice. Gapdh is used as loading control. Data are presented as mean ± SEM. **$P < 0.005$, unpaired t-test (n = 5 mice/group).

Data information: All data were presented as mean ± SEM. P values were shown in Appendix Table S6.

tumor types. Barasertib was shown to inhibit the growth of human colon, lung, and hematologic tumor xenografts by reducing cell division and inducing apoptosis-mediated cell death (Wilkinson *et al*, 2007). Barasertib was tested in clinical trials for patients with acute myeloid leukemia (AML) and various other tumors (Tsuboi *et al*, 2011; Dennis *et al*, 2012; Collins *et al*, 2015). The anti-tumor effects of barasertib were enhanced when used in combination with dexamethasone (Evans *et al*, 2008). Overall, these results indicate that fibroblast-specific expression of AURKB is a critical driver of fibroblast activation and that therapeutic targeting of AURKB may serve as an ideal therapy in IPF.

In summary, we have identified and described the pathological role for AURKB in fibroblast activation and pulmonary fibrosis. We identified a role for WT1 in AURKB expression and AURKB-driven transcripts involved in proliferation and survival of fibroblasts in the pathogenesis of pulmonary fibrosis. Our preclinical findings support the use of barasertib as an anti-fibrotic agent to attenuate fibroblast activation involved in established and ongoing pulmonary fibrosis.

Materials and Methods

Mouse models of TGFα and bleomycin-induced pulmonary fibrosis

Clara cell-specific promoter (CCSP)-driven rtTA mice (CCSP-rtTA) and TGFα overexpressing mice were generated as described previously (Hardie *et al*, 2004). Hemizygous $(TetO)_7$-cmv TGFα mice were crossed to CCSP-rtTA mice to generate bitransgenic mice (CCSP-rtTA;$TGF\alpha^{tg}$) and littermate controls (CCSP-rtTA/−). Both male and female gender mice at age 10–16 weeks were used for all the experiments. Spatiotemporal overexpression of TGFα was induced by feeding the mice with doxycycline (62.5 mg/kg) containing chow. Stock solutions of barasertib (AZD-1152-HQPA; Selleckchem, TX, USA) were prepared freshly in vehicle (5% DMSO and 50% PEG-300). Previous pharmacokinetic studies have indicated that sustained and efficient AURKB inhibition could be achieved with barasertib administered at a dose range of 25–50 mg/kg every 8–12 h in mice (Marchetti *et al*, 2013; Floc'h *et al*, 2017). Therefore,

© 2020 The Authors

we treated mice with vehicle or barasertib (40 mg/kg body weight) by intraperitoneal injections twice a day with 12-h intervals. For *in vivo* intervention studies, all groups of mice were started on Dox for total 6 weeks. At the beginning of week 3, mice were treated with either vehicle or barasertib for the final 3 weeks of the study (Sontake *et al*, 2017). For bleomycin-induced mouse model, 10- to 14-week-old C57BL/6J mice (JAX Stock # 000664) were treated intradermally with saline or bleomycin (6 U/kg body weight) 5 days per week for 4 weeks intradermally as described (Singh *et al*, 2017). For *in vivo* intervention studies, all mice were treated with saline or bleomycin for the total 4 weeks, and at the beginning of week 2, mice were treated with either vehicle or barasertib for the final 2 weeks of the study. All the mice were housed under specific pathogen-free conditions, and all animal experiments were performed under protocols approved by the Institutional Animal Care and Use Committee of the Cincinnati Children's Hospital Research Foundation.

Human samples

De-identified human IPF and control non-IPF lung tissues were obtained from the Interstitial Lung Disease Biorepository at the University of Michigan Medical School and provided by Steven Huang in the Department of Internal Medicine. Specimens consisted of paraffin-embedded and freshly isolated lung tissue of patients who underwent lung transplantation for IPF. IPF was diagnosed according to the American Thoracic Society consensus criteria (Raghu *et al*, 2011). Lung samples from donors with no lung disease were used as normal lung biopsies. All tissues were acquired using research protocols and informed consent and approved by the Michigan Medicine Institutional Review Board (HUM00105694). The experiments conformed to the principles set out in the WMA Declaration of Helsinki (https://www.wma.net/policies-post/wma-declaration-of-helsinki-ethical-principles-for-medical-research-involving-human-subjects/) and the Department of Health and Human Services Belmont Report (http://www.hhs.gov/ohrp/humansubjects/guidance/belmont.html).

RNA isolation and RT–PCR

Total RNA from primary cells and lung tissue was prepared using RNeasy kit (Qiagen Sciences, Valencia, CA) as described previously (Kasam *et al*, 2019). Real-time PCR was performed using the CFX384 Touch Real-Time PCR detection system and SYBR select master mix (Bio-Rad, Hercules, CA). Target gene transcripts in each sample were normalized to mouse hypoxanthine guanine phosphoribosyltransferase (Hprt) or human beta-actin or Gapdh. All the real-time primer details are provided in Appendix Tables S2 and S3.

Western blot

Western blot analysis was performed as described earlier (Madala *et al*, 2016a). Briefly, cell lysate was prepared either from primary cells or from lung tissue using the RIPA lysis buffer containing protease and phosphatase inhibitors. The protein concentrations in the supernatants were quantified using BCA kit (Thermo Fisher Scientific, Waltham, MA). After SDS–PAGE separation, proteins were transferred to nitrocellulose membrane and then were probed using specific primary antibodies followed by detection with HRP-conjugated secondary antibodies. Bands were quantified using the volume integration function of the phosphor imager software, Multigage (Fujifilm, Valhalla, NY). Details of antibodies used in the Western blot are provided in Appendix Table S5.

Histology and immunohistochemistry

Histology and immunostaining were performed as described previously (Sontake *et al*, 2017). Briefly, lungs were inflated and fixed with formalin. Paraffin-embedded lungs were cut into 5-μM sections and stained for masons trichrome. For immunostaining, lung sections were deparaffinized, antigen retrieval was performed using 10 mM citric acid (pH 6.0), and sections were incubated in blocking solution before they were incubated with specific primary antibody overnight. DAB-stained sections were mounted and visualized using a bright field microscope (Leica Microsystems).

Immunofluorescence and confocal imaging

Immunofluorescence, confocal imaging, and cell quantification were performed as described previously (Madala *et al*, 2014). Briefly, OCT medium-embedded lung sections were immunostained using specific primary antibodies and followed by detection with appropriate secondary antibodies conjugated with Alexa Fluor-488 or 568 or 647. For immunocytochemistry, primary cells were fixed with methanol or 4% paraformaldehyde and were blocked using BSA solution before they were incubated with primary antibodies. Lung sections or primary cells were stained with DAPI for nuclear staining. Confocal images were collected using a Nikon AIR-A1 laser scanning confocal microscope. Imaris (version 7.2.0; Bit plane) was used for image analysis and automated cell quantification. Details of the antibodies used for immunostaining are provided in Appendix Table S4.

Quantification of apoptotic death

Apoptotic cell death was measured as described previously using IncuCyte ZOOM real-time imaging system (Kasam *et al*, 2019). Briefly, primary cells were incubated in Caspase 3/7 Green apoptosis assay reagent (Caspase 3/7 substrate conjugated to green fluorophore; Essence Bioscience) at a final concentration of 5 μM/ml. Time-lapse fluorescence imaging was performed using the IncuCyte ZOOM system (Essen BioScience); 9 images per well at 20× magnification were collected every 2 h for 24–48 h. The average number of green objects produced by the apoptotic cells was measured using Incucyte ZOOM software 2015A.

BrdU cell proliferation assay

Cell proliferation was quantified using BrdU kit (Cell signaling technology, Denver, CO) as described previously (Sontake *et al*, 2017). Briefly, primary lung-resident fibroblasts that were either transiently transfected with Aurkb siRNA or treated with vehicle or barasertib were incubated with BrdU labeling solution for 24 h. The cells were then fixed 24 h after BrdU labeling, and immunodetection of BrdU was performed according to the manufacturer's protocol.

 © 2020 The Authors

siRNA-mediated knockdown

Stealth siRNA-mediated transfection was performed in human or mouse lung-resident fibroblasts using Lipofectamine 3000 transfection kit as described previously (Sontake *et al*, 2015). Stealth negative control, Aurkb stealth siRNA, and WT1 stealth siRNA were purchased from Invitrogen: Human Aurora kinase B (Cat# HSS190048), mouse Aurora kinase B (Cat# MSS209696), human WT1 (Cat# HSS111390), mouse WT1 (Cat# MSS212628), and stealth negative control siRNA (Cat# 12935300).

Adenoviral transduction

Human lung-resident fibroblasts purified from lung stromal cultures using CD45-microbeads by negative selection were transduced with control or WT1-overexpressing adenoviral particles (000488A, Abm, Richmond, Canada) as described previously (Sontake *et al*, 2018). Cells were harvested 48–72 h post-viral transduction.

Human and mouse lung primary mesenchymal cell culture

Human and mouse lung mesenchymal cell cultures were prepared as described previously (Sontake *et al*, 2018). Human and mouse mesenchymal cells were cultured in DMEM with 10% FBS and IMDM with 5% FBS media, respectively. Primary cells used in the experiments were between passages 1 and 5.

Hydroxyproline measurement and lung mechanics

Hydroxyproline was assessed by a colorimetric assay, as previously described (Madala *et al*, 2016b). Lung function parameters such as resistance, elastance, and compliance were measured using a computerized Flexi Vent system (SCIREQ, Montreal, Canada) as described previously (Singh *et al*, 2017).

RNA-sequencing and computational analysis

RNA was prepared from lung-resident fibroblasts from TGFα mice on Dox for 10 days and transfected with control or Aurkb siRNA. RNA-sequencing and differential gene expression analysis were performed as described previously (Sontake *et al*, 2018). Aurkb siRNA-generated gene signature was queried against already available IPF gene signature (GSE53845) (DePianto *et al*, 2015). Functional enrichment analysis of the negatively correlated gene sets between IPF lungs and Aurkb siRNA-treated fibroblasts was analyzed using the ToppFun application of the ToppGene Suite (Chen *et al*, 2009).

ChIP-seq PCR assay

ChIP-seq PCR was performed using the ChIP assay kit (Cell signaling technology, Denver, CO) as described previously (Sontake *et al*, 2018). Briefly, lung-resident fibroblasts were purified from lung stromal culture of CCSP/TGFα mice on Dox-containing food for 8 weeks. Cells were cross-linked with 1% formaldehyde, and immunoprecipitation was performed with anti-WT1 (catalog 12609-1-AP, Proteintech, Rosemont, IL) or isotype control IgG (Cell Signaling Technology, Denver, CO) at 4°C as described in the manufacturer's protocol. DNA was purified, and ChIP-qPCR was performed using the CFX384 Touch Real-Time PCR detection system and SYBR select master mix (Bio-Rad, Hercules, and CA).

Luciferase assay

HEK293 cells were transiently co-transfected with vectors containing empty promoter or AURKB promoter fused with luciferase reporter (SwitchGear Genomics, Menlo Park, CA) and pLJM1 alone or with pLJM1 vector expressing WT1 using lipofectamine-3000 transfection reagent (Invitrogen). After 72 h, cells were lysed, and Renilla luciferase activity was measured using LightSwitch Luciferase Assay Reagent (SwitchGear Genomics) in a Flex Station 3 microplate reader (Molecular Devices). Luciferase activity is reported as relative luminescence units (RLU).

Statistical analysis

For *in vivo* studies, we used the sample size of seven to ten per group based on our published studies using preclinical mouse model of pulmonary fibrosis. We considered sex as a biological variable and randomized both male and females animals in groups to analyze animal data in aggregate. Also, the details of experimental groups were blinded to investigators for biochemical and histological evaluations. All data were analyzed for statistical significance using Prism (version 8; Graph Pad). We used *t*-test to compar between two groups and one-way ANOVA with Turkey's multiple comparison post-test to compare between more than two experimental groups. All data were expressed as the mean ± SEM.

The paper explained

Problem
Idiopathic pulmonary fibrosis (IPF) is a fatal fibrotic lung disease caused by activation of multiple pro-fibrotic pathways in fibroblasts to induce excessive proliferation, survival, and ECM secretion. Hence, understanding converging points in fibroblast activation is essential to develop novel and effective therapies against IPF.

Results
Aurora kinase B is a key mitotic kinase that we found upregulated in lung fibroblasts of IPF and mouse models of TGFα- and bleomycin-induced pulmonary fibrosis. This increase in AURKB expression in lung-resident fibroblasts is driven by multiple pro-fibrotic growth factors and a transcription factor called Wilms tumor 1. Using both *in vitro* and *in vivo* models of pulmonary fibrosis, we demonstrate that AURKB upregulation is involved in fibroblast activation and the pharmacologic inhibition of AURKB attenuates ongoing pulmonary fibrosis in mouse models of TGFα- and bleomycin-induced pulmonary fibrosis.

Impact
This study provides the first evidence that the AURKB functions as a positive regulator for fibroproliferation and survival in the progressive expansion of fibrotic lesions in IPF. Our new findings support the mechanism of the WT1-AURKB axis to induce fibroproliferation in IPF. Barasertib treatment is an effective therapy to attenuate ongoing fibrosis in mouse models of severe fibrotic lung disease and may prove useful as a potential therapeutic option for IPF.

© 2020 The Authors

Data were considered statistically significant for $P < 0.05$. The exact P values for each figure can be found in Appendix Table S6.

Data availability

The RNA-seq datasets produced in this study are available at Gene Expression Omnibus (GEO) under the accession number GSE153898 (https://www.ncbi.nlm.nih.gov/geo/query/acc.cgi?acc=GSE153898).

Expanded View for this article is available online.

Acknowledgements
We are thankful for the veterinary services and research pathology core at Cincinnati Children's Hospital Medical Center for help in the study. This study was supported in part by the NIH 1R01 HL134801 (SKM), 1R21 AG059533 (SKM) and the US Department of Defense funds, W81XWH-17-1-0666 (SKM), and NIH NCATS grant 1UG3TR002612 (AGJ).

Author contributions
RKK and SKM conceived the project, designed experiments, analyzed data and wrote the manuscript; RKK performed most of the experiments; DS performed immunostainings; AGJ and SG performed bioinformatics analysis; SKH provided human lung tissues and edited manuscript; GBR and AGJ analyzed data and edited manuscript.

Conflict of interest
The authors declare that they have no conflict of interest.

For more information
(i) Pulmonary Fibrosis Foundation: https://www.pulmonaryfibrosis.org/
(ii) American Thoracic Society: https://www.thoracic.org/patients/patient-resources/resources/idiopathic-pulmonary-fibrosis.pdf
(iii) Dr. Madala's webpage: https://www.cincinnatichildrens.org/bio/m/satish-madala

References

Alferez DG, Goodlad RA, Odedra R, Sini P, Crafter C, Ryan AJ, Wedge SR, Wright NA, Anderson E, Wilkinson RW (2012) Inhibition of Aurora-B kinase activity confers antitumor efficacy in preclinical mouse models of early and advanced gastrointestinal neoplasia. *Int J Oncol* 41: 1475 – 1485

Allen JT, Spiteri MA (2002) Growth factors in idiopathic pulmonary fibrosis: relative roles. *Respir Res* 3: 13

Alvarez D, Cardenes N, Sellares J, Bueno M, Corey C, Hanumanthu VS, Peng Y, D'Cunha H, Sembrat J, Nouraie M *et al* (2017) IPF lung fibroblasts have a senescent phenotype. *Am J Physiol Lung Cell Mol Physiol* 313: L1164 – L1173

Barratt SL, Creamer A, Hayton C, Chaudhuri N (2018) Idiopathic pulmonary fibrosis (IPF): an overview. *J Clin Med* 7: 201

Baughman RP, Lower EE, Miller MA, Bejarano PA, Heffelfinger SC (1999) Overexpression of transforming growth factor-alpha and epidermal growth factor-receptor in idiopathic pulmonary fibrosis. *Sarcoidosis Vasc Diffuse Lung Dis* 16: 57 – 61

Bogen D, Wei JS, Azorsa DO, Ormanoglu P, Buehler E, Guha R, Keller JM, Mathews Griner LA, Ferrer M, Song YK *et al* (2015) Aurora B kinase is a potent and selective target in MYCN-driven neuroblastoma. *Oncotarget* 6: 35247 – 35262

Chaudhary NI, Roth GJ, Hilberg F, Muller-Quernheim J, Prasse A, Zissel G, Schnapp A, Park JE (2007) Inhibition of PDGF, VEGF and FGF signalling attenuates fibrosis. *Eur Respir J* 29: 976 – 985

Chen J, Bardes EE, Aronow BJ, Jegga AG (2009) ToppGene Suite for gene list enrichment analysis and candidate gene prioritization. *Nucleic Acids Res* 37: W305 – W311

Chieffi P (2018) Aurora B: a new promising therapeutic target in cancer. *Intractable Rare Dis Res* 7: 141 – 144

Collins GP, Eyre TA, Linton KM, Radford J, Vallance GD, Soilleux E, Hatton C (2015) A phase II trial of AZD1152 in relapsed/refractory diffuse large B-cell lymphoma. *Br J Haematol* 170: 886 – 890

Costabel U, Bendstrup E, Cottin V, Dewint P, Egan JJ, Ferguson J, Groves R, Hellstrom PM, Kreuter M, Maher TM *et al* (2014) Pirfenidone in idiopathic pulmonary fibrosis: expert panel discussion on the management of drug-related adverse events. *Adv Ther* 31: 375 – 391

Dennis M, Davies M, Oliver S, D'Souza R, Pike L, Stockman P (2012) Phase I study of the Aurora B kinase inhibitor barasertib (AZD1152) to assess the pharmacokinetics, metabolism and excretion in patients with acute myeloid leukemia. *Cancer Chemother Pharmacol* 70: 461 – 469

DePianto DJ, Chandriani S, Abbas AR, Jia G, N'Diaye EN, Caplazi P, Kauder SE, Biswas S, Karnik SK, Ha C *et al* (2015) Heterogeneous gene expression signatures correspond to distinct lung pathologies and biomarkers of disease severity in idiopathic pulmonary fibrosis. *Thorax* 70: 48 – 56

Desai O, Winkler J, Minasyan M, Herzog EL (2018) The role of immune and inflammatory cells in idiopathic pulmonary fibrosis. *Front Med* 5: 43

Evans RP, Naber C, Steffler T, Checkland T, Maxwell CA, Keats JJ, Belch AR, Pilarski LM, Lai R, Reiman T (2008) The selective Aurora B kinase inhibitor AZD1152 is a potential new treatment for multiple myeloma. *Br J Haematol* 140: 295 – 302

Floc'h N, Ashton S, Taylor P, Trueman D, Harris E, Odedra R, Maratea K, Derbyshire N, Caddy J, Jacobs VN *et al* (2017) Optimizing therapeutic effect of aurora B inhibition in acute myeloid leukemia with AZD2811 nanoparticles. *Mol Cancer Ther* 16: 1031 – 1040

Frangini A, Sjoberg M, Roman-Trufero M, Dharmalingam G, Haberle V, Bartke T, Lenhard B, Malumbres M, Vidal M, Dillon N (2013) The aurora B kinase and the polycomb protein ring1B combine to regulate active promoters in quiescent lymphocytes. *Mol Cell* 51: 647 – 661

Fu J, Bian M, Jiang Q, Zhang C (2007) Roles of Aurora kinases in mitosis and tumorigenesis. *Mol Cancer Res* 5: 1 – 10

Gribbin J, Hubbard RB, Le Jeune I, Smith CJ, West J, Tata LJ (2006) Incidence and mortality of idiopathic pulmonary fibrosis and sarcoidosis in the UK. *Thorax* 61: 980 – 985

Grimminger F, Gunther A, Vancheri C (2015) The role of tyrosine kinases in the pathogenesis of idiopathic pulmonary fibrosis. *Eur Respir J* 45: 1426 – 1433

Gully CP, Zhang F, Chen J, Yeung JA, Velazquez-Torres G, Wang E, Yeung SC, Lee MH (2010) Antineoplastic effects of an Aurora B kinase inhibitor in breast cancer. *Mol Cancer* 9: 42

Gully CP, Velazquez-Torres G, Shin JH, Fuentes-Mattei E, Wang E, Carlock C, Chen J, Rothenberg D, Adams HP, Choi HH *et al* (2012) Aurora B kinase phosphorylates and instigates degradation of p53. *Proc Natl Acad Sci USA* 109: E1513 – E1522

Hardie WD, Le Cras TD, Jiang K, Tichelaar JW, Azhar M, Korfhagen TR (2004) Conditional expression of transforming growth factor-alpha in adult mouse lung causes pulmonary fibrosis. *Am J Physiol Lung Cell Mol Physiol* 286: L741 – L749

 © 2020 The Authors

Hardie WD, Korfhagen TR, Sartor MA, Prestridge A, Medvedovic M, Le Cras TD, Ikegami M, Wesselkamper SC, Davidson C, Dietsch M *et al* (2007) Genomic profile of matrix and vasculature remodeling in TGF-alpha induced pulmonary fibrosis. *Am J Respir Cell Mol Biol* 37: 309 – 321

Hardie WD, Hagood JS, Dave V, Perl AK, Whitsett JA, Korfhagen TR, Glasser S (2010) Signaling pathways in the epithelial origins of pulmonary fibrosis. *Cell Cycle* 9: 2769 – 2776

Hinz B, Lagares D (2020) Evasion of apoptosis by myofibroblasts: a hallmark of fibrotic diseases. *Nat Rev Rheumatol* 16: 11 – 31

Horowitz JC, Thannickal VJ (2019) Mechanisms for the resolution of organ fibrosis. *Physiology* 34: 43 – 55

Hughes G, Toellner H, Morris H, Leonard C, Chaudhuri N (2016) Real world experiences: pirfenidone and nintedanib are effective and well tolerated treatments for idiopathic pulmonary fibrosis. *J Clin Med* 5: 78

Jha HC, Lu J, Saha A, Cai Q, Banerjee S, Prasad MA, Robertson ES (2013) EBNA3C-mediated regulation of aurora kinase B contributes to Epstein-Barr virus-induced B-cell proliferation through modulation of the activities of the retinoblastoma protein and apoptotic caspases. *J Virol* 87: 12121 – 12138

Kasam RK, Reddy GB, Jegga AG, Madala SK (2019) Dysregulation of mesenchymal cell survival pathways in severe fibrotic lung disease: the effect of nintedanib therapy. *Front Pharmacol* 10: 532

King TE Jr, Bradford WZ, Castro-Bernardini S, Fagan EA, Glaspole I, Glassberg MK, Gorina E, Hopkins PM, Kardatzke D, Lancaster L *et al* (2014) A phase 3 trial of pirfenidone in patients with idiopathic pulmonary fibrosis. *N Engl J Med* 370: 2083 – 2092

Kollareddy M, Dzubak P, Zheleva D, Hajduch M (2008) Aurora kinases: structure, functions and their association with cancer. *Biomed Pap Med Fac Univ Palacky Olomouc Czech Repub* 152: 27 – 33

Lampson MA, Cheeseman IM (2011) Sensing centromere tension: Aurora B and the regulation of kinetochore function. *Trends Cell Biol* 21: 133 – 140

Lancaster LH, de Andrade JA, Zibrak JD, Padilla ML, Albera C, Nathan SD, Wijsenbeek MS, Stauffer JL, Kirchgaessler KU, Costabel U (2017) Pirfenidone safety and adverse event management in idiopathic pulmonary fibrosis. *Eur Respir Rev* 26: 170057

Ley B, Collard HR, King TE Jr (2011) Clinical course and prediction of survival in idiopathic pulmonary fibrosis. *Am J Respir Crit Care Med* 183: 431 – 440

Lowenberg B, Muus P, Ossenkoppele G, Rousselot P, Cahn JY, Ifrah N, Martinelli G, Amadori S, Berman E, Sonneveld P *et al* (2011) Phase 1/2 study to assess the safety, efficacy, and pharmacokinetics of barasertib (AZD1152) in patients with advanced acute myeloid leukemia. *Blood* 118: 6030 – 6036

Madala SK, Schmidt S, Davidson C, Ikegami M, Wert S, Hardie WD (2012) MEK-ERK pathway modulation ameliorates pulmonary fibrosis associated with epidermal growth factor receptor activation. *Am J Respir Cell Mol Biol* 46: 380 – 388

Madala SK, Edukulla R, Schmidt S, Davidson C, Ikegami M, Hardie WD (2014) Bone marrow-derived stromal cells are invasive and hyperproliferative and alter transforming growth factor-alpha-induced pulmonary fibrosis. *Am J Respir Cell Mol Biol* 50: 777 – 786

Madala SK, Sontake V, Edukulla R, Davidson CR, Schmidt S, Hardie WD (2016a) Unique and redundant functions of p70 ribosomal S6 kinase isoforms regulate mesenchymal cell proliferation and migration in pulmonary fibrosis. *Am J Respir Cell Mol Biol* 55: 792 – 803

Madala SK, Thomas G, Edukulla R, Davidson C, Schmidt S, Schehr A, Hardie WD (2016b) p70 ribosomal S6 kinase regulates subpleural fibrosis following transforming growth factor-alpha expression in the lung. *Am J Physiol Lung Cell Mol Physiol* 310: L175 – L186

Madtes DK, Raines EW, Sakariassen KS, Assoian RK, Sporn MB, Bell GI, Ross R (1988) Induction of transforming growth factor-alpha in activated human alveolar macrophages. *Cell* 53: 285 – 293

Marchetti S, Pluim D, van Eijndhoven M, van Tellingen O, Mazzanti R, Beijnen JH, Schellens JH (2013) Effect of the drug transporters ABCG2, Abcg2, ABCB1 and ABCC2 on the disposition, brain accumulation and myelotoxicity of the aurora kinase B inhibitor barasertib and its more active form barasertib-hydroxy-QPA. *Invest New Drugs* 31: 1125 – 1135

Nigg EA (2001) Mitotic kinases as regulators of cell division and its checkpoints. *Nat Rev Mol Cell Biol* 2: 21 – 32

Pardo A, Selman M (2016) Lung fibroblasts, aging, and idiopathic pulmonary fibrosis. *Ann Am Thorac Soc* 13(Suppl 5): S417 – S421

Patel AS, Lin L, Geyer A, Haspel JA, An CH, Cao J, Rosas IO, Morse D (2012) Autophagy in idiopathic pulmonary fibrosis. *PLoS ONE* 7: e41394

Phan SH (2008) Biology of fibroblasts and myofibroblasts. *Proc Am Thorac Soc* 5: 334 – 337

Porcelli L, Guida G, Quatrale AE, Cocco T, Sidella L, Maida I, Iacobazzi RM, Ferretta A, Stolfa DA, Strippoli S *et al* (2015) Aurora kinase B inhibition reduces the proliferation of metastatic melanoma cells and enhances the response to chemotherapy. *J Transl Med* 13: 26

Portella G, Passaro C, Chieffi P (2011) Aurora B: a new prognostic marker and therapeutic target in cancer. *Curr Med Chem* 18: 482 – 496

Prele CM, Yao E, O'Donoghue RJ, Mutsaers SE, Knight DA (2012) STAT3: a central mediator of pulmonary fibrosis? *Proc Am Thorac Soc* 9: 177 – 182

Raghu G, Collard HR, Egan JJ, Martinez FJ, Behr J, Brown KK, Colby TV, Cordier JF, Flaherty KR, Lasky JA *et al* (2011) An official ATS/ERS/JRS/ALAT statement: idiopathic pulmonary fibrosis: evidence-based guidelines for diagnosis and management. *Am J Respir Crit Care Med* 183: 788 – 824

Raghu G (2017) Idiopathic pulmonary fibrosis: lessons from clinical trials over the past 25 years. *Eur Respir J* 50: 1701209

Reyfman PA, Walter JM, Joshi N, Anekalla KR, McQuattie-Pimentel AC, Chiu S, Fernandez R, Akbarpour M, Chen CI, Ren Z *et al* (2018) Single-cell transcriptomic analysis of human lung provides insights into the pathobiology of pulmonary fibrosis. *Am J Respir Crit Care Med* 199: 1517 – 1536

Richeldi L, du Bois RM, Raghu G, Azuma A, Brown KK, Costabel U, Cottin V, Flaherty KR, Hansell DM, Inoue Y *et al* (2014) Efficacy and safety of nintedanib in idiopathic pulmonary fibrosis. *N Engl J Med* 370: 2071 – 2082

Rock JR, Barkauskas CE, Cronce MJ, Xue Y, Harris JR, Liang J, Noble PW, Hogan BL (2011) Multiple stromal populations contribute to pulmonary fibrosis without evidence for epithelial to mesenchymal transition. *Proc Natl Acad Sci USA* 108: E1475 – E1483

Singh B, Kasam RK, Sontake V, Wynn TA, Madala SK (2017) Repetitive intradermal bleomycin injections evoke T-helper cell 2 cytokine-driven pulmonary fibrosis. *Am J Physiol Lung Cell Mol Physiol* 313: L796 – L806

Sontake V, Shanmukhappa SK, DiPasquale BA, Reddy GB, Medvedovic M, Hardie WD, White ES, Madala SK (2015) Fibrocytes regulate Wilms tumor 1-positive cell accumulation in severe fibrotic lung disease. *J Immunol* 195: 3978 – 3991

Sontake V, Wang Y, Kasam RK, Sinner D, Reddy GB, Naren AP, McCormack FX, White ES, Jegga AG, Madala SK (2017) Hsp90 regulation of fibroblast activation in pulmonary fibrosis. *JCI Insight* 2: e91454

Sontake V, Kasam RK, Sinner D, Korfhagen TR, Reddy GB, White ES, Jegga AG, Madala SK (2018) Wilms' tumor 1 drives fibroproliferation and myofibroblast transformation in severe fibrotic lung disease. *JCI Insight* 3: e121252

Sorrentino R, Libertini S, Pallante PL, Troncone G, Palombini L, Bavetsias V, Spalletti-Cernia D, Laccetti P, Linardopoulos S, Chieffi P *et al* (2005) Aurora

© 2020 The Authors

B overexpression associates with the thyroid carcinoma undifferentiated phenotype and is required for thyroid carcinoma cell proliferation. *J Clin Endocrinol Metab* 90: 928 – 935

Tang A, Gao K, Chu L, Zhang R, Yang J, Zheng J (2017) Aurora kinases: novel therapy targets in cancers. *Oncotarget* 8: 23937 – 23954

Thannickal VJ, Horowitz JC (2006) Evolving concepts of apoptosis in idiopathic pulmonary fibrosis. *Proc Am Thorac Soc* 3: 350 – 356

Tsuboi K, Yokozawa T, Sakura T, Watanabe T, Fujisawa S, Yamauchi T, Uike N, Ando K, Kihara R, Tobinai K *et al* (2011) A Phase I study to assess the safety, pharmacokinetics and efficacy of barasertib (AZD1152), an Aurora B kinase inhibitor, in Japanese patients with advanced acute myeloid leukemia. *Leuk Res* 35: 1384 – 1389

Tsukui T, Sun KH, Wetter JB, Wilson-Kanamori JR, Hazelwood LA, Henderson NC, Adams TS, Schupp JC, Poli SD, Rosas IO *et al* (2020) Collagen-producing lung cell atlas identifies multiple subsets with distinct localization and relevance to fibrosis. *Nat Commun* 11: 1920

Vallath S, Hynds RE, Succony L, Janes SM, Giangreco A (2014) Targeting EGFR signalling in chronic lung disease: therapeutic challenges and opportunities. *Eur Respir J* 44: 513 – 522

Walton KL, Johnson KE, Harrison CA (2017) Targeting TGF-beta mediated SMAD signaling for the prevention of fibrosis. *Front Pharmacol* 8: 461

Wilkinson RW, Odedra R, Heaton SP, Wedge SR, Keen NJ, Crafter C, Foster JR, Brady MC, Bigley A, Brown E *et al* (2007) AZD1152, a selective inhibitor of Aurora B kinase, inhibits human tumor xenograft growth by inducing apoptosis. *Clin Cancer Res* 13: 3682 – 3688

Willems E, Dedobbeleer M, Digregorio M, Lombard A, Lumapat PN, Rogister B (2018) The functional diversity of Aurora kinases: a comprehensive review. *Cell Div* 13: 7

Wilson MS, Wynn TA (2009) Pulmonary fibrosis: pathogenesis, etiology and regulation. *Mucosal Immunol* 2: 103 – 121

Wollin L, Wex E, Pautsch A, Schnapp G, Hostettler KE, Stowasser S, Kolb M (2015) Mode of action of nintedanib in the treatment of idiopathic pulmonary fibrosis. *Eur Respir J* 45: 1434 – 1445

Wu L, Ma CA, Zhao Y, Jain A (2011) Aurora B interacts with NIR-p53, leading to p53 phosphorylation in its DNA-binding domain and subsequent functional suppression. *J Biol Chem* 286: 2236 – 2244

Wynn TA (2011) Integrating mechanisms of pulmonary fibrosis. *J Exp Med* 208: 1339 – 1350

Wynn TA, Ramalingam TR (2012) Mechanisms of fibrosis: therapeutic translation for fibrotic disease. *Nat Med* 18: 1028 – 1040

Xia H, Gilbertsen A, Herrera J, Racila E, Smith K, Peterson M, Griffin T, Benyumov A, Yang L, Bitterman PB *et al* (2017) Calcium-binding protein S100A4 confers mesenchymal progenitor cell fibrogenicity in idiopathic pulmonary fibrosis. *J Clin Invest* 127: 2586 – 2597

Yamauchi T, Uzui K, Shigemi H, Negoro E, Yoshida A, Ueda T (2013) Aurora B inhibitor barasertib and cytarabine exert a greater-than-additive cytotoxicity in acute myeloid leukemia cells. *Cancer Sci* 104: 926 – 933

Yang J, Ikezoe T, Nishioka C, Tasaka T, Taniguchi A, Kuwayama Y, Komatsu N, Bandobashi K, Togitani K, Koeffler HP *et al* (2007) AZD1152, a novel and selective aurora B kinase inhibitor, induces growth arrest, apoptosis, and sensitization for tubulin depolymerizing agent or topoisomerase II inhibitor in human acute leukemia cells *in vitro* and *in vivo*. *Blood* 110: 2034 – 2040

License: This is an open access article under the terms of the Creative Commons Attribution 4.0 License, which permits use, distribution and reproduction in any medium, provided the original work is properly cited.

Dysregulated overexpression of Sox9 induces fibroblast activation in pulmonary fibrosis

Prathibha R. Gajjala[1,2], Rajesh K. Kasam[1,2], Divya Soundararajan[1,2], Debora Sinner[1,3], Steven K. Huang[4], Anil G. Jegga[1,5] and Satish K. Madala[1,2]*

[1] Department of Pediatrics, University of Cincinnati, College of Medicine, Cincinnati, OH, USA

[2] Division of Pulmonary Medicine, Cincinnati Children's Hospital Medical Center, Cincinnati, OH, USA

[3] Division of Neonatology and Pulmonary Biology, Perinatal Institute, Cincinnati Children's Hospital Medical Center, Cincinnati, OH, USA

[4] Division of Pulmonary and Critical Care Medicine, University of Michigan Medical School, Ann Arbor, MI, USA

[5] Division of Biomedical Informatics, Cincinnati Children's Hospital Medical Center, Cincinnati, OH, USA

*** Correspondence:** Satish K. Madala, Division of Pulmonary Medicine, Cincinnati Children's Hospital Medical Center, MLC 2021, 3333 Burnet Avenue, Cincinnati, OH 45229. Email: satish.madala@cchmc.org Phone: (513) 636-9852 Fax: (513) 636-9946

Conflict of interest

The authors have declared that no conflict of interest exists.

Abstract

Idiopathic pulmonary fibrosis (IPF) is a fatal fibrotic lung disease associated with unremitting fibroblast activation including fibroblast-to-myofibroblast transformation (FMT), migration, resistance to apoptotic clearance, and excessive deposition of extracellular matrix (ECM) proteins in the distal lung parenchyma. Aberrant activation of lung-developmental pathways is associated with severe fibrotic lung disease; however, the mechanisms through which these pathways activate fibroblasts in IPF remain unclear. Sox9 is a member of the HMG box family of DNA-binding transcription factors that are selectively expressed by epithelial cell progenitors to modulate branching morphogenesis during lung development. We demonstrate that Sox9 is upregulated via MAPK/PI3K-dependent signaling and by the transcription factor Wilms' tumor 1 in distal lung-resident fibroblasts in IPF. Mechanistically, using fibroblast activation assays, we demonstrate that Sox9 functions as a positive regulator of FMT, migration, survival, and ECM production. Importantly, our in vivo studies demonstrate that fibroblast-specific deletion of Sox9 is sufficient to attenuate collagen deposition and improve lung function during TGFα-induced pulmonary fibrosis. Using a mouse model of bleomycin-induced pulmonary fibrosis, we show that myofibroblast-specific Sox9 overexpression augments fibroblast activation and pulmonary fibrosis. Thus, Sox9 functions as a profibrotic transcription factor in activating fibroblasts, illustrating the potential utility of targeting Sox9 in IPF treatment.

Introduction

Pulmonary fibrosis is the final common pathway of several lung diseases caused by dysregulated healing responses to chronic lung injury. Fibrosis is often associated with fibroproliferation, survival, and excessive deposition of the extracellular matrix (ECM) proteins, leading to progressive lung parenchyma scarring (1, 2). Idiopathic pulmonary fibrosis (IPF) is perhaps the most severe and enigmatic form of interstitial lung disease, and recent epidemiological studies suggest that the prevalence of the disease is increasing in the U.S. and globally. The mortality rate of IPF is increasing every year as well, and the disease is one of the leading causes of death among the aging population (2). The survival rate after diagnosis is typically 3–5 years, which is partly due to a lack of effective treatments or cure. However, the major impediment to developing new therapies is the lack of knowledge regarding mechanisms underlying fibroblast activation in IPF. Therefore, it is essential to characterize and understand these underlying molecular mechanisms in order to develop new treatments that attenuate fibroblast activation in IPF.

Transcription factors play a critical role in orchestrating cell-specific gene networks that support the early stages of lung development. The expression of these transcription factors is typically suppressed in fully developed adult lungs, preventing cellular overgrowth and lung dysfunction. Studies using single-cell transcriptomic analysis of lung cells suggest the existence of a cell-specific expression pattern and aberrant reactivation of these developmental transcription factors in a cell-specific manner in IPF (3, 4). In particular, frequent injury and damage to epithelial cells have been shown to reactivate several profibrotic transcription factors in lung cells; reactivation results in dysregulated repair and regeneration in IPF and in several chronic mouse models of severe fibrotic

lung disease. Recent studies from our lab and others have demonstrated the reactivation of Wilms' tumor 1 (WT1) in both fibroblasts and mesothelial cells in IPF lungs. In contrast, during lung development, WT1 expression is limited to mesothelial cells, and the lack of such expression is lethal to mice. Furthermore, our next-generation RNA-seq studies using WT1-positive fibroblasts identified several important transcriptional regulators, such as *Sox9*, that are epithelial cell-specific and involved in lung development (5). Sox9 is a transcription factor that belongs to Sry-related HMG box-containing proteins. Insights into Sox9 expression and function have been primarily obtained from studies of embryonic organ development; chondrogenesis in the trachea, branching morphogenesis in the lung, and male gonad development are examples (6-8). In developing lungs, Sox9 is highly expressed in the distal tips of the branching epithelium. Sox9 expression is downregulated by the onset of terminal differentiation into type I and type II epithelial cells and is restricted to only few airway epithelial cells (5). The overexpression or deletion of Sox9 leads to branching defects and affects proliferation, differentiation, and ECM production (6, 9).

Although the role of Sox9 in the epithelium during lung development is well documented, Sox9 expression in the distal fibroblasts of the lung and its potential role in fibroblast activation has never been explored in the context of pulmonary fibrosis. In the present study, we evaluated whether Sox9 is upregulated in fibroblasts and the possible pathogenic role of Sox9, and its target genes, in fibroblast activation and pulmonary fibrosis. Our study demonstrates that Sox9 upregulation in fibroblasts contributes to pulmonary fibrosis and thus provides a therapeutic target for IPF.

Results

SOX9 is upregulated in distal lung fibroblasts in IPF. To identify the kinetics of SOX9 expression, we measured *SOX9* transcripts during the embryonic and postnatal stages of lung development and observed that *Sox9* RNA levels were the highest in the early lung (E14.5), and subsequently declined before birth, with the lowest RNA levels observed in the adult lungs (Supplemental Figure 1A). Immunofluorescence staining of SOX9 in the lung sections of alpha-actin-2 (ACTA2) reporter mice supported earlier findings that SOX9 is selectively expressed by distal epithelial progenitor cells; however, there was limited or no staining observed in the ACTA2-positive mesenchymal cells of developing lungs at E15.5 (Supplemental Figure 1B). Furthermore, measurement of *SOX9* transcript levels revealed a significant increase in the total lung transcripts of *SOX9* in individuals with IPF compared to those in healthy controls (Figure 1A). Immunohistochemistry revealed a previously unreported finding that SOX9 is predominantly localized to the nuclei of spindle-shaped cells in the distal fibrotic lesions including fibrotic foci and thickened subpleural, which are the predominant pathological features of IPF (Figure 1B and Supplemental Figure 2A). Quantification of the number of SOX9-positive cells and total cells in these fibrotic lesions indicated a significant increase in the percentage of SOX9-positive cells in IPF compared to that in healthy controls (Figure 1C). To show that SOX9 is upregulated in IPF fibroblasts, we measured *SOX9* transcripts in the distal lung fibroblasts isolated from IPF and healthy donor lungs. Indeed, we observed a marked increase in the *SOX9* transcripts in the total transcripts of fibroblasts isolated from IPF lungs, compared with that in fibroblasts from normal lungs (Figure 1D). Analysis of IPF and normal lung sections co-immunostained with antibodies

against SOX9 and vimentin showed a marked increase in the number of SOX9 and vimentin dual positive cells in IPF lungs compared to those in normal lungs (Figure 1E). Similarly, analysis of fibroblasts from distal lung cultures showed a significant increase in the number of SOX9-positive fibroblasts in IPF (Supplemental Figure 2B-2C).

Sox9 is upregulated in a mouse model of TGFα-induced pulmonary fibrosis. To determine whether SOX9 is upregulated during TGFα-induced pulmonary fibrosis, we measured the *Sox9* levels in the total lung transcripts of *TGFα^{OE}* mice that developed severe fibrotic lung disease by 28 days after Dox treatment (10). *Sox9* transcript levels in the lungs of Dox-treated *TGFα^{OE}* mice were the highest at day 28 compared to those at day 0 (Figure 1F). Co-immunostaining analyses revealed an increase in the dual positive cells for ACTA2 and SOX9, or vimentin and SOX9, in the fibrotic lesions of *TGFα^{OE}* mice compared to control mice treated with Dox for six weeks (Figure 1G). We also observed a significant increase in SOX9 protein levels in lysates of the distal lung fibroblasts isolated from *TGFα^{OE}* mice compared to that from control mice treated with Dox for 4 weeks (Figure 1H). These results suggest that Sox9 is upregulated in the distal lung fibroblasts of IPF and a mouse model of TGFα-induced pulmonary fibrosis.

The TGFα/WT1 axis is involved in the upregulation of SOX9 in fibroblasts. To determine the potential effects of multiple profibrotic growth factors on SOX9 expression, we treated distal human lung fibroblasts (HLF) with multiple growth factors including TGFα, bone morphogenic protein 2 (BMP2), connective tissue growth factor (CTGF), and insulin growth factor 1 (IGF1). *SOX9* levels were elevated in HLF treated with TGFα, BMP2, and CTGF; however, there was limited or no effect of IGF1 on *SOX9* levels (Figure 2A). We next studied the effects of TGFα on SOX9 expression in fibroblasts from IPF and normal

lungs. We observed that *SOX9* levels were high in both normal and IPF fibroblasts treated with TGFα compared to those in media-treated fibroblasts (Figure 2B). To determine the signaling pathway involved in TGFα-induced SOX9 expression, we treated IPF fibroblasts with inhibitors of MEK (ARRY) and PI3 kinase (PX-866) in the presence and absence of TGFα. As expected, TGFα treatment resulted in a notable increase in the phosphorylation of Erk1/2 at 30 min compared with that in media-treated fibroblasts (Supplemental Figure 3A–C). This increase in TGFα-induced pErk1/2 was significantly attenuated in IPF fibroblasts treated with ARRY compared with that in vehicle-treated controls (Supplemental Figure 3A-C). Notably, we observed a significant decrease in TGFα-induced SOX9 expression in IPF fibroblasts treated with ARRY (Figure 2C). Although basal levels of pAKT were decreased in the presence of TGFα compared to vehicle treatment, further inhibition of pAKT with PX-866 resulted in a significant reduction in *SOX9* levels in IPF fibroblasts treated with TGFα (Figure 2C). Next, we quantified the changes in SOX9 protein levels in IPF fibroblasts treated with TGFα in the presence and absence of ARRY and observed a significant reduction in TGFα-induced SOX9 protein in IPF fibroblasts (Figure 2D). Recent studies from our laboratory have shown that WT1 is upregulated in activated fibroblasts, and it coincides with the increase in profibrotic gene networks, including *Sox9*, during TGFα-induced pulmonary fibrosis (3, 4). To test whether WT1 is a positive regulator of SOX9, we knocked down WT1 in distal lung fibroblasts isolated from IPF lungs. Compared with control siRNA, the knockdown of WT1 was sufficient to attenuate *SOX9* expression in IPF fibroblasts (Figure 2E and Supplemental Figure 3D). We next assessed the effect of adenovirus-mediated overexpression of WT1 on *SOX9* levels in normal HLF. Overexpressing WT1 in fibroblasts significantly increased

both transcript and protein levels of SOX9 (Figure 2F and Supplemental Figures 3E-3H). To test whether the TGFα-WT1 axis is involved in upregulation of *Sox9*, we treated cultured lung fibroblasts from *WT1*$^{f/f}$ (Control) and *Col1α2*^{CreER}*WT1*$^{f/f}$ mice with 4-hydroxy tamoxifen in the presence and absence of TGFα. With the loss of WT1, we observed a significant decrease in *Sox9* levels in fibroblasts treated with TGFα (Supplemental Figures 3I-J). To determine whether WT1 is a transcription factor that directly binds to the *SOX9* promoter, we performed a computational analysis of the promoter region of human *SOX9* and found the presence of a WT1 binding site (Figure 2G). We next generated *SOX9* promoter-driven luciferase reporter clones that either contained a WT1-binding site (*SOX9*^{WT1}) or did not (*SOX9*$^{\Delta WT1}$) to validate the role of the TGFα/WT1 axis in inducing SOX9 expression. We transfected HEK293 cells with either an empty plasmid containing the luciferase reporter gene or a *SOX9* promoter-driven luciferase reporter gene (*SOX9*^{WT1} or *SOX9*$^{\Delta WT1}$) and treated cells with TGFα to observe changes in the luciferase activity (Figure 2H). Compared with cells treated with the empty reporter plasmid, cells transfected with *SOX9* promoter-driven luciferase reporter clones showed increased luciferase activity (Figure 2H). This increase in *SOX9* promoter-driven luciferase activity was further elevated in cells treated with TGFα compared to media-treated cells. In the presence of TGFα, the deletion of the *WT1* binding element in the *SOX9* promoter (*SOX9*$^{\Delta WT1}$) markedly decreased *SOX9* promoter activity compared to cells transfected with the *SOX9*^{WT1} promoter plasmid (Figure 2H). We next overexpressed WT1 in HEK293 cells co-transfected with either the *SOX9*^{WT1} or *SOX9*$^{\Delta WT1}$ luciferase reporter plasmid. We observed a significant increase in luciferase activity in cells co-transfected with the *WT1* overexpression plasmid compared to cells transfected with the

control plasmid (Figure 2I). Importantly, the observed increase in the *SOX9* promoter activity with WT1 overexpression was significantly attenuated with the deletion of the *WT1* binding site in the *SOX9*-luciferase promoter. Together, our new findings suggest that WT1 functions as a positive regulator of SOX9 by directly binding to the *SOX9* promoter in the distal lung fibroblasts during TGFα-induced fibroblast activation and pulmonary fibrosis.

SOX9 is a positive regulator of fibrosis-associated gene networks. To gain additional insights into the role of SOX9 in fibroblast activation, we assessed differentially expressed gene transcripts with the loss of SOX9. Specifically, we performed next-generation sequencing of total RNA from IPF fibroblasts treated with SOX9-specific siRNA in comparison with those treated with control siRNA for 72 hours. As shown in the heat map, SOX9 knockdown resulted in 572 upregulated and 763 downregulated genes (≥1.5-fold change; $p \leq 0.05$) (Supplemental Figure 4A). To identify SOX9-driven profibrotic gene transcripts in IPF, we next compared differentially expressed genes in SOX9-deficient IPF fibroblasts with up- or downregulated gene transcripts in IPF lungs (GSE53845) (11). Our comparative analysis identified multiple differentially expressed gene transcripts that were either upregulated (74 genes) or downregulated (71 genes) by SOX9 in IPF, as shown in the Venn diagram (Figure 3A). The list of genes is shown in Supplemental Table S1. Functional enrichment analysis of negatively correlated gene sets, using the ToppFun application of the ToppGene Suite, identified several important fibroblast-specific biological processes; these genes were found to be associated with ECM production and organization, migration, and mesenchymal cell differentiation (Figure 3B and Supplemental Figure 4A). To validate the SOX9-driven profibrotic genes in IPF

fibroblasts, we quantified transcripts using real-time PCR for ECM genes (*COL1*A*1*, *COL3*A*1*, *COL14*A*1*, *COL15*A*1*, and *ACTA2*) and proteoglycan-associated genes (*ASPN*, *OGN*, *POSTN*, and *CTGF*) (Figure 3C). Additionally, the loss of SOX9 resulted in a significant decrease in gene transcripts associated with mesenchymal cell differentiation and development (*SFRP2*, *OSR2*, *TGFB2*, and *LOXL2*), as well as migration (*FGF1*, *THBS4*, *MMP10*, and *DPYSL3*) (Figure 3D and 3E). We next confirmed the knockdown effects of SOX9 on ECM protein levels through western blot analysis of IPF fibroblasts treated with SOX9-specific siRNA compared to those treated with control siRNA for 72 hours. Consistent with changes in gene transcripts, we observed a significant decrease in ECM-associated protein levels with the loss of SOX9 in IPF fibroblasts (COL1α1, ACTA2, POSTN, and LOXL2) (Figure 3F and Supplemental Figure 4B).

SOX9 is a positive regulator of fibroblast migration, transformation, and survival. Bioinformatics analysis of Sox9 knockdown transcriptome in IPF fibroblasts suggested that SOX9 may function as a positive regulator of fibroblast migration, fibroblast-to-myofibroblast transformation (FMT), and survival in IPF. To test whether SOX9 induces the migration of fibroblasts, we performed real-time scratch assays using IPF fibroblasts treated with control or SOX9-specific siRNA for 48 hours. We then measured the kinetics of migration. With SOX9 knocked down, IPF fibroblasts showed a significant reduction in their ability to migrate (Figure 4A and Supplemental Figure 5A). Functional enrichment analyses of SOX9-regulated genes involved in migration identified dihydropyrimidinase-like-3 (DPYSL3) as a potential downstream target of SOX9 in mediating fibroblast migration in IPF. Therefore, we assessed whether DPYSL3 is upregulated in IPF and observed a significant increase in *DPYSL3* gene transcripts in the total lung transcripts of

IPF compared with that in normal lungs (Figure 4B). SOX9 knockdown significantly reduced *DPYSL3* gene transcript levels in IPF fibroblasts (Figure 4C). These results suggest that SOX9 is a positive regulator of fibroblast migration and induces migration-associated genes, including *DPYSL3*, in IPF fibroblasts. As we observed altered ACTA2 expression with the loss or overexpression of SOX9, we also assessed whether SOX9 induces FMT. To evaluate the role of SOX9 in FMT, we used a cell-fate mapping strategy based on the lineage-specific expression of ACTA2 in lung-resident fibroblasts isolated from *Acta2* reporter mice ($\alpha SMA^{CreERT}ROSA^{mTmG}$ mice). In this model, the distal lung fibroblasts of the *Acta2* reporter mice were infected with either control or SOX9-overexpressing lentiviruses in the presence of 4-hydroxy-tamoxifen for 72 hours. Upon Lenti-mediated overexpression of SOX9, we observed a significant increase in the number of myofibroblasts (green cells) suggesting that SOX9 induces FMT (Figure 4D and 4E). To determine whether SOX9 contributes to the contractile function of myofibroblasts, we treated IPF fibroblasts with control or SOX9-specific siRNA for 72 hours and seeded them into rat tail collagen gels. We observed a significant reduction in the contractility of collagen gels with the loss of SOX9 in IPF fibroblasts (Figure 4F and Supplemental Figure 4B). To determine whether SOX9 induces resistance to Fas-induced apoptosis in fibroblasts, we performed a TUNEL assay in IPF fibroblasts treated with either control or SOX9-specific siRNA for 72 hours. SOX9 knockdown in IPF fibroblasts resulted in a significant increase in TUNEL-positive fibroblasts with the treatment of anti-Fas antibody compared to control antibody (Figure 4G & 4H). Therefore, we measured the changes in anti-apoptotic gene transcripts and observed a significant decrease in the transcripts of anti-apoptotic genes, including *BCL-XL* and *BCL-2L2*, in

SOX9-deficient fibroblasts (Figure 4I). These new findings suggest that SOX9 induces the anti-apoptotic pathway genes responsible for enhanced survival of IPF fibroblasts. Taken together, our in vitro results establish that SOX9 upregulation in distal lung fibroblasts augments fibroblast activation including migration, FMT, survival, and ECM production.

Fibroblast-specific deletion of Sox9 attenuates TGFα-induced pulmonary fibrosis in mice. To investigate the in vivo effects of fibroblast-specific Sox9 deletion in the pathogenesis of pulmonary fibrosis, we crossed *TGFα^{OE}* mice with Sox9 floxed mice and *Col1α2^{CreER}* mice. Through breeding, we successfully generated three groups of mice including control (*CCSP;Sox9$^{f/f}$*) mice and *TGFα^{OE}* mice containing fibroblast-specific Cre and the floxed Sox9 alleles (*TGFα^{OE}Sox9$^{f/f}$* mice or *TGFα^{OE}Col1α2^{CreER}Sox9$^{f/f}$* mice). To identify whether fibroblast-specific Sox9 deletion influences the susceptibility to fibrosis, all groups of mice were treated with Dox for six weeks and simultaneously treated with tamoxifen to delete Sox9 in fibroblasts (Figure 5A). To assess whether TGFα expression is similar in both the *TGFα^{OE}Sox9$^{f/f}$* and *TGFα^{OE}Col1α2^{CreER}Sox9$^{f/f}$* groups, we quantified its transcripts and found the expression to be similar in both groups (Figure 5B). To determine the efficiency of *Col1α2^{CreER}*-driven Sox9 deletion, we measured transcripts of *Sox9* in all three groups of mice. As expected, we observed an increase in the *Sox9* transcript levels in Dox-treated *TGFα^{OE}Sox9$^{f/f}$* mice compared with *Sox9$^{f/f}$* mice. Approximately 50% *Sox9* transcripts that were elevated in the lungs of *TGFα^{OE}Sox9$^{f/f}$* mice were attenuated in *TGFα^{OE}Col1α2^{CreER}Sox9$^{f/f}$* mice (Figure 5B). Importantly, the reduction in *Sox9* transcripts was associated with a significant decrease in collagen staining and in the total lung hydroxyproline levels in *TGFα^{OE}Col1α2^{CreER}Sox9$^{f/f}$* mice compared to *TGFα^{OE}Sox9$^{f/f}$*

mice (Figure 5C and 5D). Consistent with changes in lung collagen levels, we observed a significant improvement in lung function parameters including resistance, compliance, and elastance in *TGFα^{OE}Col1α2^{CreER}Sox9$^{f/f}$* mice compared to *TGFα^{OE}Sox9$^{f/f}$* mice (Figure 5E, 5F, and 5G). Furthermore, transcripts of several ECM-associated genes, including *Col1a1*, *Col3a1*, *Ctgf*, and *Loxl2*, that were elevated in *TGFα^{OE}Sox9$^{f/f}$* mice compared to control mice were significantly attenuated in *TGFα^{OE}Sox9$^{f/f}$* mice (Figure 5H). To identify Sox9-positive myofibroblast accumulation, lung sections were immunostained with antibodies against ACTA2 and SOX9. Accumulation of SOX9-positive myofibroblasts was attenuated in fibrotic lung lesions of Dox-treated *TGFα^{OE}Col1α2^{CreER}Sox9$^{f/f}$* mice compared to *TGFα^{OE}Sox9$^{f/f}$* mice (Figure 5I and 5J). Thus, our findings provide direct in vivo evidence that Sox9 expression in fibroblasts plays a pathogenic role during TGFα-induced pulmonary fibrosis.

Sox9 is required for the maintenance of fibroblast activation. To examine whether Sox9 is required for the maintenance of fibroblast activation, we isolated activated fibroblasts from fibrotic lung lesions of Dox-treated *TGFα^{OE}Sox9$^{f/f}$* mice for 6 weeks. As shown in Figure 6A, we selectively deleted Sox9 in activated fibroblasts by treating them with Cre-expressing adenovirus and assessed the changes in ECM gene expression, contractility, and apoptosis. Western blot analysis indicated a significant loss in SOX9 protein levels in fibroblasts infected with Cre adenovirus compared to those in fibroblasts treated with control adenovirus for 72 hours (Figure 6B). *Sox9* knockdown resulted in a significant decrease in ECM-associated genes including *Acta2*, *Col1α1*, and *Loxl2* compared to those in control fibroblasts (Figure 6C). To measure the changes in the contractile function, we seeded fibroblasts infected with Cre or control adenovirus in collagen gels

and observed a significant reduction in the contraction of collagen gels (Figure 6D). In addition, the TUNEL assays further confirmed that the knockdown of *Sox9* increased the number of TUNEL-positive cells in the presence of anti-Fas antibodies (Figure 6E and 6F). Thus, our findings provide complementary evidence that Sox9 is required for the maintenance of the profibrotic functions of activated fibroblasts.

Overexpression of Sox9 in myofibroblasts augments bleomycin-induced pulmonary fibrosis. To further substantiate our findings, we investigated whether Sox9 overexpression augments bleomycin-induced pulmonary fibrosis. We bred $\alpha SMA^{CreERT2}$ mice with *CAG-Sox9* mice to generate myofibroblast-specific conditional Sox9 overexpressing mice ($\alpha SMA^{CreERT2}Sox9^{OE}$) and control mice ($\alpha SMA^{CreERT2}$). As shown in Schemata in Figure 7A, the mice in both groups were treated with two tamoxifen injections per week for two weeks prior to intratracheal bleomycin instillation, and an additional injection was administered one week after bleomycin treatment. We monitored the changes in body weights post bleomycin instillation; the mice were sacrificed at the end of week two post bleomycin instillation. Notably, we observed a significant decline in the bodyweight of bleomycin-treated $Sox9^{OE}$ mice compared to bleomycin-treated control mice (Figure 7B). Levels of SOX9 protein were increased in the total lung lysates of bleomycin-treated $Sox9^{OE}$ mice compared with that in bleomycin-treated control mice (Figure 7C). To assess Sox9 upregulation in myofibroblasts, we co-immunostained lung sections with antibodies against SOX9 and ACTA2. We observed selective SOX9 overexpression in myofibroblasts of bleomycin-treated $Sox9^{OE}$ mice compared to that in myofibroblasts of bleomycin-treated control mice (Figure 7D). When we quantified the SOX9-positive myofibroblasts in total myofibroblasts that accumulated in the fibrotic

lesions, we observed that a large percentage (~80%) of myofibroblasts overexpressed SOX9 in bleomycin-treated *Sox9*^{OE} mice compared to bleomycin-treated control mice (Figure 7D and 7E). Masson's trichrome staining exhibited a substantial increase in collagen staining in the lung sections of bleomycin-treated *Sox9*^{OE} mice compared with that in bleomycin-treated control mice (Figure 7F). We quantified the fibrotic area in the whole lung section from all mice and observed a significant increase in the percentage of the fibrotic area, normalized to the total scanned area in the lung sections of bleomycin-treated *Sox9*^{OE} mice compared with that in bleomycin-treated control mice (Figure 7F). We measured the changes in lung resistance as a measure of lung function and observed significant deterioration of lung function of bleomycin-treated *Sox9*^{OE} mice compared with that of bleomycin-treated control mice (Figure 7G). To assess myofibroblast accumulation, lung sections were immunostained with antibodies against ACTA2. ACTA2 staining increased in the lung parenchyma of bleomycin-treated *Sox9*^{OE} mice compared with that in bleomycin-treated control mice (Figure 8A). We next quantified the ACTA2 staining area that was significantly increased in bleomycin-treated *Sox9*^{OE} mice compared to bleomycin-treated control mice (Figure 8B). We also quantified the changes in ECM-associated genes in the total lung transcripts of bleomycin-treated *Sox9*^{OE} and control mice. Consistent with changes in collagen levels, we observed a significant increase in transcripts of ECM-associated genes including *Acta2*, *Col1a1*, *Col3a1*, *Col5a1*, *Fn1*, *Postn*, *Loxl2*, *Osr2*, and *Mmp7* in bleomycin-treated *Sox9*^{OE} mice compared to bleomycin-treated control mice (Figure 8C). We quantified the transcripts of several profibrotic growth factors including *TGFb1*, *Il6*, *Il13*, and *Il17* and found that their levels were elevated in the lungs of bleomycin-treated *Sox9*^{OE} mice compared to those in the

lungs of bleomycin-treated control mice (Figure 8D). Consistent with changes in transcripts levels, we observed a marked increase in the levels of ACTA2, LOXL2, FN1, and COL1α1 in the lung lysates of bleomycin-treated *Sox9*^{OE} mice compared with that in bleomycin-treated control mice (Figure 8E and 8F). Taken together, our findings provide complementary in vivo evidence that Sox9 upregulation in fibroblasts is responsible for fibroblast activation and accumulation and plays an integral role in the pathogenesis of pulmonary fibrosis.

Discussion

In this study, we show that SOX9 is aberrantly activated in fibroblasts of distal lung fibrotic lesions in both human IPF and a mouse model of TGFα-induced pulmonary fibrosis. For the first time, we demonstrated that the TGFα/WT1 axis is involved in SOX9 upregulation in pulmonary fibrosis. Using in vitro fibroblast activation assays, we showed that SOX9 upregulation causes excessive migration, FMT, ECM gene expression, and resistance to apoptosis in IPF fibroblasts. To investigate the in vivo relevance of Sox9 upregulation in fibroblasts, we performed fibroblast or myofibroblast-specific deletion or overexpression of Sox9. Both loss-of-function and gain-of-function studies suggest a pathologic role for Sox9 in fibroblast activation and pulmonary fibrosis in two alternative mouse models of pulmonary fibrosis.

Recent advances in quantitative transcriptomics using next-generation RNA-seq and single-cell genomics have helped us identify the loss of lineage specificity in transcription factors between proximal and distal lung cells in IPF pathogenesis (13, 14). Particularly, fibroblast dysregulation is important in IPF due to its direct involvement in excessive collagen deposition and the progressive expansion of fibrotic lung lesions in

IPF (15, 16). Here, we report a pathogenic fibroblast that overexpresses SOX9, a key transcription factor that is thought to be epithelial progenitor cell-specific during lung development or in adult lungs. We show that SOX9-positive fibroblasts and myofibroblasts accumulate in the distal areas of IPF lungs, including fibroblastic foci and subpleural fibrotic lesions. Consistent with the findings in IPF lungs, we found that these SOX9-expressing fibroblasts accumulate in the distal fibrotic lung lesions during TGFα-induced pulmonary fibrosis. However, in normal lung sections, we observed limited or no expression of SOX9 in fibroblasts or myofibroblasts. Mechanistically, using the *SOX9* promoter-driven luciferase assays, we showed that the TGFα/WT1 axis is responsible for the upregulation of Sox9 in fibroblasts, which results in an increase in the migration, FMT, survival, and ECM gene expression. We demonstrated that both bleomycin and TGFα-induced pulmonary fibrosis depend on SOX9-driven increases in profibrotic gene networks and fibroblast activation. Together, these studies identified SOX9 as a positive regulator of fibroblast activation in the pathogenesis of pulmonary fibrosis, illustrating the potential utility of targeting SOX9 or SOX9 downstream targets in the treatment of IPF and other fibrotic diseases.

The Sox family of transcription factors in airway epithelial cells, including SOX2 and SOX9, have been extensively studied in the context of proximal-distal patterning of the lung (17, 18). Specifically, Sox9 plays a critical role in lung branching morphogenesis and is highly expressed during the pseudo glandular stage in epithelial progenitor cells. Later, its expression is downregulated with the onset of alveolarization, and limited or no expression of SOX9 is observed in either epithelial cells or mesenchymal cells of adult distal lungs (6, 9). Our novel findings demonstrate that SOX9 is upregulated in the distal

lung fibroblasts of IPF. Importantly, our findings showed that multiple profibrotic growth factors including *BMP2*, *CTGF*, and *TGFα* can upregulate *SOX9*. Previous studies identified the role of BMPs and FGFs in upregulating SOX9 in epithelial progenitor cells during lung development, whereas the role of TGFα remained unclear (19, 20). During TGFα-induced pulmonary fibrosis, WT1-positive fibroblasts have been shown to accumulate in distal fibrotic lesions, similar to SOX9-positive fibroblasts (3, 4). Recent studies from our lab and others showed that WT1 upregulation in fibroblasts is involved in fibroblast activation and the pathogenesis of pulmonary fibrosis (3, 4, 21). Here, we demonstrate that the loss of WT1 is sufficient to attenuate TGFα-induced SOX9 expression in fibroblasts. Additionally, we performed bioinformatics analysis on the *SOX9* promoter region and identified a potential binding site for WT1. Using luciferase reporter assays, we demonstrated that WT1 indeed binds to the *SOX9* promoter and functions as a positive regulator of SOX9 expression in fibroblasts. However, it is important to note that multiple growth factors can upregulate SOX9 in fibroblasts and epithelial cells(18, 22). Therefore, we cannot rule out the possibility that other mechanisms are involved in SOX9-induced pulmonary fibrosis. While we implicated a role for SOX9 in fibroblast activation and pulmonary fibrosis, further work is necessary to determine the impact of SOX9 in other lung cells including epithelial cells during the initiation, maintenance, and resolution of pulmonary fibrosis.

IPF is a severe fibrotic disease in which fibroblasts are transformed into an activated state, called myofibroblasts, and deposit excess ECM in response to chronic injury; this process ultimately leads to the formation of scar tissue (23-25). Activated fibroblasts are highly proliferative, secrete excessive ECM, are invasive and migrative,

and are resistant to apoptosis (26). Myofibroblasts are the main culprits involved in the progression of fibrosis. Lineage-tracing studies on the origins of myofibroblasts have shown that tissue-resident fibroblasts, including WT1-positive fibroblasts, are a source of myofibroblasts (4, 27). However, SOX9-driven gene networks in fibroblasts that cause the pathological features observed in IPF are poorly defined. Therefore, we performed transcriptional profiling of SOX9 knockdown in IPF fibroblasts and identified SOX9-driven gene networks and biological processes that are dysregulated in IPF fibroblasts. Particularly, enrichment analysis of SOX9-knockdown downregulated genes with IPF gene datasets indicated the role of SOX9 in ECM production and organization, migration, FMT, and the survival of the fibroblasts. In support of its profibrotic actions, SOX9 knockdown in IPF fibroblasts resulted in reduced migration and downregulation of several ECM-related genes. Similar observations were made in mouse fibrotic fibroblasts, where SOX9 affected ECM gene expression. Notably, SOX9 regulates the expression of LOXL2 an important ECM organizing enzyme that plays a crucial role in matrix remodeling and fibrogenesis (28). Previous studies have demonstrated that LOXL2 is a marker for IPF progression, and its inhibition resulted in the slower progression of the disease (28-30). SOX9 is well recognized as a transcriptional regulator for various ECM-related genes based on the studies related to chondrogenesis and cancer cell types (31, 32). For the first time, we have highlighted the role of SOX9 in FMT and migration of distal fibroblasts by regulating the expression of DPYSL3 and mitogens such as FGF1, whose levels are highly increased in IPF fibroblasts (33). Using fibroblasts with gain or loss of SOX9 expression, we showed that SOX9 functions as a positive regulator of ACTA2 expression and regulates the contractility of collagen gels. Likewise, in the FMT assay, SOX9

overexpression promoted FMT. These findings suggest that the profibrotic activity of SOX9 may, at least in part, be attributed to the induction of ACTA2. However, the mechanisms underlying SOX9-driven ACTA2 expression and contractility remain to be investigated in fibroblasts. Previous studies have identified increased expression of the BCL family of anti-apoptotic genes, including BCL-2, BCL-XL, and BCL2L2 in IPF fibroblasts (34). These genes contribute to resistance against Fas-mediated apoptotic clearance in fibroblasts and myofibroblasts (35-38). Therefore, we analyzed the role of SOX9 in fibroblast survival; our novel findings suggest that SOX9 promotes the survival of fibroblasts by inducing the expression of anti-apoptotic genes (*BCL-XL* and *BCL-2L2*). Strikingly, the resistance against Fas-induced apoptosis observed in IPF fibroblasts was reversed with the loss of SOX9. Thus, our results indicate that enhanced expression of SOX9 in IPF and TGFα-fibroblasts allows the cells to resist Fas-mediated apoptosis. Consequently, survival and accumulation of activated fibroblasts likely occurs in IPF during TGFα-induced pulmonary fibrosis. Overall, our new findings indicate that SOX9 is a positive regulator of fibroblast activation by inducing migration, FMT, survival, and production of ECM in pulmonary fibrosis.

Previous studies have identified the important roles of WT1 in both TGFα- and bleomycin-induced pulmonary fibrosis, whereas the role of SOX9 has remained unclear. To determine whether SOX9 alters TGFα and bleomycin-induced pulmonary fibrosis, we generated conditional fibroblast- or myofibroblast-specific *Sox9* knockout or overexpressing mice. We employed a commonly used *Col1α2^{CreERT}* fibroblast-specific Cre driver to delete Sox9 in fibroblasts (39, 40). Strikingly, the increase in TGFα-induced fibroblast activation and pulmonary fibrosis in *TGFα^{OE}* mice was attenuated with the loss

of SOX9, which supports the profibrotic function of SOX9. Consistent with our findings, few studies have demonstrated that either ECM proteins or loss of SOX9 affects the cytoskeletal organization and interferes with cell morphology (6, 41, 42). In addition, we documented the important role of SOX9 in fibroblast activation using an alternative mouse model of bleomycin-induced pulmonary fibrosis. In IPF, myofibroblasts are the ultimate differentiated cells that deposit excess ECM components and destroy the architecture of the lung; therefore, we overexpressed SOX9 in myofibroblasts (4, 43). Our novel findings demonstrated that SOX9 overexpression leads to a decrease in body weight compared to control mice, and a decline in lung function. Additionally, the histology of the lung sections indicated an increase in collagen deposition with an increase in SOX9 levels; a parallel increase in the ECM-related proteins accompanied the escalation of fibrosis. Interestingly, SOX9 overexpression in myofibroblasts led to an increase in the profibrotic factors such as TGFβ1 and inflammatory cytokines (*Il6*, *Il-13*, and *Il-17*) resulting in tissue remodeling. TGFβ1 is considered a master regulator of fibrosis and is secreted by injured epithelial and inflammatory cells and partly by (myo)fibroblasts in patients with IPF (44-46). Numerous studies have shown a positive association between TGFβ1 and Sox9 expression or stabilization (47, 48). Our studies suggest that SOX9 regulates the expression of these profibrotic factors in the myofibroblasts either directly or indirectly and likely forms a positive feed-forward loop resulting in progressive fibrosis. A recent study on IPF fibroblasts confirmed that fibroblasts also secrete Il6 and activate STAT3/SMAD3 signaling, which could trigger additional fibrotic events (49). However, the mechanisms by which SOX9 regulates these factors have yet to be determined. Additionally, the role of SOX9 in the epithelial progenitor population in IPF must be determined to

therapeutically target this molecule. The pathogenic role of SOX9 in inducing fibrosis was confirmed in other organs such as the liver, kidney, and heart (32, 50-52). In the heart, SOX9 is predominantly expressed by cardiomyocytes and cardiac fibroblasts after myocardial infarction injury in mice. Importantly, fibroblast specific SOX9 deletion was sufficient to attenuate migration, proliferation, and contractility of cardiac fibroblasts and improve cardiac function (52). Likewise, we found that the loss of SOX9 attenuates migration and contractility but not the proliferation in lung fibroblasts (unpublished data), further suggesting the importance of SOX9-positive fibroblasts as a part of the pro-fibrotic response in multiple organs. In the liver, the deletion of SOX9 in vivo has been shown to attenuate CCL4-induced liver fibrosis (50). Importantly, elevated levels of SOX9 or SOX9 regulated matrix proteins have been shown to correlate with the progression towards cirrhosis in these patients (32, 50). Our genomic studies have identified several downstream targets of SOX9 that may have an important role in predicting the disease progression or mediating the pathology in lung fibrosis. To substantiate our findings, we further evaluated upregulation of SOX9 and its targets in an independent cohort data of 160 IPF patients and 108 controls (GSE47460) as described previously (12). Consistent with our findings, we observed a significant increase in *SOX9* transcripts levels in the lungs of IPF compared to healthy controls (Supplementary Figure 6A). Several of the SOX9-dependent ECM genes including *COL15A1, COL14A1, SFRP2, OSR2, ASPN, COL3A1, ACTA2, OGN, and LOXL2* were found upregulated and positively correlated with Sox9 levels (Supplemental Figure 6B). Further, the levels of Sox9 and its target genes were negatively correlated with the forced vital capacity (FVC) and the diffusing capacity of the lung for carbon monoxide (DLCO) (Supplemental Figure 6C). However,

further studies are needed to identify the potential associations between cell-specific SOX9 targets and the decline in lung function which could potentially assist in the stratification of patients with IPF. Nevertheless, the pathological role of SOX9 in activating fibroblasts and orchestrating fibrosis in multiple organs might open up opportunities for drug discovery, precision targets, and therapeutic interventions (32, 50-52).

Taken together, our results established multiple roles for SOX9 in fibroblasts that promote fibrosis. We demonstrated that SOX9 is a positive regulator of migration, ECM production, and organization, which promotes FMT processes and allows fibroblasts to resist apoptosis. Importantly, using two complementary mouse models of pulmonary fibrosis, we demonstrated that SOX9 upregulation in the distal lung fibroblasts causes severe fibrotic lung disease. These new findings highlight how excessive SOX9 activity in fibroblasts can contribute to the progressive expansion of fibrotic lesions in the lung and that targeting the aberrant activation of SOX9 could be a therapeutic strategy to mitigate ongoing pulmonary fibrosis in IPF.

Methods

Mouse models of TGFα^{OE} and bleomycin-induced pulmonary fibrosis. Floxed *Sox9, WT1* mice, and *Col1α2^{CreER}* transgenic mice were characterized previously (53-56). The *WT1* flox mice were a kind gift from Dr. Christoph Englert from Molecular Genectic lab, Leibniz Institute, Jena, Germany. To generate fibroblast-specific Sox9-deficient mice, *Sox9$^{f/f}$* mice were bred with heterozygous *Col1α2^{CreER}* mice to generate *Col1α2^{CreER}Sox9$^{f/f}$* mice. The generation of Dox-inducible and Clara-cell-specific TGFα overexpression mice was previously described and is herein termed as *TGFα^{OE}* mice (57). We bred *TGFα^{OE}* mice with *Col1α2^{CreER}Sox9$^{f/f}$* mice to generate *CCSP-rtTASox9$^{f/f}$* (control mice), *TGFα^{OE}Sox9$^{f/f}$*,

and *TGFα^{OE}Col1α2^{CreER}Sox9$^{f/f}$* mice. All the mice used were aged between 11 and 16 weeks in our animal studies. Mice were fed a diet containing doxycycline (62.5 mg/kg) to induce TGFα overexpression, which causes the mice to develop a significant amount of fibrotic lung disease by 4 to 6 weeks. To induce cell-specific CreER-driven recombination, mice were administered 100 μl of tamoxifen (100 mg/kg) twice weekly via i.p. injection, as described previously (4). The generation of SOX9 overexpressing (*Sox9^{OE}*) and *αSMA^{CreERT2}* mice has been described previously (58, 59). We bred *Sox9^{OE}* mice with *αSMA^{CreERT2}* mice to generate *αSMA^{CreERT2}Sox9^{OE}* and *αSMA^{CreERT2}* (control) mice. As mentioned previously, tamoxifen was administered via the i.p. route twice in one week before two weeks of intratracheal bleomycin (3 U/kg) instillation, and for a week after bleomycin injury; the mice were sacrificed after two weeks of bleomycin instillation. To generate *Col1α2^{CreER}WT1$^{f/f}$* mice, we bred *Col1α2^{CreER}* mice with *WT1$^{f/f}$* and generated lung fibroblasts by culturing lungs in vitro as detailed in our published studies (60).

Lung function parameters were measured using Flexi Vent (SCIREQ Inc., Montreal, Canada). The mice were sacrificed, and the lungs were collected for histology, RNA, protein, and hydroxyproline. Hydroxyproline from the right lung was measured using colorimetry, as described previously (61).

Human samples. IPF and nonfibrotic lung specimens were obtained from the Interstitial Lung Disease Biorepository at the University of Michigan Medical School and provided by Dr. Steven Huang in the Division of Pulmonary and Critical Care Medicine. IPF was diagnosed according to the guidelines of the American Thoracic Society (62) and confirmed in a multidisciplinary fashion through weekly consensus conference. All tissues were acquired using research protocols that were approved by the Michigan Medicine

Institutional Review Board (HUM00105694) and all patients provided informed consent. Lung tissue was obtained from explanted lungs after lung transplantation.

RNA isolation and RT-PCR. The RNA from tissues and primary cells was isolated using an RNeasy kit (Qiagen Sciences, Valencia, CA) as per the instructions described in a previous study (63). cDNA was synthesized, and real-time PCR was performed using the SYBR select master mix (Bio-Rad, Hercules, CA) and CFX384 Touch Real-Time PCR instrument (Bio-Rad, Hercules, CA) and analyzed using CFX maestro software version 4.0. The target gene transcripts from mice and humans were normalized to either hypoxanthine-guanine phosphor ribosyl transferase (Hprt) or human β-actin, respectively. The primer lists for both human and mouse genes are provided in Supplemental Table S2 and S3, respectively.

Histology and immunohistochemistry. Histological procedures were performed as mentioned previously (4). Briefly, paraffin-embedded tissues were cut into 5 μm sections and deparaffinized for Masson's trichrome staining. For immunohistochemistry, lung sections were deparaffinized followed by citric acid antigen retrieval (pH 6.0) and methanol treatment, blocked in 5% donkey serum, incubated with the primary antibody overnight, followed by incubation with species-specific secondary peroxidase antibodies, and then stained with DAB (3,3'-diaminobenzidine). Bright-field images were captured through Keyence BZ series microscopy and quantified using a BZ-X-analyzer.

Immunofluorescence and confocal imaging. Isolated lungs or tissues were fixed overnight with 4% paraformaldehyde at 4°C, followed by PBS washes. Thereafter, the tissues were cryoprotected with 30% sucrose and embedded in OCT (Tissue-Tek). The procedure for immunofluorescence was performed as previously described (10). Briefly, we performed

citric acid antigen retrieval (pH 6.0) and blocked the sections using 5% donkey serum, followed by overnight incubation of the samples with specific primary antibodies. The next day, samples were incubated with species-specific Donkey Alexa Fluor-488, 568, or 647 antibodies, and DAPI was applied for nuclear staining. Primary cells were fixed with 4% paraformaldehyde for 10 minutes. Images were captured using a Nikon AIR-A1 confocal microscope and analyzed using the Imaris or Elements software. Details of antibodies used and their dilutions are provided in Supplemental Table S4.

TUNEL staining. Depending on the experiment, human or mouse fibrotic fibroblasts were treated with either siRNA or transduced with adenovirus, respectively, for 48 hours. Cells were then treated with species-specific anti-Fas antibody (250 ng/ml, 05-201clone CH11, or EMD Millipore) for 24 hours. Nuclei were stained using DAPI, and DNA fragmentation of apoptotic cells was performed using the terminal deoxynucleotidyl Transferase Biotin-dUTP Nick End Labeling (TUNEL) method using an In Situ Cell Death Detection kit, TMR red (12156792910, Roche Diagnostics); staining was performed according to the manufacturer's instructions. The images were captured at 20× magnification using a confocal microscope and quantified using Elements software version 9.1.

Western blot. Western blotting analysis was performed as described previously (61) using cell lysis buffer (CST, Danvers, Massachusetts). Briefly, the lysates were electrophoresed and then transferred onto a nitrocellulose membrane. The membranes were blocked and incubated with primary antibodies overnight, which are listed with their dilutions in Supplemental Table S3. The western blots were visualized and quantified using phosphorimager software, Multi gage (Fujifilm, Valhalla, NY). The target proteins were normalized with GAPDH.

Primary fibroblast cultures and treatments. Adult human lung primary fibroblasts from normal tissue, patients with IPF, and mice were isolated using collagenase digestion, as described previously (4), and then cultured in DMEM (10% FBS) for human fibroblasts or IMDM media for mouse fibroblasts (5% FBS). The fibroblasts used in the experiments were between passages 1 and 4. Cells were treated with TGFα (100 ng/ml, 100-16A, Peprotech), BMP2 (200 ng/ml, 355-BM-010, R&D systems), IGF-1 (100 ng/ml, 291-G1-200 R&D systems), or CTGF (50 ng/ml, SRP4702, Sigma-Aldrich) overnight at low serum conditions. EGFR pathway inhibitors were used as described in our published studies with few modifications (64). Briefly, fibroblasts were pretreated with 0.1 μM ARRY (MEK inhibitor) or PX-866 (PI3K inhibitor) before 1 hour of stimulation with TGFα and the appropriate controls for different periods.

Transfection and Transduction of cells. For stealth siRNA-mediated studies, IPF fibroblasts were transfected with stealth siRNA control (Cat# 12935300) or target siRNA (Sox9: HSS110100, WT1: HSS111390, Invitrogen) for 72 hours using a lipofectamine 3000 transfection kit (Life Technologies, Carlsbad, California) as described previously (10). Similarly, using lipofectamine 3000, we transfected the plasmids for the luciferase assays. Depending on the experiment, human primary fibroblasts were treated with either a control virus, Sox9, or WT1 overexpressing viral particles. Cells were harvested after 48–72 hours for RNA or protein lysates, as mentioned previously (10). For Cre-mediated in vitro experiments, $TGF\alpha^{OE}$ and $Sox9^{f/f}$ mice were treated with Dox for 6 weeks, and the lung fibroblasts were cultured. The purified fibroblasts were transduced with either adeno-Cre-expressing adenovirus (AdCre) or control adeno (AdControl) viral particles to excise

lox-p sites that flanked the Sox9 gene for 48–72 hours. Then, we performed the gel contraction assay, TUNEL assay, and RNA isolation.

Migration assay. The IPF lung fibroblasts were transfected with either siControl or si*SOX9* siRNA for 48 hours, and a scratch was made in the wells. Migration was measured using the IncuCyte Zoom real-time imaging system for the next 48 hours. Images were acquired every three hours on 10× magnification, and the percentage of wound closure was measured using IncuCyte Zoom software 2018A.

Myofibroblast differentiation assay. Primary lung fibroblasts were isolated from $\alpha SMA^{CreERT2}$ and $Rosa^{mTmG}$ for the fibroblast-myofibroblast transformation assay, as described previously (59). Briefly, the fibroblasts were transduced with either control lenti or Sox9 overexpressing lentiviral particles and were treated with 4-hydroxy tamoxifen (2 μM, H7904, Millipore Sigma) for 72 hours. Then, cells were fixed with 4% paraformaldehyde, and the nucleus was stained with DAPI. Confocal images were obtained at 20× magnification and, for quantification of myofibroblasts, the MetaMorph imaging software was employed.

Collagen contraction assay. Depending on the experiment, after 48 hours of transfection or infection, fibroblasts were seeded into rat tail collagen (1 mg/ml, A10483-01, Gibco™) gel matrices, as described previously (65). Briefly, gels were detached from the wells, images were captured using a stereomicroscope, and the area of contraction was measured using ImageJ software.

Luciferase activity assay. Luciferase assay was performed as previously described (10). Briefly, HEK293 cells were transfected with either an empty promoter vector (S790005, Switchgear Genomics), human *Sox9* promoter ($SOX9^{WT1}$) (S705795, Switchgear

Genomics), or WT1 binding element deleted *Sox9* promoter (*SOX9*$^{\Delta WT1}$) with Renilla luciferase reporter for 48 hours. Then, the cells were adapted to low serum DMEM-F12 media followed by treatment with TGFα for 24 hours. *SOX9*$^{\Delta WT1}$ that lacked 16 bp (-327 to -311) from *SOX9*^{WT1} was generated using a site-directed mutagenesis kit (Cat# 200524, QuikChange II Site-Directed Mutagenesis Kit, Agilent technologies). In another experiment, the cells were co-transfected with either pLJM1 control or pLJM1 WT1 overexpressing lentivector with either an empty promoter, *SOX9* promoter, or *SOX9*$^{\Delta WT1}$ promoter for 48 hours and with TGFα for 24 hours with appropriate controls. The luciferase assay was performed using the LightSwitch Luciferase Assay kit, and Renilla luciferase activity was measured using a Glomax luminometer.

RNA-sequencing and bioinformatic analysis. RNA-sequencing was performed using RNA isolated from the Sox9 knockdown studies in IPF fibroblasts. The RNA-sequencing method and differential gene expression analysis have been described previously (4). The RNA-seq data were deposited in the GEO with the ID: GSE171532. Briefly, Sox9 siRNA-generated gene signatures were intersected with available IPF gene data sets (GSE53845) (11). Enrichment analysis was performed on downregulated genes with Sox9 siRNA and upregulated in IPF using ToppFun application of the ToppGene Suite (66).

Statistics. For multiple comparisons, one-way ANOVA with post hoc Tukey's test or two-way ANOVA with post hoc Sidak's test was performed. Student's unpaired *t*-test was used to determine statistical significance among two groups. P values of less than 0.05 were considered statistically significant. The averaged or mean data are presented with SEM

to indicate variability. For SOX9 and its target gene correlation studies, we used Pearson coefficient analysis.

Study approval. All animal experiments were performed under protocols approved by the Institutional Animal Care and Use Committee of Cincinnati Children's Hospital Research Foundation. Informed consent was obtained from the patients undergoing lung transplants and the study protocols were approved by the Michigan Medicine Institutional Review Board (HUM00105694).

Author contributions

PRG and SKM devised the project, were involved in designing and executing the experiments, analyzed data, and wrote the manuscript; PRG performed most of the experiments; DS performed immunostaining and cloning experiments; AGJ performed bioinformatic analysis and edited the manuscript; SHK provided human lung tissues and edited the manuscript; DS shared the $Sox9^{OE}$ mice and edited the manuscript; RKK performed RT-PCR and immunostaining experiments.

Acknowledgments

We are thankful for the veterinary services, research pathology, and confocal core at Cincinnati Children's Hospital Medical center for their help in performing this study. We like to thank Mihika Sharma for helping us with GEO submission of RNA-seq data.

Funding

This study was supported in part by the NIH 1R01 HL134801 (SKM), 1R01 HL157176 (SKM), 5R01HL144774 (DS) and the U.S. Department of Defense funds, W81XWH-17-1-0666 (SKM).

Conflict of interest

The authors have declared that no conflict of interest exists.

References

1. Wynn TA. Cellular and molecular mechanisms of fibrosis. *J Pathol.* 2008;214(2):199-210.
2. Henderson NC, Rieder F, and Wynn TA. Fibrosis: from mechanisms to medicines. *Nature.* 2020;587(7835):555-66.
3. Sontake V, Shanmukhappa SK, DiPasquale BA, Reddy GB, Medvedovic M, Hardie WD, et al. Fibrocytes Regulate Wilms Tumor 1-Positive Cell Accumulation in Severe Fibrotic Lung Disease. *J Immunol.* 2015;195(8):3978-91.
4. Sontake V, Kasam RK, Sinner D, Korfhagen TR, Reddy GB, White ES, et al. Wilms' tumor 1 drives fibroproliferation and myofibroblast transformation in severe fibrotic lung disease. *JCI Insight.* 2018;3(16).
5. Hogan BL, Barkauskas CE, Chapman HA, Epstein JA, Jain R, Hsia CC, et al. Repair and regeneration of the respiratory system: complexity, plasticity, and mechanisms of lung stem cell function. *Cell Stem Cell.* 2014;15(2):123-38.
6. Rockich BE, Hrycaj SM, Shih HP, Nagy MS, Ferguson MA, Kopp JL, et al. Sox9 plays multiple roles in the lung epithelium during branching morphogenesis. *Proc Natl Acad Sci U S A.* 2013;110(47):E4456-64.
7. Lefebvre V, and Dvir-Ginzberg M. SOX9 and the many facets of its regulation in the chondrocyte lineage. *Connect Tissue Res.* 2017;58(1):2-14.
8. Gonen N, and Lovell-Badge R. The regulation of Sox9 expression in the gonad. *Curr Top Dev Biol.* 2019;134:223-52.
9. Perl AK, Kist R, Shan Z, Scherer G, and Whitsett JA. Normal lung development and function after Sox9 inactivation in the respiratory epithelium. *Genesis.* 2005;41(1):23-32.
10. Kasam RK, Ghandikota S, Soundararajan D, Reddy GB, Huang SK, Jegga AG, et al. Inhibition of Aurora Kinase B attenuates fibroblast activation and pulmonary fibrosis. *EMBO Mol Med.* 2020;12(9):e12131.
11. DePianto DJ, Chandriani S, Abbas AR, Jia G, N'Diaye EN, Caplazi P, et al. Heterogeneous gene expression signatures correspond to distinct lung pathologies and biomarkers of disease severity in idiopathic pulmonary fibrosis. *Thorax.* 2015;70(1):48-56.
12. Wang Y, Yella J, Chen J, McCormack FX, Madala SK, and Jegga AG. Unsupervised gene expression analyses identify IPF-severity correlated signatures, associated genes and biomarkers. *BMC Pulm Med.* 2017;17(1):133.
13. Adams TS, Schupp JC, Poli S, Ayaub EA, Neumark N, Ahangari F, et al. Single-cell RNA-seq reveals ectopic and aberrant lung-resident cell populations in idiopathic pulmonary fibrosis. *Sci Adv.* 2020;6(28):eaba1983.
14. Reyfman PA, Walter JM, Joshi N, Anekalla KR, McQuattie-Pimentel AC, Chiu S, et al. Single-Cell Transcriptomic Analysis of Human Lung Provides Insights into the Pathobiology of Pulmonary Fibrosis. *Am J Respir Crit Care Med.* 2019;199(12):1517-36.
15. Ramos C, Montano M, Garcia-Alvarez J, Ruiz V, Uhal BD, Selman M, et al. Fibroblasts from idiopathic pulmonary fibrosis and normal lungs differ in growth

rate, apoptosis, and tissue inhibitor of metalloproteinases expression. *Am J Respir Cell Mol Biol.* 2001;24(5):591-8.
16. Hetzel M, Bachem M, Anders D, Trischler G, and Faehling M. Different effects of growth factors on proliferation and matrix production of normal and fibrotic human lung fibroblasts. *Lung.* 2005;183(4):225-37.
17. Que J, Luo X, Schwartz RJ, and Hogan BL. Multiple roles for Sox2 in the developing and adult mouse trachea. *Development.* 2009;136(11):1899-907.
18. Danopoulos S, Alonso I, Thornton ME, Grubbs BH, Bellusci S, Warburton D, et al. Human lung branching morphogenesis is orchestrated by the spatiotemporal distribution of ACTA2, SOX2, and SOX9. *Am J Physiol Lung Cell Mol Physiol.* 2018;314(1):L144-L9.
19. Abler LL, Mansour SL, and Sun X. Conditional gene inactivation reveals roles for Fgf10 and Fgfr2 in establishing a normal pattern of epithelial branching in the mouse lung. *Dev Dyn.* 2009;238(8):1999-2013.
20. Morrisey EE, and Hogan BL. Preparing for the first breath: genetic and cellular mechanisms in lung development. *Dev Cell.* 2010;18(1):8-23.
21. Karki S, Surolia R, Hock TD, Guroji P, Zolak JS, Duggal R, et al. Wilms' tumor 1 (Wt1) regulates pleural mesothelial cell plasticity and transition into myofibroblasts in idiopathic pulmonary fibrosis. *FASEB J.* 2014;28(3):1122-31.
22. Danopoulos S, Thornton ME, Grubbs BH, Frey MR, Warburton D, Bellusci S, et al. Discordant roles for FGF ligands in lung branching morphogenesis between human and mouse. *J Pathol.* 2019;247(2):254-65.
23. Lederer DJ, and Martinez FJ. Idiopathic Pulmonary Fibrosis. *N Engl J Med.* 2018;378(19):1811-23.
24. Martinez FJ, Collard HR, Pardo A, Raghu G, Richeldi L, Selman M, et al. Idiopathic pulmonary fibrosis. *Nat Rev Dis Primers.* 2017;3:17074.
25. Sontake V, Gajjala PR, Kasam RK, and Madala SK. New therapeutics based on emerging concepts in pulmonary fibrosis. *Expert Opin Ther Targets.* 2019;23(1):69-81.
26. Sgalla G, Iovene B, Calvello M, Ori M, Varone F, and Richeldi L. Idiopathic pulmonary fibrosis: pathogenesis and management. *Respir Res.* 2018;19(1):32.
27. Rock JR, Barkauskas CE, Cronce MJ, Xue Y, Harris JR, Liang J, et al. Multiple stromal populations contribute to pulmonary fibrosis without evidence for epithelial to mesenchymal transition. *Proc Natl Acad Sci U S A.* 2011;108(52):E1475-83.
28. Chien JW, Richards TJ, Gibson KF, Zhang Y, Lindell KO, Shao L, et al. Serum lysyl oxidase-like 2 levels and idiopathic pulmonary fibrosis disease progression. *Eur Respir J.* 2014;43(5):1430-8.
29. Chapman HA, Wei Y, Montas G, Leong D, Golden JA, Trinh BN, et al. Reversal of TGFbeta1-Driven Profibrotic State in Patients with Pulmonary Fibrosis. *N Engl J Med.* 2020;382(11):1068-70.
30. Wei Y, Dong W, Jackson J, Ho TC, Le Saux CJ, Brumwell A, et al. Blocking LOXL2 and TGFbeta1 signalling induces collagen I turnover in precision-cut lung slices derived from patients with idiopathic pulmonary fibrosis. *Thorax.* 2021.
31. Jo A, Denduluri S, Zhang B, Wang Z, Yin L, Yan Z, et al. The versatile functions of Sox9 in development, stem cells, and human diseases. *Genes Dis.* 2014;1(2):149-61.

32. Athwal VS, Pritchett J, Martin K, Llewellyn J, Scott J, Harvey E, et al. SOX9 regulated matrix proteins are increased in patients serum and correlate with severity of liver fibrosis. *Sci Rep.* 2018;8(1):17905.
33. MacKenzie B, Korfei M, Henneke I, Sibinska Z, Tian X, Hezel S, et al. Increased FGF1-FGFRc expression in idiopathic pulmonary fibrosis. *Respir Res.* 2015;16:83.
34. Safaeian L, Abed A, and Vaseghi G. The role of Bcl-2 family proteins in pulmonary fibrosis. *Eur J Pharmacol.* 2014;741:281-9.
35. Hernandez-Segura A, de Jong TV, Melov S, Guryev V, Campisi J, and Demaria M. Unmasking Transcriptional Heterogeneity in Senescent Cells. *Curr Biol.* 2017;27(17):2652-60 e4.
36. Redente EF, Chakraborty S, Sajuthi S, Black BP, Edelman BL, Seibold MA, et al. Loss of Fas signaling in fibroblasts impairs homeostatic fibrosis resolution and promotes persistent pulmonary fibrosis. *JCI Insight.* 2020;6(1).
37. Huang SK, Scruggs AM, Donaghy J, Horowitz JC, Zaslona Z, Przybranowski S, et al. Histone modifications are responsible for decreased Fas expression and apoptosis resistance in fibrotic lung fibroblasts. *Cell Death Dis.* 2013;4:e621.
38. Tanaka T, Yoshimi M, Maeyama T, Hagimoto N, Kuwano K, and Hara N. Resistance to Fas-mediated apoptosis in human lung fibroblast. *Eur Respir J.* 2002;20(2):359-68.
39. Penke LR, Speth JM, Dommeti VL, White ES, Bergin IL, and Peters-Golden M. FOXM1 is a critical driver of lung fibroblast activation and fibrogenesis. *J Clin Invest.* 2018;128(6):2389-405.
40. Lee TH, Yeh CF, Lee YT, Shih YC, Chen YT, Hung CT, et al. Fibroblast-enriched endoplasmic reticulum protein TXNDC5 promotes pulmonary fibrosis by augmenting TGFbeta signaling through TGFBR1 stabilization. *Nat Commun.* 2020;11(1):4254.
41. Nishizaka T, Shi Q, and Sheetz MP. Position-dependent linkages of fibronectin-integrin-cytoskeleton. *Proc Natl Acad Sci U S A.* 2000;97(2):692-7.
42. Hay ED. Interaction of embryonic surface and cytoskeleton with extracellular matrix. *Am J Anat.* 1982;165(1):1-12.
43. Upagupta C, Shimbori C, Alsilmi R, and Kolb M. Matrix abnormalities in pulmonary fibrosis. *Eur Respir Rev.* 2018;27(148).
44. Fernandez IE, and Eickelberg O. The impact of TGF-beta on lung fibrosis: from targeting to biomarkers. *Proc Am Thorac Soc.* 2012;9(3):111-6.
45. Khalil N, Parekh TV, O'Connor R, Antman N, Kepron W, Yehaulaeshet T, et al. Regulation of the effects of TGF-beta 1 by activation of latent TGF-beta 1 and differential expression of TGF-beta receptors (T beta R-I and T beta R-II) in idiopathic pulmonary fibrosis. *Thorax.* 2001;56(12):907-15.
46. Bergeron A, Soler P, Kambouchner M, Loiseau P, Milleron B, Valeyre D, et al. Cytokine profiles in idiopathic pulmonary fibrosis suggest an important role for TGF-beta and IL-10. *Eur Respir J.* 2003;22(1):69-76.
47. Li H, Cai H, Deng J, Tu X, Sun Y, Huang Z, et al. TGF-beta-mediated upregulation of Sox9 in fibroblast promotes renal fibrosis. *Biochim Biophys Acta Mol Basis Dis.* 2018;1864(2):520-32.

48. Chavez RD, Coricor G, Perez J, Seo HS, and Serra R. SOX9 protein is stabilized by TGF-beta and regulates PAPSS2 mRNA expression in chondrocytes. *Osteoarthritis Cartilage.* 2017;25(2):332-40.
49. Epstein Shochet G, Brook E, Bardenstein-Wald B, and Shitrit D. TGF-beta pathway activation by idiopathic pulmonary fibrosis (IPF) fibroblast derived soluble factors is mediated by IL-6 trans-signaling. *Respir Res.* 2020;21(1):56.
50. Athwal VS, Pritchett J, Llewellyn J, Martin K, Camacho E, Raza SM, et al. SOX9 predicts progression toward cirrhosis in patients while its loss protects against liver fibrosis. *EMBO Mol Med.* 2017;9(12):1696-710.
51. Raza S, Jokl E, Pritchett J, Martin K, Su K, Simpson K, et al. SOX9 is required for kidney fibrosis and activates NAV3 to drive renal myofibroblast function. *Sci Signal.* 2021;14(672).
52. Scharf GM, Kilian K, Cordero J, Wang Y, Grund A, Hofmann M, et al. Inactivation of Sox9 in fibroblasts reduces cardiac fibrosis and inflammation. *JCI Insight.* 2019;5.
53. Akiyama H, Chaboissier MC, Martin JF, Schedl A, and de Crombrugghe B. The transcription factor Sox9 has essential roles in successive steps of the chondrocyte differentiation pathway and is required for expression of Sox5 and Sox6. *Genes Dev.* 2002;16(21):2813-28.
54. Zheng B, Zhang Z, Black CM, de Crombrugghe B, and Denton CP. Ligand-dependent genetic recombination in fibroblasts : a potentially powerful technique for investigating gene function in fibrosis. *Am J Pathol.* 2002;160(5):1609-17.
55. Gebeshuber CA, Kornauth C, Dong L, Sierig R, Seibler J, Reiss M, et al. Focal segmental glomerulosclerosis is induced by microRNA-193a and its downregulation of WT1. *Nat Med.* 2013;19(4):481-7.
56. Nathan A, Reinhardt P, Kruspe D, Jorss T, Groth M, Nolte H, et al. The Wilms tumor protein Wt1 contributes to female fertility by regulating oviductal proteostasis. *Hum Mol Genet.* 2017;26(9):1694-705.
57. Hardie WD, Le Cras TD, Jiang K, Tichelaar JW, Azhar M, and Korfhagen TR. Conditional expression of transforming growth factor-alpha in adult mouse lung causes pulmonary fibrosis. *Am J Physiol Lung Cell Mol Physiol.* 2004;286(4):L741-9.
58. Kim Y, Murao H, Yamamoto K, Deng JM, Behringer RR, Nakamura T, et al. Generation of transgenic mice for conditional overexpression of Sox9. *J Bone Miner Metab.* 2011;29(1):123-9.
59. Sontake V, Wang Y, Kasam RK, Sinner D, Reddy GB, Naren AP, et al. Hsp90 regulation of fibroblast activation in pulmonary fibrosis. *JCI Insight.* 2017;2(4):e91454.
60. Madala SK, Edukulla R, Schmidt S, Davidson C, Ikegami M, and Hardie WD. Bone marrow-derived stromal cells are invasive and hyperproliferative and alter transforming growth factor-alpha-induced pulmonary fibrosis. *Am J Respir Cell Mol Biol.* 2014;50(4):777-86.
61. Madala SK, Thomas G, Edukulla R, Davidson C, Schmidt S, Schehr A, et al. p70 ribosomal S6 kinase regulates subpleural fibrosis following transforming growth factor-alpha expression in the lung. *Am J Physiol Lung Cell Mol Physiol.* 2016;310(2):L175-86.

62. Raghu G, Collard HR, Egan JJ, Martinez FJ, Behr J, Brown KK, et al. An official ATS/ERS/JRS/ALAT statement: idiopathic pulmonary fibrosis: evidence-based guidelines for diagnosis and management. *Am J Respir Crit Care Med.* 2011;183(6):788-824.
63. Kasam RK, Gajjala PR, Jegga AG, Courtney JA, Randell SH, Kramer EL, et al. Fibrocyte accumulation in the lungs of cystic fibrosis patients. *J Cyst Fibros.* 2020;19(5):815-22.
64. Madala SK, Edukulla R, Phatak M, Schmidt S, Davidson C, Acciani TH, et al. Dual targeting of MEK and PI3K pathways attenuates established and progressive pulmonary fibrosis. *PloS one.* 2014;9(1):e86536.
65. Ngo P, Ramalingam P, Phillips JA, and Furuta GT. Collagen gel contraction assay. *Methods Mol Biol.* 2006;341:103-9.
66. Chen J, Bardes EE, Aronow BJ, and Jegga AG. ToppGene Suite for gene list enrichment analysis and candidate gene prioritization. *Nucleic Acids Res.* 2009;37(Web Server issue):W305-11.

Figure legends

Figure 1. SOX9 is upregulated in the distal lung fibroblasts during the pathogenesis of pulmonary fibrosis. (A) Quantification of *SOX9* transcripts from the total lung RNA of normal individuals and patients with IPF by RT-PCR. (*P < 0.05; n = 5–6/group; unpaired *t*-test). **(B)** Immunostaining was performed with the anti-SOX9 antibody on lung sections of normal individuals and patients with IPF. Representative images were obtained at 40× magnification, Scale bar, 150 μm (n = 5/group). **(C)** Quantification of SOX9-positive cells normalized to the total lung cells in images of lung sections from normal individuals and patients with IPF was performed using a Bz-X analyzer. (****P < 0.00005; n = 5/group; unpaired *t*-test). **(D)** Quantification of *SOX9* transcripts in primary lung fibroblasts grown from normal and IPF lungs by RT-PCR. (**P < 0.005; n = 4/group; unpaired *t*-test). **(E)** Confocal microscopy images of lung sections from normal individuals and patients with IPF stained with anti-SOX9 (green color) and anti-vimentin (red color) antibodies and nuclei stained with DAPI (blue color). Cells positive for both SOX9 and vimentin are highlighted with white arrows. Images obtained at 60× magnification. Scale bar, 50 μm (n = 5/group). **(F)** Quantification of *Sox9* transcripts in the total lung transcripts of $TGF\alpha^{OE}$ mice treated with Dox for 0, 1, 4, 14, and 28 days (****P < 0.00005; n = 4-5/group; one-way ANOVA). **(G)** Confocal images of lung sections from control and $TGF\alpha^{OE}$ mice stained with anti-SOX9 (green color) and anti-ACTA2 (red color) or anti-vimentin (red color) antibodies and nuclei stained with DAPI (blue color). Images obtained at 60× magnification. Scale bar, 50 μm (n = 5/group). **(H)** Primary lung-resident fibroblasts isolated from lung cultures of control and $TGF\alpha^{OE}$ mice treated with Dox for 4 weeks were immunoblotted with antibodies against SOX9 and GAPDH. SOX9 protein levels were

normalized to GAPDH and are shown as fold induced change using a bar graph (**P < 0.005, n = 3/group; unpaired *t*-test).

Figure 2. The TGFα/WT1 axis induces SOX9 in the distal lung fibroblasts. (A) *SOX9* transcripts were measured by RT-PCR in normal lung fibroblasts treated with media or BMP2 (200 ng/ml), CTGF (50 ng/ml), TGFα (100 ng/ml), and IGF1 (100 ng/ml) for 16 hours. (****P < 0.00005, *P < 0.05; n = 4–8/group; one-way ANOVA). **(B)** Quantification of *SOX9* transcripts by RT-PCR in normal and IPF lung fibroblasts treated with media or TGFα (100 ng/ml) for 16 hours. (****P < 0.00005, ***P < 0.0005; n = 4; one-way ANOVA). **(C)** Quantification of *SOX9* transcripts by RT-PCR in IPF fibroblasts treated with vehicle, MEK inhibitor (ARRY, 0.1 μM), or PI3K inhibitor (PX-866, 0.1 μM) in the presence and absence of TGFα (100 ng/ml) for 16 hours. (****P < 0.00005, *P < 0.05; n = 4; one-way ANOVA). **(D)** IPF fibroblasts were treated with vehicle or MEK inhibitor (ARRY, 1 μM) in the presence and absence of TGFα (100 ng/ml) for 48 hours and immunoblotted with antibodies against SOX9 and GAPDH. SOX9 protein levels were normalized to GAPDH and are shown as fold induced change using a bar graph (**P < 0.005; n = 3; unpaired *t*-test). **(E)** IPF lung fibroblasts were transiently transfected with control or WT1 siRNA for 72 hours and *SOX9* transcripts were quantified using RT-PCR (**P < 0.005; n = 4; unpaired *t*-test). **(F)** Normal lung fibroblasts were transduced with control or WT1-adenoviral particles for 72 hours, and cell lysates were immunoblotted with antibodies against SOX9, WT1, and GAPDH. **(G)** Schemata show a human *SOX9* promoter ($Sox9^{WT1}$) clone or the WT1 binding site with the *SOX9* promoter clone deleted ($Sox9^{\triangle WT1}$). **(H)** Luciferase activity was measured in HEK293 cells that are transiently

transfected with empty, *SOX9*^{WT1}, or *SOX9*$^{\Delta WT1}$ promoter plasmids and cells treated with media or TGFα (100 ng/ml) for 16 hours (****P < 0.00005, ***P < 0.0005; n = 6; one-way ANOVA) **(I)** Luciferase activity was measured in HEK293 cells co-transfected with WT1 overexpression plasmid and *SOX9*^{WT1} or *SOX9*$^{\Delta WT1}$ promoter-luciferase plasmids for 48 hours and then treated with either media or TGFα (100 ng/ml) for another 16 hours. (****P < 0.00005; n = 6, one-way ANOVA).

Figure 3. Loss of SOX9 attenuates the genes involved in fibroblast activation in IPF. **(A)** The Venn diagram shows an overlap between differentially expressed genes in SOX9-deficient IPF fibroblasts and IPF lungs. **(B)** SOX9-driven gene networks in IPF fibroblasts were analyzed using ToppFun and visualized using Cytoscape. Red and purple colored oval shapes represent SOX9-driven genes that are up- or downregulated in IPF lungs, respectively. The turquoise-color squares represent enriched biological processes for inversely correlated genes between SOX9-deficient fibroblasts and IPF lungs. **(C)** Quantification of ECM-related gene transcripts by RT-PCR in IPF fibroblasts treated with either control or *SOX9*-specific siRNA for 72 hours. (****P < 0.00005, ***P < 0.0005, **P < 0.005; n = 4; unpaired *t*-test). **(D)** Quantification of gene transcripts implicated in mesenchymal cell differentiation by RT-PCR in IPF fibroblasts treated with either control or *SOX9*-specific siRNA for 72 hours (****P < 0.00005; n = 4; unpaired *t*-test). **(E)** Quantification of migration-associated gene transcripts by RT-PCR in IPF fibroblasts treated with either control or *SOX9*-specific siRNA for 72 hours. (****P < 0.00005, ***P < 0.0005; n = 4; unpaired *t*-test). **(F)** IPF fibroblasts were treated with either

control or *SOX9*-specific siRNA for 72 hours, and cell lysates were immunoblotted with antibodies against SOX9, ACTA2, COL1α1, POSTN, LOXL2, and GAPDH.

Figure 4. SOX9 is a positive regulator of migration, transformation, and survival of IPF fibroblasts. (A) Quantification of migration of IPF fibroblasts treated with either control or *SOX9* siRNA for 72 hours. (****P < 0.00005, (**P < 0.005; n = 12; two-way ANOVA). **(B)** Quantification of *DPYSL3* gene transcripts in the total transcripts of IPF compared to normal lungs (*P < 0.05; n = 4; unpaired *t*-test). **(C)** Quantification of *DPYSL3* gene transcripts in IPF fibroblasts treated with either control or *SOX9* siRNA for 72 hours (***P < 0.0005; n = 4; unpaired *t*-test). **(D)** Fibroblasts isolated from distal lung cultures of $\alpha SMA^{CreERT}Rosa^{mTmG}$ mice were transduced with either control or SOX9 overexpressing lentivirus in the presence of 4-hydroxy tamoxifen for 72 hours. Representative confocal images were obtained at 60× magnification. Scale bar, 100 μm (n = 4/group). **(E)** The number of ACTA2 positive (GFP or green color) cells in the total cells (DAPI or blue color) were quantified using MetaMorph image analysis software and are presented as the percentage of ACTA2-positive cells in total fibroblasts (**P < 0.005; n = 4; unpaired *t*-test). **(F)** IPF fibroblasts were treated with either control or *SOX9* siRNA for 72 hours and cultured with collagen gels to measure the changes in collagen gel contraction after 6 hours (****P < 0.00005; n = 6; unpaired *t*-test). **(G)** IPF fibroblasts were treated with either control or *SOX9* siRNA for 48 hours, followed by anti-Fas treatment for another 24 hours and cells stained to quantify the total TUNEL-positive cells. Representative confocal images were obtained at 20× magnification. Scale bar, 200 μm. **(H)** The number of TUNEL-positive (red color) cells and the total cells (DAPI or blue color) were quantified

using Elements image analysis software and are presented as the percentage of TUNEL-positive cells in total cells. (**P < 0.005, *P < 0.05; n = 3/group; one-way ANOVA) **(I)** Quantification of anti-apoptotic gene transcripts, *BCL-XL* and *BCL-2L2*, in IPF fibroblasts treated with either control or *SOX9*-specific siRNA for 72 hours (***P < 0.0005, **P < 0.005; n = 4; unpaired *t*-test).

Figure 5. Fibroblast-specific deletion of SOX9 attenuates TGFα-induced pulmonary fibrosis in vivo. (A) Schemata of representation of animal experiments performed with three groups of $Sox9^{f/f}$, $TGF\alpha^{OE}Sox9^{f/f}$, and $TGF\alpha^{OE}Col1\alpha2^{CreER}Sox9^{f/f}$ mice. All mice were treated with Dox for six weeks in conjunction with two intraperitoneal tamoxifen injections per week. **(B)** Quantification of *TGFα* and *Sox9* gene transcripts in the total lungs of control and Sox9-deficient mice. (***P < 0.0005, *P < 0.05; n = 3-4/group; one-way ANOVA). **(C)** Representative images of Masson's trichrome-stained lung sections from $CCSPSox9^{f/f}$, $TGF\alpha^{OE}Sox9^{f/f}$, and $TGF\alpha^{OE}Col1\alpha2^{CreER}Sox9^{f/f}$ mice. Images were captured at 10× magnification. Scale bar, 500 μm. **(D)** Quantification of hydroxyproline levels in the right lung of mice. (**P < 0.005, *P < 0.05; n = 3-4/group; one-way ANOVA). **(E–G)** Quantification of lung mechanics (resistance, compliance, and elastance) among three groups of mice using FlexiVent (**P < 0.005, *P < 0.05; n = 3–4/group; one-way ANOVA). **(H)** Quantification of *Col1a1*, *Col3a1*, *Ctgf*, and *Loxl2* gene transcripts in the total lungs of control and Sox9-deficient mice (****P < 0.00005, ***P < 0.0005, **P < 0.005, *P < 0.05; n = 3–4/group; one-way ANOVA). **(I)** Lung sections of fibrosis control ($TGF\alpha^{OE}Sox9^{f/f}$) and Sox9-deficient ($TGF\alpha^{OE}Col1\alpha2^{CreER}Sox9^{f/f}$) mice were immunostained with antibodies against SOX9 (green color) and ACTA2 (red color). Representative confocal

images were obtained at 60× magnification, and DAPI was used to stain nuclei (blue color). Scale bar, 40 μm. White arrowheads were used to highlight cells positive for both SOX9 and ACTA2. **(J)** The SOX9 and ACTA2-positive cells in the total cells were quantified using Elements image analysis software.

Figure 6. SOX9 is required for the maintenance of fibroblast activation. (A) Schematic representation of the workflow for isolating fibroblasts from lung cultures of *TGFα*^{OE}*Sox9*$^{f/f}$ mice treated with Dox for 6 weeks. Fibroblasts were infected with either control adeno or Cre-expressing adenovirus for 48 hours or 72 hours to delete SOX9 in activated fibroblasts. **(B)** Fibroblasts were infected with control or Cre-expressing adenovirus for 72 hours, and cell lysates were immunoblotted with antibodies against SOX9 and GAPDH. SOX9 protein levels were normalized to GAPDH and are shown as induced fold change using a bar graph (***P < 0.0005; n = 3, unpaired *t*-test). **(C)** Fibroblasts were transduced with control or Cre-expressing adenovirus for 72 hours and were measured the transcripts of *Sox9*, *Acta2*, *Col1a1*, and *Loxl2* by RT-PCR. (***P < 0.0005, **P < 0.005, *P < 0.05; n = 3; unpaired *t*-test). **(D)** Fibroblasts were transduced with control or Cre-expressing adenovirus for 72 hours and seeded with collagen gels to measure the percent contraction of collagen gels after 6 hours (***P < 0.0005; n = 6; unpaired *t*-test). **(E, F)** Fibroblasts were transduced with control or Cre-expressing adenovirus for 48 hours and treated with anti-Fas or control antibody for another 24 hours. The percentage of TUNEL-positive (red color) cells in the total cells (DAPI or blue color) was quantified using Elements image analysis software. Scale bar: 200 μm (****P < 0.00005, ***P < 0.0005; n = 3/group; one-way ANOVA).

Figure 7. Overexpression of SOX9 in myofibroblasts augments bleomycin-induced pulmonary fibrosis. (A) Schematic representation of animal experiments with *αSMA*^{CreERT2} (control) and *αSMA*^{CreERT2}*CAG-Sox9* (*Sox9*^{OE}) mice treated with bleomycin and tamoxifen via intratracheal and intraperitoneal routes, respectively. **(B)** The progressive weight loss after bleomycin treatment in control and *Sox9*^{OE} mice. (**P < 0.005; n = 6/group; two-way ANOVA). **(C)** The lung lysates of control and *Sox9*^{OE} mice were immunoblotted with antibodies against SOX9 and GAPDH. SOX9 protein levels were normalized to GAPDH and are shown as fold induced change using a bar graph (***P < 0.005; n = 4; unpaired *t*-test). **(D)** Representative confocal images of lung sections stained for SOX9 (green color), ACTA2 (red color), and DAPI (blue color). Scale bar: 50 μm. **(E)** The efficiency of SOX9 overexpression was quantified by counting the percentage of SOX9- and ACTA2-positive cells in total ACTA2-positive cells. (****P < 0.00005; n = 4; unpaired *t*-test). **(F)** Masson's trichrome-stained lung sections of the control and *Sox9*^{OE} mice treated with bleomycin. Images were captured at 4× magnification and 20× magnification with scale bars of 1500 and 200 μm, respectively. The percentage of the fibrotic area was quantified in the images of control and *Sox9*^{OE} mice using BZx image analysis (**P < 0.005; n = 6; unpaired *t*-test). **(G)** The lung resistance was measured using FlexiVent in control and *Sox9*^{OE} mice treated with bleomycin (*P < 0.05; n = 6; unpaired *t*-test).

Figure 8. SOX9 overexpression in myofibroblasts augments bleomycin-induced pulmonary fibrosis in vivo. (A) Representative images of ACTA2-stained lung sections of α*SMA*^{CreERT2} (control) and α*SMA*^{CreERT2}*; CAG-Sox9* (*Sox9*^{OE}) mice captured at 4× (low)

and 20× (high) magnification, respectively. Scale bar: 1500 and 200 μm. **(B)** Quantification of ACTA2 positive area in the whole lung section (***P < 0.0005, n = 6/group, unpaired *t*-test). **(C, D)** Quantification of ECM and inflammatory-related gene transcripts among two groups. (****P < 0.00005, **P < 0.005, *P < 0.05 n = 6/group, unpaired *t*-test). **(E, F)** Immunoblots for ACTA2, LOXL2, FN1, COL1α1, and GAPDH expression in the whole lung tissue lysates of control and *Sox9*^{OE} mice and its quantification (****P < 0.00005, **P < 0.005, *P < 0.005 n = 4, unpaired *t*-test). Immunoblots for figure 7C and 8E were from the same experiment and blots were run in parallel to normalize with GAPDH levels.

Figure 1

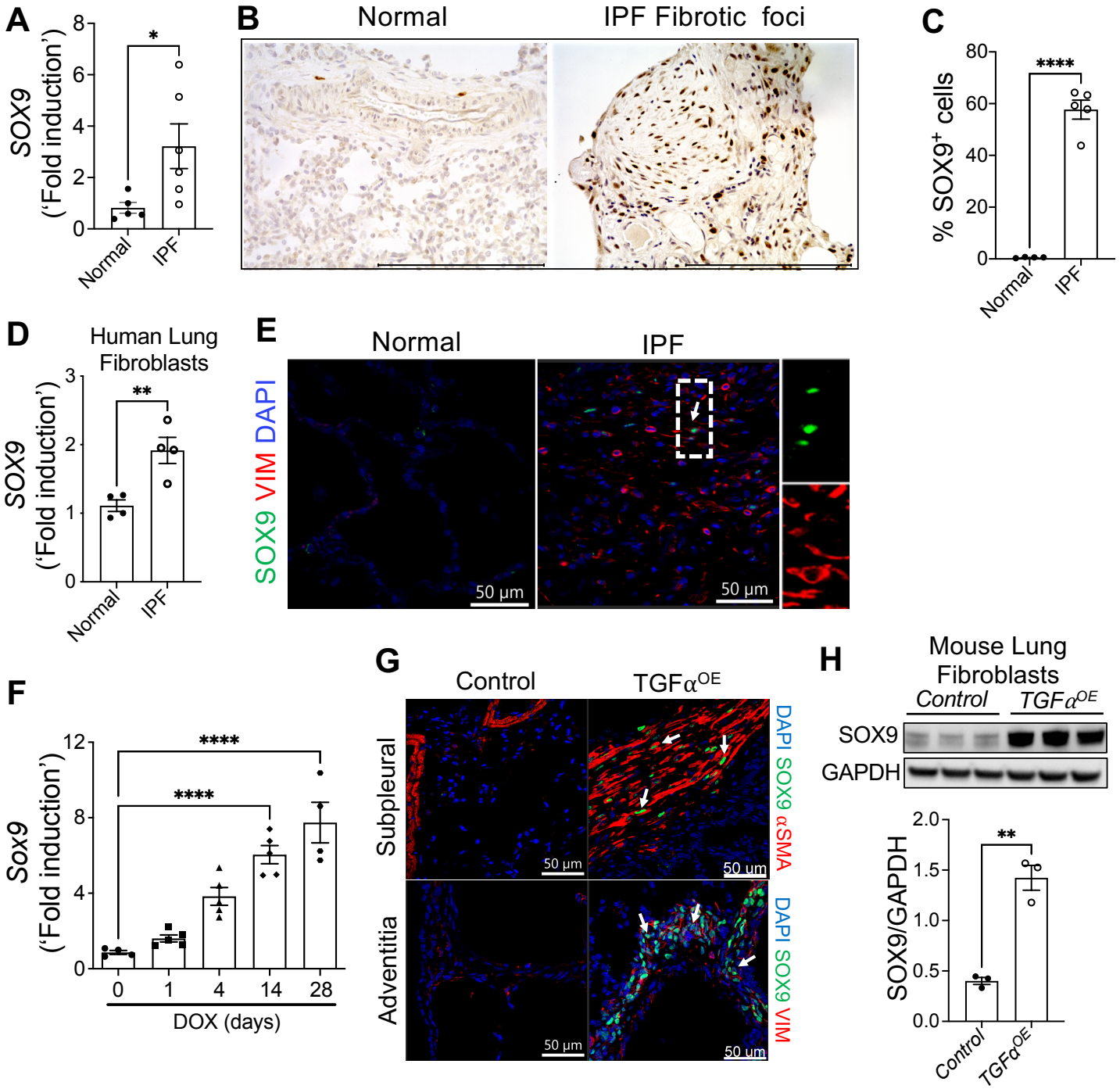

A
SOX9 ('Fold induction')
Normal
IPF
B
Normal
IPF Fibrotic foci
C
% SOX9+ cells
****
D
Human Lung Fibroblasts
SOX9 ('Fold induction')
**
E
Normal
IPF
SOX9 VIM DAPI
50 µm
F
Sox9 ('Fold induction')
****
DOX (days)
G
Control
TGFα^OE
Subpleural
Adventitia
DAPI SOX9 αSMA
DAPI SOX9 VIM
50 µm
H
Mouse Lung Fibroblasts
Control
TGFα^OE
SOX9
GAPDH
SOX9/GAPDH

Figure 2

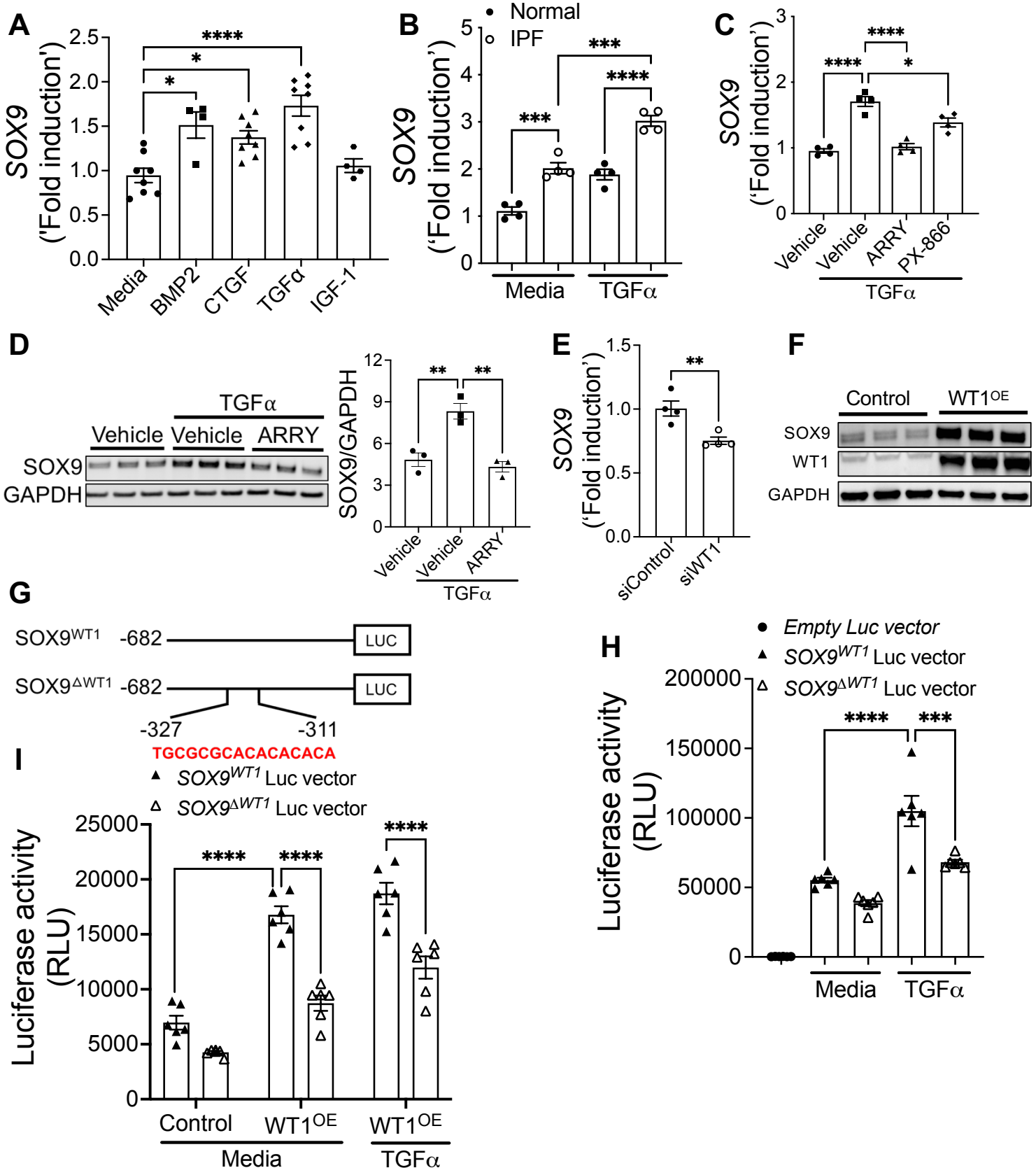

A
SOX9 ('Fold induction')
Media
BMP2
CTGF
TGFα
IGF-1
B
Normal
IPF
SOX9 ('Fold induction')
Media
TGFα
C
SOX9 ('Fold induction')
Vehicle
Vehicle
ARRY
PX-866
TGFα
D
TGFα
Vehicle
Vehicle
ARRY
SOX9
GAPDH
SOX9/GAPDH
E
SOX9 ('Fold induction')
siControl
siWT1
F
Control
WT1OE
SOX9
WT1
GAPDH
G
SOX9WT1 -682 LUC
SOX9ΔWT1 -682 LUC
-327
-311
TGCGCGCACACACACA
H
Empty Luc vector
SOX9WT1 Luc vector
SOX9ΔWT1 Luc vector
Luciferase activity (RLU)
Media
TGFα
I
SOX9WT1 Luc vector
SOX9ΔWT1 Luc vector
Luciferase activity (RLU)
Control
WT1OE
WT1OE
Media
TGFα

Figure 3

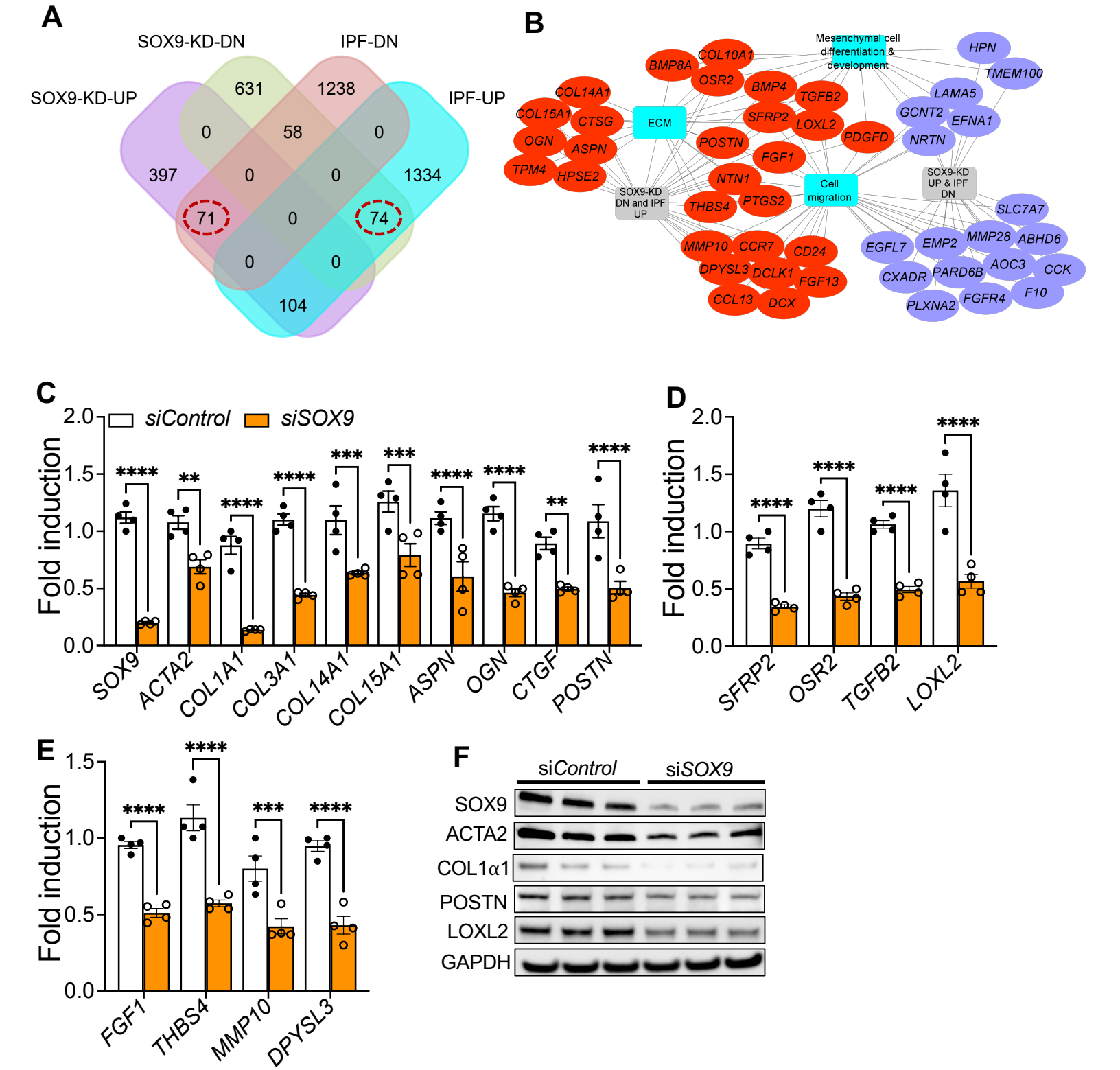
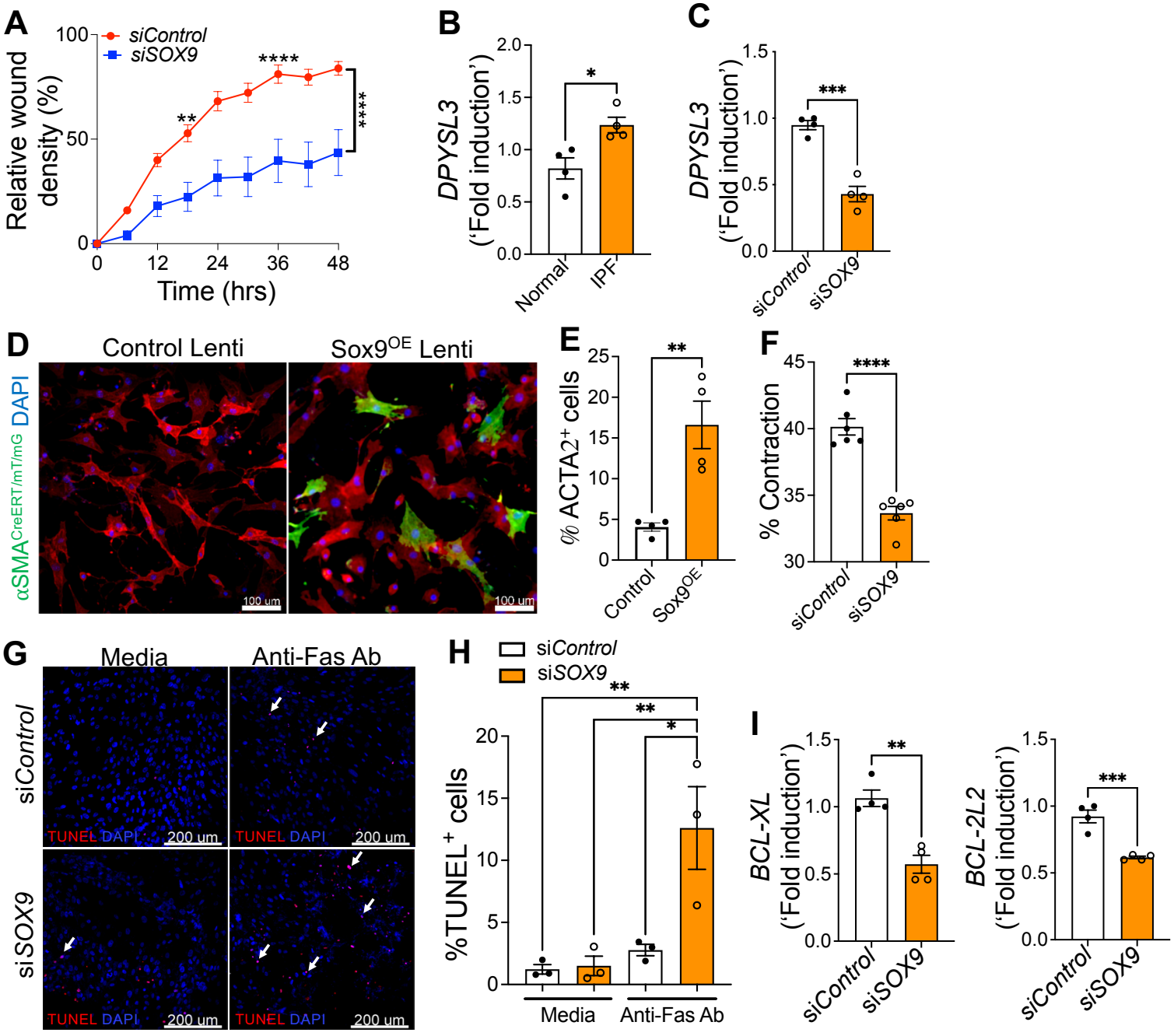

A
SOX9-KD-DN
IPF-DN
SOX9-KD-UP
IPF-UP
631
1238
0
58
0
397
0
0
1334
71
0
74
0
0
104
B
Mesenchymal cell differentiation & development
ECM
Cell migration
SOX9-KD DN and IPF UP
SOX9-KD UP & IPF DN
COL10A1
BMP8A
OSR2
BMP4
TGFB2
COL14A1
COL15A1
CTSG
SFRP2
LOXL2
PDGFD
OGN
ASPN
POSTN
FGF1
TPM4
HPSE2
NTN1
THBS4
PTGS2
MMP10
CCR7
CD24
DPYSL3
DCLK1
FGF13
CCL13
DCX
HPN
TMEM100
LAMA5
GCNT2
EFNA1
NRTN
SLC7A7
EGFL7
EMP2
MMP28
ABHD6
AOC3
CCK
CXADR
PARD6B
PLXNA2
FGFR4
F10
C
siControl
siSOX9
Fold induction
SOX9
ACTA2
COL1A1
COL3A1
COL14A1
COL15A1
ASPN
OGN
CTGF
POSTN
D
Fold induction
SFRP2
OSR2
TGFB2
LOXL2
E
Fold induction
FGF1
THBS4
MMP10
DPYSL3
F
siControl
siSOX9
SOX9
ACTA2
COL1α1
POSTN
LOXL2
GAPDH

Figure 4


A
siControl
siSOX9
Relative wound density (%)
Time (hrs)
B
DPYSL3 ('Fold induction')
Normal
IPF
C
DPYSL3 ('Fold induction')
siControl
siSOX9
D
Control Lenti
Sox9OE Lenti
αSMACreERT/mT/mG DAPI
100 um
E
% ACTA2+ cells
Control
Sox9OE
F
% Contraction
siControl
siSOX9
G
Media
Anti-Fas Ab
siControl
siSOX9
TUNEL DAPI
200 um
H
siControl
siSOX9
%TUNEL+ cells
Media
Anti-Fas Ab
I
BCL-XL ('Fold induction')
BCL-2L2 ('Fold induction')
siControl
siSOX9

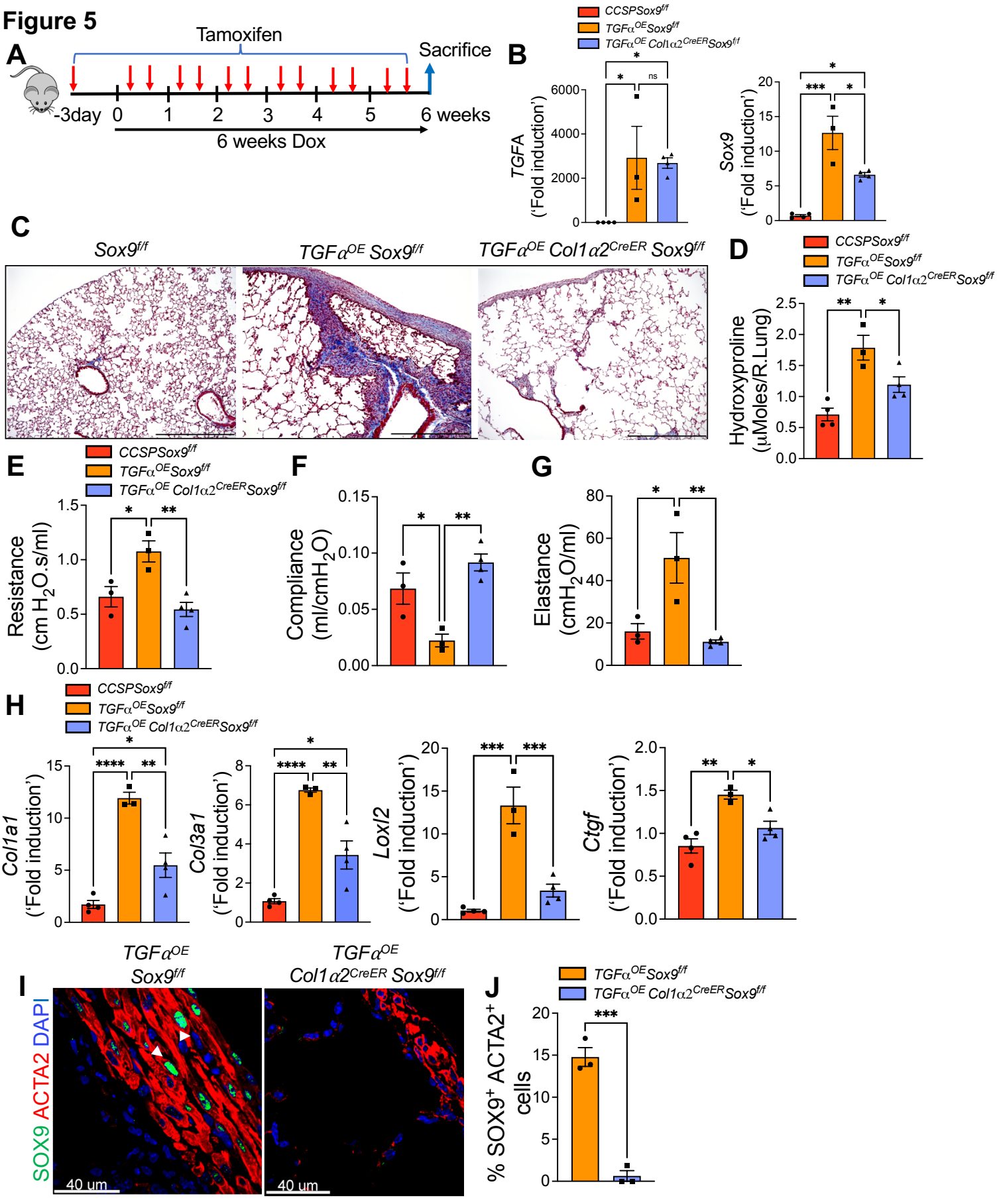

Figure 5
A
Tamoxifen
Sacrifice
-3day
0
1
2
3
4
5
6 weeks
6 weeks Dox
B
CCSPSox9f/f
TGFαOESox9f/f
TGFαOE Col1α2CreERSox9f/f
TGFA (‘Fold induction’)
Sox9 (‘Fold induction’)
C
Sox9f/f
TGFαOE Sox9f/f
TGFαOE Col1α2CreER Sox9f/f
D
Hydroxyproline (µMoles/R.Lung)
E
Resistance (cm H2O.s/ml)
F
Compliance (ml/cmH2O)
G
Elastance (cmH2O/ml)
H
Col1a1 (‘Fold induction’)
Col3a1 (‘Fold induction’)
Lox/2 (‘Fold induction’)
Ctgf (‘Fold induction’)
I
SOX9 ACTA2 DAPI
40 um
J
% SOX9+ ACTA2+ cells

Figure 6

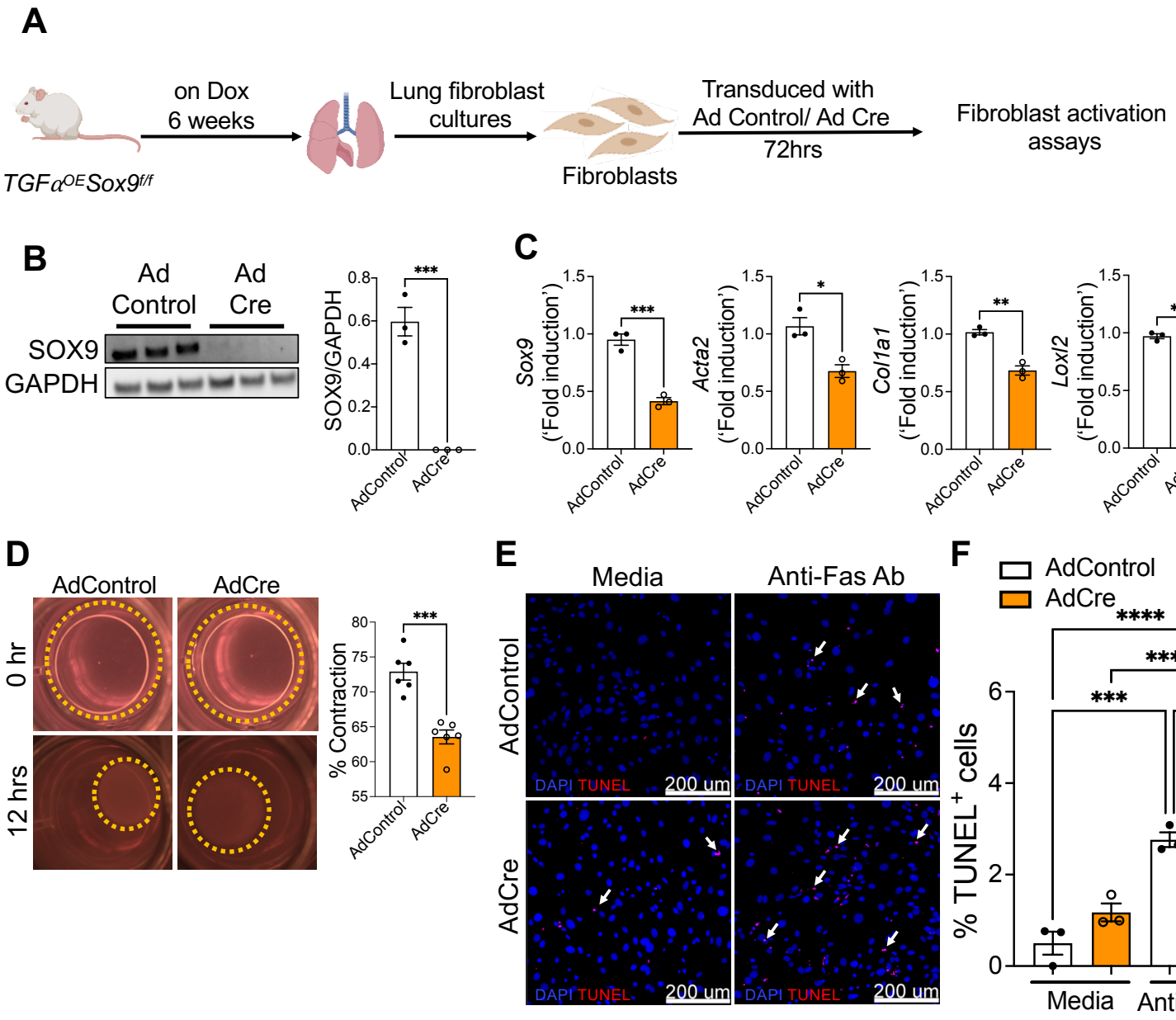

A
on Dox
6 weeks
Lung fibroblast
cultures
Fibroblasts
Transduced with
Ad Control/ Ad Cre
72hrs
Fibroblast activation
assays
TGFα^OE Sox9^f/f
B
Ad
Control
Ad
Cre
SOX9
GAPDH
SOX9/GAPDH
AdControl
AdCre
C
Sox9
('Fold induction')
Acta2
('Fold induction')
Col1a1
('Fold induction')
Loxl2
('Fold induction')
D
AdControl
AdCre
0 hr
12 hrs
% Contraction
E
Media
Anti-Fas Ab
AdControl
AdCre
DAPI TUNEL
200 um
F
AdControl
AdCre
% TUNEL+ cells
Media
Anti-Fas Ab

Figure 7

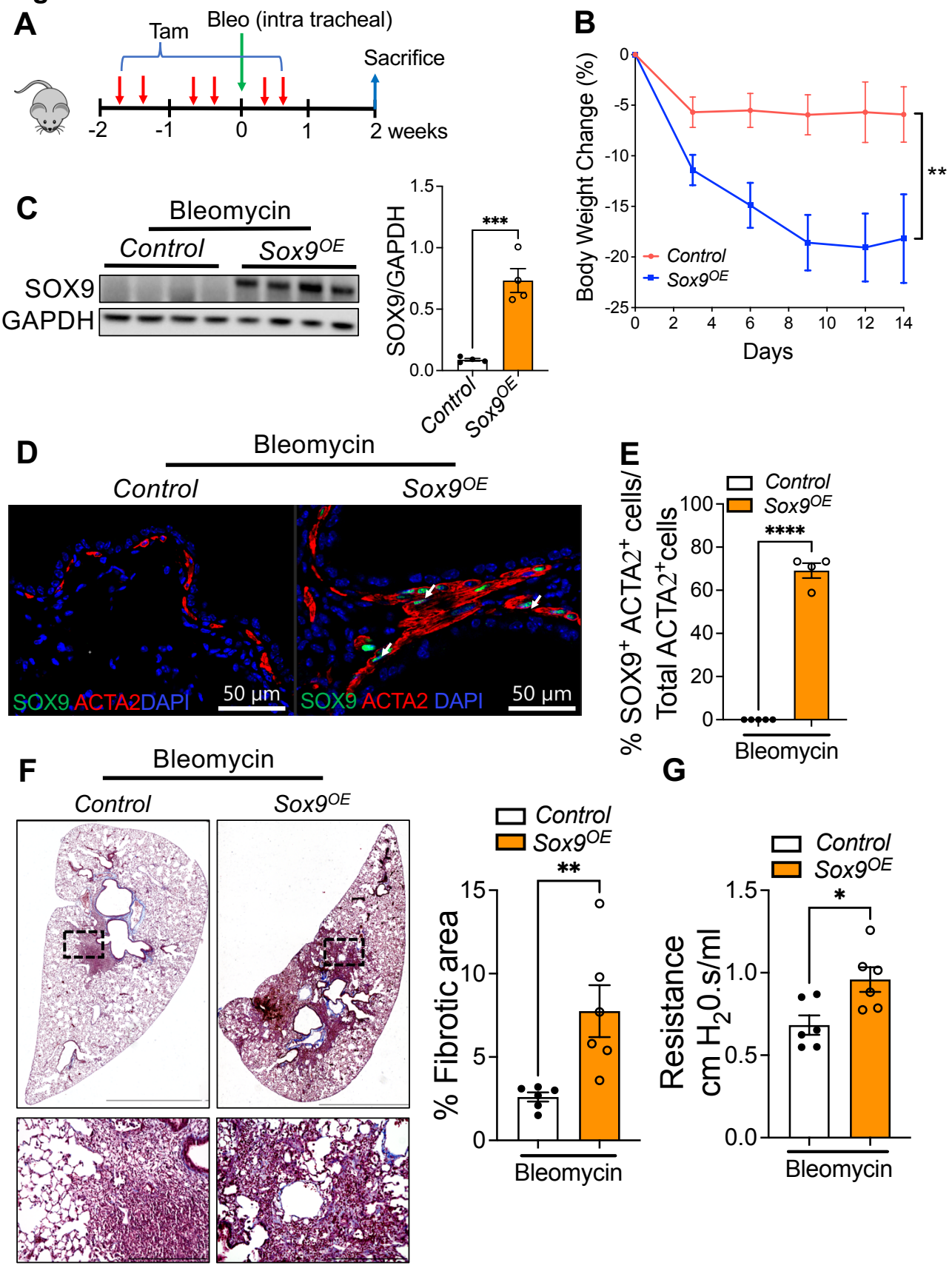
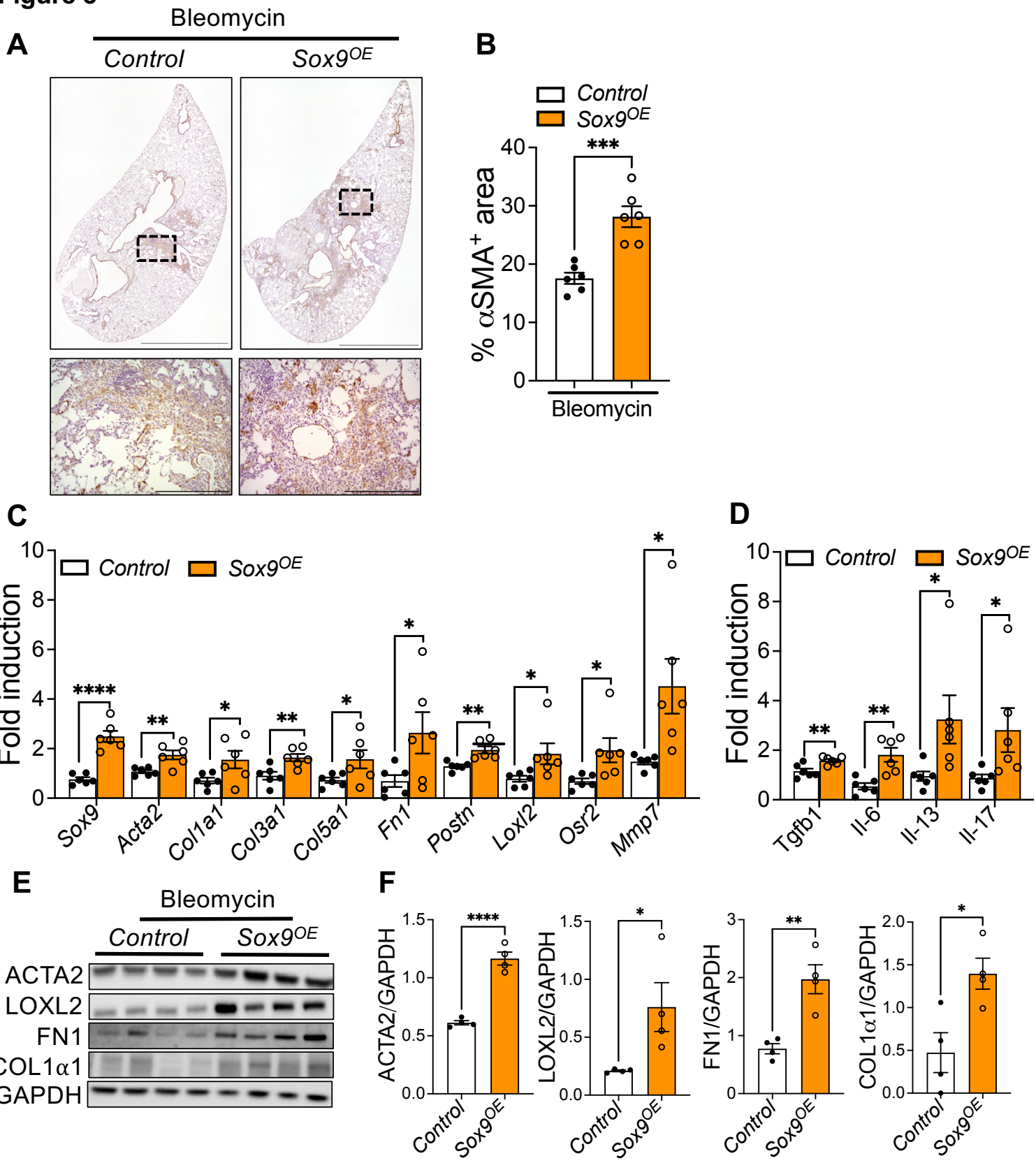

A
Tam
Bleo (intra tracheal)
Sacrifice
-2
-1
0
1
2 weeks
B
Body Weight Change (%)
Days
Control
Sox9OE
**
C
Bleomycin
Control
Sox9OE
SOX9
GAPDH
SOX9/GAPDH
***
D
Bleomycin
Control
Sox9OE
SOX9 ACTA2 DAPI
50 μm
E
% SOX9+ ACTA2+ cells/ Total ACTA2+cells
****
Bleomycin
F
Bleomycin
Control
Sox9OE
% Fibrotic area
**
G
Resistance cm H2O.s/ml
*

Figure 8


A
Bleomycin
Control
Sox9OE
B
Control
Sox9OE
% αSMA+ area
***
Bleomycin
C
Control
Sox9OE
Fold induction
Sox9
Acta2
Col1a1
Col3a1
Col5a1
Fn1
Postn
Loxl2
Osr2
Mmp7
D
Control
Sox9OE
Fold induction
Tgfb1
Il-6
Il-13
Il-17
E
Bleomycin
Control
Sox9OE
ACTA2
LOXL2
FN1
COL1α1
GAPDH
F
ACTA2/GAPDH
LOXL2/GAPDH
FN1/GAPDH
COL1α1/GAPDH
Control
Sox9OE